Fall 2011

Mixing and Melt Sources in the Miocene Aztec Wash pluton (Nevada, USA) as Revealed by Zircon Hf and O and Whole Rock Sr, Nd and Hf Isotopes

Mark Ryan
San Jose State University

MIXING AND MELT SOURCES IN THE MIOCENE AZTEC WASH PLUTON (NEVADA, USA) AS REVEALED BY ZIRCON Hf AND O AND WHOLE ROCK Sr, Nd AND Hf ISOTOPES

A Thesis

Presented to

The Faculty of the Department of Geology

San Jose State University

In partial fulfillment

of the requirements for the degree

Master of Science

by

Mark Ryan

December 2011

The Designated Committee Approves the Thesis Titled

MIXING AND MELT SOURCES IN THE MIOCENE AZTEC WASH PLUTON (NEVADA, USA) AS REVEALED BY ZIRCON Hf AND O AND WHOLE ROCK Sr, Nd AND Hf ISOTOPES

by

Mark Ryan

APPROVED FOR THE DEPARTMENT OF GEOLOGY

SAN JOSE STATE UNIVERSITY

DECEMBER 2011

Prof. Jonathan Miller	Department of Geology
Dr. Ellen Metzger	Department of Geology
Dr. Richard Sedlock	Department of Geology

ABSTRACT

MIXING AND MELT SOURCES IN THE MIOCENE AZTEC WASH PLUTON (NEVADA, USA) AS REVEALED BY ZIRCON Hf AND O AND WHOLE ROCK Sr, Nd AND Hf ISOTOPES

by Mark Ryan

The 15.6 Ma Aztec Wash pluton, within the northern Colorado River extensional corridor (Nevada), displays abundant field evidence for open system processes. Previous geochemical studies documented physical and chemical mixing processes that produced a wide spectrum of compositional and textural variants. To better understand the mixing pathways and melt sources, whole rock and zircon isotopes were analyzed from samples that document the range of rock compositions and textural variety and that contain zircons that have trace element variations indicative of large thermal and chemical fluctuations. The new whole rock isotope data show that all rocks are mixtures of Precambrian crust and enriched lithospheric mantle components, with mixtures having a large mantle fraction (≥50%). New Hf (n=189) and O (n=241) isotope analyses of zircon from all samples show heterogeneous isotopic compositions (-5 to -18 εHf; 4.5-7.5‰ $\delta^{18}O$), which are interpreted to reflect recycling of crystals from many intrusive increments. Paucity of Precambrian zircons (n=1) indicates that initial melts were zircon-undersaturated and that zircon grew mainly from magmas in Aztec Wash magma chamber(s) or conduits. Silicic melt was derived from a deep crustal “hot zone” formed by injection of enriched mantle basalt into Proterozoic crust; mixing of this melt with enriched mantle-derived basalts produced the observed spread in isotopic data.

ACKNOWLEDGMENTS

I would like to express my sincere thanks to my advisor, Professor Jonathan Miller, for allowing me this great opportunity to work with him and be a part of a fantastic team in the Geology Department at San Jose State University. His expertise in this subject has been invaluable to me in the classroom, out in the field, and during our thought-provoking discussions relating to this project and beyond. I feel I will leave a better geologist for it. National Science Foundation grants EAR0409882 and EAR0409876 provided funding that supported this project. I would like to also extend my thanks to my committee members, Dr. Richard Sedlock and Dr. Ellen Metzger, for their contributions toward this project. Both have been a part of my education as a graduate student and each have assisted me in advancing my knowledge in the subject in their unique and successful teaching methods. They have not only helped me develop as a student in geology but each has been a fantastic work colleague and mentor during my time as a teacher in Geology. I would also like to thank the team at Vanderbilt University for their help. Dr. Calvin Miller provided many insights during our brief excursion to the Aztec Wash pluton. Ashley Bromley provided me with the necessary samples to complete the study, and Vanderbilt graduate students Ayla Pamukcu, Abraham Padilla, and Tamara Carley, and SJSU graduate student Kaye Evleth, were a welcome addition in the field and offered helpful assistance and support during this project. I would also like to extend my deepest thanks to all those involved in the data collection for this study. To Professor Gareth Davies in the Faculty of Earth and Life

Sciences at Vrije University (VU Amsterdam), thank you for not only opening up your department and lab to me whilst offering useful information about the data, but also for welcoming me into your home. Both you and Joanne were excellent hosts during my stay. Thanks to Bas van der Wagt (VU Amsterdam) for his amazing dedication and technical support in the laser ablation lab in Amsterdam both day and night. The knowledge he shared and the friendship we developed was very important to me. And a small thanks for the beers too! Thank you to Dr. Axel Schmitt at the University of California, Los Angeles and to Dr. Joseph Wooden at Stanford University for welcoming me into their respective labs, answering questions and providing assistance in data collection and data reduction. Thanks also to the technical staff at the MC-ICP-MS lab at the University of California, Davis for running samples for whole-rock isotope analyses. Finally, a special thanks to my wife, Sierra Ryan. Her unwavering support for me during my time at San Jose and her constant motivation to continue during this project has been the base from which I have pushed myself. I certainly would not be where I am today if not for her being at my side.

TABLE OF CONTENTS

INTRODUCTION 1

GEOLOGIC BACKGROUND 5

Geological Setting: The Aztec Wash Pluton 5

Previous Geochemical Studies 14

Hafnium and Oxygen Isotopes in Zircon 17

Zirconium in Sphene Thermometry 22

SAMPLES AND METHODS 24

Sample Descriptions 24

Grain Separation and Imaging 27

Zircon Age and Zircon and Sphene Trace Element Analysis 28

Oxygen in Zircon 30

Hafnium in Zircon 33

Whole Rock Strontium, Neodymium, and Hafnium Isotope Analysis 40

RESULTS 44

Whole Rock Radiogenic Sr-Nd-Hf Analysis 44

In-situ Age and Trace Element Analysis of Zircon 57

Hafnium Isotopes in Zircon 60

Granites 79
Mechanically Contaminated 79
Grey Hybrids 79
Dark Pods 80
Mafic Sheets 80
Oxygen Isotopes in Zircon 81
Granites 91
Mechanically Contaminated 91
Grey Hybrids 91
Dark Pods 92
Mafic Sheets 92
Zircon core-rim relationships 93
Combined Hafnium and Oxygen in Zircon 95
Trace Element and Zr-in-Sphene Temperature Analysis 98
DISCUSSION 112
Sources of Magmatic Input 122
Generalized Model for Melt Derivation and Zircon Growth in the Aztec Wash pluton 130

Late-stage assimilation and/or hydrothermal alteration? 134

Further Work Required 136

CONCLUSIONS 138

REFERENCES 140

APPENDIX A: Whole rock data..... 148

APPENDIX B: Zircon trace element data..... 154

APPENDIX C: Zircon SHRIMP age data..... 160

APPENDIX D: LA-ICP-MS zircon Hf isotope composition data..... 163

APPENDIX E: Ion Mircroprobe zircon O isotope data..... 178

APPENDIX F: Spehene SHRIMP data..... 194

APPENDIX G: Zircon CL images..... 271

APPENDIX H: Sphene BSE images..... 350

APPENDIX I: Mixing curve data..... 393

LIST OF FIGURES

Figure 1. Location of the Aztec Wash pluton (AWP) within the northern Colorado River extension corridor 6

Figure 2. Schematic geological map of the Aztec Wash pluton 10

Figure 3. Field relationships of mafic and felsic melt in the Heterogeneous Zone 11

Figure 4. Schematic cartoon for construction of the Aztec Wash pluton 13

Figure 5. Flowcharts highlighting the open-system nature of the Aztec Wash pluton 15

Figure 6. Variation of $\delta^{18}O$ in different rocks on Earth including values of igneous zircons relative to VSMOW 20

Figure 7. Measured results and external errors for zircon standard R33 32

Figure 8. Monitoring of laser ablation runs during Hf isotope analysis of zircon 35

Figure 9. Recorded measurements and associated errors for zircon standard GJ-1 39

Figure 10. Whole rock $(^{87}Sr/^{86}Sr)_i$, $\varepsilon Nd_{(t)}$ $\varepsilon Hf_{(t)}$ vs. SiO_2 45

Figure 11. Whole rock reciprocal plots of initial Sr, Hf and Nd isotope ratios against respective elemental concentrations 50

Figure 12.Whole rock $\varepsilon Hf_{(t)}$ vs. $\varepsilon Nd_{(t)}$ for samples in Granite and Heterogeneous zones 53

Figure 13. Whole rock Nd and Sr compositions for Aztec Wash pluton and regional lithologies 55

Figure 14. Calculated binary mixing curves for Nd and Sr isotopic compositions..... 56

Figure 15. Cumulate probability curves for zircon ages of AWM-1 (a) and AWM-2 (b) .. 58

Figure 16. REE spider diagram for zircons in AWM-1 59

Figure 17. Zircon (zirc) εHf vs. whole-rock (WR) εHf 63

Figure 18. Cumulative probability plots for εHf-in-zircon data 64

Figure 19. Ranked plot for individual spot values of $\delta^{18}O$ in zircon 82

Figure 20. Cumulative probability plots for $\delta^{18}O$ in zircon 83

Figure 21. Cathodoluminescence images for targeted zircon grains highlighting $\delta^{18}O$ core-rim relationships 94

Figure 22. Combined Hf vs. O isotopic data 96

Figure 23. REE concentration diagrams of sphene 101

Figure 24. Zr-in-sphene temperature vs. bulk Zr saturation temperatures 106

Figure 25. Cumulative probability curves of Zr-in-sphene (dashed black) and Ti-in-zircon (solid red) 107

Figure 26. εHf in zircon vs. whole-rock SiO_2 115

Figure 27. $\delta^{18}O$ of zircon vs. whole-rock SiO_2 117

Figure 28. $\delta^{18}O$ vs. Ti-in-zircon temperatures for cores and rims of zircons in units sampled 121

Figure 29. Cartoon for potential mechanism to create heterogeneity in zircon population within felsic units 129

Figure 30. Schematic cartoon of proposed model for construction of the Aztec Wash pluton 133

Figure G1. Zircon images for sample NAWZ-13 272

Figure G2. Zircon images for sample NAWZ-16 276

Figure G3. Zircon images for sample NAWZ-26 281

Figure G4. Zircon images for sample NAWZ-50 287

Figure G5. Zircon images for sample AWAG-1A 292

Figure G6. Zircon images for sample AWAG-1B 297

Figure G7. Zircon images for sample AWAG-1C 303

Figure G8. Zircon images for sample AWAG-2 306

Figure G9. Zircon images for sample AWAG-3 311

Figure G10. Zircon images for sample AWAG-4 316

Figure G11. Zircon images for sample AWAG-5 321

Figure G12. Zircon images for sample AWAG-6 326

Figure G13. Zircon images for sample AWAG-7 330

Figure G14. Zircon images for sample AWM-1 335

Figure G15. Zircon images for sample AWM-2 341

Figure H1. Back-scatter Electron Imaging of sample AWAG-1A 351

Figure H2. Back-scatter Electron Imaging of sample AWAG-1B 355

Figure H3. Back-scatter Electron Imaging of sample AWAG-2 359

Figure H4. Back-scatter Electron Imaging of sample AWAG-3 363

Figure H5. Back-scatter Electron Imaging of sample AWAG-4 367

Figure H6. Back-scatter Electron Imaging of sample AWAG-5 371

Figure H7. Back-scatter Electron Imaging of sample AWAG-6 375

Figure H8. Back-scatter Electron Imaging of sample AWAG-7 378

Figure H9. Back-scatter Electron Imaging of sample AWM-1 382

Figure H10. Back-scatter Electron Imaging of sample AWM-2 388

LIST OF TABLES

Table 1. Sample Descriptions 26

Table 2. LA-ICP-MS Hf Cup Collector Configuration 36

Table A1. Whole-rock major element analysis 149

Table A2. Whole-rock trace element analysis 150

Table A3. Whole-rock major element analysis of AWM-1 and 2 152

Table A4. Whole-rock trace element analysis of AWM1 and 2 152

Table A5. Whole-rock Sr, Hf and Nd isotope analysis 153

Table B1. Zircon *in-situ* compositions from SHRIMP-RG 155

Table C1. SHRIMP U/Pb age data for AWM-1 161

Table C2. SHRIMP U/Pb age data for AWM-2 162

Table D1. LA-ICP-MS in-situ zircon data 165

Table E1. Micro-ionprobe *in-situ* zircon oxygen isotope data 180

Table F1. Sphene SHRIMP trace element data 196

Table F2. Sphene SHRIMP trace element data for standard BLR 244

Table F3. SHRIMP titanium in sphene temperatures 256

Table I1. Calculated results for binary mixing of whole-rock Sr and Nd isotopic data 394

Table I2. Calculated results for binary mixing of in-situ zircon Hf and O isotopic data 395

INTRODUCTION

Today it is generally accepted that most modest to very large granitoid plutons are formed incrementally via multiple magmatic injections rather than as single large pulses (e.g., Wiebe and Collins, 1998; Miller and Patterson, 2004; Glazner et al., 2004; Annen et al., 2006; Matzel et al., 2006; Walker et al., 2007; Michel et al., 2008; Schaltegger et al., 2009). However, questions still remain about the sources of the various magmas that construct granitoid plutons and about the physical and chemical evolution of the plutons during their growth. Are they mainly derived from juvenile material recently extracted from the Earth's mantle, the product of melting of continental crust following large heat transfer from depth, or a combination of these two end members? To what extent are magma chamber processes captured and preserved within these granitoids?

Within large granitoid plutons, mixing or mingling of magma types is often evident where there is strong compositional contrast (mafic enclaves and localized hybrids in larger felsic bodies), but across larger, more superficially homogeneous or compositionally restricted plutonic masses the evidence for mixing or even multiple magmatic inputs can be cryptic (e.g., Coleman et al., 2004; Matzel et al., 2006; Walker et al., 2007). Homogenization and production of hybrid intermediate magmas in magma chambers probably follows magma injection events that periodically stir the magma chamber. Lower solidus temperatures of intermediate to felsic magma chambers allow

for repeated stirring and extended crystal-melt interaction with sufficient magma injection rates and volatile transfer following new magma input (Bachmann and Bergantz, 2008).

For hybrid intrusions that are otherwise superficially homogeneous, a complex record of thermal and compositional evolution in magma systems may manifest itself especially between zones of a single crystal (compositional and/or disequilibrium isotopic zoning; cf. Davidson et al., 2007). Single crystals are potentially also powerful recorders of magma chamber evolution, particularly in plutons where multiple injections are clearly evident (e.g., layered mafic-silicic plutons), and together with other geochemical and isotopic data give a richer understanding of the history of pluton construction and pluton-building processes that occur in the magma chambers that build plutons. Accessory minerals, such as zircon and sphene, may be particularly useful for assessing the melt source and subsequent thermal and physical processes in the magma chamber.

The accessory mineral zircon is a ubiquitous phase in intermediate to felsic igneous rocks and is also common in mafic igneous rocks and metamorphic rocks (Hawkesworth and Kemp, 2006). Much use has been made of zircon as a geochronometer through the U-Pb-Th systems in both igneous and metamorphic rocks. The chemically robust nature of zircon, its ubiquity in common crustal rocks, and recent advances in microanalytical capabilities have opened new pathways for using zircon to

study the geology of the Earth's crust and its evolution over time (Hanchar, 2003). Among the most recent developments is the ability to acquire information from whole single grain and sub-grain-scale studies of zircon (age, geochemistry, geothermometry, isotopic composition). Of these, two have proven particularly useful for tracking melt sources and open-system changes in magmas: using secondary ion mass spectrometry (SIMS) and laser ablation multi-collector, inductively coupled plasma mass spectrometry (LA-MC-ICPMS) to obtain O and Hf isotopic compositions, respectively (Hawkesworth and Kemp, 2006; Kemp et al., 2007; Zheng et al., 2007; Schmitt and Vazquez, 2009).

This thesis research used the archival record of zircon (and to a lesser extent sphene) to evaluate melt sources and examine the evolution of a shallow mafic-silicic layered pluton in southern Nevada in the Aztec Wash pluton. Specifically, the goal is to link zircon trace element geochemistry and whole rock isotope geochemistry with grain-scale (*"in-situ"*) hafnium (Hf) and oxygen (O) isotope data on zircon to better understand the internal dynamics of the Aztec Wash magma system during its construction. The following questions in particular are addressed: What were the primary source(s) that fed mafic and felsic magmas into the Aztec Wash Pluton? What can the accessory minerals tell us about the various mixing processes that may have produced the spectrum of rock compositions observed in the Aztec Wash pluton? Previous work has suggested that formation of intermediate magmas by mixing of mafic and felsic materials involved mechanical mixing of crystal-rich "slurries" and accumulated crystals with new magmas, mixing between compositionally distinct crystal-poor magmas,

mixing fractionated mafic magmas with extant felsic melts in the magma chamber, and disaggregation and assimilation of Precambrian host rocks into the magma chamber. This research addressed whether these processes can be distinguished and to what extent they are captured by zircon.

GEOLOGIC BACKGROUND

Geological Setting: The Aztec Wash Pluton

The Aztec Wash pluton is located within the northern Colorado River extensional corridor, southernmost Nevada, and is part of a group of mostly Early to Middle Miocene plutons in the Eldorado Mountains (Fig. 1; Miller and Miller, 2002). The northern Colorado River extensional corridor is a 70 to 100 km wide area that underwent a large amount of extension during the mid-Miocene and experienced pre-, syn-, and post-extensional volcanic episodes. Volcanism includes mafic to felsic lavas, volcanic breccias, and ash-flow tuffs and is largely coeval with the Miocene plutons of the region (Faulds et al., 1995; Feuerbach et al., 1998; Bachl et al., 2001; Faulds et al., 2002; Harper et al., 2004). Extensive E-W tilting of fault blocks and subsequent erosion has exposed many of the plutons from their roofs to fairly deep structural levels (5-15 km; Bachl et al. 2001; Miller and Miller, 2002; Walker et al., 2007). This makes the northern Colorado River extensional corridor an excellent location to gain insight into the full workings of diverse plutonic systems.

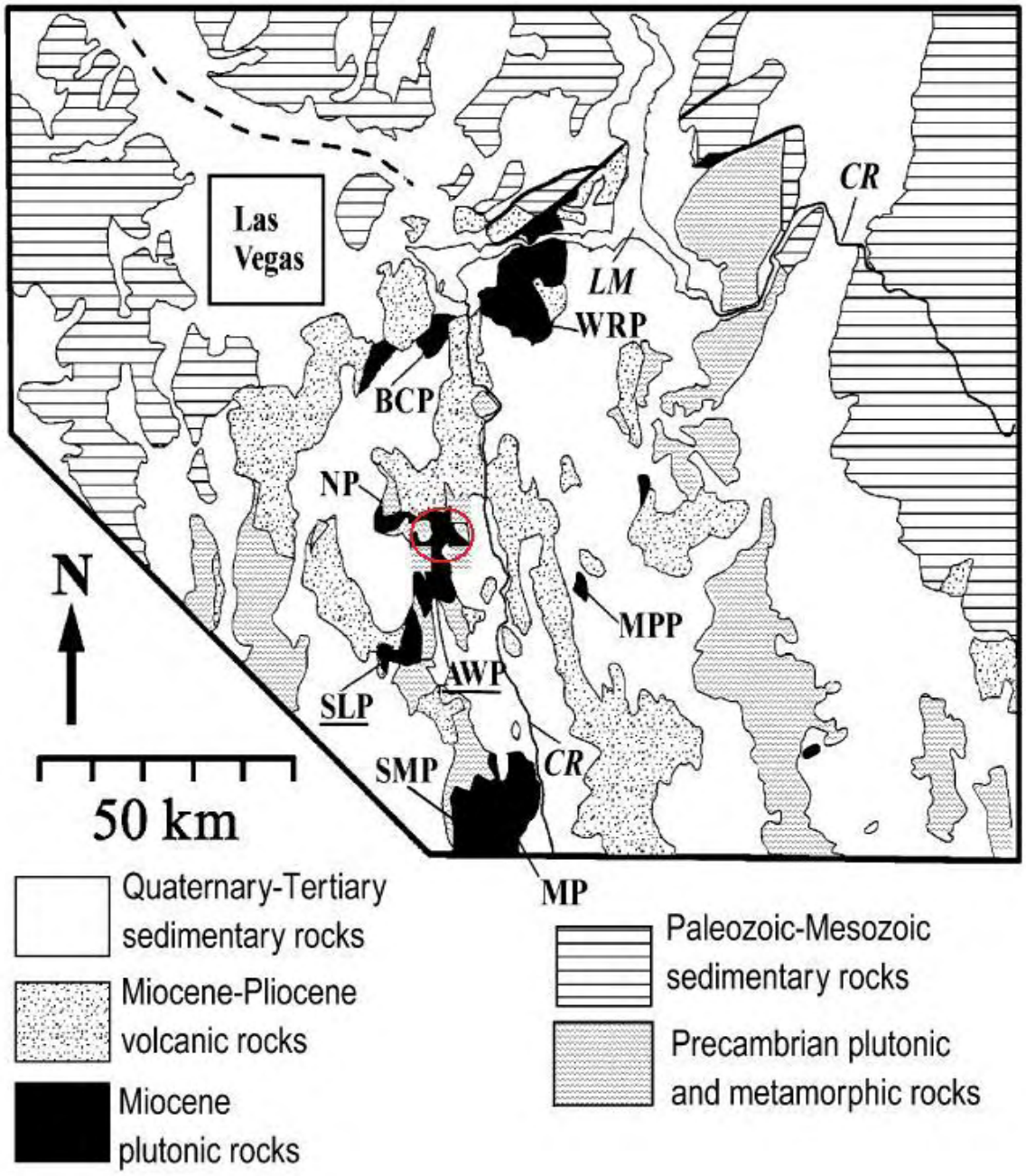

Figure 1. Location of the Aztec Wash pluton (AWP) within the northern Colorado River extension corridor. CR= Colorado River. Figure also highlights spacial relationships of Miocene plutons with volcanism during extension of the region at that time. Modified from Miller & Miller (2001).

Structural restoration of the mid-Miocene Aztec Wash pluton has shown that map view represents a partial cross-section of the pluton (Miller and Miller, 2002; Harper et al., 2004) with the roof exposed along the eastern contact and structurally deeper toward the west (Fig. 2; Harper et al., 2004). A minimum of ~5 km of structural depth is exposed, but the very bottom of the pluton is cut out by a younger fault. The Aztec Wash pluton can be subdivided into two chemically and physically distinct zones, the Granite Zone and the Heterogeneous Zone (Robinson & Miller, 1999; Harper et al. 2004). The Granite Zone is relatively homogenous granite with subtle differences in textures and felsic mineralogy that Harper et al. (2004) subdivided into seven units. The Heterogeneous Zone interfingers with the Granite Zone and is far more variable both texturally and chemically, such that breaking out individual facies is not possible. The Heterogeneous Zone contains evidence for mafic and felsic magma input with a wide compositional range (42-78 wt% SiO_2) and a variety of rock types including troctolite, olivine-pyroxene gabbro, hornblende gabbro, fine-grained gabbros (essentially trachybasaltic sheets and enclaves), diorites, monzonites, quartz monzonites, and granites with varying textures (Erickson, 2006). Vertically stacked and laterally continuous to semi-continuous mafic sheets that show evidence for extensive physical and chemical interaction with the granite unit are the most prominent features of the Heterogeneous Zone (Fig. 3) (Patrick and Miller, 1997; Miller and Miller, 2002; Bleick et al., 2005; Ericksen, 2006). In previous studies of such sequences, has been

found that mafic injections into a pluton will form by laterally spreading of mafic magma below less dense felsic melt but above a denser crystal-rich floor (Wiebe et al., 2002).

The generalized model for the growth of Aztec Wash pluton (first summarized in Harper et al., 2004) is similar in many respects to models for layered mafic-silicic intrusions developed by Wiebe (1996). The model is generalized from extensive field, petrographic, and geochemical work, some of which is discussed in more detail below as it pertains to the current study (Fig. 4).

Initial felsic magma emplacement occurred in the shallow crust where closed-system fractional crystallization then took place and felsic (feldspar-rich, quartz-poor) cumulates (quartz monzonites and monzonites) developed at the base of the active magma chamber. Mafic magmas were later injected into the magma chamber and spread laterally along the floor at the rheologic transition between relatively strong/rigid crystal mush (quartz monzonites) and the relatively crystal-poor magma (granites). Thermal perturbations from this mafic input allowed for extensive hybridization with silicic magma and resorption of earlier felsic crystal mush. Quenching and disaggregation of mafic sheets and chamber stirring resulting from thermally induced convection account for mafic enclaves that are widespread throughout the Heterogeneous Zone but commonly concentrated above and at the distal edges of mafic sheets. Episodic recharge produced a sequence of mafic lobes comprised mainly of the

previously mentioned stacked mafic sheet sequences that show varying degrees of hybridization across the pluton.

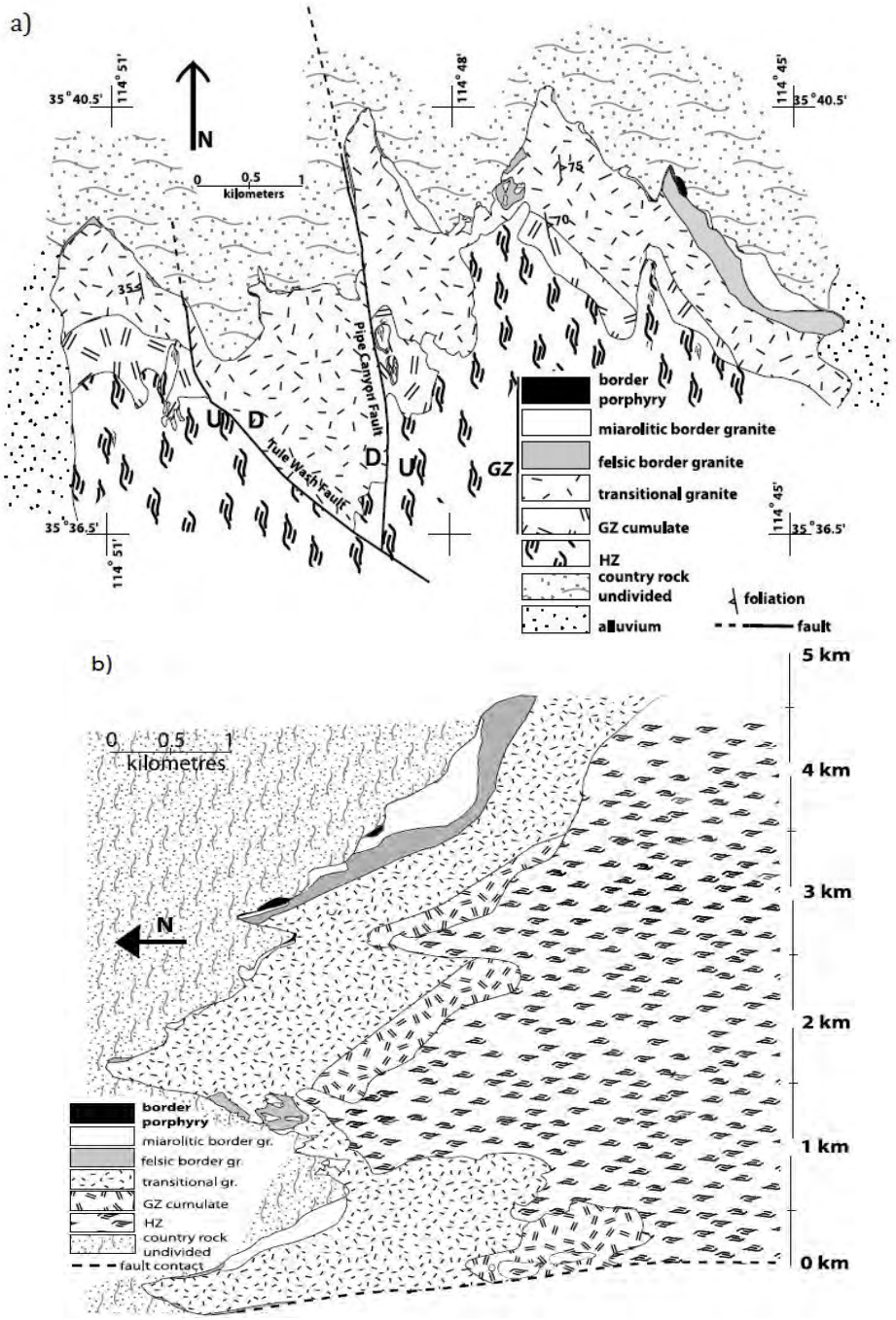

Figure 2. a) Schematic geological map of the Aztec Wash pluton showing the relationship of the Granite Zone with the Heterogeneous Zone discussed in text. Note also the transitional granite between them that is likely a mixing of the two zones. b) Reconstruction of the true orientation for the Aztec Wash pluton. Restoration assumes 62° ENE tilting from palaeohorizontal indicators. Taken from Harper et al., 2004. The structural roof of pluton is at the top of figure 2b.

a)

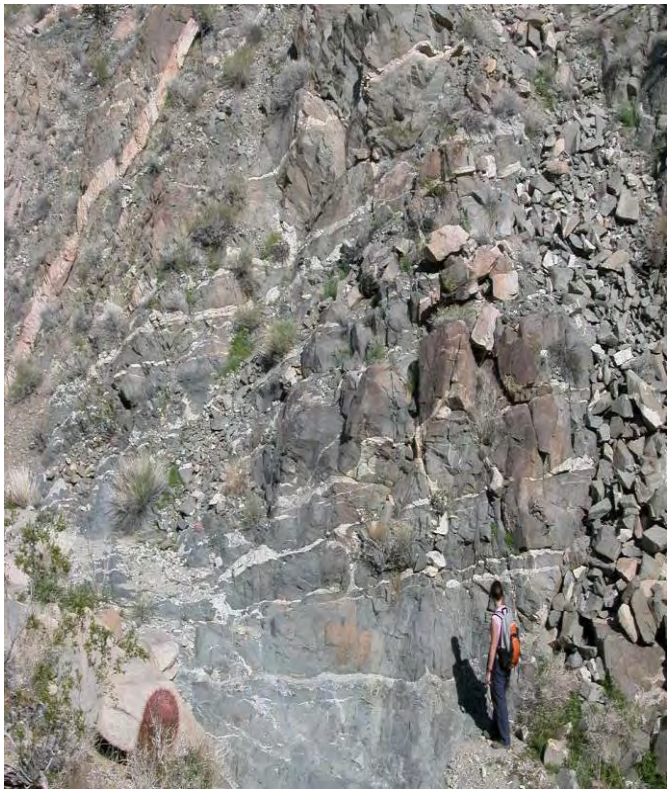

Figure 3. Field relationships of mafic and felsic melt in the Heterogeneous Zone of the Aztec Wash Pluton. a) Multiple vertical stacks of mafic sheets (0.5 – 1 m thick) injected into a felsic mush (Ericksen 2006). b) Interaction between mafic (left) and felsic (right) melts producing a hybridized unit (center). Such relationships are common across the Heterogeneous Zone. c) Felsic pipes within a mafic rock unit driven by mafic loading on felsic melt below. Compass clinometer (~6” in length) used for b) and c).

b)

c)

Figure 3 (continued)

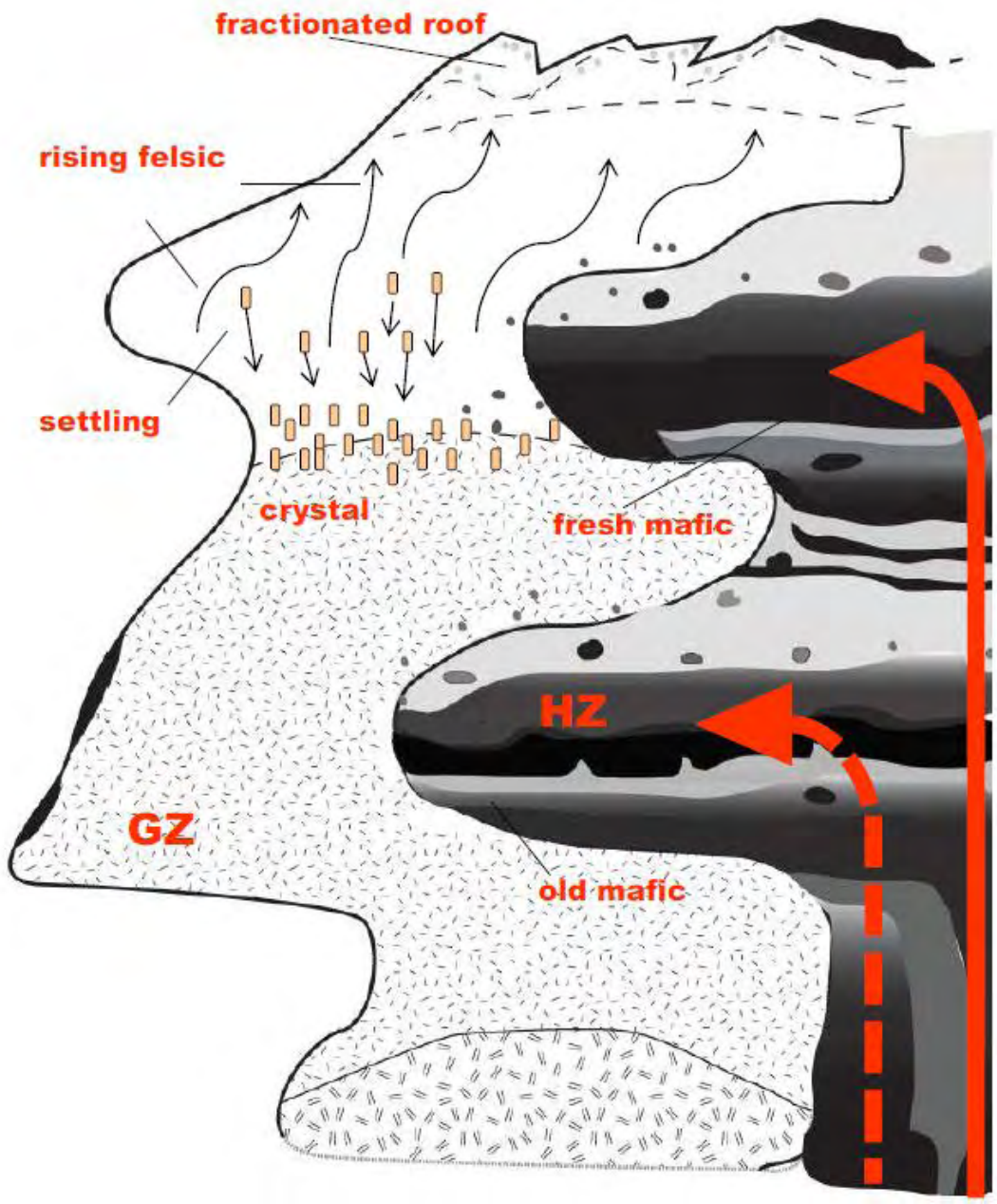

Figure 4. Schematic cartoon for construction of the Aztec Wash pluton. Mafic sheets are periodically injected into a fractionally crystallizing felsic chamber forming lobate structures younging upward. Mafic-felsic melt interaction and hybridization is localized around mafic lobe contacts. HZ = Heterogeneous Zone, GZ = Granite Zone. Taken from Bromley (2008).

Previous Geochemical Studies

Work by Falkner et al (1995), Ericksen et al (2004), and Ericksen (2006) recognized that mafic magmas of the Aztec Wash pluton were primarily derived from an enriched lithospheric mantle source. The isotopic data also support field observations that extensive hybridization took place between magmatic end-members at the level of the pluton. Notably, scattered but nevertheless strong correlations between Sr and Nd isotopic composition and bulk composition (e.g., bulk SiO_2) show that the Aztec Wash magma chamber behaved as an open system during its construction. The isotopic scatter, particularly among the Granite Zone rocks, demonstrates that simple two-component mixing could not apply to the Aztec Wash (ε_{Nd} and $^{87}Sr/^{86}Sr$ values range from –12.9 to -8.4 and 0.7089 to 0.7116 respectively in the Granite Zone; Miller and Miller, 2002; Ericksen, 2006). A series of flow charts proposed by Ericksen (2006) highlighted this conclusion (Fig. 5). The figure shows that from a given input of parent mafic magma mixing with residual fractionates or parent felsic magma (Field 1), it is possible to derive hybrid products which, in turn, can experience a variety of mixing pathways involving parent magma, fractionates, or other hybridized melts (fields 2 and 3). The array of ε_{Nd} and $^{87}Sr/^{86}Sr$ compositions from these fields could therefore account for observed data (Ericksen, 2006).

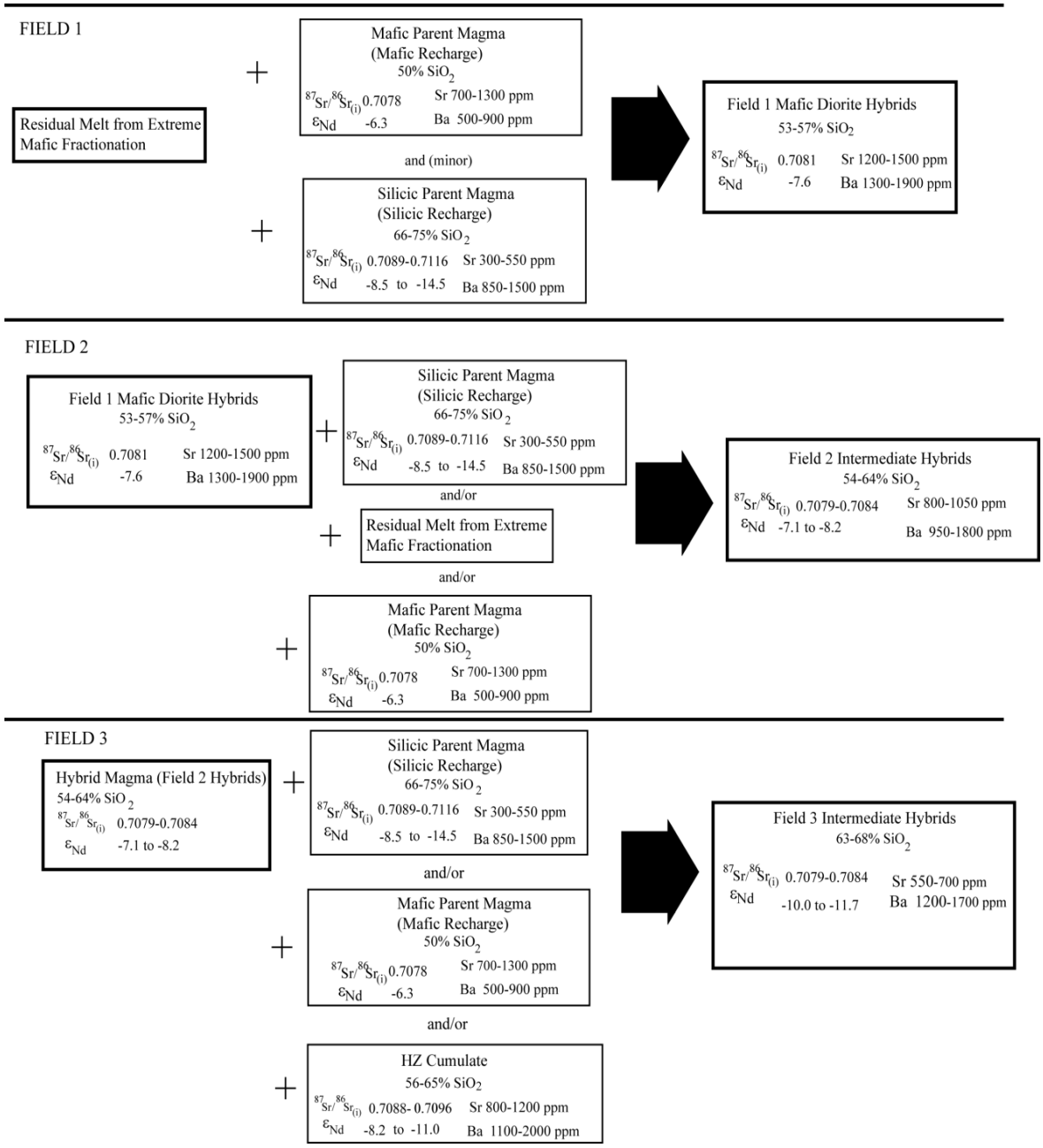

Figure 5. Flowcharts highlighting the open-system nature of the Aztec Wash pluton Ericksen (2006). Compositionally variable hybrids are formed through potential mixing scenarios between hybrids and parent magmas.

Most recently, Bromley (2008) undertook an *in-situ* trace element study of zircons within various lithologies in the Heterogeneous Zone and attempted to correlate these changes with the Ti-in-zircon (T_{TiZ}) thermometer as proposed by Watson et al. (2006). Bromley (2008) found generally that zircon REE concentrations and certain REE ratios (e.g., Gd/Yb) are positively correlated with T_{TiZ}, whereas Hf concentrations are negatively correlated with T_{TiZ}. Decreasing core-rim T_{TiZ} accompanied by increasing core-rim Hf concentration reflects fractional crystallization of zircon and growth of zircon from more Hf-rich melt (e.g., Claiborne et al., 2010). In the Aztec Wash pluton, Bromley (2008) observed simple core-to-rim increases in Hf and decreases T_{TiZ} but many zircons show a more complicated history of increasing Hf accompanying decreasing T_{TiZ} (i.e., cooling and zircon growth from more fractionated melts) followed by increasing T_{TiZ} and decreasing Hf (i.e., a temperature and compositional reversal), which she interpreted as a heating event accompanying new magma input. These were particularly evident in samples where interaction between mafic and more felsic materials was observed in field and petrographic data. Overall T_{TiZ} in each sample population reflects the increased interaction with mafic magma input as is also observed in the field.

Hafnium and Oxygen Isotopes in Zircon

^{176}Lu decays through β emission to ^{176}Hf with a half life of 35.4 ± 1.1 Byr (Dickin, 1995). The concentration of the stable isotope ^{177}Hf can be used to produce a decay equation:

$$\frac{^{176}Hf}{^{177}Hf} = \left(\frac{^{176}Hf}{^{177}Hf}\right)I + \frac{^{176}Lu}{^{177}Hf}(e^{\lambda t} - 1)$$

The Lu-Hf system has many similarities with the Sm-Nd isotope system. In each, the daughter atoms (Hf and Nd) are more incompatible than their respective parents (Lu and Sm). Therefore, during partial melting of mantle material Hf and Nd will preferentially enter the melt producing an enrichment of Hf and Nd in crustal material and a depleted mantle. This leads to high ^{176}Lu/^{177}Hf and high ^{143}Sm/^{144}Nd (corresponding to high ^{176}Hf/^{177}Hf, ^{143}Nd/^{144}Nd respectively) in the mantle (Nowell et al., 1998). This relationship is useful in bulk rock isotopic analysis owing to the changes in the isotopic compositions of different reservoirs that arise via fractionation of parent and daughter over Earth history.

One of the rapidly growing developments in Lu/Hf geochemistry is the use of zircon to capture ^{176}Hf/^{177}Hf ratios of melt sources (Griffin et al., 2000; Griffin et al., 2002; Hawkesworth and Kemp, 2006; Kemp et al., 2007; Zheng et al., 2007). Zircon potentially provides a much more complete record of its history than bulk rock analysis, although the current analytical protocols and precisions limit this somewhat to larger

grains with large isotopic contrasts. Hf is much more compatible in the zircon crystal structure than Lu, and at the crystal scale the concentration of Hf in zircon reaches beyond trace amounts (~1 wt.%), leading to very low Lu/Hf ratios (Hawkesworth & Kemp, 2006). Due to the low time-integrated Lu/Hf in zircon, Hf isotope data in zircon grains are able to provide initial $^{176}Hf/^{177}Hf$ ratios of melt sources (particularly for relatively young igneous rocks as in the present study), thereby distinguishing magmas that were derived from sources having low Lu/Hf ratios (e.g., ancient crust) from those having high Lu/Hf (e.g., young, asthenospheric mantle). As with the Sm-Nd system, isotope ratios are typically expressed as part per 10^4 deviations relative to the Chondritic Uniform Reservoir (CHUR) using the epsilon notation. Calculation of εHf is thus the same as that for ε_{Nd} (Dickin, 1995):

$$\varepsilon_{Hf} = \left[\frac{\left(\frac{^{176}Hf}{^{177}Hf}\right) sample}{\left(\frac{^{176}Hf}{^{177}Hf}\right) CHUR} - 1 \right] 10^4$$

Relative to an initial chondritic Earth (εHf = 0), juvenile mantle material will have a large positive εHf value (high time-integrated Lu/Hf) whereas ancient continental crust material will generally have a large negative εHf (low time-integrated Lu/Hf). Ancient enriched lithospheric mantle will typically have negative but higher εHf than juvenile asthenospheric mantle (Beard and Johnson, 1997), owing to the enrichment of this

mantle in Hf during earlier melting events (i.e., such that it has also has a much lower time-integrated Lu/Hf in comparison to modern asthenospheric mantle).

In contrast to the Lu/Hf isotopic system, in which variations in isotopic reservoirs are produced by fractionation of parent and daughter isotopes and subsequent radioactive decay, oxygen isotopic variation is a function of how ^{18}O and ^{16}O partition in water during low-temperature geochemical processes that fractionate light, stable isotopes (e.g., condensation, evaporation) and also how they are fractionated into different minerals during crystallization of melts. Variations in the ratio of ^{18}O to ^{16}O are expressed as $\delta^{18}O$ through the equation:

$$\delta^{18}O = (R_{SA}/R_{ST} - 1) \times 1000$$

where R_{SA}/R_{ST} is the ratio $^{18}O/\ ^{16}O$ in the sample and standard respectively. The global standard is the Vienna Mean Standard Ocean Water (VSMOW), which has a ratio of 0.020052 (Bindeman, 2008). Geologic materials show a wide range of $\delta^{18}O$ values ranging from -55‰ (meteoric water) to +40‰ (siliceous oozes). Igneous rocks have a somewhat narrower range. Mafic and ultramafic melts typically have values between 5.3‰ and 5.9‰. Increasing the silica content through closed-system fractionation leads to higher $\delta^{18}O$ because stronger Si-O bonds favor the heavier ^{18}O isotope. Typical rhyolites or metaluminous granites will therefore higher $\delta^{18}O$ value (typically 6.0-6.5‰). Figure 6 (Bindeman, 2008) gives a summary of ranges in $\delta^{18}O$ for different Earth materials.

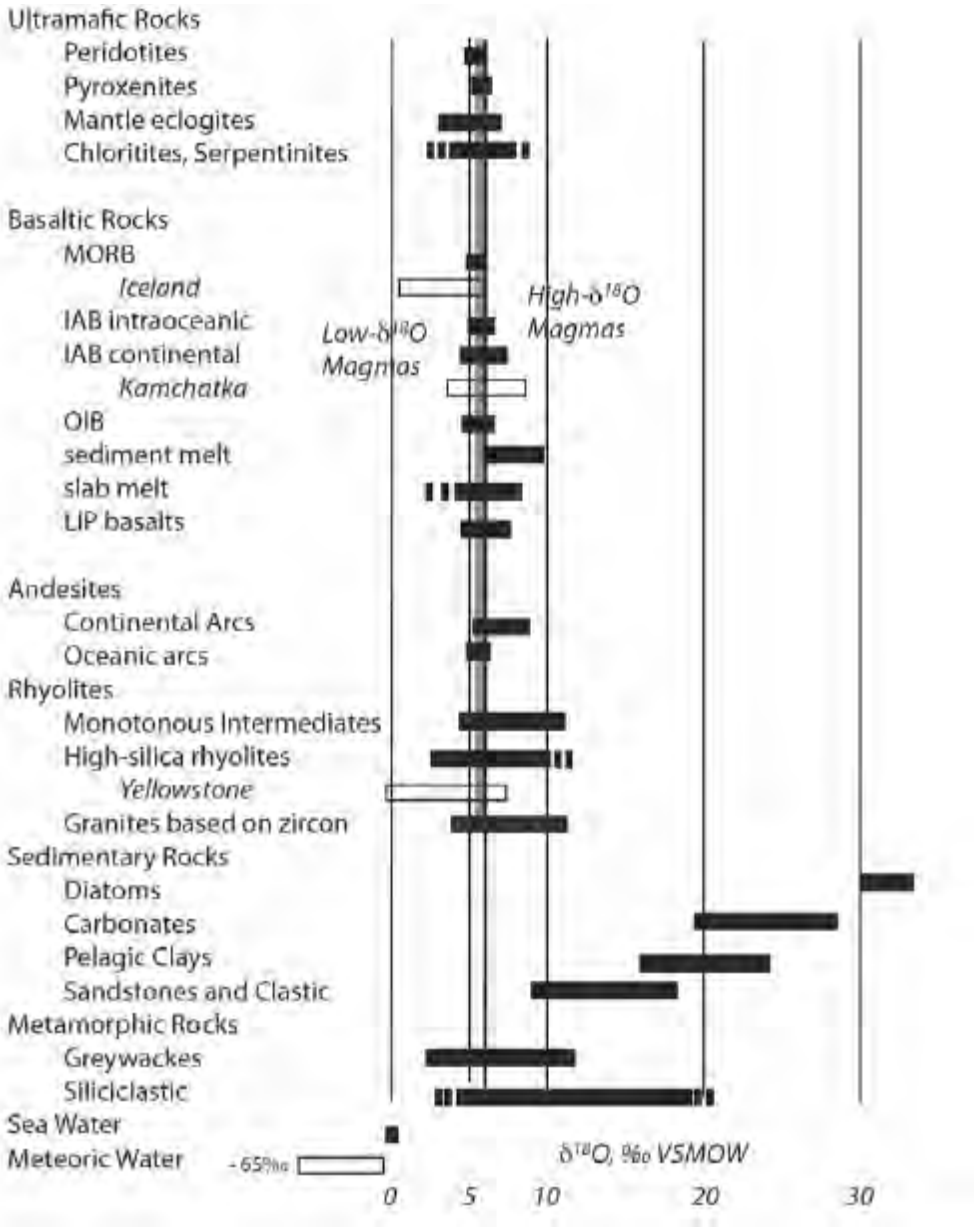

Figure 6. Variation of $\boldsymbol{\delta}^{18}$O in different rocks on Earth including values for igneous zircons relative to VSMOW. Oceanic sediments typically have elevated $\boldsymbol{\delta}^{18}$O values due to differentiation of oxygen isotopes after natural distillation processes leading to very low $\boldsymbol{\delta}^{18}$O in meteoric waters. Contamination of rocks by meteoric water can drastically affect the range of $\boldsymbol{\delta}^{18}$O values. Typical mantle zircon values are within 5.3 ± 0.3‰. Taken from Bindeman (2008)

Because bulk rock $\delta^{18}O$ can be affected by processes such as hydrothermal alteration and weathering, it is necessary to study individual minerals that are resistant to these processes (e.g., quartz, zircon). Zircon is relatively unaltered by low temperature (sub-solidus) processes and can therefore retain the original magmatic O isotopic ratios. Variations in $\delta^{18}O$ can, like Hf, be used to infer melt sources and various magmatic processes that cause the variation (Kemp et al., 2007). Zircons that are in equilibrium with mantle magmas typically have a small range of $\delta^{18}O$ values on the order of 5.3 ± 0.3‰ (Valley et al., 2005; see also Figure 6). Metasedimentary rocks and strongly peraluminous ('S-type') granites typically have high- $\delta^{18}O$ values due to the incorporation of or derivation from rocks that have experienced a weathering cycle in Earth surface environments (e.g., pelites). Alternatively, should an igneous or metamorphic rock become altered over time through interaction of meteoric or hydrothermal waters any subsequently grown zircon crystals will inherit a relatively low-$\delta^{18}O$ value (Bindeman, 2008).

By combining Hf and O isotope data, the *in-situ* analysis of zircon is especially powerful. For example, magmas with relatively high- $\delta^{18}O$ signature and low negative ε_{Hf} likely reflects derivation from or involvement of ancient metasedimentary material, whereas relatively low- $\delta^{18}O$ signatures and high positive ε_{Hf} imply a deeper, asthenospheric mantle magma source (Kemp et al., 2007; Bindeman, 2008). Zonal variation (e.g., core-rim) in Hf and O can further expand our understanding of magma interaction during pluton construction (Bolhar et al., 2008), because variation requires

distinct inputs of magmas and transfer of zircons between separate, isotopically distinct pulses. Importantly, both variation between different zircons, and within individual zircons requires mixing of different pulses, even if whole rock isotopic variation is relatively minimal.

Zirconium in Sphene Thermometry

Sphene is receiving increasing attention as a potentially powerful tracker of open-system magmatic processes (e.g., McCleod et al., 2011). Recently, Hayden et al. (2008) have proposed that sphene can be used as a magmatic geothermometer, with its Zr content being temperature sensitive. Sphene commonly occurs alongside zircon as an accessory phase. This allows for Zr^{4+} – Ti^{4+} ionic substitution between crystal lattices governed by the equilibrium:

$$CaTiSiO(sphene) + ZrSiO_4(zircon) \leftrightarrow CaZrSiO_5(sphene) + TiO_2(rutile) + SiO_2(quartz)$$

If the concentration of Zr in sphene grains is known and an assumed activity, *a*, is assigned to rutile (*i.e.*, TiO_2), quartz and sphene, then direct calculation for temperature of crystallization at a given pressure (P) can be generated from the equation (Hayden et al., 2008):

$$T(^{\circ}C) = \frac{[7708 + 960P]}{[10.52 - \log(aTiO_2) - \log(aSiO_2) - \log(ppm\ Zr, sphene)]} - 273$$

In a similar method devised for Hf and O isotopes in zircon, a core-to-rim or sector analysis of sphene can be applied to track potential changes in the temperature at which a specific grain grew. Hayden et al (2008) also found that the Zr concentration in sphene is pressure-sensitive. In the case of the Aztec Wash pluton, the depth of intrusion is well established from geologic map relations (e.g., Miller and Miller, 2002), and the pressure correction is likely very small. Less well known are the appropriate activities for TiO_2 and SiO_2.

SAMPLES AND METHODS

Sample Descriptions

Because one of the main goals of this project was to link (if possible) results from Hf and O isotopes in zircon with their geochemistry, the samples consist of previously analyzed zircons from Bromley (2008) along with new samples obtained in the field. Table 1 gives a list of all samples used by Bromley (2008) as well as unit descriptions and pertinent T_{TiZ}, Hf concentration ranges, and calculated bulk zircon saturation temperatures (Watson and Harrison, 1983).

Bromley (2008) divided the samples into four distinct groups: Granites, "Grey Hybrids," "Mechanically Contaminated" and "Dark Pods" (Table 1). The Granites were chosen from a highly fractionated leucogranite, a felsic dike, a coarse-grained granite typical of the Granite Zone and an uncontaminated cumulate within the Heterogeneous Zone. These granites were chosen due to no obvious evidence for interaction with mafic magma. The "Mechanically Contaminated" samples were taken from lithologies that demonstrated physical incorporation of mafic magma into felsic (*i.e.*, mafic enclaves and mafic mineral "clots"). Thermal exchange between mafic and felsic magmas were important in the formation of these samples with limited chemical diffusion. The "Grey Hybrids" were selected from lithologies that experienced thorough hybridization between mafic and felsic magmas within the Heterogeneous Zone. Diffusive mixing was a major process in forming these fine-grained, equigranular

samples. Finally, the "Dark Pods," from the Heterogeneous Zone, were sampled from a quenched margin, a coarse-grained interior, and wet fractionated pocket of a dark rock unit. These samples had a stronger mafic affinity than the Grey Hybrids.

Two additional samples grouped as Mafic Sheets (AWM-1 and AWM-2 in Table 1) were collected during a field excursion to the Heterogeneous Zone of the Aztec Wash Pluton because Bromley's previous study focused more on the felsic and intermediate lithologies in this zone. The first, AWM-1, was taken from a fine to medium-grained mafic diorite sheet that shows quenching and forms enclaves within and mingles locally with more felsic host. The second (AWM-2) was a re-sampling of a coarse-grained gabbro with visible euhedral zircon that Bromley (2008) sampled and obtained trace element data for, but for which reliable U-Pb age information were never obtained.

Table 1. SAMPLE DESCRIPTION AND RELEVANT DATA FOR THIS STUDY

Group/Sample Name	Description	Bulk zircon saturation T / °C	T_{TiZ} / °C	Ranges for Hf concentration / ppm
Granites				
NAWZ-13	GZ dike: late felsic dike - microgranite	764	740 - 1031	~ 9000 – 13000
NAWZ-26	GZ miarolitic granite: highly fractionated GZ leucogranite	766	702 - 869	~ 8000 – 12700
NAWZ-50	True GZ granite	793	720 - 864	~ 8500 – 11400
AWAG-6	HZ felsic cumulate	810	717 - 891	~ 7600 – 10000
Mechanically Contaminated				
NAWZ-16	HZ cumulate: highly resorbed feldspar, abundant mafic clots	888	751 - 923	~ 7800 – 12000
AWAG-2	HZ: Crystal-rich felsic host for extensive basaltic enclaves	845	721 - 873	~ 7700 – 11700
AWAG-3	HZ fine-grained felsic unit in more hybridized material. Contains resorbed feldspars	819	707 - 876	~ 7800 – 12600
AWAG-7	HZ highly contaminated felsic sheet. Resorbed feldspars and abundant mafic enclaves	834	703 - 854	~ 9700 – 12100
Grey Hybrids				
AWAG-4	HZ fine-grained equigranular “grey” sheet	795	745 - 858	~ 7700 – 11500
AWAG-5	HZ fine-grained equigranular “grey” sheet	852	720 - 907	~ 7600 – 11000
Dark Pods				
AWAG-1A	HZ: Quenched margin of dark grey pod. Fine-grained equigranular	796	740 - 852	~ 6700 – 10800
AWAG-1B	HZ: Dark pod interior. Fine-grained equigranular	794	714 - 912	~ 6800 – 8000
AWAG-1C	HZ: Dark pod interior. Increasing evolved and hydrous material. Abundant biotite and hornblende	808	686 - 872	~ 5100 – 8400
Mafic Sheets				
AWM-1	HZ: Quenched medium-grained diorite sheet	730	767 - 877	~ 6400 - 9000
AWM-2 (AWSC-2)	HZ: Coarse-grained gabbro cumulate with visible euhedral zircon grains	699	732 - 852	~ 7200 - 12600

Grain Separation and Imaging

Grain separation was carried out at San Jose State University. Approximately 2 kg samples were jaw crushed and a split was reserved for whole-rock geochemistry and isotopic analysis. The remainder was sent through a hardened steel disk mill to reduce the grain sizes to <1 mm. To ensure minimal contamination the equipment was pre-contaminated with some of each sample that was then discarded and then thoroughly cleaned using a steel brush, compressed air and ethanol. The heavier minerals, including zircon and sphene, were separated out using the wet gravity-based technique of a Wilfley shaking table, magnetic separation, and heavy liquids.

The final mineral separate from each sample was taken to Stanford University for grain mount preparation and imaging. Grains were picked out using a binocular microscope and mounted in clean epoxy resin. Around 90 zircon and 35 sphene grains were taken from AWM-1, and 35 zircon and 30 sphene from AWM-2. New sphene mounts were also prepared for the other samples of the Aztec Wash pluton used in this study with 25 – 30 sphene grains in each set. Sphene separates were not available for samples NAWZ-13, 16, 26, and 50, and AWAG-1C. The mounts were then gold coated, polished, and imaged using scanning electron and transmitted light microscopy. The zircon grains from AWM-1 and 2 were imaged using cathodoluminescence (CL) on the SEM to distinguish zones of growth, and to help identify crystal heterogeneities and inclusions. Backscatter electron imaging (BSE) was used for all sphene grain mounts.

The jaw crushed sample splits of AWM-1 and AWM-2 were sent to Washington State University for major and trace element analysis and these are included in Appendix B. Information pertaining to these analyses and reproducibility can be found at http://www.sees.wsu.edu/Geolab/note.html.

Zircon Age and Zircon and Sphene Trace Element Analysis

Analysis of zircon grains from two samples was carried out using the Sensitive High-Resolution Ion Microprobe-Reverse Geometry (SHRIMP-RG) at Stanford. Age data on zircon were collected for samples AWM-1 and AWM-2, and trace element data were collected for AWM-1 as well, to complement the existing data set of trace elements from Bromley (2008). Locations for spots were selected using the CL images taken for each sample. Points of interest included any distinct zonation and subtle contrasts in brightness between and within grains. Crystal defects and likely inclusions were carefully avoided during this process.

For each U-Pb age analysis of zircon, a 10 nA $^{16}O^{2-}$ primary ion beam was rastered across the grain for 120 seconds to remove the gold coat and surface contamination. The beam was then used to excavate an approximately 1 µm deep circular pit, approximately 25 µm to 35 µm in diameter, thereby generating positive secondary ions. For each analysis, a minimum of six scans of peaks at ^{90}Zr, ^{16}O, ^{204}Pb, ^{206}Pb, ^{207}Pb, ^{238}U, $^{232}Th^{16}O$ and $^{238}U^{16}O$ were collected. Count times ranged from 2 to 14 s, with maximum

count times for ^{206}Pb and ^{207}Pb. Isotopic compositions for all zircons analyzed are referenced to the R33 zircon standard (419 Ma) and U and Th concentration measurements were determined relative to zircon standard SL13 (238 ppm U).

For zircon and sphene trace element analyses, an O^{2-} primary beam operating at 1.5-2.5 nA current was used, achieving mass resolution M/ΔM = approximately 11000 at 10% peak height. Masses ranging from $^{19}F^{+}$ through $^{238}U^{16}O^{+}$, and including the REE and key transition metals were measured. Data was collected for each mass sequentially after an initial 30 second raster period. The analysis used auto-centering with peak centering on guide peaks with known mass offsets adjacent to low-abundance species or species close to large mass peaks. Beam diameter was 15-20 µm, which allowed multiple analyses within individual zoned crystals, although typical oscillatory zoning in the zircons was too fine-scale to analyze individual zones. Spot locations on the unknowns were selected to sample the diversity of observed CL (zircon) and BSE zonation (sphene). Measurements on unknowns were interspersed with periodic measurements on a well-characterized zircon standard (MAD-green) or titanite standard (BLR-1; Aleinikoff et al. 2007). Data reduction was performed offline using count rates of each element of interest ratioed to $^{30}Si^{+}$ to account for differences in primary and secondary beam intensities. The derived ratios for the unknowns were compared to an average of those for MAD-green or BLR-1 to determine concentrations following the procedure of Mazdab (2009). The full set of trace elements analyzed included: Be, B, F, Al, Si, P, Ca, Sc, Ti, V, Fe, Y, Nb, Zr, Hf, Pb, Th, U, and the rare earth elements. Spot to

spot precisions (as measured on the standards) varied according to ionization efficiency and concentration. For zircon, precisions were ± 3% for Hf, ± 5% for the HREE, ± 10-15% for P, Sc, Y and the MREE, and up to ± 40% for La (1 SD). For sphene, precisions ranged from ± 4-7% for Ti, Y, Zr, Cr, Fe, and Al, ± 4-9% for the REEs, and ± 10-15% for H, Ta, U, Th, and Pb (1 SD). All data reported were screened for inclusions, which can affect REE patterns and calculated Ti-in-zircon and Zr-in-sphene temperatures. A total of 27 spots were analyzed for trace element data on zircons from AWM-2 and 42 spots for ages from AWM-1 and AWM-2.

Oxygen in Zircon

Determination of $\delta^{18}O$ zircon values was made using the UCLA CAMECA ims 1270 high-resolution ion microprobe in Faraday multicollection mode. Analysis spots focused on the same areas on grains previously analyzed for trace element and U-Th-Pb ages where possible, and were complemented by additional analysis spots on grains that had not been previously analyzed. However, all grains had to be repolished to remove earlier ion probe burn spots before any data collection took place because of possible contamination with implanted O from the earlier SHRIMP-RG analysis. Cracks, defects and probable inclusions were avoided following careful inspection of CL images but also live monitor images were utilized as polishing removed grain layers, altering their shape slightly.

The analysis followed the methods described in Trail et al (2007). A ~5nA Cs^+ beam was focused to a ~20 µm spot and 10 keV secondary ions were admitted to the mass spectrometer after passing through a 30 eV energy slit. Mass spectrometer entrance and exit slits were tuned to a mass resolving power of ~2400 to resolve hydride interferences such as $H_2{}^{16}O$. Average count rates for $^{16}O^-$ and $^{18}O^-$ were ~2 x 10^9 and ~4 x 10^6 cps, respectively under these conditions. Total integration time per analysis was ~5 min, with 1 minute presputtering. A total of 241 analyses were made. Zircon standard R33 was used with an accepted $\delta^{18}O$ value of 5.55 ‰ (Valley, 2003). External errors based on analysis of R33 were 0.2 ‰ for the first and second days of analysis and 0.3 – 0.5 ‰ for the third day (1 SD) (Fig. 7).

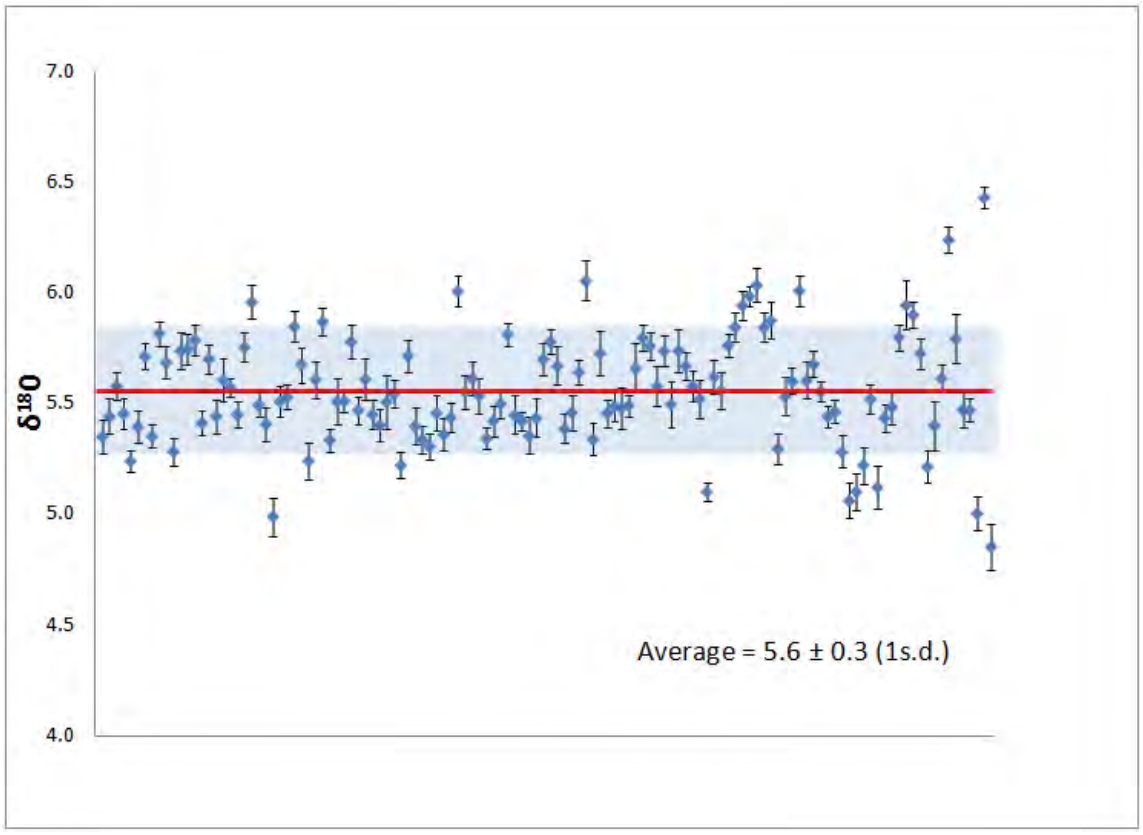

Figure 7. Measured results and external errors for zircon standard R33. Line with field indicates average value of measurements with error recorded to 1SD.

Hafnium in Zircon

After O analysis, measurements of Hf isotopic compositions were performed on the zircon mounts from all samples using a 193 nm Lambda Physik excimer laser ablation system with GeoLas optics operating at 26 kV coupled to a Thermo-Finnigan Neptune multi-collector, inductively coupled, plasma mass-spectrometer at the Vrije Universiteit (VU), Amsterdam.

For all analyses a spot size of 49 μm was selected using an energy beam of 7 J/cm^2 with a pulse frequency of 7 Hz in a He atmosphere. A mixed He and Ar carrier gas was used to transport ablated material to the plasma source of the mass spectrometer.

A total of 189 Hf isotope ratio measurements were made over three lab days. Sites for ablation were selected using CL and live monitor images. As before, spots were chosen for close proximity to those previously made for trace element, age and O isotope analyses. Equivalent zones were chosen where an absolute match could not be made. However, because of the large ablation spot size, many analysis spots extended across multiple growth zones, or even entire crystals thus potentially blending variable Hf isotopic compositions from different zones (even more so than in the case of the ion probe analyses). As a result, these points represent average Hf isotopic compositions over the fairly large volume of the ablation pit (Fig. 8a and 8b) or even over most of the crystal, about half or slightly more of which had been removed by earlier analyses. To a first approximation, isotopic zoning can be checked by examining the sequential

$^{176}Hf/^{177}Hf$ ratios for each ablation (i.e., a depth profile from the exposed center down through the crystal face that remains buried in the epoxy). Ablation checks were systematically made both during lab time and follow-up analysis (Fig. 8c), to look for any obvious isotopic zoning.

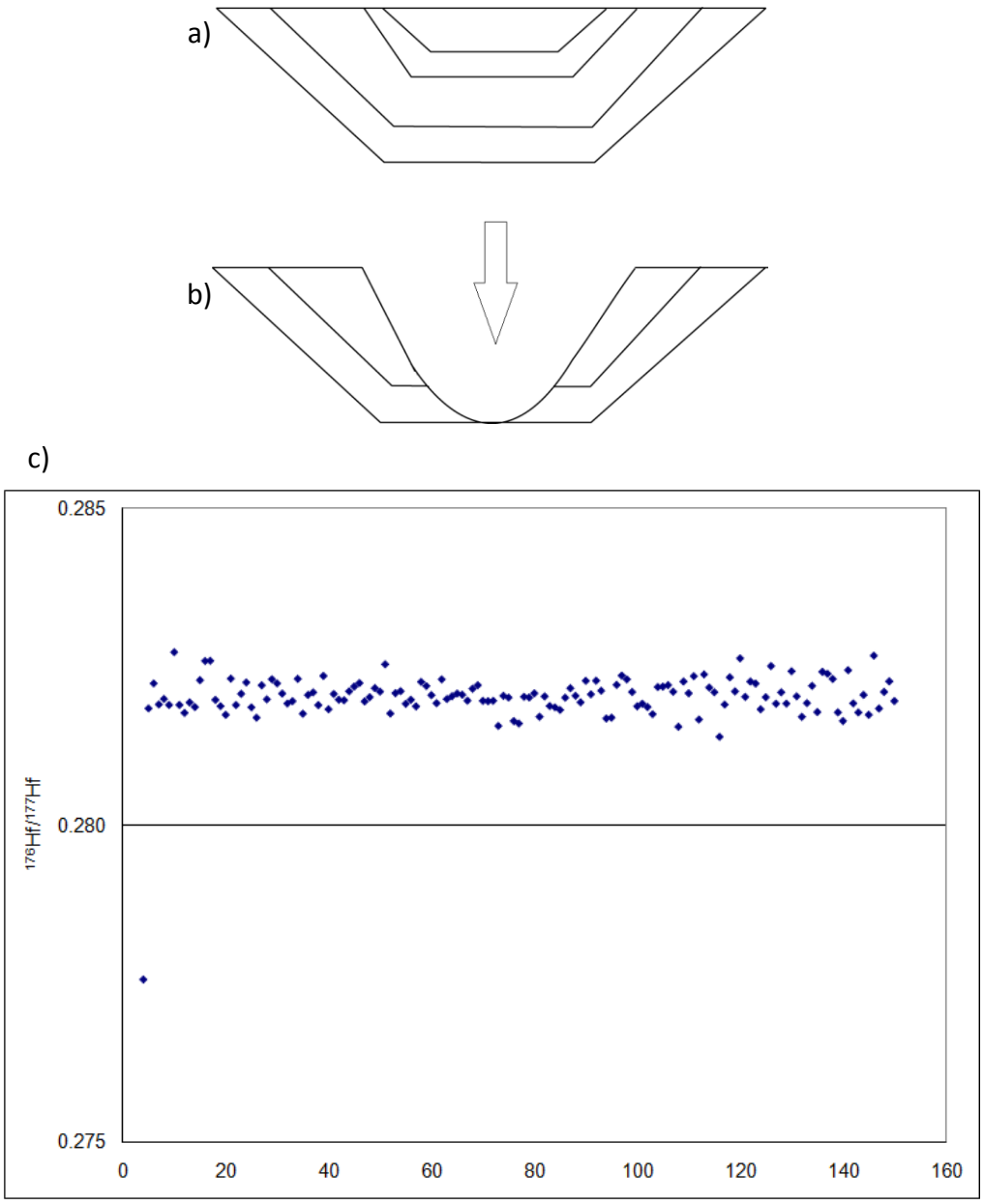

Figure 8. Monitoring of laser ablation runs during Hf isotope analysis of zircon. Multiple zones of a zircon grain (a) can be sampled during a single ablation run (b). Systematic checks of these runs are made to monitor any notable change in isotopic composition either through zonation or sampling of inclusions (c). Constrained field of data points indicates relatively homogenous grain.

Beam intensity was monitored on ^{180}Hf with signals on the Neptune ranging from ~1.5 to 4 V, and with each ablation analysis typically lasting between ~40 and 150 seconds (1 s = 1 cycle) depending on grain depth. Table 2 gives the Faraday collector configuration used during the measurements of Hf isotopes. Prior to each laser ablation analysis there was a 60 second background measurement monitoring online blank corrections.

Table 2. LA MC-ICP-MS HF COLLECTOR CONFIGURATION

Cup	L1	L2	L3	L4	Centre	H1	H2	H3	H4
Mass	^{171}Yb	^{173}Yb	^{175}Lu	^{176}Hf (^{176}Lu) (^{176}Yb)	^{177}Hf	^{178}Hf	^{179}Hf	^{180}Hf (^{180}W)	^{182}W

Isobaric interferences on ^{176}Hf by ^{176}Yb and ^{176}Lu can be significant for zircons because the laser ablation technique does not permit chemical separation of Hf in advance of the analysis (Woodhead et al., 2004). This poses significant challenges, and as yet there is no universally agreed upon method within the laser ablation community to correct for these interferences. Using the collector configuration shown in Table 2 allows for the intensities of interference-free Yb isotopes ^{171}Yb and ^{173}Yb to be measured, which can then be used for interference correction of ^{176}Yb on ^{176}Hf given a canonical value of $^{176}Yb/^{173}Yb = 0.79631$ (Vervoort et al., 2004). This was the approach taken here for correcting for Yb interference but it should be noted that the beam intensities for the Yb isotopes may be fairly small (20-30 mV), and therefore also subject

to appreciable measurement uncertainty. This ratio must also be corrected for instrumental mass fractionation, which can be very large in plasma mass spectrometry and is assumed to follow an exponential law (Russell et al., 1978). The $^{176}Yb/^{173}Yb$ ratio for each measurement was thus artificially mass-fractionated by measuring $^{171}Yb/^{173}Yb$ for each spot and using this ratio to calculate a Yb mass fractionation factor (βYb) relative to an accepted $^{171}Yb/^{173}Yb$ value of 0.8848. The mass-fractionation corrected $^{176}Yb/^{173}Yb$ was then used to correct for isobaric ^{176}Yb interference on ^{176}Hf. A similar correction was made for ^{176}Lu interference using $^{176}Lu/^{175}Lu = 0.02655$ (Vervoort et al., 2004). This ratio was artificially mass fractionated using βHf calculated from the measured $^{179}Hf/^{177}Hf$ relative to an accepted value of 0.7325, and then used to subtract out ^{176}Lu interference on ^{176}Hf. Time-integrated data reduction was performed offline with an Excel spreadsheet.

Hf isotopic compositions were monitored for any systematic bias using the international standard GJ-1 (Elhlou et al., 2006) with $^{176}Hf/^{177}Hf = 0.282000 \pm 0.000005$ (2SD, weighted mean, multiple solution analyses on different grain fragments; Morel et al., 2008). Other reported $^{176}Hf/^{177}Hf$ for GJ-1 include: 0.281998 ± 0.000007 (2SD solution; Gerdes and Zeh, 2006); 0.282018 ± 0.000062 (2SD; n=115, laser analysis; Andersen et al., 2009). Averages for $^{176}Hf/^{177}Hf$ for GJ-1 during the period of analysis were as follows: 0.282017 ± 0.000070 (2SD) for day one, 0.282037 ± 0.000086 (2SD) for day two, and 0.282048 ± 0.000036 (2SD) for day three. Combining all three days gives a mean of 0.282032 ± 0.00004 (2SD) (Fig. 9). This corresponds to a 113 ppm bias

(approximately +1 εHf unit) relative to the value of Morel et al. (2008), but is within 2 standard deviations of the ablation mean over the three days. The data reported in the Results section have not been corrected for systematic bias.

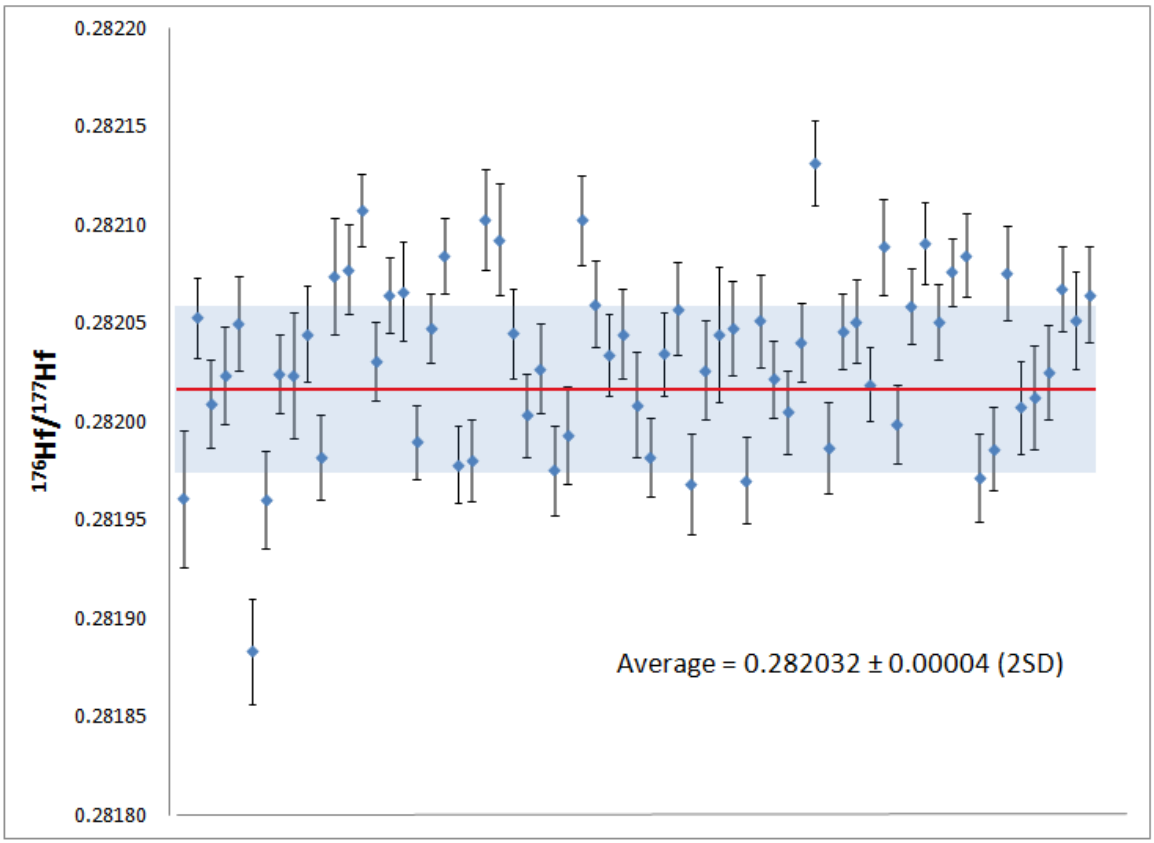

Figure 9. Recorded measurements and associated errors for zircon standard GJ-1. Central line with field indicates average for all results error recorded to 2SD.

Whole Rock Strontium, Neodymium, and Hafnium Isotope Analysis

All dissolution and isotope elutions were done at the UC Davis Interdisciplinary Center for Plasma Mass Spectrometry (ICPMS). Approximately 100 mg was weighed out for each silicate sample. These were digested in closed Savillex™ PFA containers in a mix of concentrated HF-HNO_3 on the hotplate at about 150°C for 24 hours. Following dry-down, fluoride complexes were removed at high temperature (~ 170°C) until dry in an orthoboric-hydrochloric acid mixture. Finally, 6 N HCl was added to the samples to ensure complete dissolution. For Hf and Nd purification, solutions were loaded in 1N HCl + 0.1N HF onto a first–stage column containing AG50W–X12 (100 – 200 mesh) resin. Hafnium was eluted directly followed by rinsing with 2.5 N HCl to remove matrix and trace elements such as LREE. This was followed by Nd elution in 6N HCl. Fractions collected from the first – stage column were dried down and loaded onto the second stage column. Second stage columns for separation of Hf from other similar elements (e.g., Ti, Zr, Nb) uses LN-Spec and requires the use of different concentrations of HCl, H_2O, citric acid, HNO_3, H_2O_2, and HF prior to Hf elution in a HCl-HF mixture. Likewise, second-stage columns for Nd uses LN-Spec, but requires only a simple elution scheme involving removal of other REE using 0.18N HCl followed by Nd elution in 0.5 N HCl. Sr purifcation for $^{87}Sr/^{86}Sr$ analysis was carried out using an aliquot of digested material estimated to contain 1-10µg of Sr dried down and redissolved into 8N HNO_3. This 8N HNO_3 solution was loaded on a Teflon micro-column filled with Sr Spec resin (50-100 mesh size) with a resin bed of volume of approximately 300uL and washed with more

than twenty column volumes of 3N HNO_3 to ensure good separation of rubidium. Sr was then eluted with warm 0.05 N HNO_3. Only distilled and/or Optima® – grade reagents were used for all chemical procedures.

Hf isotopic compositions were analyzed by static multi-collection using a Nu Plasma HR MC-ICP-MS and introduced via a DSN-100 desolvating nebulizer. The collector array on the Nu Plasma was fixed and a post magnet zoom lens system is used to position the masses in the collectors. For Hf analyses, the collectors H4 to L3 are used. The configuration used enables simultaneous collection of Hf (masses 180, 179, 178, 177, 176 and 174) together with monitoring of Lu at mass 175 and Yb at mass 172. The latter two measurements allow interference corrections to be applied to masses 174 and 176. Hf isotope measurements were normalized internally to a $^{179}Hf/^{177}Hf$ ratio of 0.7325 using an exponential correction. The ^{176}Lu, ^{176}Yb and ^{174}Yb corrections were made assuming natural abundances ($^{175}Lu = 0.97416$, $^{176}Lu = 0.02584$, $^{172}Yb = 0.2183$, $^{174}Yb = 0.3138$, $^{176}Yb = 0.1276$) corrected for instrumental mass discrimination as monitored by $^{179}Hf/^{177}Hf$. The configuration used does not permit correction of mass 180 for the presence of ^{180}Ta, because ^{181}Ta is too small to be monitored for a meaningful correction for Ta on mass 180. Although the ^{180}W correction could be applied through monitoring of ^{182}W or ^{184}W, this was not done because in the absence of a ^{180}Ta correction only a partial correction can be made. The presence of ^{180}Ta and ^{180}W can be assessed by comparing $^{180}Hf/^{177}Hf$ values of samples to the mean values measured on the standards. Samples were run using a modified sample-standard

bracketing approach with JMC-475 Hf standard solution analyzed after every six samples to monitor systematic in-run drift in the standard value. The average of the 6 JMC-475 Hf standard measurements was 0.282179 with an internal precision of 0.000013 (2SD) and a true value of 0.282160.

Purified Nd solutions were introduced into the Nu Plasma MC-ICPMS with a DSN-100 desolvating nebulizer. Neodymium isotope ratios were measured in static collection mode, where the collector configuration for Nd isotope analysis is such that all Nd isotopes plus ^{147}Sm are analyzed (to monitor interference of ^{144}Sm on ^{144}Nd), with mass 144 on the axial channel. Like with Hf, Nd isobar corrections assume natural abundances of isotopic compositions and are subtracted proportionally, with calibrated instrumental mass discrimination. Mass fractionation is corrected by normalizing to a ^{146}Nd/^{144}Nd of 0.7219. There was no correction made on Ce since this isobar does not interfere with ^{143}Nd/^{144}Nd.

^{87}Sr/^{86}Sr ratios are measured on a Nu Plasma HR which is a double-focusing, plasma-source mass spectrometer equipped with fixed detectors and high-precision and high-resolution capabilities. Samples introduced with a desolvating nebulizer system (DSN-100) and a 0.1mL/min quartz nebulizer result in instrument sensitivity typically ranging from 160 - 200V/ppm Sr. Ratios include 50-60 data points and each data point integrates for 10 seconds. The software automatically runs 2SE statistics and allows/disallows outliers (~95% confidence) in real time. Baselines are measured for 30

seconds by ESA deflection (ion beams are defocused away from detectors). ^{88}Sr signals typically range from 3 – 18 volts. $^{87}Sr/^{86}Sr$ data is internally normalized by the measured $^{86}Sr/^{88}Sr$ ratio relative to $^{86}Sr/^{88}Sr = 0.1194$, which proportionally corrects for instrumental mass discrimination assuming exponential fractionation on other isotope ratios. ^{85}Rb is measured to correct for any small amount of ^{87}Rb present, again assuming the exponential fractionation of Sr to apply proportionally. $^{84}Sr/^{86}Sr$ is assumed to be 0.00675476 and is used to estimate ^{84}Kr and ^{86}Kr. Kr is subtracted until the $^{84}Sr/^{86}Sr$ ratio equals the canonical value of 0.00675476 (while iterating the mass-bias correction). This allows a robust correction to be made on mass 86 with large error demagnification in this process, due to the fact that $^{86}Kr/^{84}Kr$ is approximately 0.30, while the $^{86}Sr/^{84}Sr$ ratio is approximately 17.7.

RESULTS

Whole Rock Radiogenic Sr-Nd-Hf Analysis

A total of 15 whole-rock samples were analyzed for radiogenic Sr, Nd, and Hf isotopes (Table A3; Appendix A). For the data set as a whole, $(^{87}Sr/^{86}Sr)_i$ ranges from 0.70800 to 0.71442, $\varepsilon Nd_{(t)}$ ranges from = -7.32 to -11.62, and $\varepsilon Hf_{(t)}$ ranges from -6.75 to -13.11.

To best illustrate relationships throughout the sample groups, isotope data was plotted against SiO_2 (Fig. 10). Reciprocal plots were also made for each isotope type to examine binary mixing (Fig. 11). Finally, the Hf and Nd isotope data were plotted against each other (Fig. 12). Where possible, whole rock data from Ericksen (2006) were incorporated to further constrain relationships.

For $(^{87}Sr/^{86}Sr)_i$ vs. SiO_2 (Fig. 10a) there is an overall positive trend with data in this study conforming well with data from Ericksen (2006). Ratios are expectedly lowest in the mafic sheets ($(^{87}Sr/^{86}Sr)_i$ = 0.70800 – 0.70850) and highest in the granites (0.71011 – 0.71189) with the largest spread in ratios for the granites. However, within each group the more evolved samples do not necessarily equate to the greater $(^{87}Sr/^{86}Sr)_i$ ratios. For example, for the Mafic Sheet samples AWM-1 and 2 the SiO_2 contents are 56% and 54%, and $(^{87}Sr/^{86}Sr)_i$ = 0.70800 and 0.70850 respectively.

a)

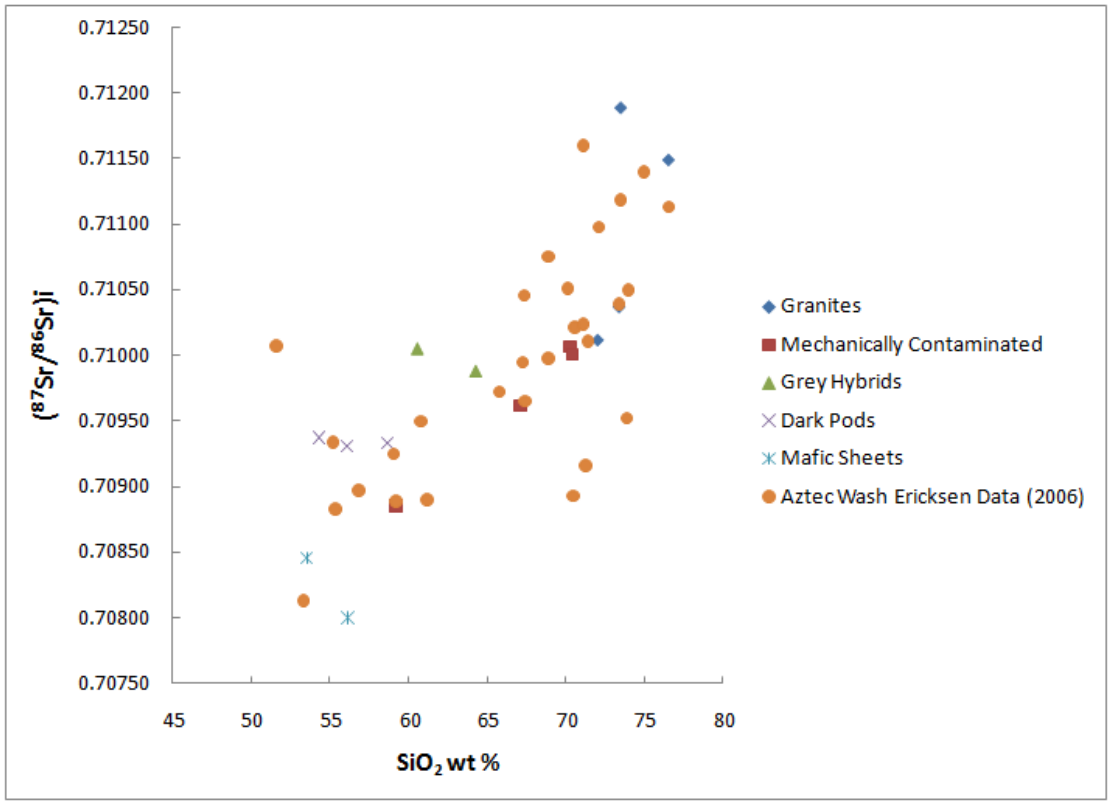

Figure 10. Whole rock $(^{87}Sr/^{86}Sr)_i$, $\varepsilon Nd_{(t)}$ $\varepsilon Hf_{(t)}$ vs. SiO_2. Plots (a) and (b) include relevant data from Ericksen (2006). Age corrected for 15.6 Ma Aztec Wash pluton.

b)

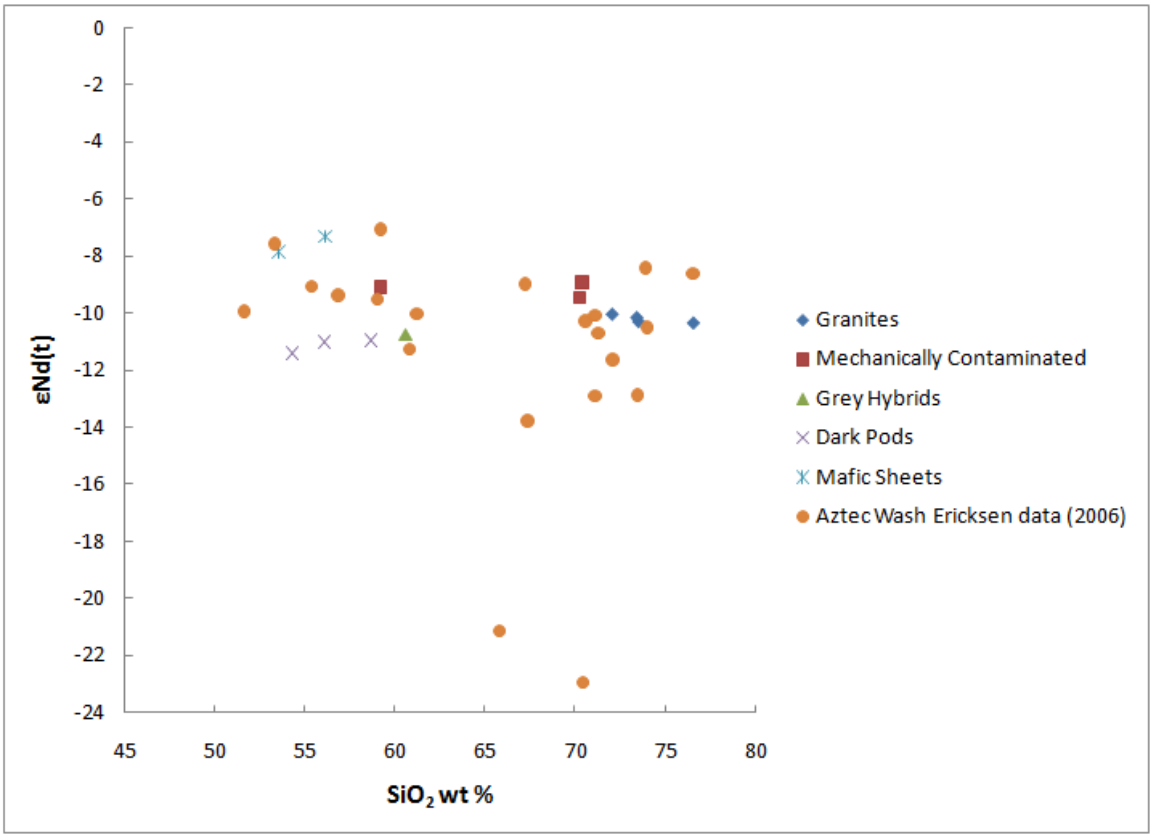

Figure 10 (continued)

c)

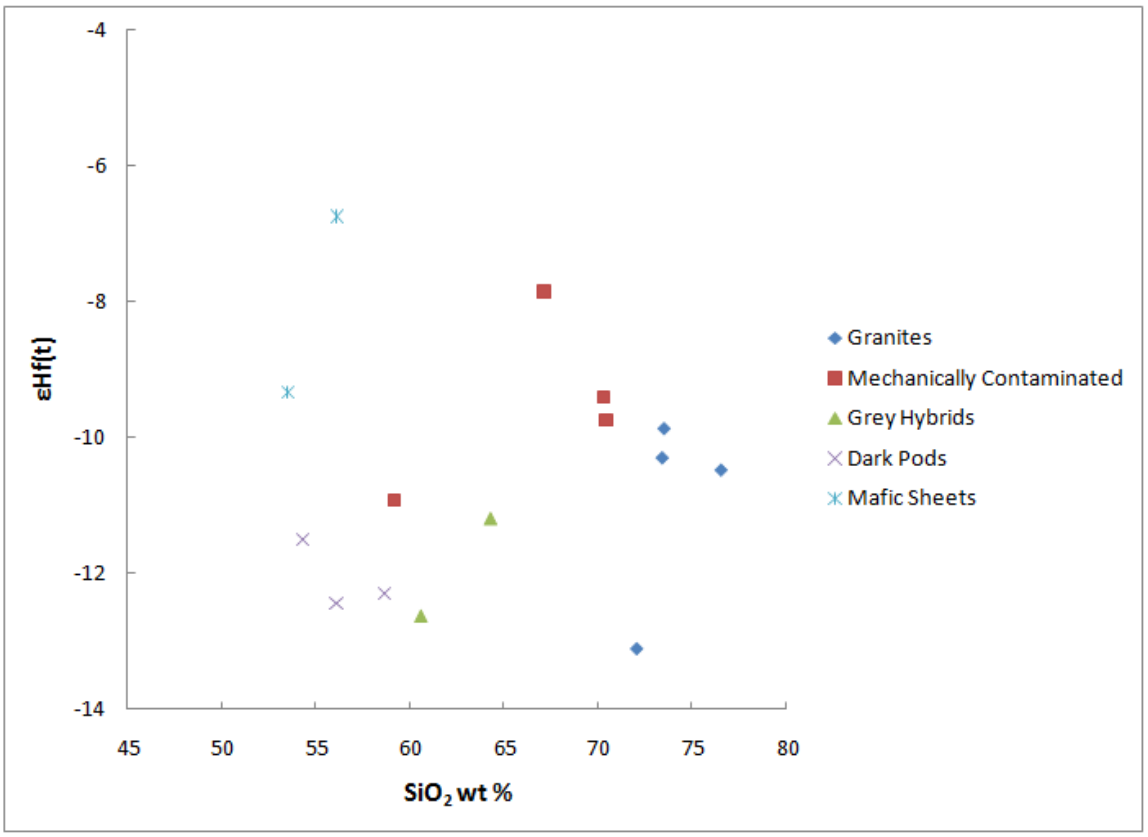

Figure 10 (continued)

The Mechanically Contaminated and Grey Hybrid samples are intermediate between the most mafic and felsic samples with $(^{87}Sr/^{86}Sr)_i$ = 0.70889 – 0.71025, and 0.70998 – 0.71011 respectively. The Dark Pods have relatively elevated $(^{87}Sr/^{86}Sr)_i$ ratios given their SiO_2 contents (0.70934 – 0.70942).

When Nd and Hf isotopes are plotted against SiO_2 (Figs. 10b and 10c) the trends are not as clear or obvious as the trends in $(^{87}Sr/^{86}Sr)_i$ ratios. Total variability in $\varepsilon Nd_{(t)}$ across all sample groups is relatively restricted to approximately 4 epsilon units. The Mafic Sheets have the highest $\varepsilon Nd_{(t)}$ (-7.3 and -7.6) as might be expected, but all other samples are within 2.5 $\varepsilon Nd_{(t)}$ units of each other (-9 to -11.4), with the relatively mafic Dark Pods showing the most negative values ($\varepsilon Nd_{(t)}$ = -11 to -11.4).

Unlike $\varepsilon Nd_{(t)}$, the $\varepsilon Hf_{(t)}$ values have a slightly broader range of approximately 6 εHf units, but this is reflected mainly by greater variation in the Mafic Sheets where values range from -6.7 (AWM-1) to -9.3 (AWM-2). All other samples again range over approximately 2.5 $\varepsilon Hf_{(t)}$ units, with Dark Pods having somewhat distinctly lower $\varepsilon Hf_{(t)}$ values (-11.5 to -12.3) given their low SiO_2 values.

Plotting reciprocals of isotope compositions (Fig. 11) provides evidence that mixing is occurring but that it is not a simple binary model, agreeing well with initial observations from Ericksen (2006). The plot of $(^{87}Sr/^{86}Sr)_i$ vs. 1/Sr (Fig. 11a) is perhaps the closest to a binary model with a strong positive correlation between the most mafic samples and the most felsic. The reciprocal plot for Hf composition (Fig. 11b) has a

potentially strong negative trend but the Dark Pod samples do not lie along this trend, and some granite samples (NAWZ-26, 50 and AWAG-6) do not form part of one specific end-member that their SiO_2 compositions might suggest they should. For Nd compositions (Fig. 11c), where data from Ericksen (2006) may show a weak negative linear trend, data from samples in this study do not show any specific trend.

a)

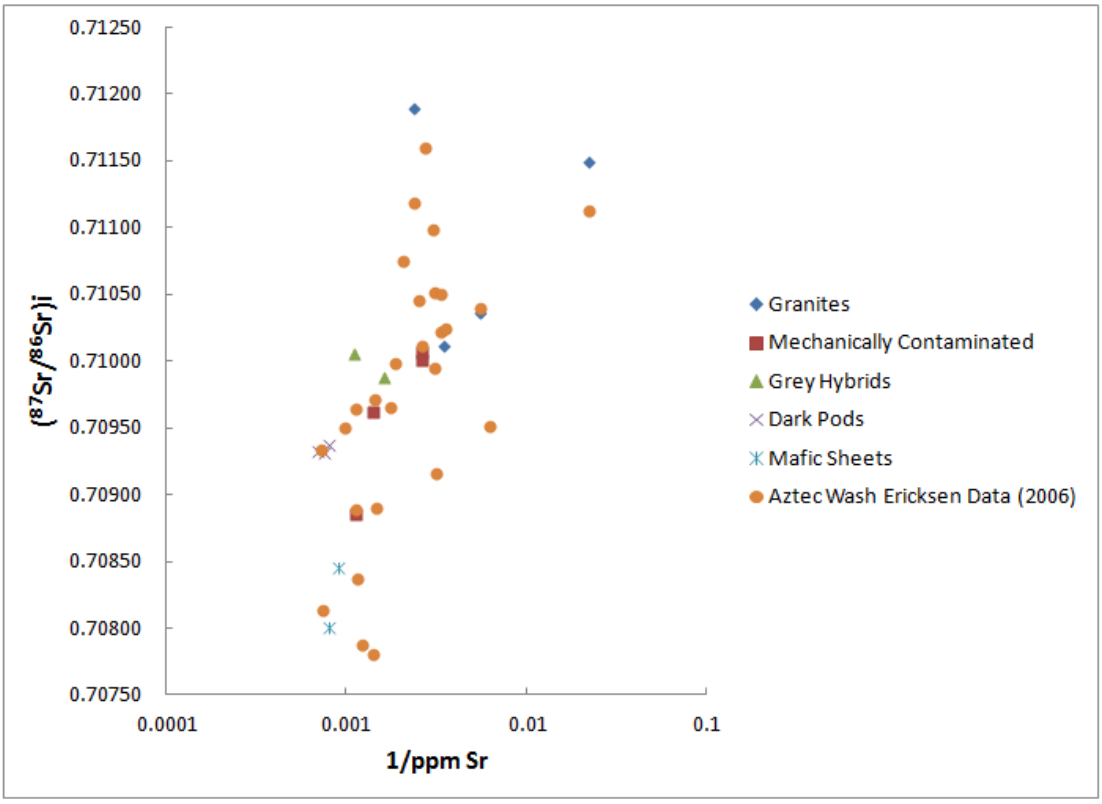

Figure 11. Whole rock reciprocal plots of initial Sr, Hf and Nd isotope ratios against respective elemental concentrations. Plots (a) and (c) include relevant data from Ericksen (2006). Age corrected for 15.6 Ma Aztec Wash pluton.

b)

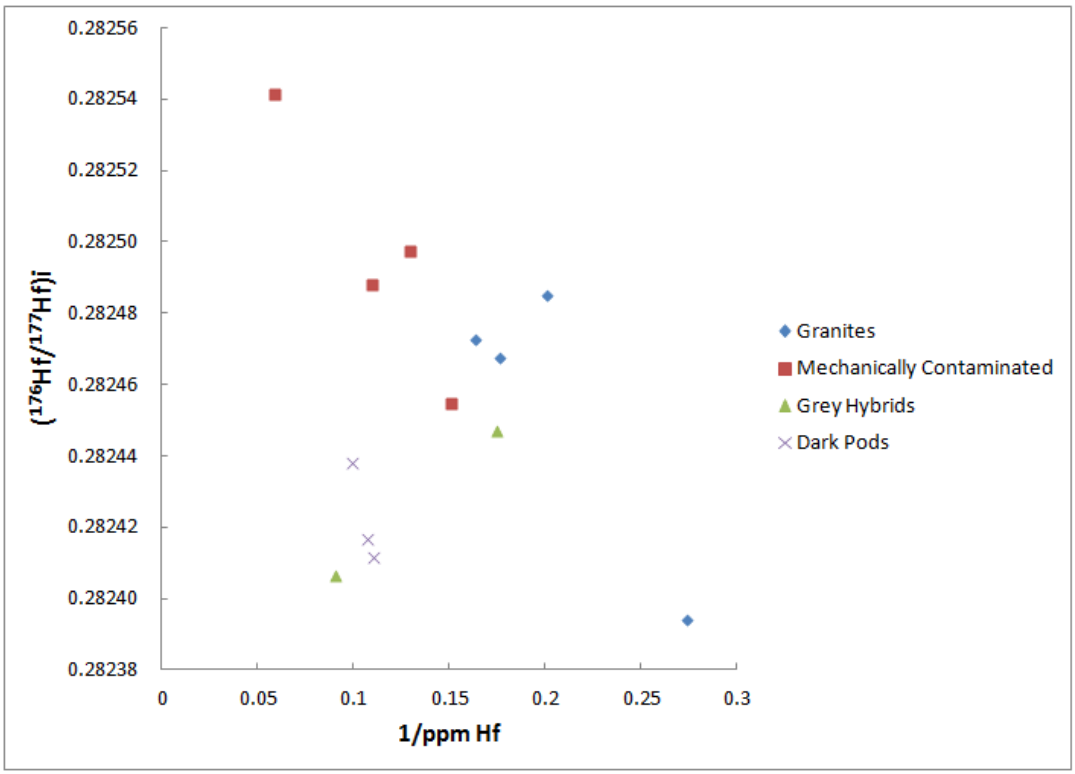

Figure 11 (continued)

c)

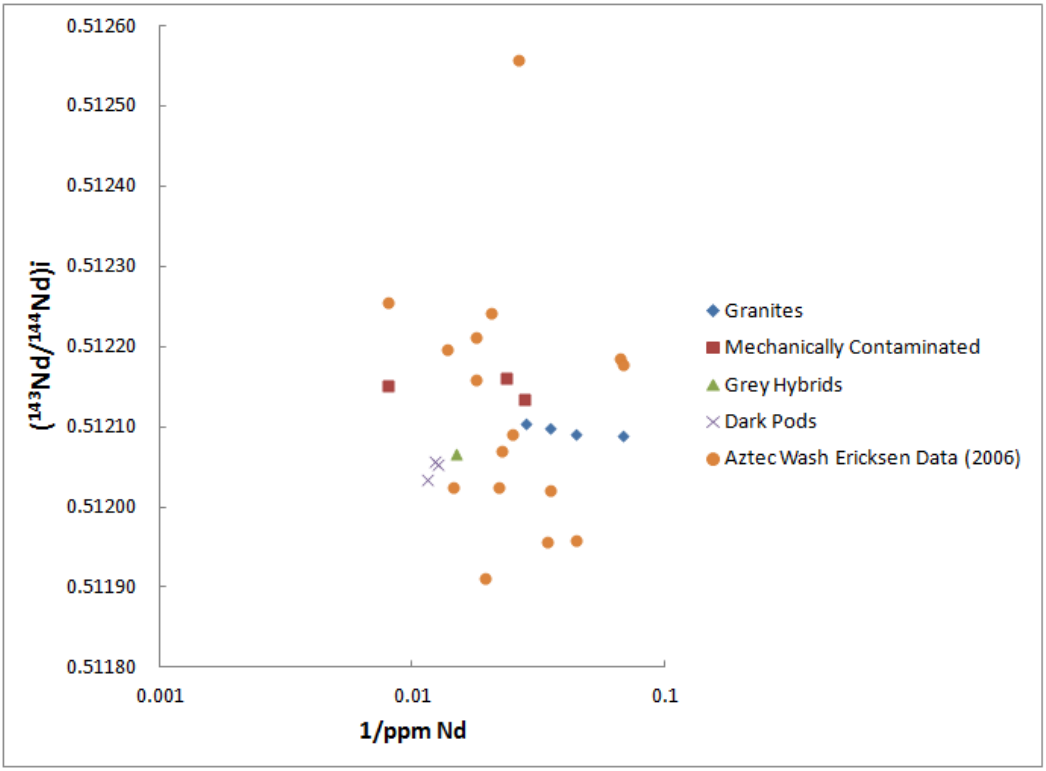

Figure 11 (continued)

As expected $\varepsilon Hf_{(t)}$ and $\varepsilon Nd_{(t)}$ show a strong positive correlation due to relatively similar parent-daughter systematics during melting processes (Fig. 12). Each particular unit type can also be distinguished by its εNd values. There is much more overlap, however, in $\varepsilon Hf_{(t)}$ values for each sample set.

Figure 13 shows the relationship of $\varepsilon Nd_{(t)}$ vs. $(^{87}Sr/^{86}Sr)_i$ for the Aztec Wash pluton and neighboring Eldorado Mountain plutons (Searchlight and Ireteba). Overall there is a strong negative trend with overlap in $\varepsilon Nd_{(t)}$ and $(^{87}Sr/^{86}Sr)_i$ between the Aztec Wash pluton and Searchlight pluton.

Figure 13 also shows the εNd vs. $(^{87}Sr/^{86}Sr)_i$ plot of regional basement units considered to be the potential host rocks for Aztec Wash pluton intrusion, as well as an inferred enriched mantle basalt (εNd = -6, $(^{87}Sr/^{86}Sr)_i$ = 0.7065; Miller and Wooden, 1994), likely to be a melt source during emplacement. Again there is a strong negative correlation, and it is also clear that some overlap exists between Aztec Wash pluton, Searchlight pluton, Old Woman basement rocks, and Ireteba pluton mafic-intermediate units. Figure 14 shows potential mixing curves between Aztec Wash lithologies and these basement units and will be addressed in the discussion.

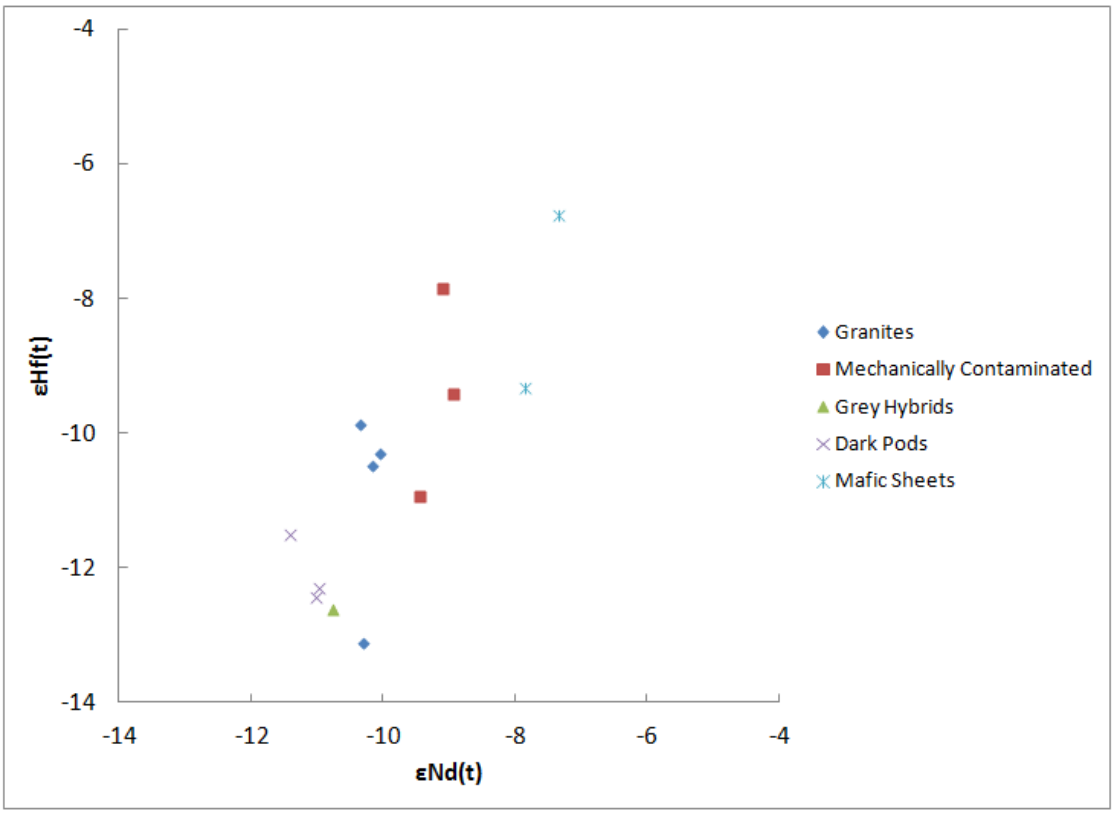

Figure 12. Whole rock $\varepsilon Hf_{(t)}$ vs. $\varepsilon Nd_{(t)}$ for samples in Granite and Heterogeneous zones. Age corrected for 15.6 Ma Aztec Wash pluton.

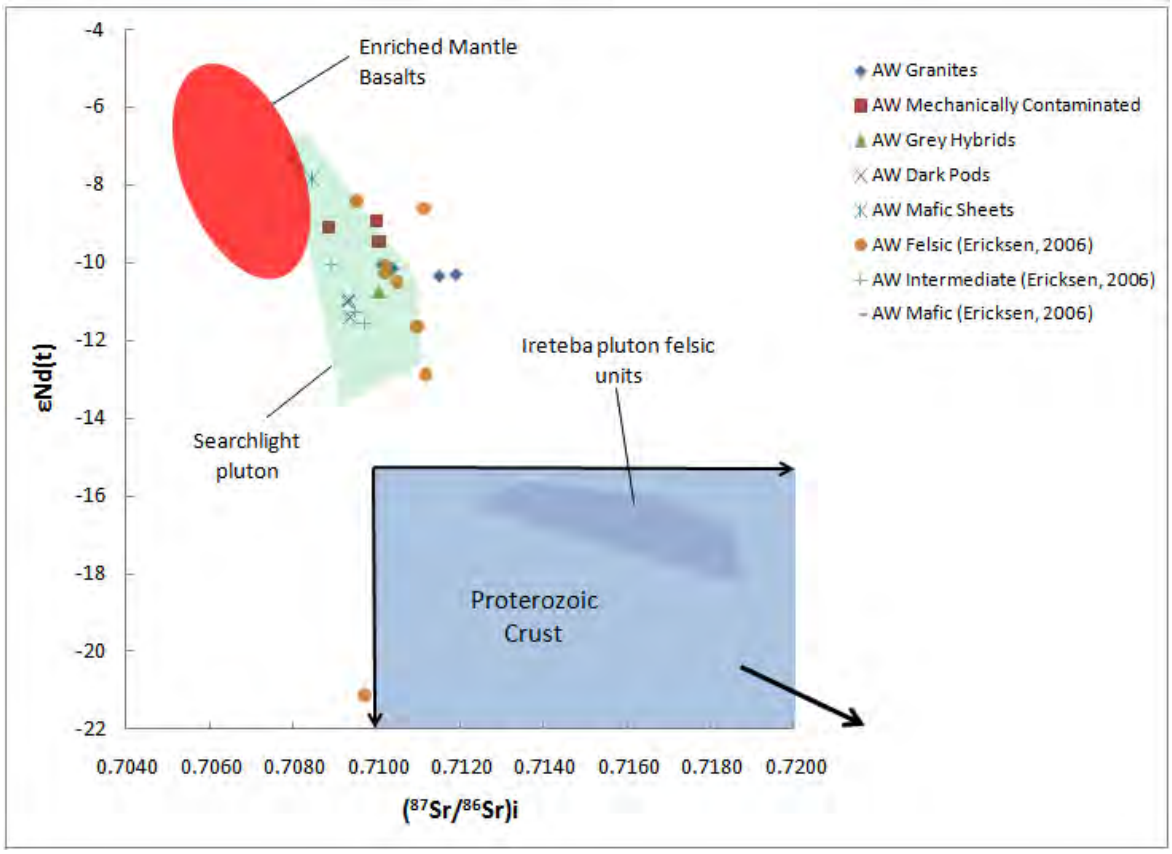

Figure 13. Whole rock Nd and Sr compositions for Aztec Wash pluton and regional lithologies. Compositional fields used for Ireteba pluton (Kapp et al., 2002), Searchlight pluton (Bachl et al., 2001). Fields for enriched mantle basalts and Proterozoic crust from, and relevant data from Aztec Wash pluton taken from Ericksen (2006). Age corrected for 15.6 Ma Aztec Wash pluton.

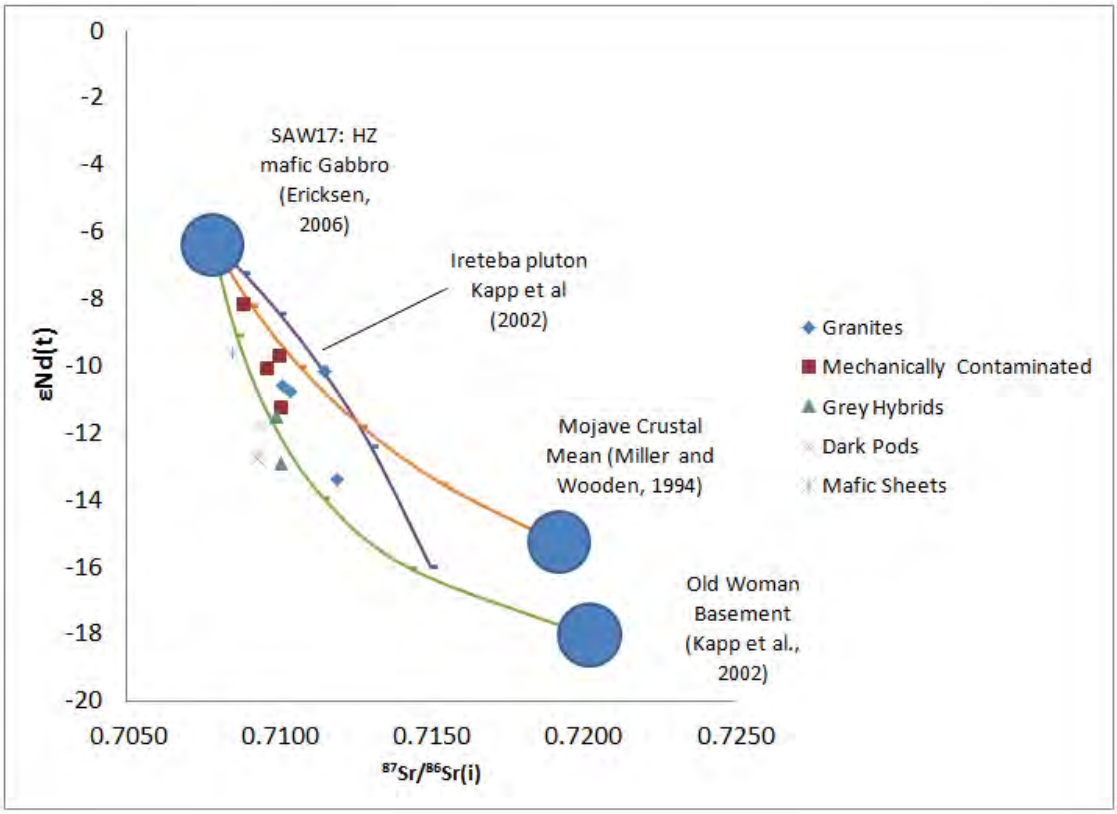

Figure 14. Calculated binary mixing curves for Nd and Sr isotopic compositions. Sample SAW17 (Ericksen, 2006) is assumed as candidate for mafic end-member constructing Aztec Wash. Tick marks in 20 % fraction increments. Values used are as follows: SAW17 (Ericksen, 2006): Sr = 700ppm, Nd = 40ppm, $^{87}Sr/^{86}Sr$ = 0.7078, εNd = -6.3; Ireteba pluton (Kapp et al., 2002): Sr = 465ppm, Nd = 17ppm, $^{87}Sr/^{86}Sr$ = 0.715, εNd = -16; Mojave (Miller and Wooden, 1994): Sr = 361ppm, Nd = 42.9ppm, $^{87}Sr/^{86}Sr$ = 0.719, εNd = -15.2; Old Woman basement (Kapp et al., 2002): Sr = 200ppm, Nd = 50ppm, $^{87}Sr/^{86}Sr$ = 0.720, εNd = -18. See Appendix I for calculated mixing data.

In-situ Age and Trace Element Analysis of Zircon

U-Pb age data for the two mafic sheets (AWM-1 and AWM-2) and additional and trace element analyses for AWM-1 obtained by SHRIMP are given in tables C1 and C2 (Appendix C) and B1 (Appendix B) respectively. The best age estimate for the two sheets is given by the error weighted mean $^{206}Pb/^{238}U$ age corrected for Common Pb using ^{207}Pb (Fig. 15). The age of AWM-1 is 15.7 ±0.1 Ma (1SD) and the age of AWM-2 is 15.7 ±0.2 Ma (1SD).

Chondrite-normalized REE concentrations for AWM-1 are also displayed in Figure 16 and show typical strong enrichment of HREEs expected in zircon, creating a convex upward pattern. Concentrations of HREE are generally four orders of magnitude greater than LREE. There are notable positive Ce anomalies caused by Ce^{4+} substituting for Zr^{4+} in the crystal lattice, along with slightly negative Eu anomalies.

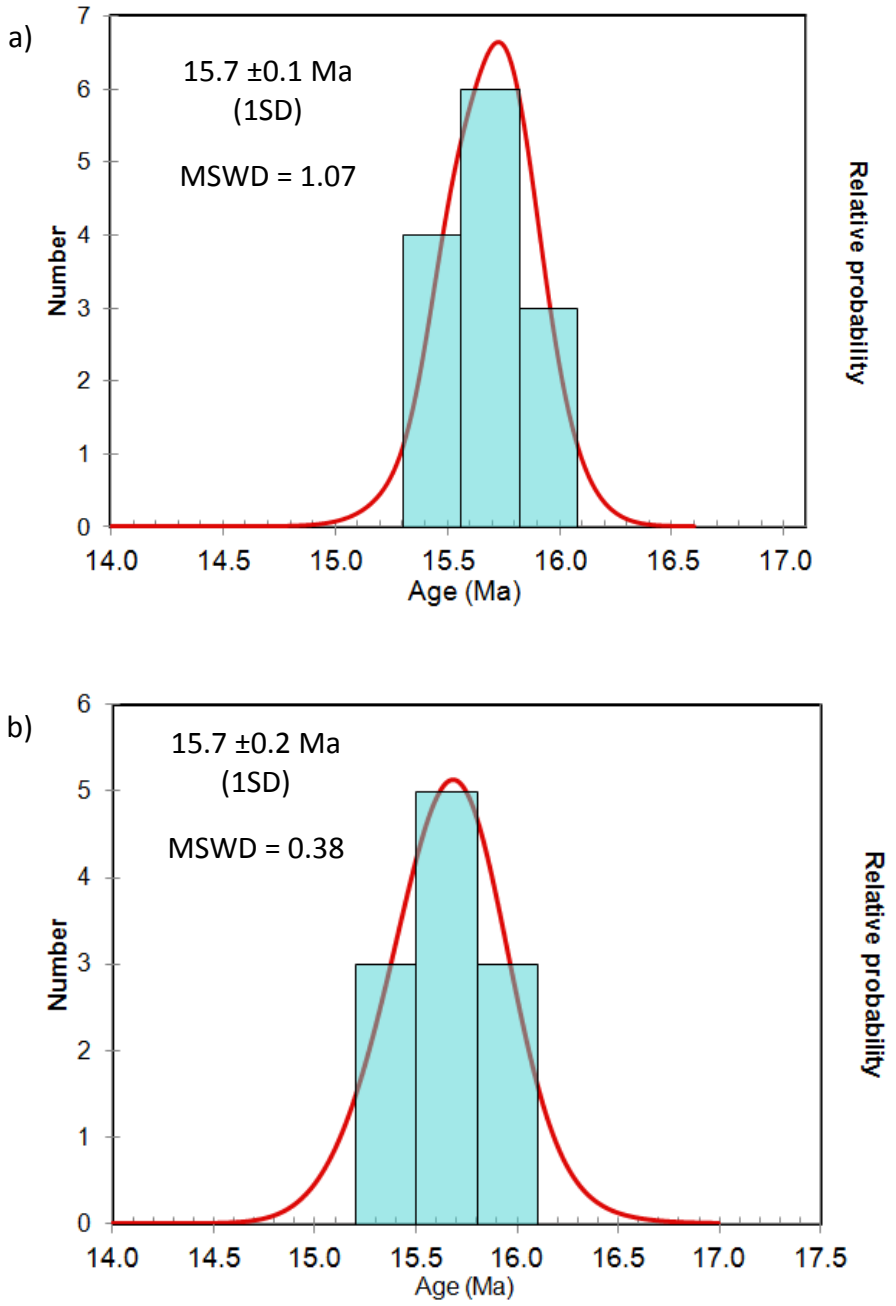

Figure 15. Cumulate probability curves for zircon ages of AWM-1 (a) and AWM-2 (b). Ages calculated using $^{206}U/^{238}U$ and corrected by ^{207}Pb.

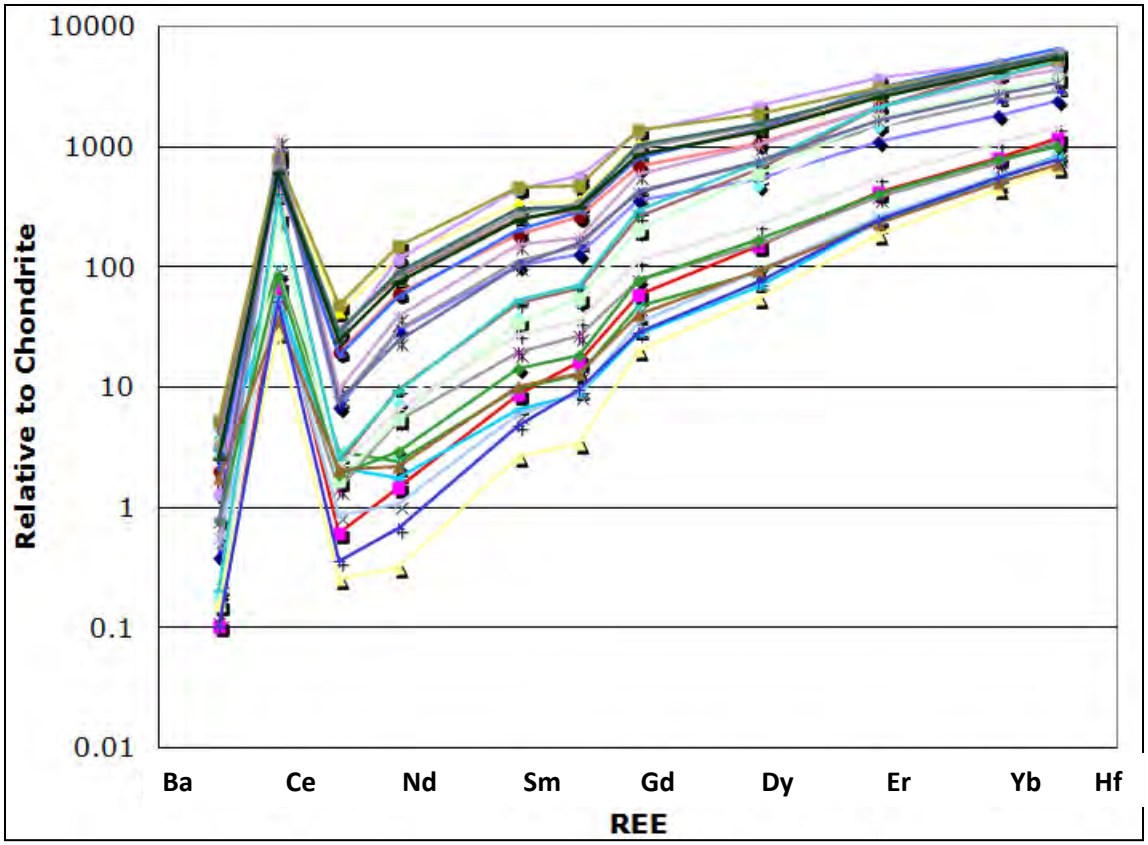

Figure 16. REE spider diagram for zircons in AWM-1. Normalized the chondrite figures from Anders and Grevesse (1989).

Hafnium Isotopes in Zircon

The laser ablation zircon Hf data are given in Table D1 (Appendix D) and Figures 17, 18. Comparison of the whole-rock εHf values for each sample to the εHf of individual zircon ablation spots and their 2-sigma internal precisions (Fig. 17) gives a crude assessment of the degree of internal consistency between the two different data sets.

Assuming that nearly all of the Hf in the rock resides in zircon, the individual arrays of zircon εHf should generally overlap the whole rock εHf (for a sufficient number of data points). This is the case for all of the samples except AWAG-1A (n=16; Dark Pod). Relatively limited numbers of zircons were analyzed from all samples, and so it is possible that analysis of greater numbers of zircons for sample AWAG-1A would capture somewhat more variation than observed. This is discussed more below in relation to the error-weighted Hf isotope distributions. In addition, as noted above, there is an approximately +1 εHf unit bias on the GJ-1 standard run with the zircon sample data, which, if applied systematically to all zircon data points, would shift them down (i.e., by -1 εHf) and cause the low εHf end of the array for AWAG-1A to overlap the bulk rock εHf.

The data arrays in Figure 17 show the total spread in Hf isotopic composition measured for the zircons, but given the relatively large errors associated with individual data points, it is important to try to assess the degree to which the spread of the data is

real or simply within expected analytical scatter. In addition, the lack of statistically resolvable intracrystal variation in the zircons (i.e., distinct cores vs. rims) necessitates a different approach to assessing the degree to which we see isotopic heterogeneity in the analyzed zircons.

In Figure 18 the data for each sample are shown as histograms with superimposed cumulative probability curves calculated in Isoplot 3.0 (Ludwig, 2003). These provide a more robust way to potentially distinguish true isotopic heterogeneity within the analyzed zircons for each rock (and for the compositional groups). The whole-rock εHf(t) is also shown as a vertical dashed line for comparison with the zircon data.

The principal challenge to examining the data this way is to decide how to assign error to the input data. Figure 18 illustrates the impact of different error estimates on the calculated cumulative probability curves for each sample. One could assign the unique two standard error (2SE) from each individual analysis to the data (i.e., the internal precision of each data point based on each individual ablation). This is usually the least conservative estimate of the error. However, in many cases the "internal precision" exceeds the 2SD external reproducibility for multiple $^{176}Hf/^{177}Hf$ analyses of the GJ-1 standard (± 1.4 εHf units), which is not what would be typically expected (Appendix D). Assigning the 2SD external reproducibility as the error results in cumulative probability curves that show even more distinct peakedness, even though this is usually regarded as a more conservative way to assign error.

The relatively large 2SE internal precisions seen in many zircons relative to the standard can sometimes be attributed to short ablation times owing to the small size of the zircon (i.e., counting statistics), but in other cases where ablation times were not limited, it probably indicates that the sample zircons are not homogeneous over the ablation volume, even though the ablation checks do not show an obvious shift in Hf isotopic composition. Zoning of 4 or 5 εHf units in a sample zircon would be difficult to detect in the ablation. Also, the relatively large laser spot size makes ablation across multiple zones (and therefore mixing of Hf from these different zones during ablation) inevitable. Appreciable mixing of distinct but not necessarily widely variable isotopic compositions could be expected. All of these issues argue that significantly more data points per sample are warranted in order to have greater statistical power when dealing with mixtures of zircons where isotopic variation is near the external reproducibility limit.

Using the 2SE internal precisions allows a unique error to be assigned to each measurement, such that the cumulative probability curve is weighted to reflect the isotopic variation of the individual ablation measurements, and is therefore preferred (Fig. 18). In several samples, there are clearly non-Gaussian distributions regardless of the assigned errors (e.g., NAWZ-13, NAWZ-26, AWAG-6, AWAG-1A, AWAG-5), and these unequivocally demonstrate that zircons with distinctly different isotopic compositions are present in these samples. Bearing these limitations in mind, the general variation that is observed in each of the compositional/petrographic groups is presented below.

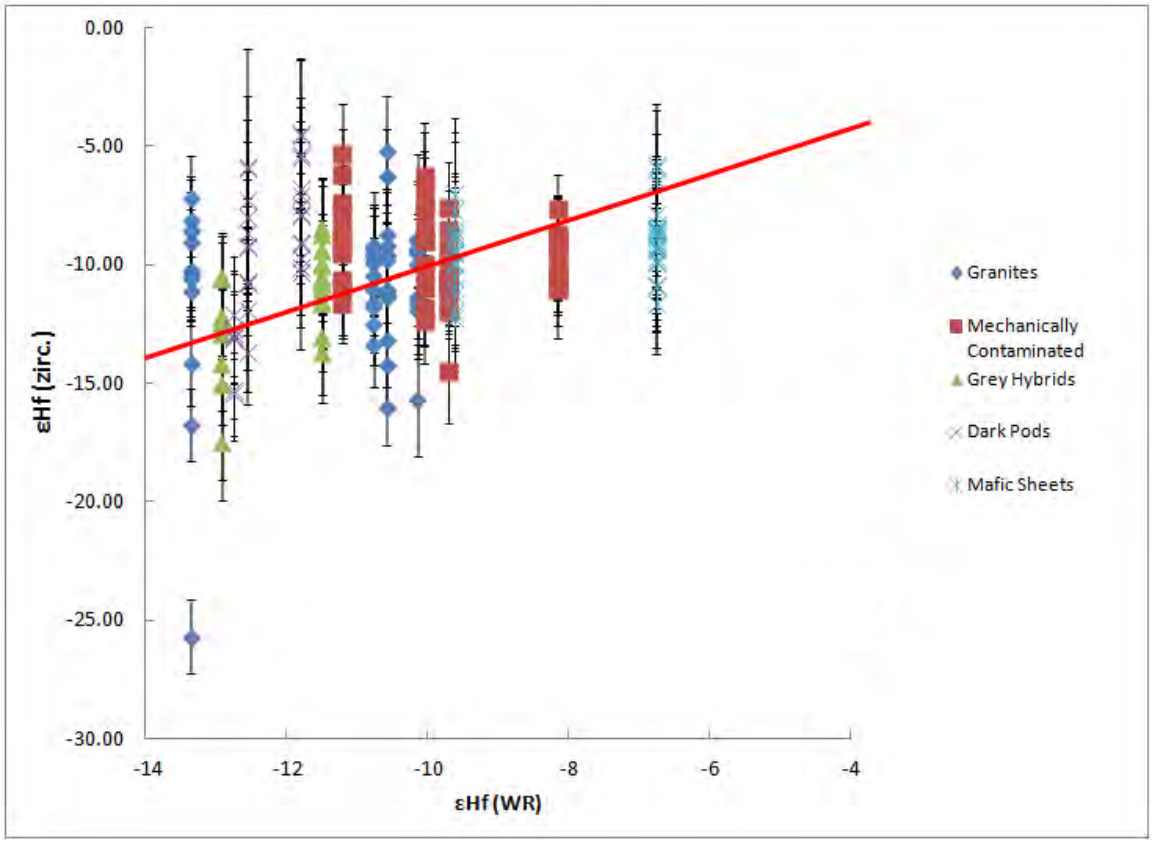

Figure 17. Zircon (zirc) εHf vs. whole-rock (WR) εHf. Error bars for individual zircon spots indicate 1SD.

Granites

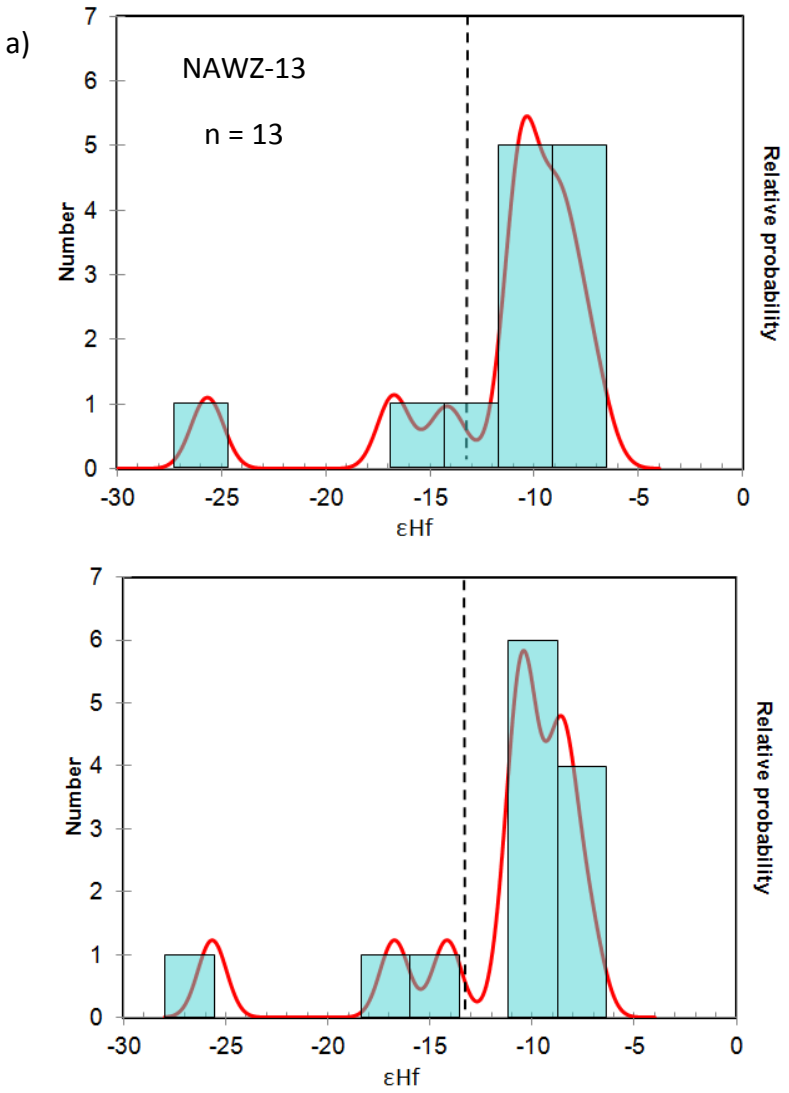

Figure 18. Cumulative probability plots for εHf-in-zircon data. Each pair is of same sample with top plot providing name and number of data points used for both. Top plots generated using internal precision (2SE). Bottom plots generated using external reproducibility (2SD) of zircon standard GJ-1 of ±1.4 epsilon units. Dashed line indicates measured whole rock εHf. Plots produced with Isoplot 3.0 (Ludwig, 2003).

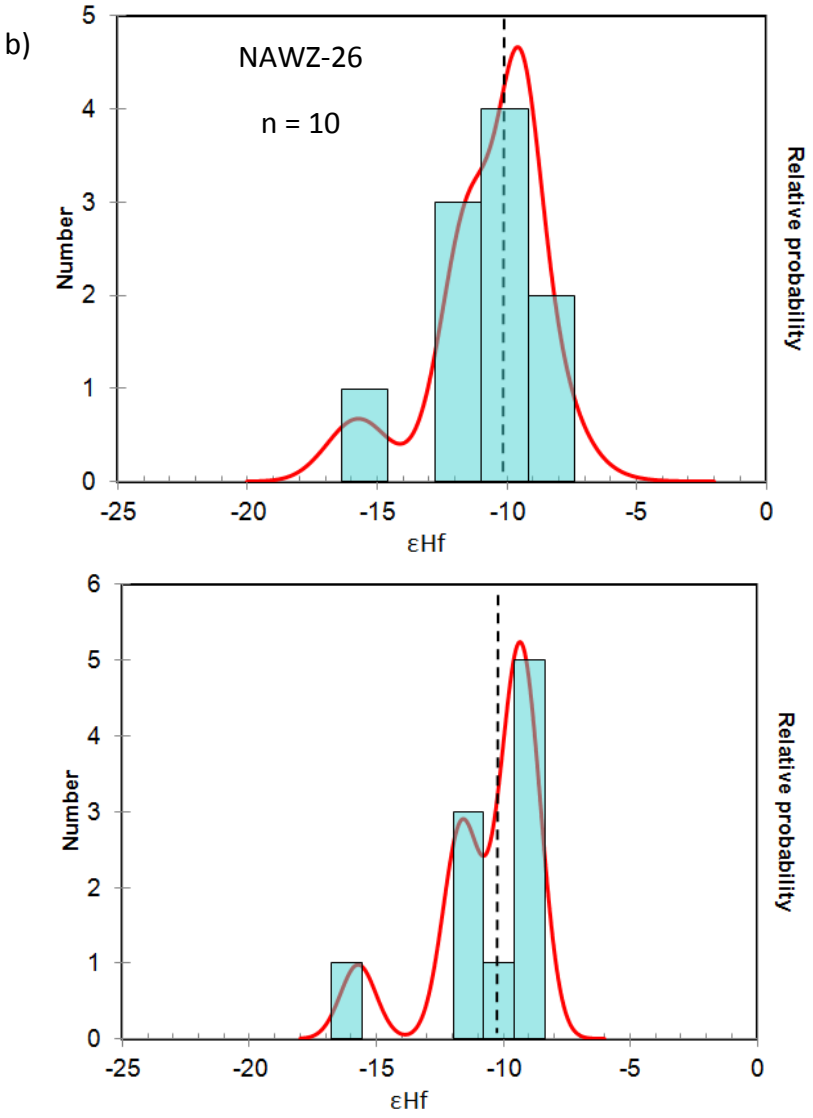

Figure 18 (continued)

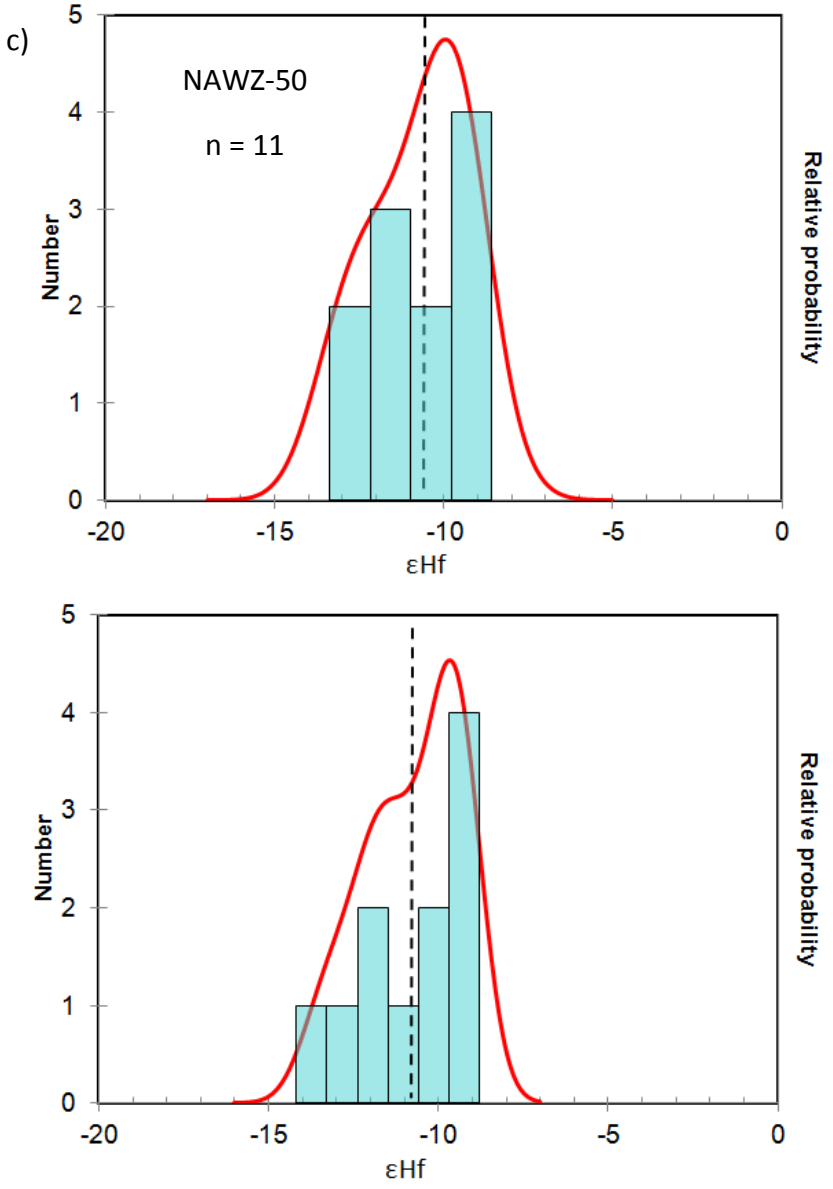

Figure 18 (continued)

d)

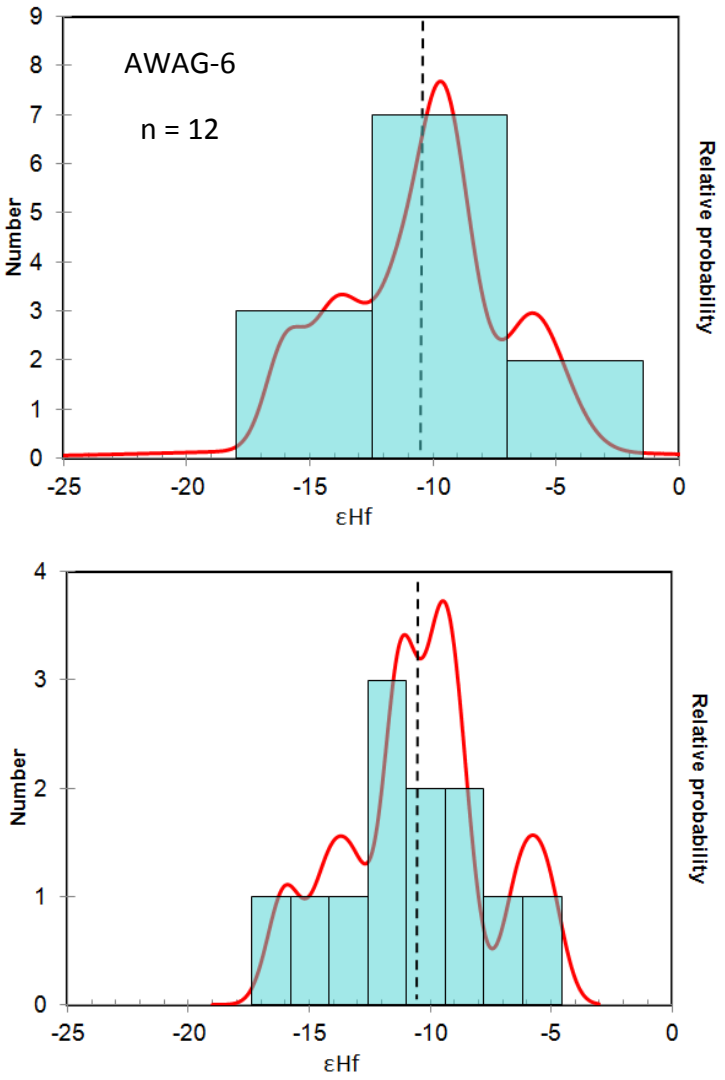

Figure 18 (continued)

Mechanically Contaminated

e)

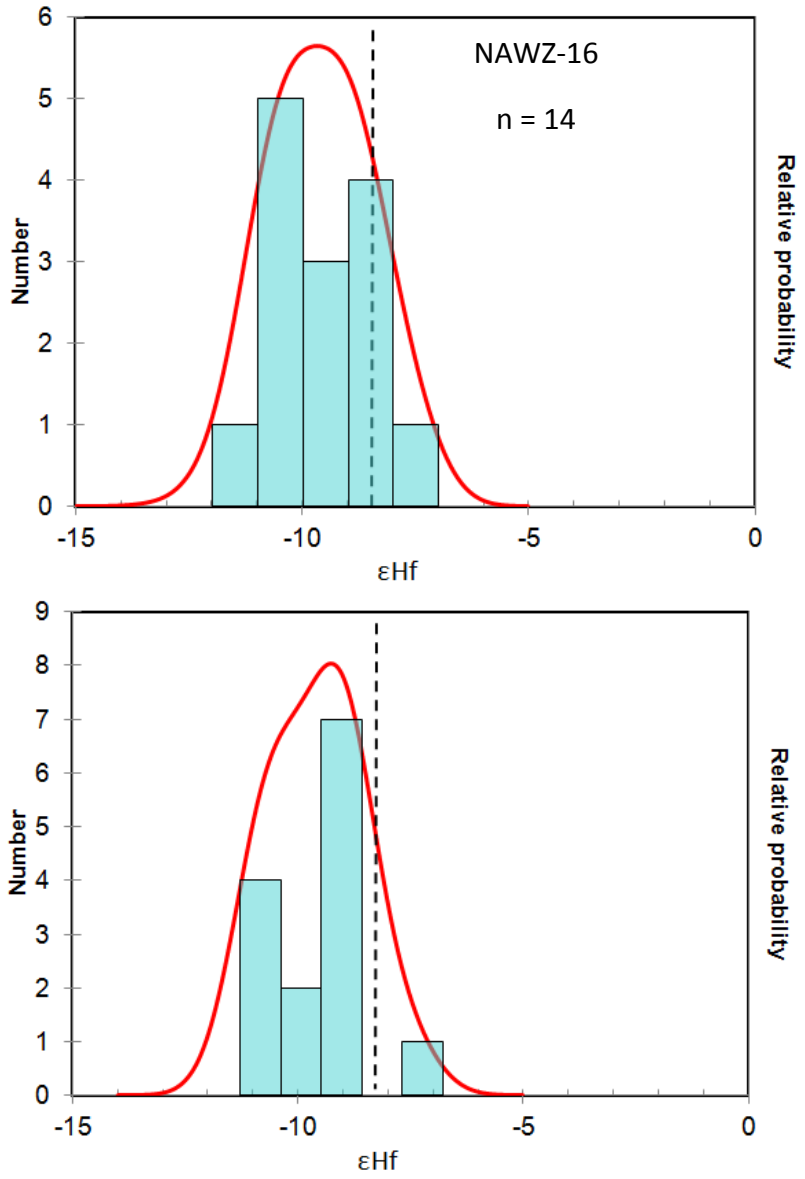

Figure 18 (continued)

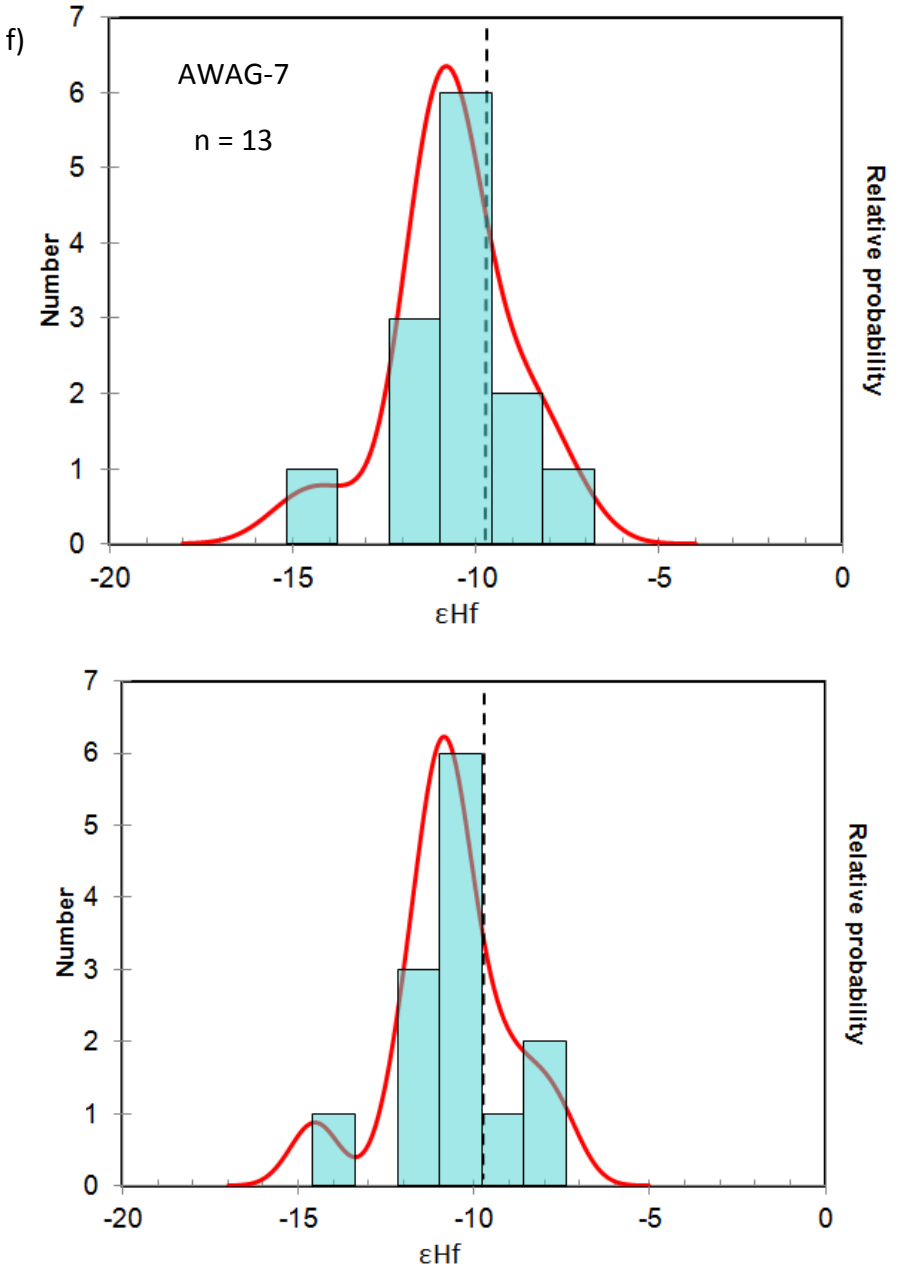

Figure 18 (continued)

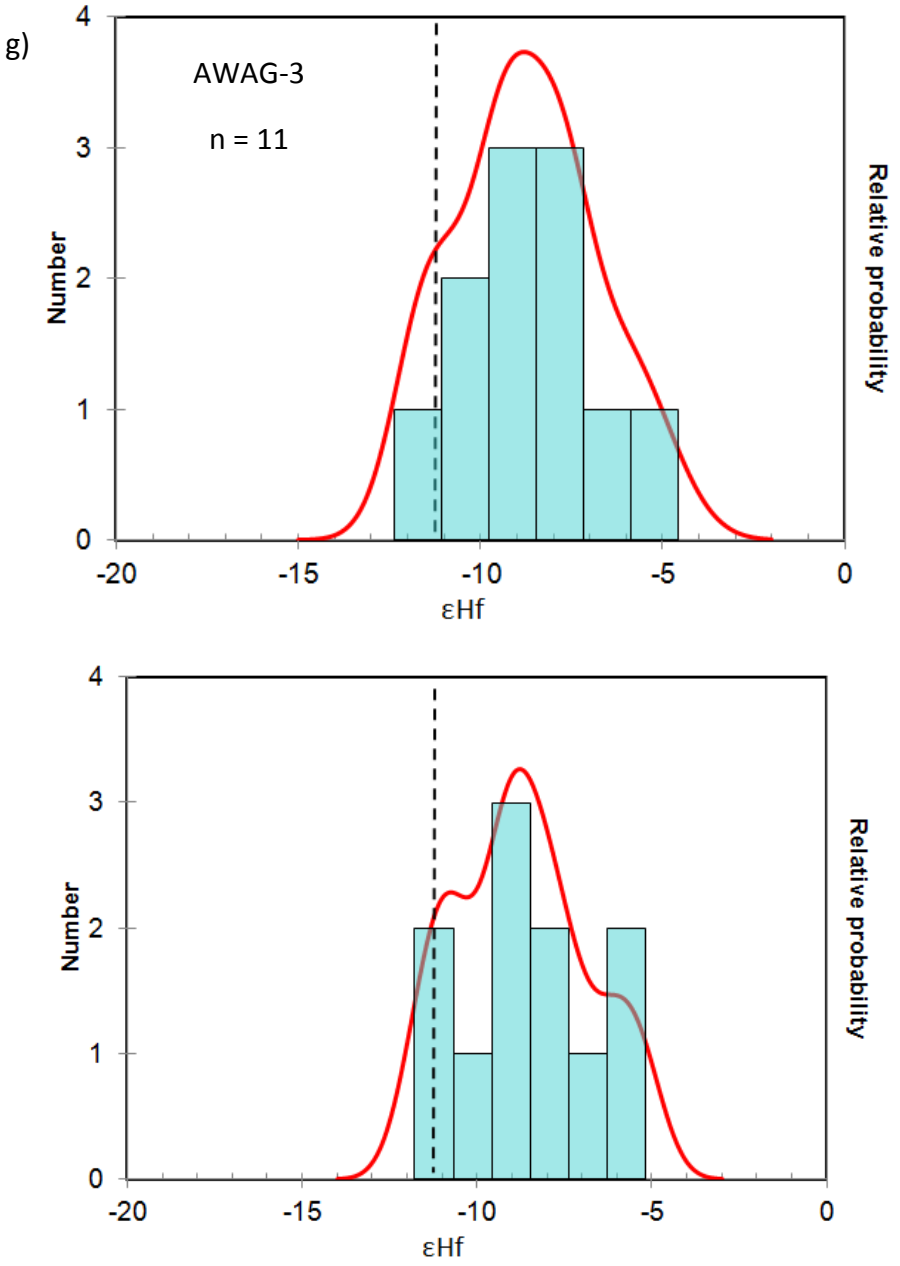

Figure 18 (continued)

h)

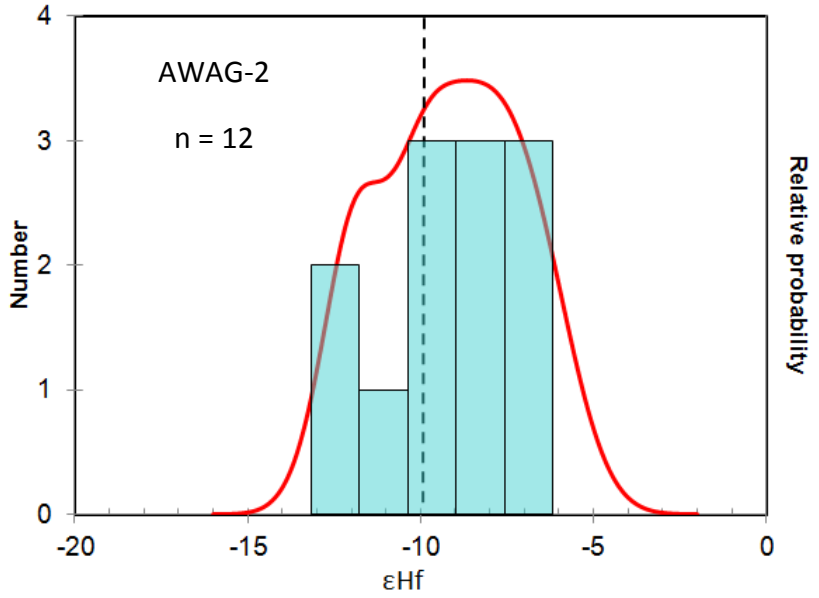

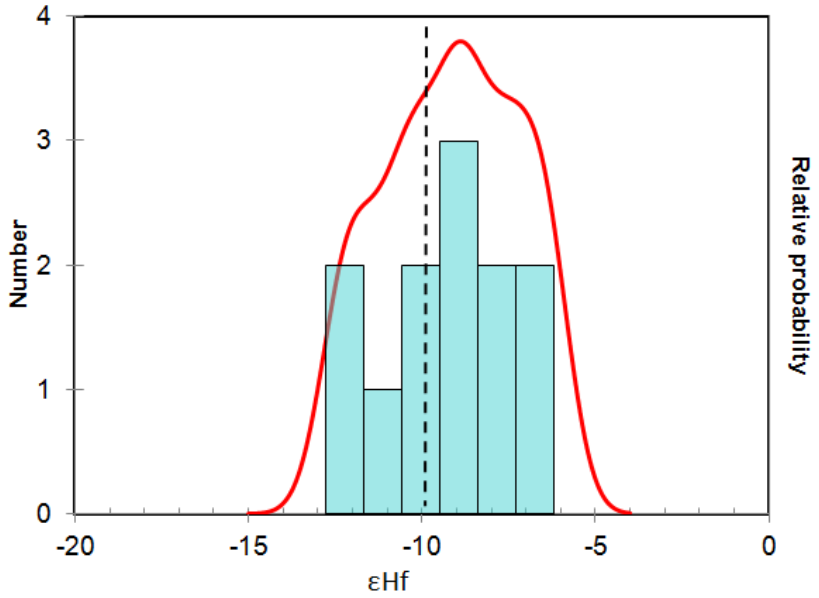

Figure 18 (continued)

Dark Pods

i)

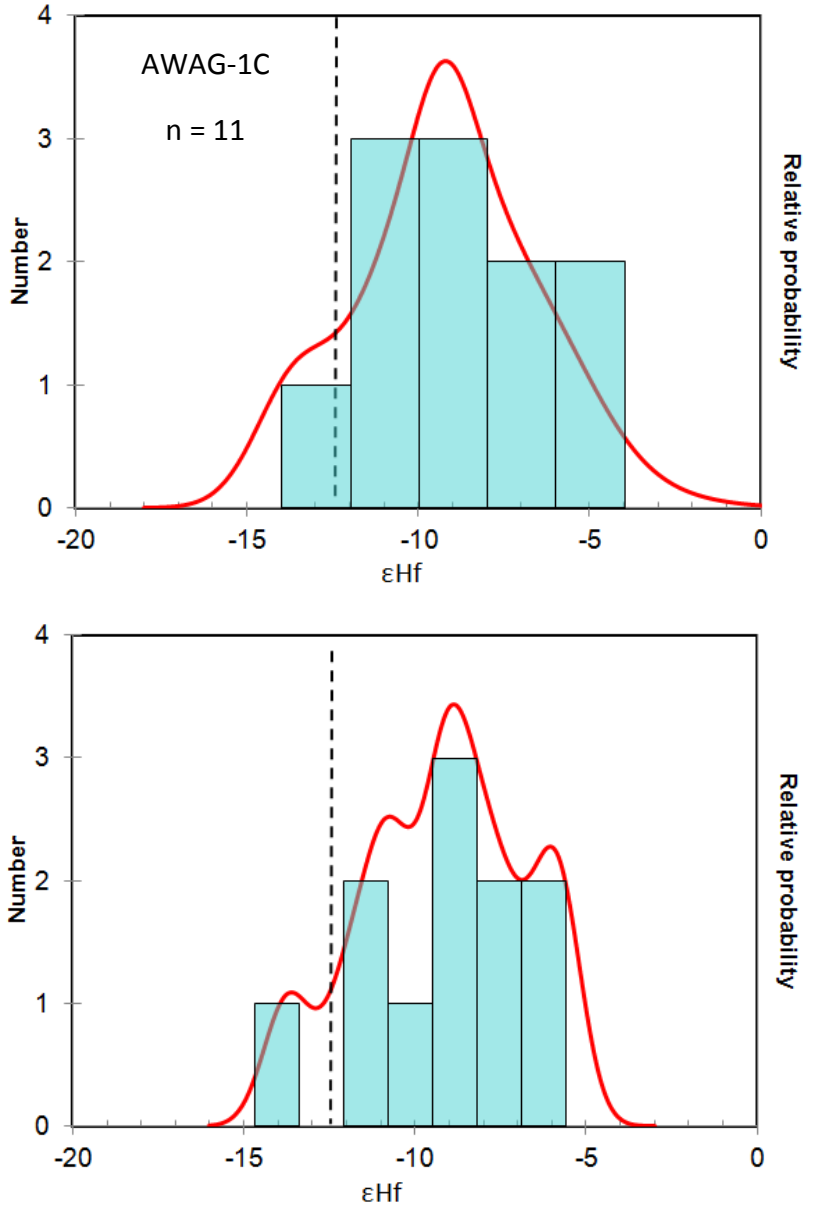

Figure 18 (continued)

j)

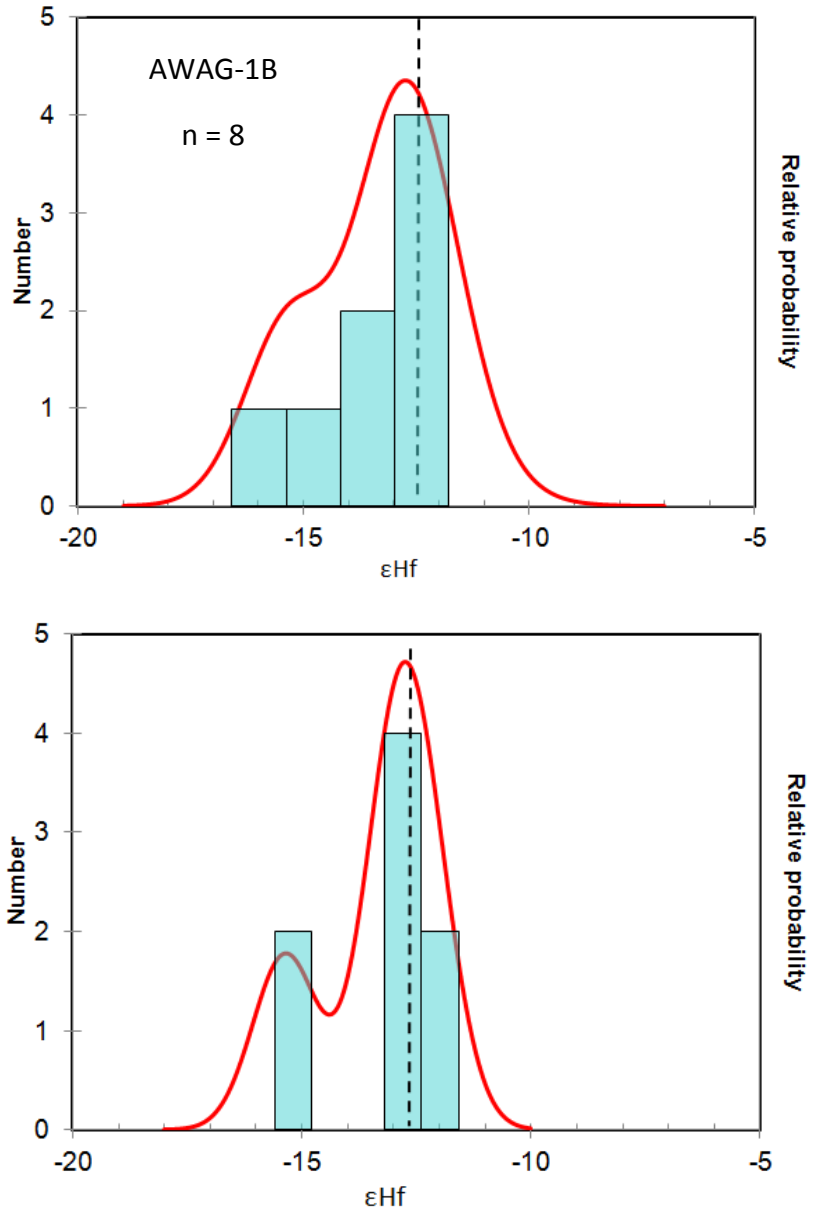

Figure 18 (continued)

k)

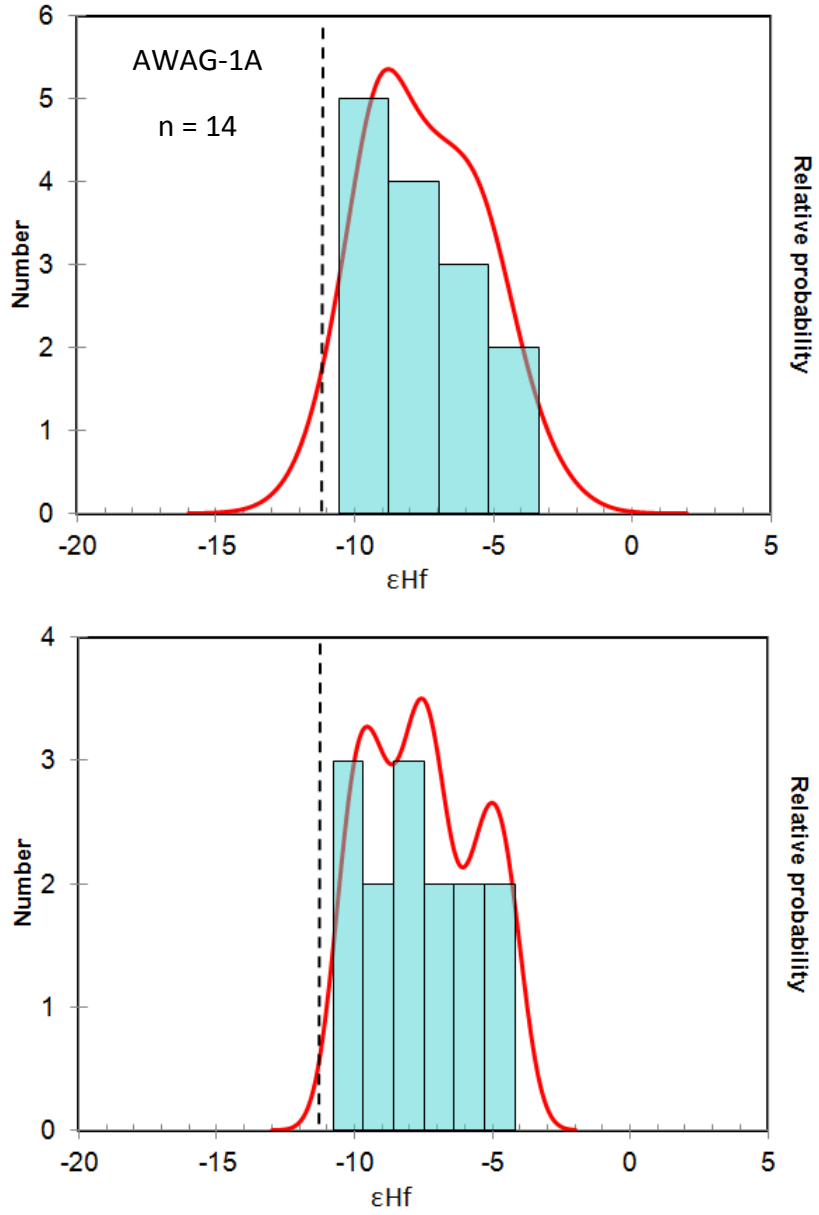

Figure 18 (continued)

Grey Hybrids

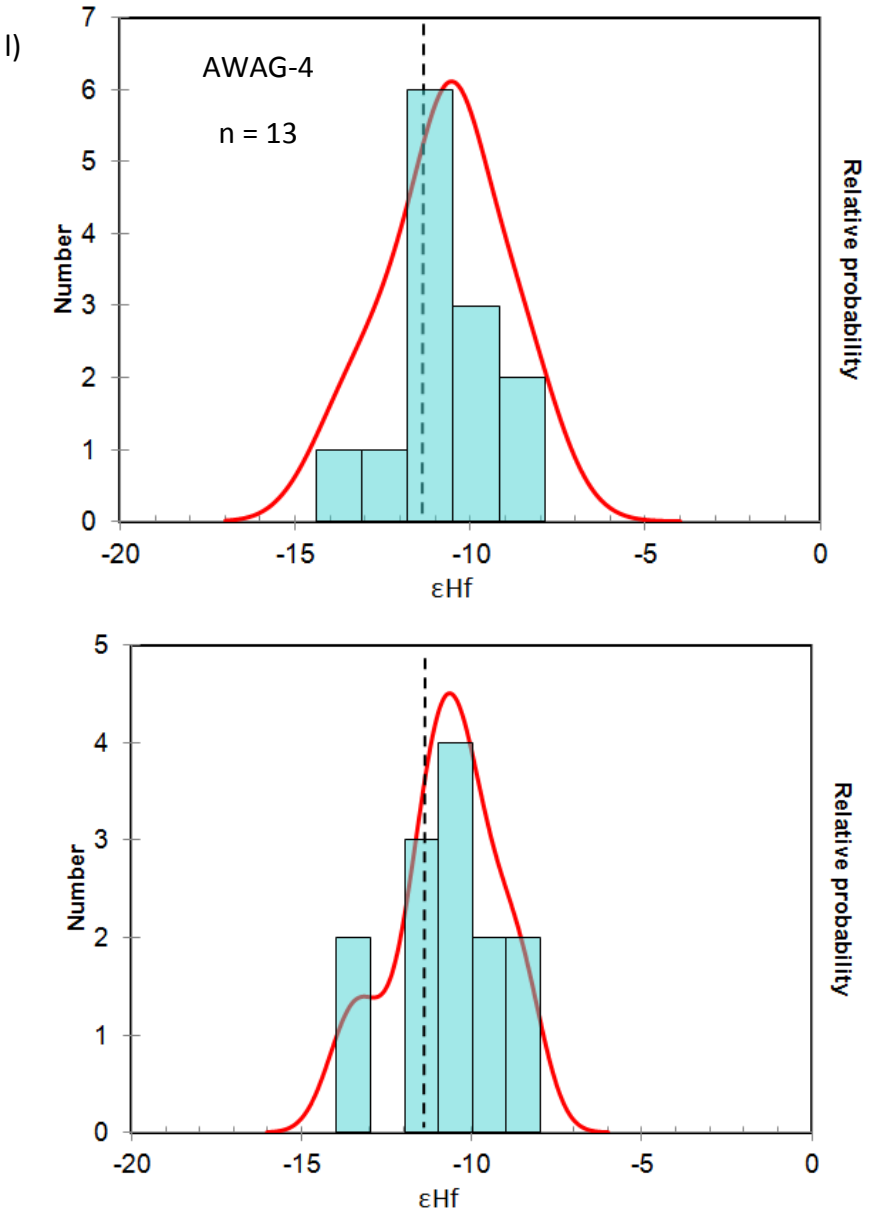

Figure 18 (continued)

m)

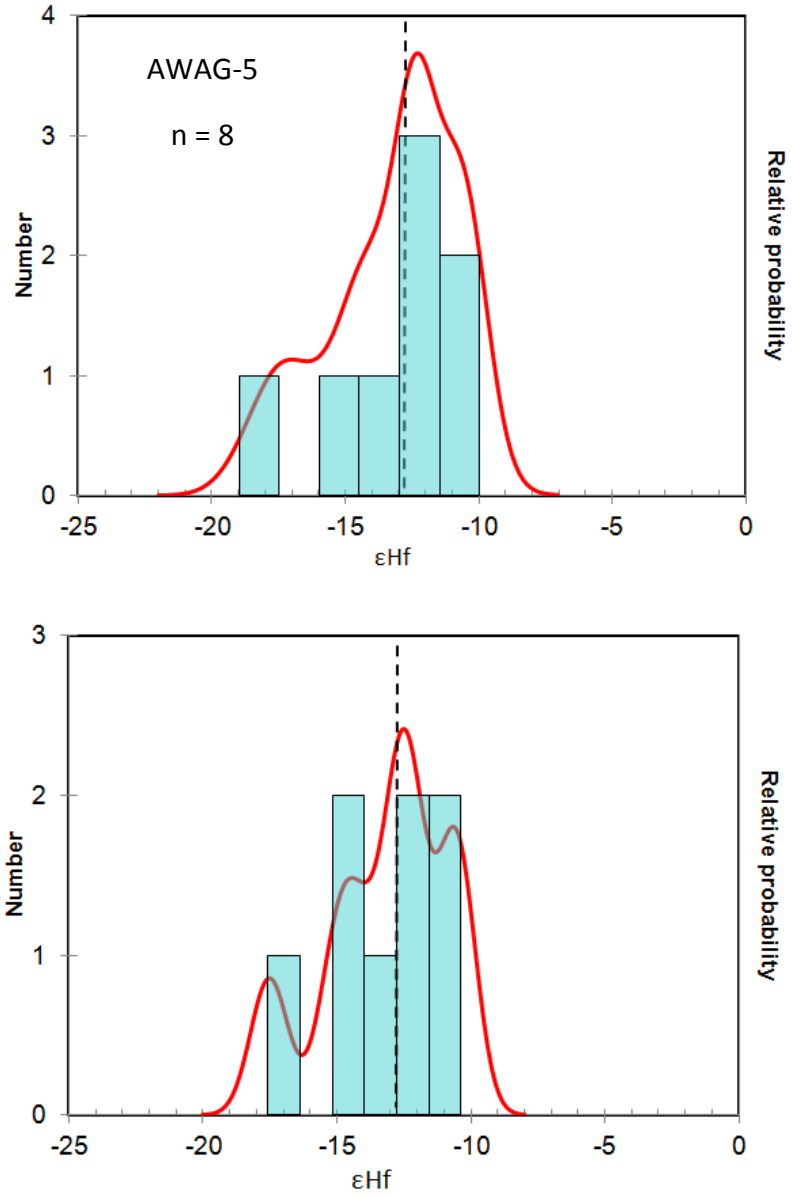

Figure 18 (continued)

Mafic Sheets

n)

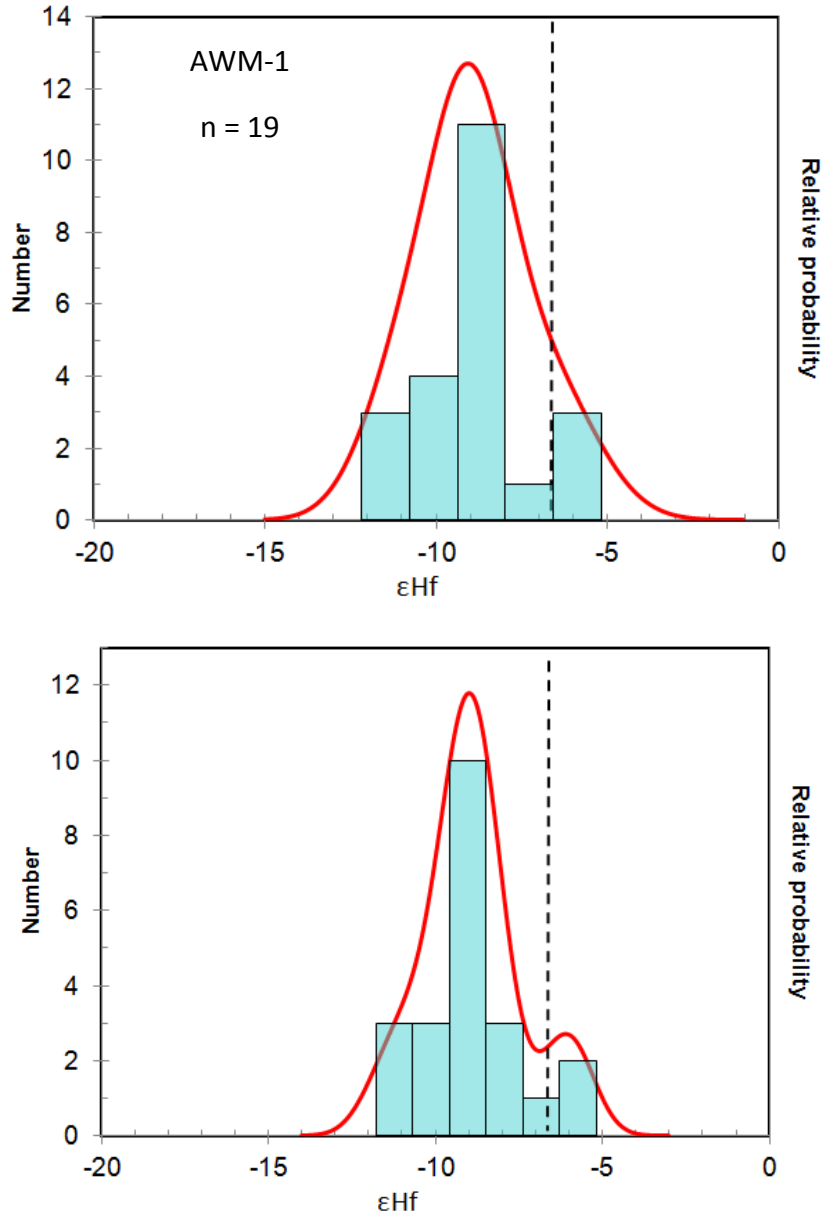

Figure 18 (continued)

o)

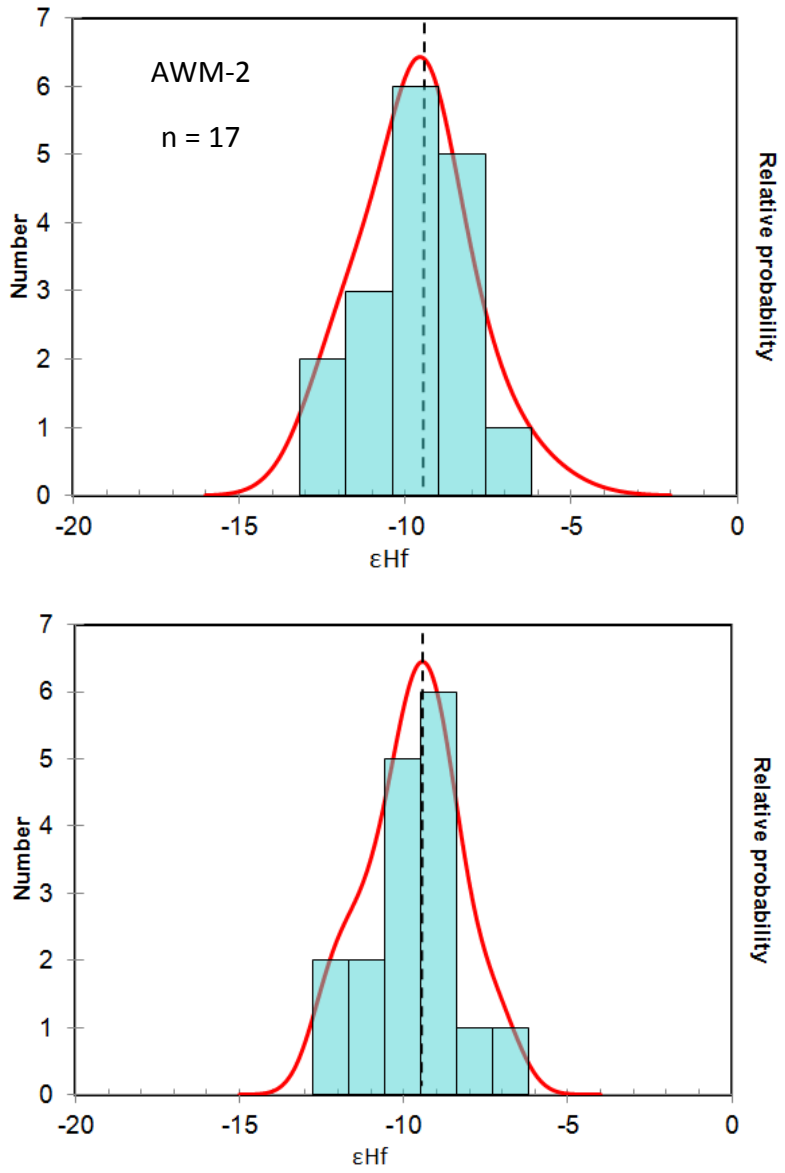

Figure 18 (continued)

Granites

A total of 45 measurements for zircons from 4 granitic samples of the Aztec Wash pluton were determined (Figs. 18a-d). Granites have the broadest range of εHf values, ranging from -5.2 to -25 (20 εHf units). One grain within sample AWAG-6 accounts for the relatively lower values of -5.2 and -6.3. The grain with εHf = -25, found in sample NAWZ-13, is the lowest in the entire data set in this study. Excluding this single grain gives a more modest spread of 11 εHf units. Although separate core and rim analyses were not obtained for this zircon, the ablation profile for this grain showed no evidence of isotopic zonation (e.g., higher εHf on a much lower εHf core).

Mechanically Contaminated

Fifty measurements were made on the 4 mechanically contaminated samples (Figs. 18e-h). Values of εHf range from -5.4 to -15. Sample NAWZ-16 had the smallest spread of εHf data (-7.7 to -11) with a mean of -9.6 and could reflect a somewhat homogeneous sampling. AWAG-2 and 3 had values ranging between -6.3 to -12 and -5.4 to -12, respectively.

Grey Hybrids

Only two samples of grey hybrids were analyzed, with data for 21 spots acquired (Figs. 18l and 18m). Total spread of εHf values was 9 units (-8.5 to -18). AWAG-5 values for εHf were overall consistently lower than those in AWAG-4 (-11 to -18 and -8.5 to -14, respectively).

Dark Pods

Thirty-three analyses for Hf isotopes from the 3 samples in the Dark Pod unit (Figs. 18i-k) gave an approximately 11 εHf unit spread (-4.5 to -15.5), with appreciable isotopic heterogeneity apparent in the histogram and cumulative probability plots for the 3 samples. Sample AWAG-1A, the fine-grained (quenched margin), had highly variable εHf (-4.5 to -10). AWAG-1C (hydrous melt of dark pod) showed a slightly larger spread of εHf units (-5.8 to -13.7). AWAG-1B (interior) appeared to sample a more homogeneous population, with a variation of approximately 4 εHf units (-12 to -16).

Mafic Sheets

The mafic sheets were sampled to potentially garner information on the likely mantle source for much of the Aztec Wash pluton. A total of 39 spots were analyzed for Hf isotopes from 2 samples (Figs. 18n and 18o) AWM-1 εHf values extend across approximately 6 units (-5.8 to -12). The largest cluster of data points were between εHf = -8 to -10, with only 7 spots falling beyond this narrow boundary. AWM-2 showed a slightly lower range in εHf than AWM-1 (-7.0 to -12).

Oxygen Isotopes in Zircon

Figure 19 gives an overview of all data points (n = 241) for the different groups of samples. For the data set as a whole the spread in zircon $\delta^{18}O$ ranges from just under 5 to just over 8 per mil, with the spread within the compositional/petrographic groups typically about 1 to 1.5 per mil. In the following discussion of the groups, the data are also presented as histograms with cumulative probability plots generated using the external reproducibility of the R33 standard over the period of analysis (± 0.3‰ 1SD) (Fig. 20). In the case of the O isotopes, the internal precision of the individual data points is better than the external reproducibility, so the cumulative probability plots shown are generated using the most conservative estimate of the errors. This is to be expected because, in contrast to the laser ablation analysis, the ion probe spot is smaller and mills down only about 2 microns into the grain.

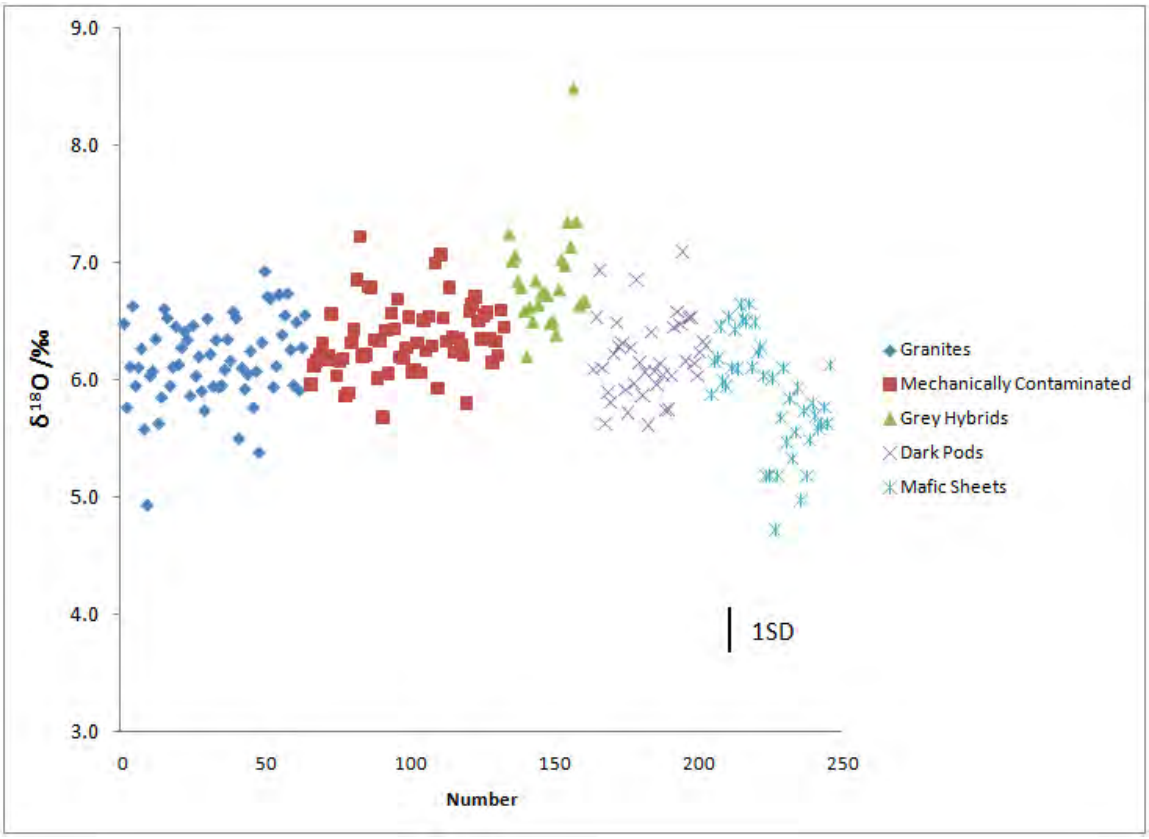

Figure 19. Ranked plot for individual spot values of $\delta^{18}O$ in zircon. Error bar is for zircon standard R33 of ± 0.3‰ (1SD).

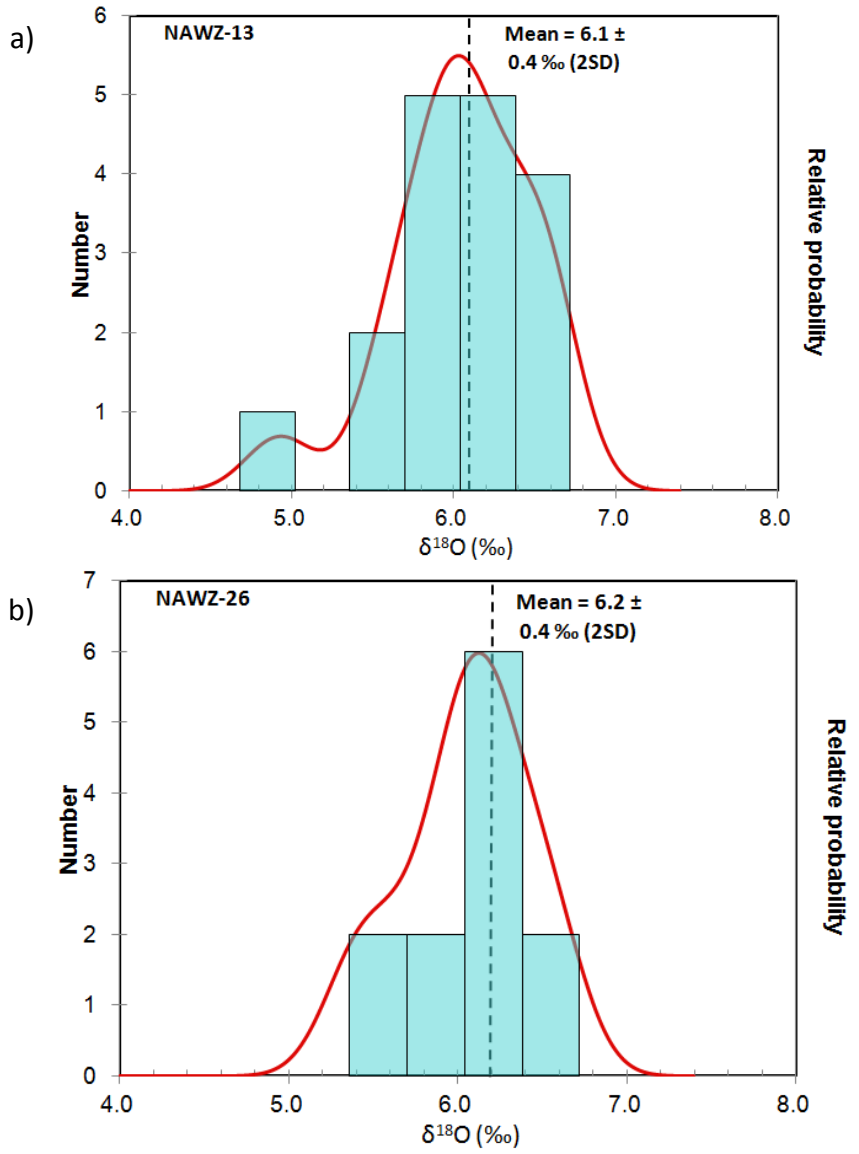

Figure 20. Cumulative probability plots for $\delta^{18}O$ in zircon. Sample name given in each. Dashed lines indicate mean of each sample population and errors reported from zircon standard R33 (2SD). Plots generated using Isoplot 3.0 (Ludwig, 2003).

c)

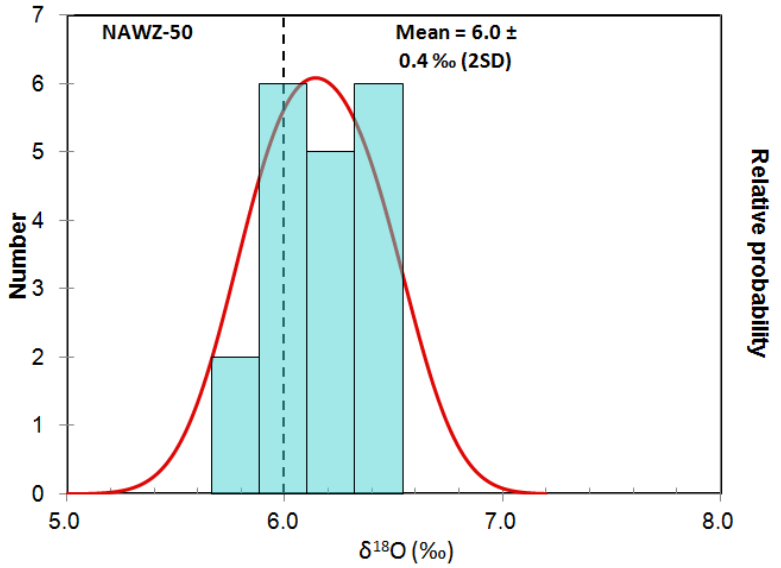

d)

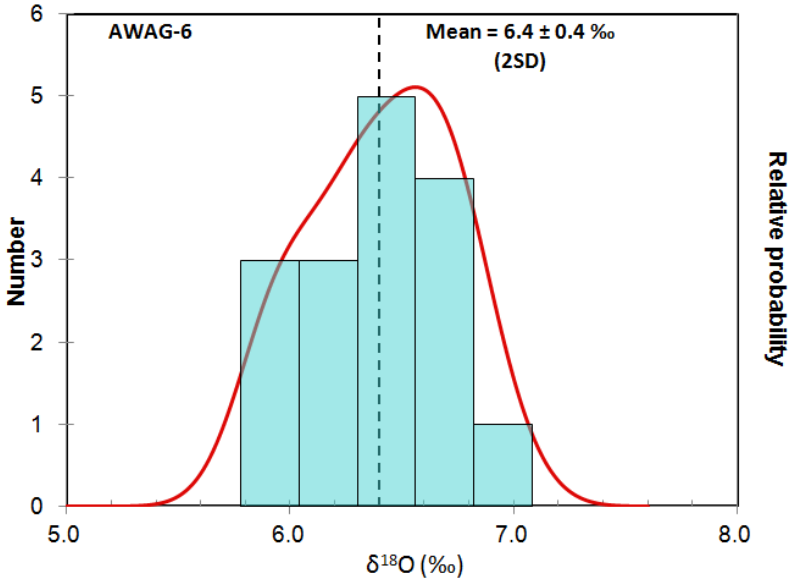

Figure 20 (continued)

e)

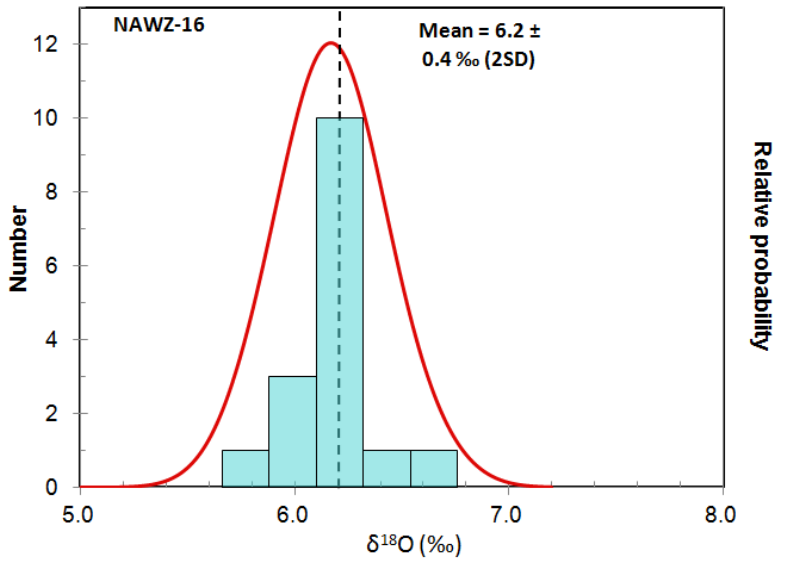

f)

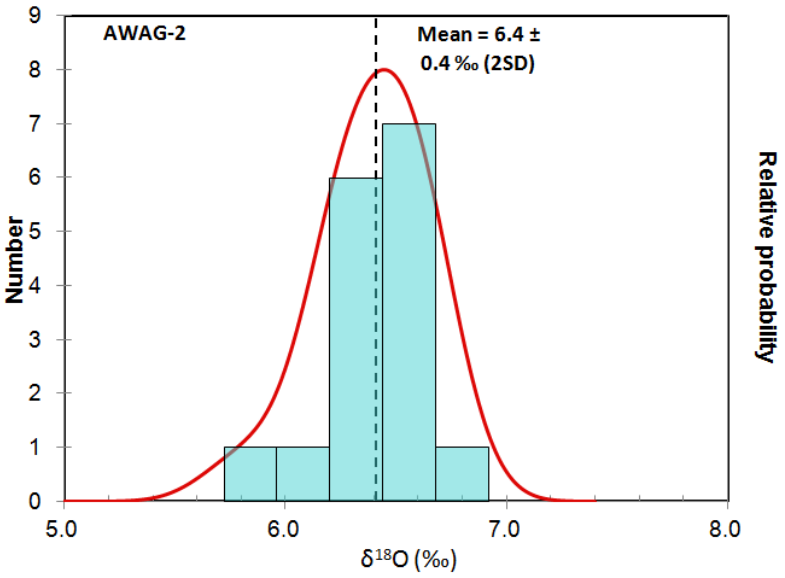

Figure 20 (continued)

g)

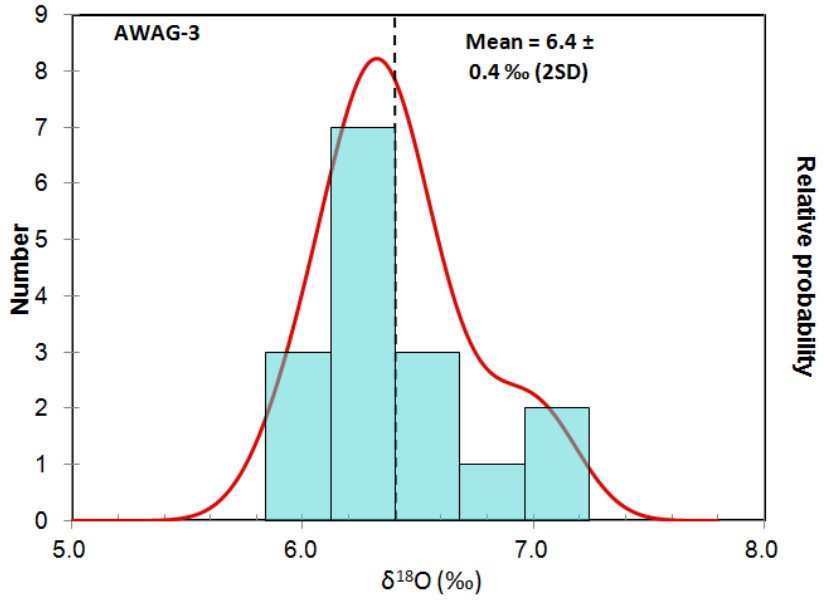

h)

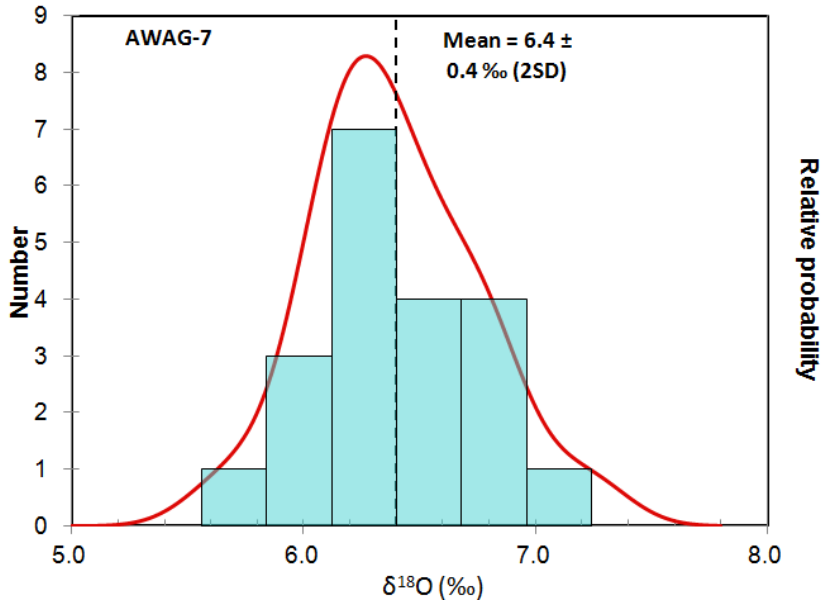

Figure 20 (continued)

i)

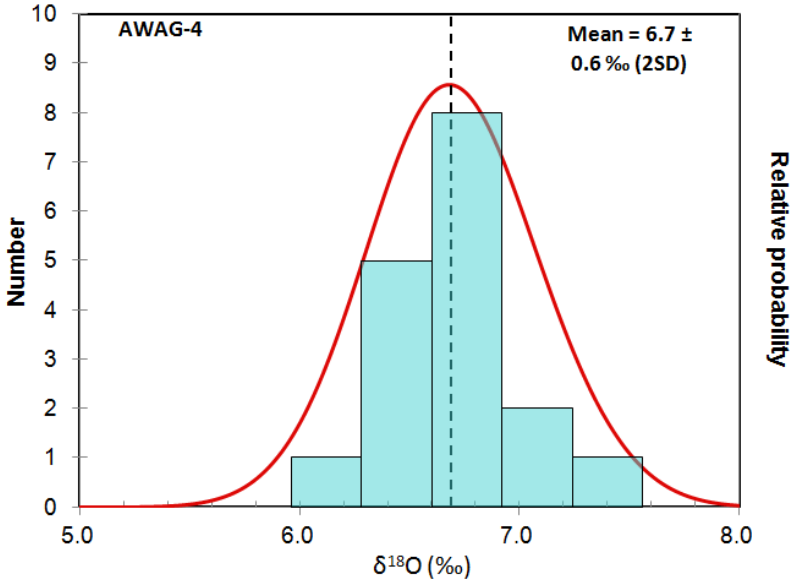

j)

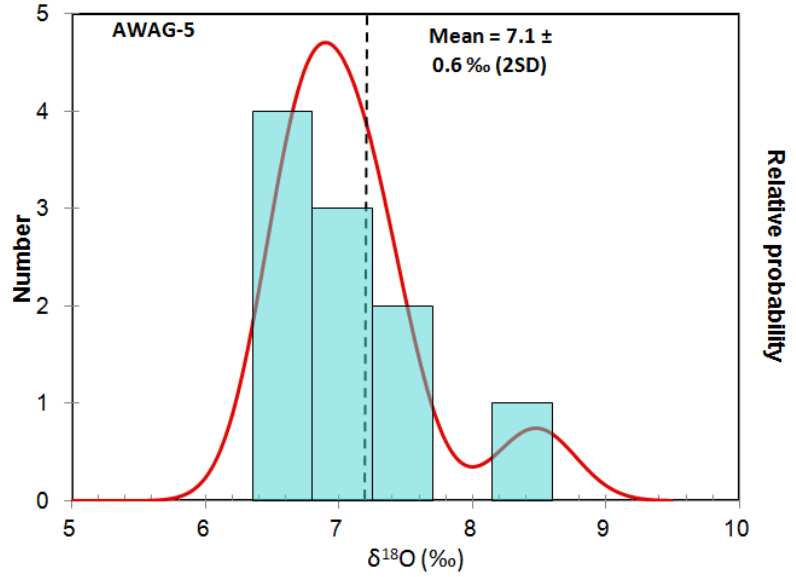

Figure 20 (continued)

k)

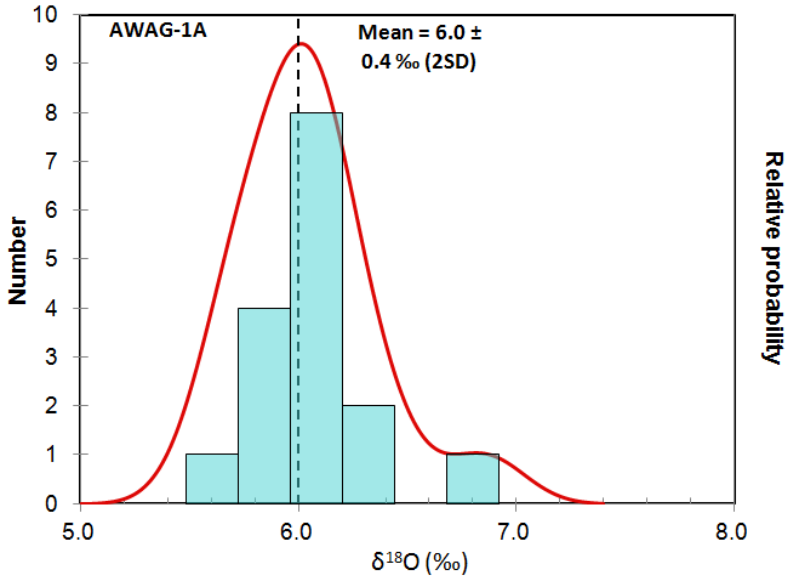

l)

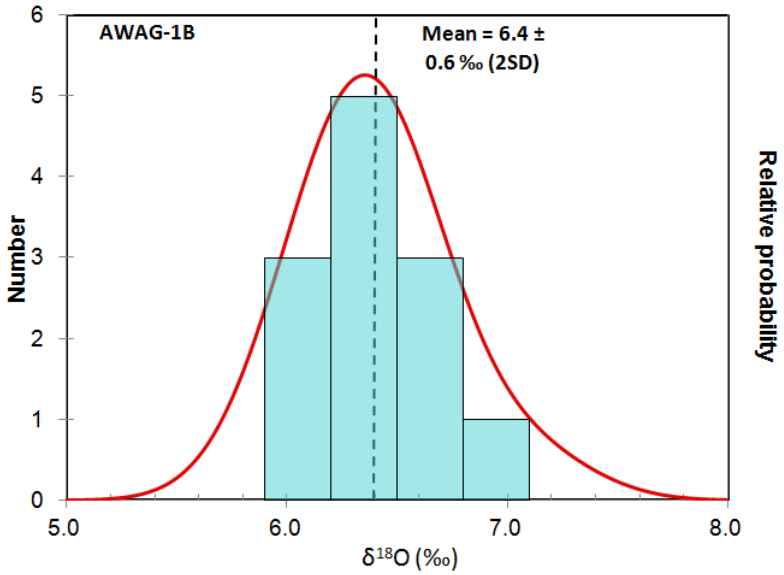

Figure 20 (continued)

m)

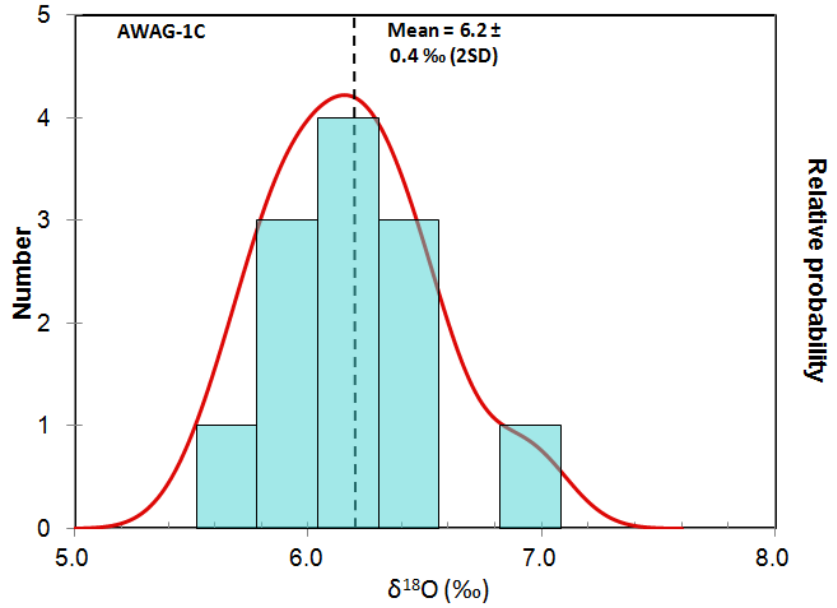

n)

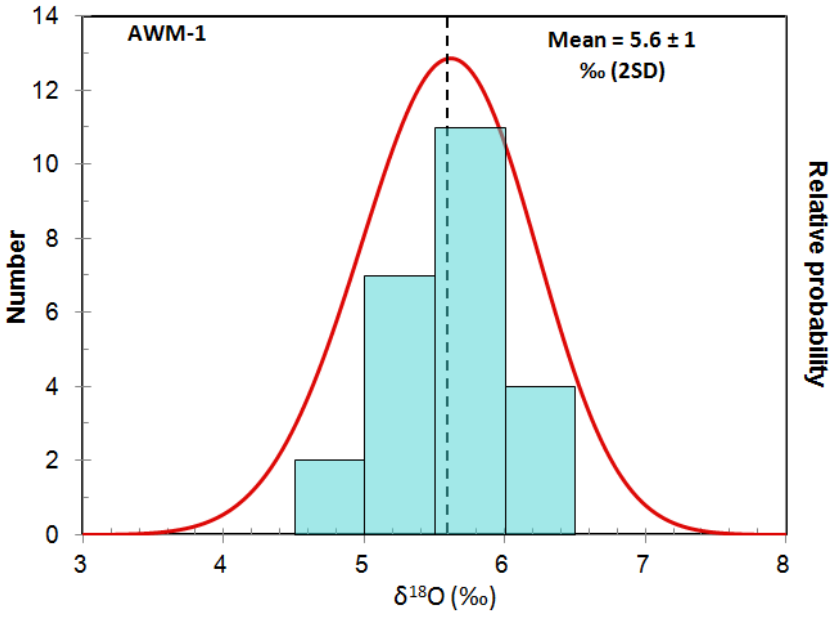

Figure 20 (continued)

o)

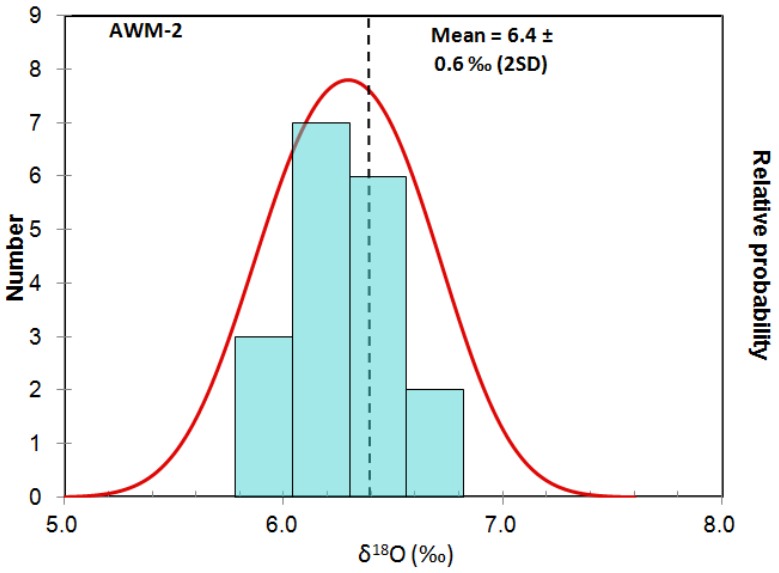

Figure 20 (continued)

Granites

Across the 4 granitic samples, 64 spots were measured for $\delta^{18}O$ (Figs. 20a-d). The total spread of data covers 2‰ (4.9 – 6.9‰). NAWZ-13 has the largest spread for the granite samples (1.7 ‰ difference) and contains the lowest $\delta^{18}O$ value of 4.9‰, which comes from a zircon core. In contrast the highest value of 6.9‰ (AWAG-6) is from a spot on the rim of a grain. The $\delta^{18}O$ means for each sample are as follows: NAWZ-13 = 6.0‰, NAWZ-26 = 6.1‰, NAWZ-50 = 6.2‰, AWAG-6 = 6.4‰.

Mechanically Contaminated

The total spot count for the mechanically contaminated samples was 68 (Figs. 20e-h). Total spread of $\delta^{18}O$ values for this unit type is 1.5‰ (5.7 to 7.2‰), seen in sample AWAG-7. Overall, data for these samples can be largely bracketed between $\delta^{18}O \approx 6.0 – 6.6‰$. AWAG-3 has a similar range in $\delta^{18}O$ as AWAG-7 of 1.2‰ (5.9 – 7.1‰). Sample NAWZ-16 has the lowest mean (6.2‰) and has a relatively homogeneous population of results, consistently plotting around the mean. All other samples have a mean of 6.4‰.

Grey Hybrids

The $\delta^{18}O$ values from 27 spots in zircons from the grey hybrids are the highest of all units in the Aztec Wash pluton (Figs. 20i and 20j) No spot has a $\delta^{18}O$ below 6.2‰. The highest $\delta^{18}O$ value of 8.5‰ is found close to the rim of a well-zoned grain in AWAG-5 and is a distinct outlier in the O data set as a whole. AWAG-5 shows the highest levels

with spots measuring consistently above 7.0 ‰ with a mean of 7.1‰. AWAG-4 has a sample mean of 6.7‰, which is distinctly higher than the mean of samples from the other groups.

Dark Pods

For the three samples analyzed for $\delta^{18}O$, 40 spots were produced (Figs. 20k-m). Values for the dark pod samples range from 5.6 to 7.1‰. AWAG-1A and C have a very similar total data spread with $\delta^{18}O$ values between 5.6 to 6.9‰. AWAG-1B overall has slightly elevated $\delta^{18}O$ values between 6.0 to 7.1‰. Means of AWAG-1A, B and C also support this notion (6.0‰, 6.4‰, and 6.2‰ respectively).

Mafic Sheets

The two mafic sheet samples yielded 42 data points for $\delta^{18}O$ and each perhaps shows contrasting magmatic histories (Figs. 20n and 20o) The total spread in $\delta^{18}O$ ranges from 4.7‰ and 6.6 ‰. AWM-1 has a mean = 5.6‰ with 6 spots having $\delta^{18}O$ <5.3‰). In AWM-2, $\delta^{18}O$ values range from 5.8 to 6.6‰ (mean = 6.3‰).

Zircon core-rim relationships

Highlighting definite differences in Hf isotopic compositions from core to rim on zircon grains becomes problematic due to the spot sizes. However, O isotope intragrain variation can potentially be observed because the beam sizes are smaller (25 microns). Figure 21 shows specific examples of this and provides a better understanding of how zonation on single grains may reflect the sample population. The grain in the granitic sample NAWZ-13 with the lowest $\delta^{18}O$ value in the entire dataset of 4.9‰ is a spot on the core of the grain. Figure 21a shows that a spot measured on the rim of this grain has a significantly increased $\delta^{18}O$ value of 5.6‰. In a separate granitic sample (AWAG-6) the highest $\delta^{18}O$ value of 6.9‰ was measured on the rim of one zircon and is the highest measured among the granites (Fig. 21b). Analysis of the core of this grain gave a $\delta^{18}O$ value of 6.3‰; an increase of 0.6‰ from core to rim. This is not the overall pattern in this sample: one grain shows a consistent $\delta^{18}O$ levels at 5.9‰ and another shows apparent fluctuations in the $\delta^{18}O$ of the melt during grain growth. Changes in $\delta^{18}O$ values are not, however, limited to the granitic samples (Fig. 21c). The grain with highest $\delta^{18}O$ in the whole dataset (8.5‰) is found in a Grey Hybrid sample (AWAG-5); the respective core gave a value of 7.1‰ (Fig. 21c); a 1.4‰ core-to-rim increase. A second grain studied in this sample also shows core-to-rim variation (0.2‰) that is within the external reproducibility.

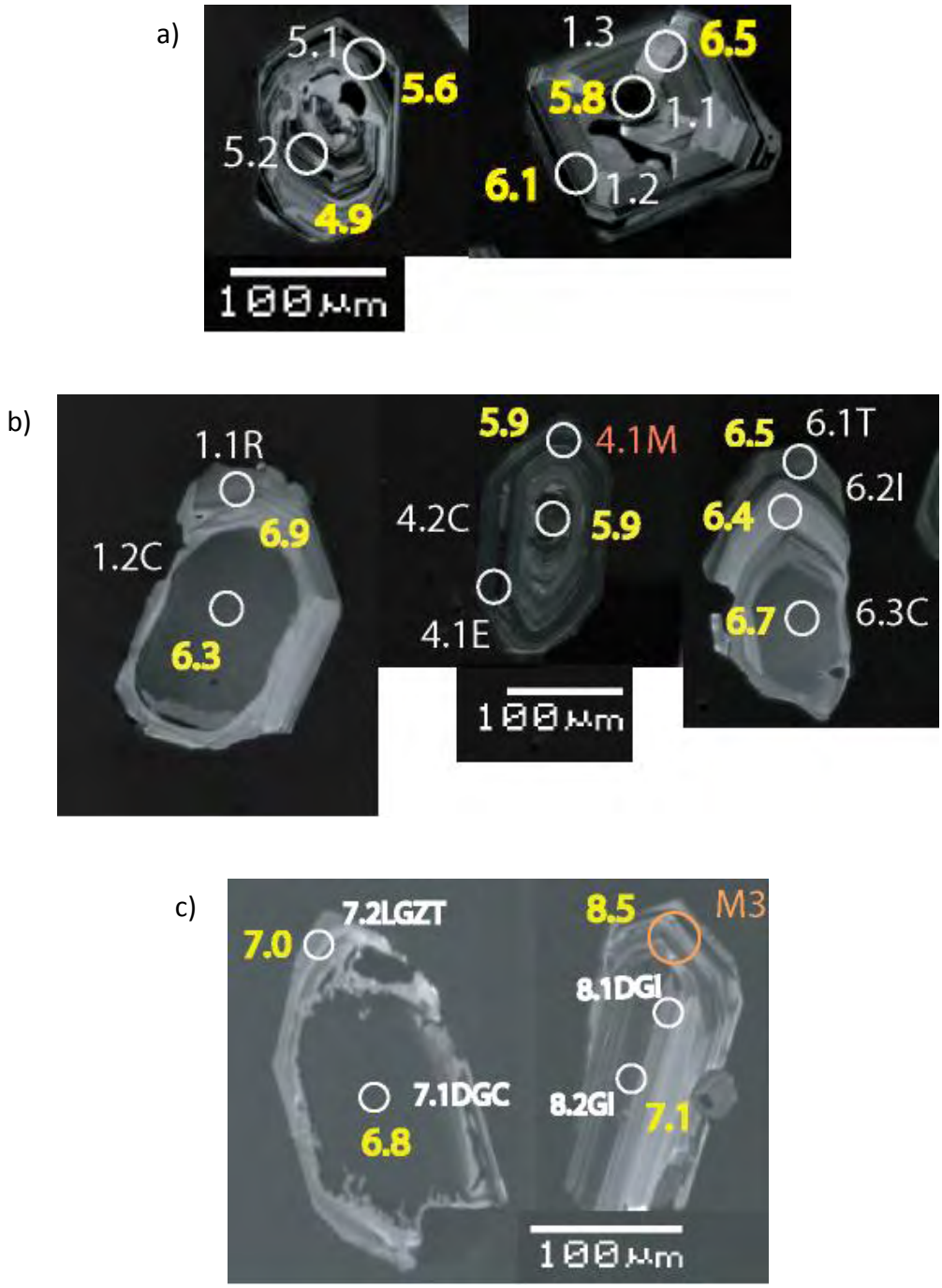

Figure 21. Cathodoluminescence images for targeted zircon grains highlighting $\delta^{18}O$ core-rim relationships. Grains are from samples NAWZ-13 (a), AWAG-6 (b), and AWAG-5 (c). Spot locations and names are shown (white/red) along with $\delta^{18}O$ values (yellow). Figures illustrate increases, decreases and fluctuations in $\delta^{18}O$ values in all zircon sample populations.

Combined Hafnium and Oxygen in Zircon

Plotting all samples on a Hf-O covariation diagram shows a large cluster of data points between εHf = -5 to -14, and $\delta^{18}O$ = 5.5 to 7.0 with varying but generally a large degree of overlap between samples across unit types (Fig. 22a). This cluster generally has a 'fan-like' pattern with increasing $\delta^{18}O$ and εHf increasingly spreading out over a broad range between relatively high values and relatively low values. Increasing $\delta^{18}O$ is generally negatively correlated with εHf, but not necessarily at the scale of a single sample. Sample AWM-1 (mafic sheet) has the lowest $\delta^{18}O$ and highest εHf in the data set and thus anchors the high εHf-low $\delta^{18}O$ terminus of the data fan. Only 2 noticeable outliers exist for the entire data set: the zircon rim from AWAG-5 (grey hybrid) that has anomalously high $\delta^{18}O$ = 8.5‰ (at an εHf = -14.2) and NAWZ-13 (granite) with anomalously low εHf (-25.7 at $\delta^{18}O$ = 5.6‰). Possible mixing curves are shown on Figure 22b and are discussed later.

a)

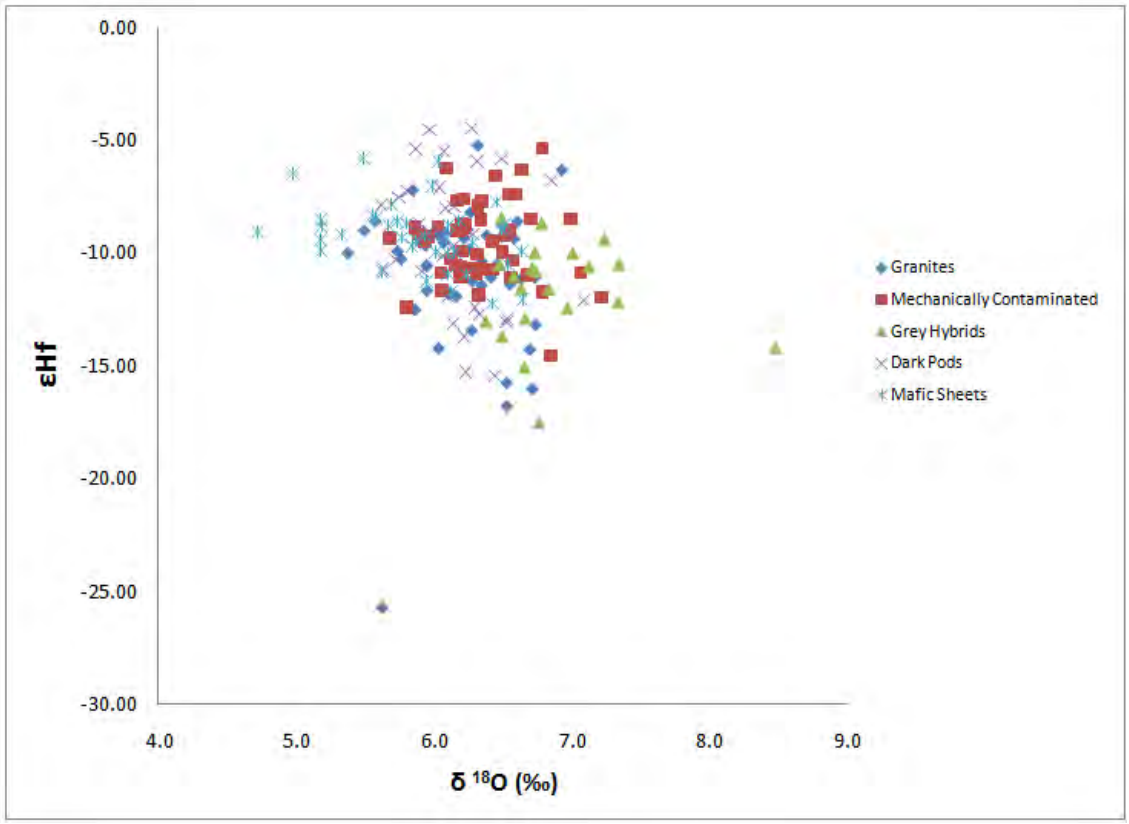

Figure 22. Combined Hf vs O isotopic data (a). Proposed mixing curves of Hf and O isotopes for Proterozoic basement rock with depleted mantle or enriched mantle (b).

b)

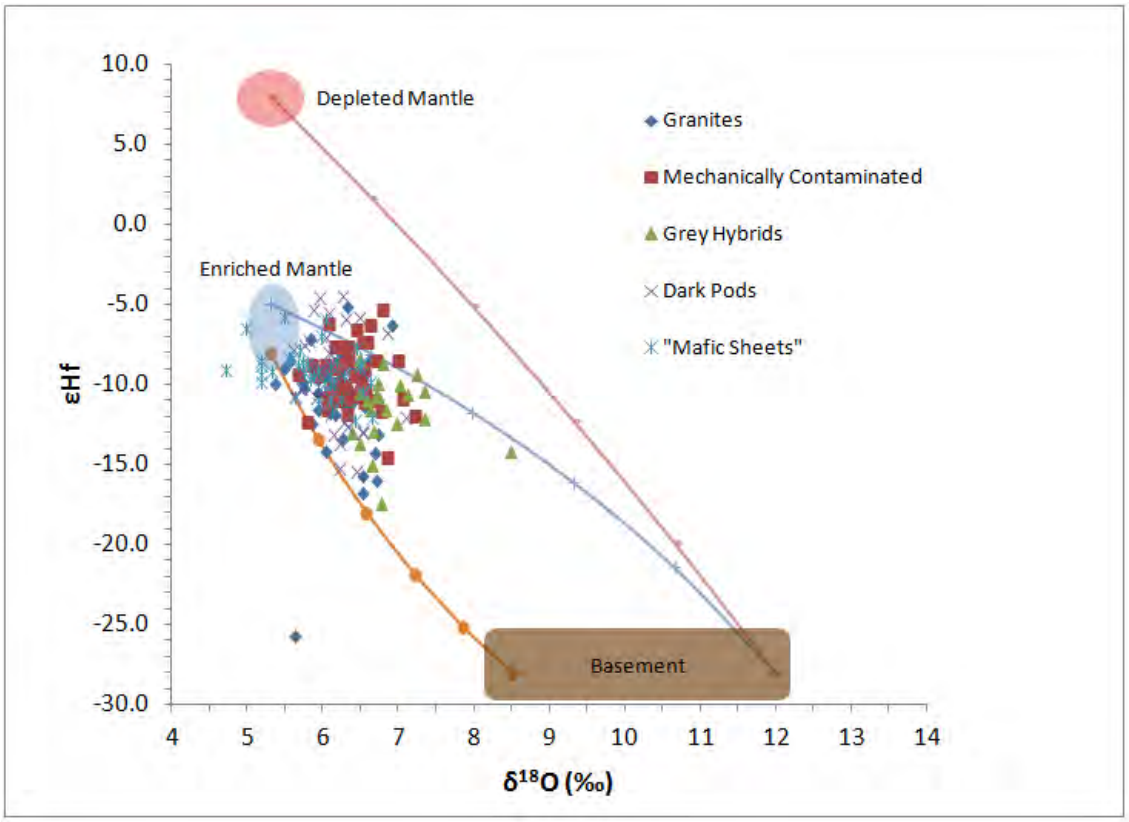

Figure 22 (continued). Data used for mixing curves: Enriched Mantle: Hf = 5ppm εHf = -5 and -8 (this study), $\delta^{18}O$ = 5.3 (based on uncontaminated mafic sheets); Depleted Mantle: Hf = 7ppm, εHf = +8 (Beard and Johnson, 1997), $\delta^{18}O$ = 5.3; Precambrian Basement: Hf = 6ppm (Taylor and McLennan, 1995) εHf = -28, $\delta^{18}O$ = 8.5 (Kapp et al., 2002), and 12 (Bender et al., 1993). See Appendix I for full calculated mixing data.

Trace Element and Zr-in-Sphene Temperature Analysis

Rare earth element (REE) plots of sphene populations within each sample (Fig. 23) show a general pattern of greater concentration of lighter to middle REEs than the heavier REEs. This conforms well to the compatibility behavior of these elements within the sphene crystal lattice (Bachmann et al., 2005). Beyond this there are some patterns that can be highlighted between lithological types.

The most mafic samples (AWM-1 and 2) are enriched in light to middle REEs but are more depleted in heavier REEs than the more felsic samples, particularly in the single granitic sample (AWAG-6). Pure hybrids (AWAG-4 and 5) have relatively consistent REE patterns and Eu anomalies. However, the mechanically contaminated (AWAG-2, 3 and 7) and dark pod samples (AWAG-1A and 1B) show more variable patterns, including a positive Eu anomaly.

The total range of Zr-in-sphene temperatures measured ($T_{Zr\text{-}sphene}$) for all spots (n = 282) is 280°C (~630 – 910°C). A standard deviation of ± 12°C was assigned to all spots using the measurements taken from standard BLR, a_{TiO2} was set at 0.7, and a_{SiO2} was set to 0.7 for all calculated temperatures (see Section "Zirconium in sphene thermometry" for discussion of the thermometer). This is a remarkable spread in temperature given the few studies that have so far employed the Zr-in-sphene thermometer of Hayden et al (2008). Colombini et al. (2011) concluded that sphene typically does not crystallize until very late and reported temperatures of 750°C or less, although their study focused

exclusively on granite/rhyolite systems. Moore and Sisson (2008) also reported temperatures generally well below 800°C but their study focused on granodiorite intrusions in the Sierra Nevada. The felsic samples in this study also generally show relatively low $T_{Zr\text{-}sphene}$ but the mafic samples (mafic sheets and dark pod especially) show crystallization at much higher temperatures.

Sample AWAG-1A has the largest $T_{Zr\text{-}sphene}$ spread encompassing 251 °C (656 – 907°C), and AWAG-5 has the smallest temperature range (69 °C or 698 – 767 °C). Excluding an outlier the second grey hybrid sample (AWAG-4) has a similar narrow range in temperatures (72°C or 673 – 745°C). The two mafic samples (AWM-1 and 2) have a wide range of crystallizing temperatures of 668 – 884°C and 679 – 868°C, respectively. Inclusive of an outlier the single granitic sample (AWAG-6) has a relatively large range of $T_{Zr\text{-}sphene}$ temperatures of 205°C (between 684 – 889°C). The mechanically contaminated samples (AWAG-2, 3 and 7) cover a temperature range of 174°C (631 – 805°C) with AWAG-7 having the highest variability (161°C). Figure 24 shows these values plotted against related bulk Zr saturation temperatures ($T_{Zr\text{-}sat}$) for each sample. Although there appears to be minor overlap with some samples (AWM-1, 2, AWAG-1A and 1B), overall there does not appear to be any relationship between $T_{Zr\text{-}sphene}$ and $T_{Zr\text{-}sat}$ meaning $T_{Zr\text{-}sphene}$ is likely to be independent of Zr saturation in the melt. Probability curves were produced using the one standard deviation error to illustrate any possible heterogeneity in the sample population (Fig. 25). The plots were merged with probability curves of $T_{Ti\text{-}zircon}$ data from Bromley (2008) to analyze any potential crystallizing relationships. The

plots suggest that heterogeneity does exist across all samples apart from AWAG-5 (Fig. 25f), which shows minimal variability but still lacks a normal distribution. This heterogeneity may be a product of either magma chamber dynamics or multiple episodes of sphene crystallization.

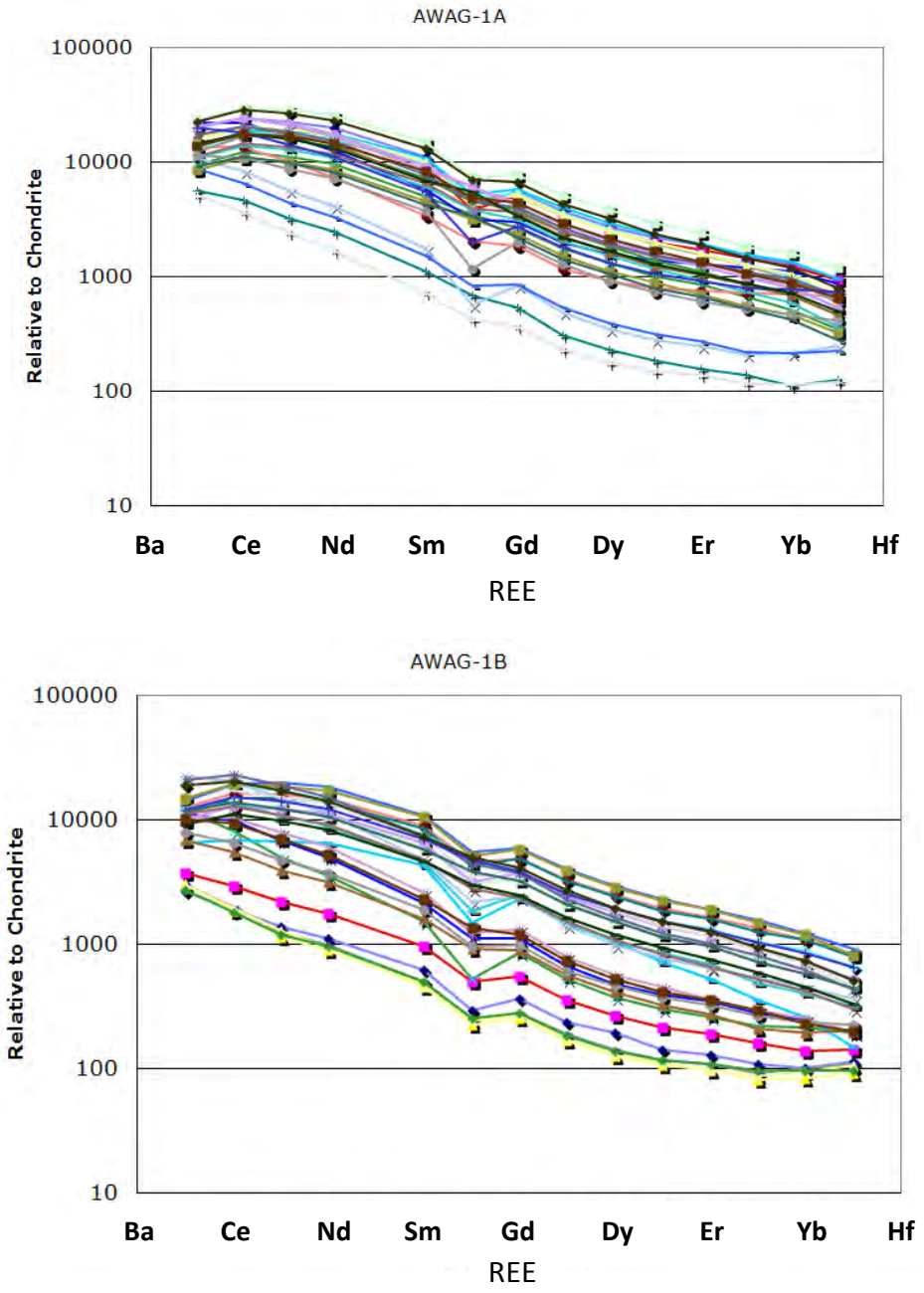

Figure 23. REE concentration diagrams of sphene. Data normalized to chondrite following Anders and Grevesse (1989).

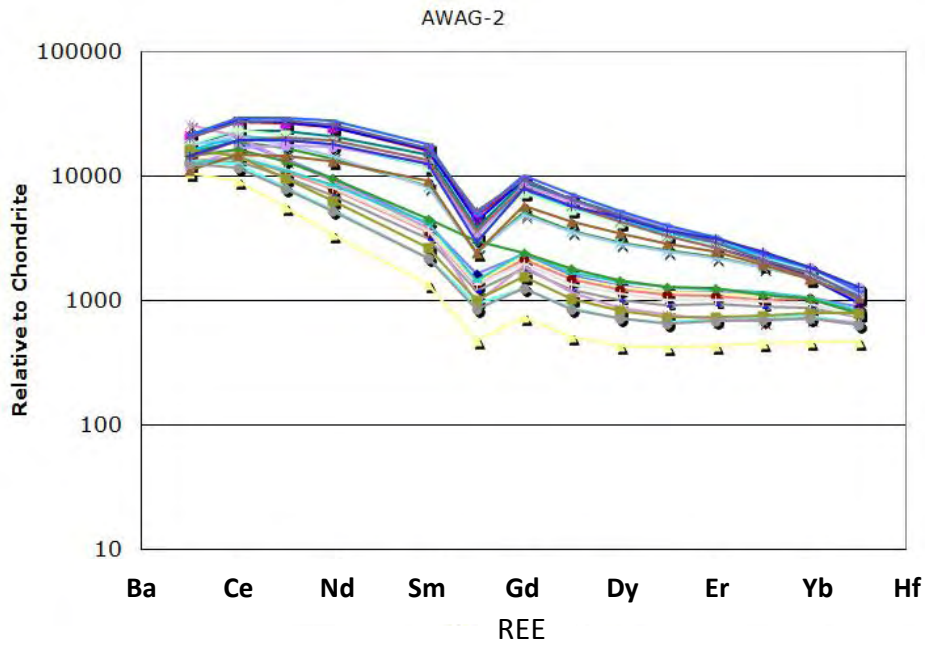

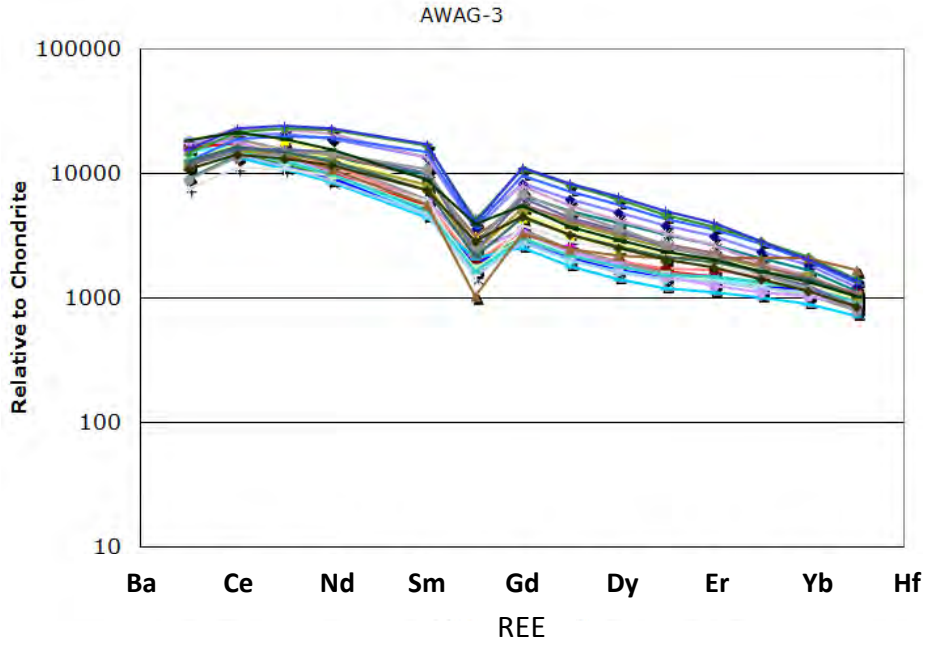

Figure 23 (continued)

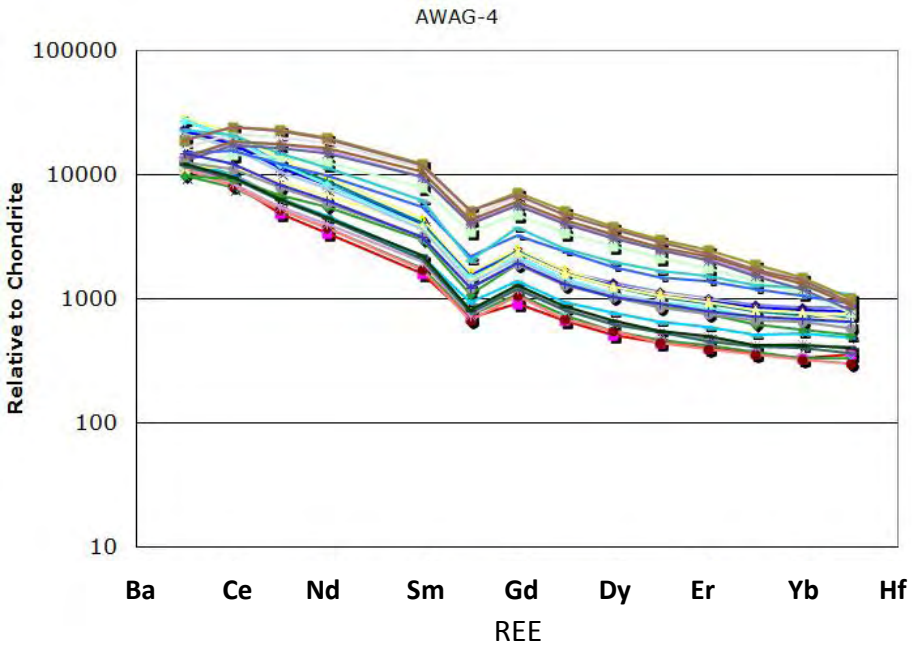

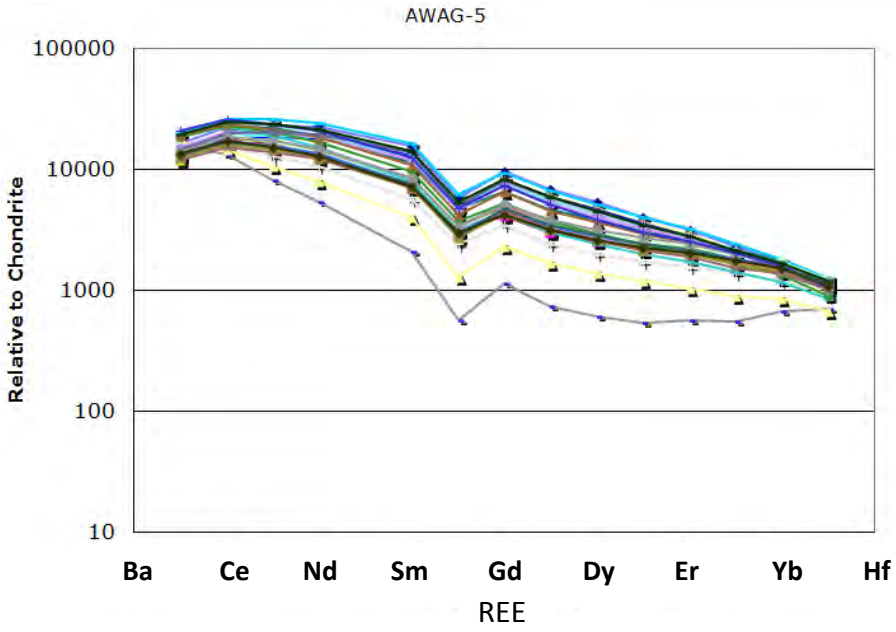

Figure 23 (continued)

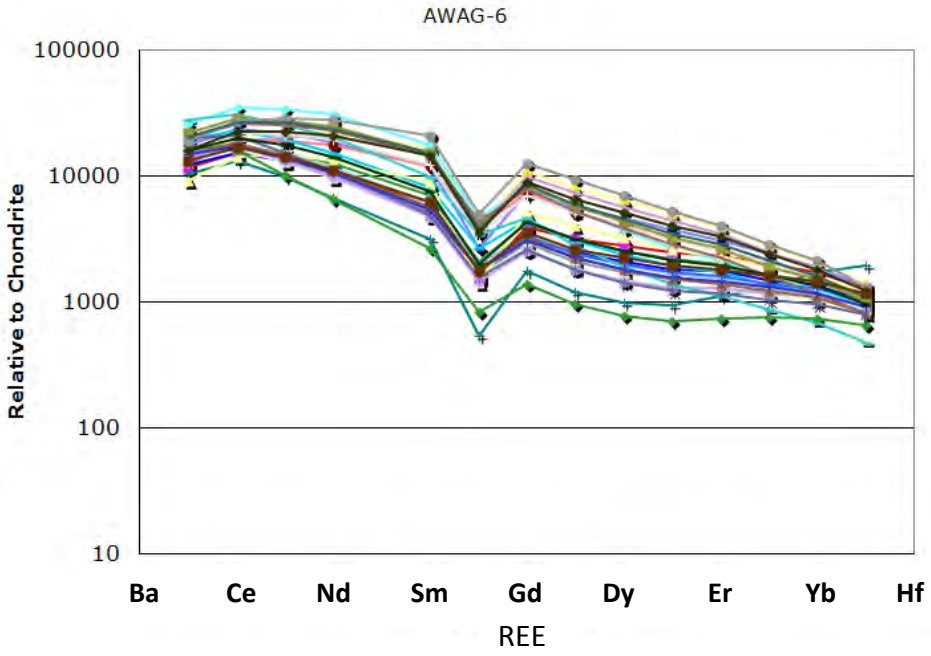

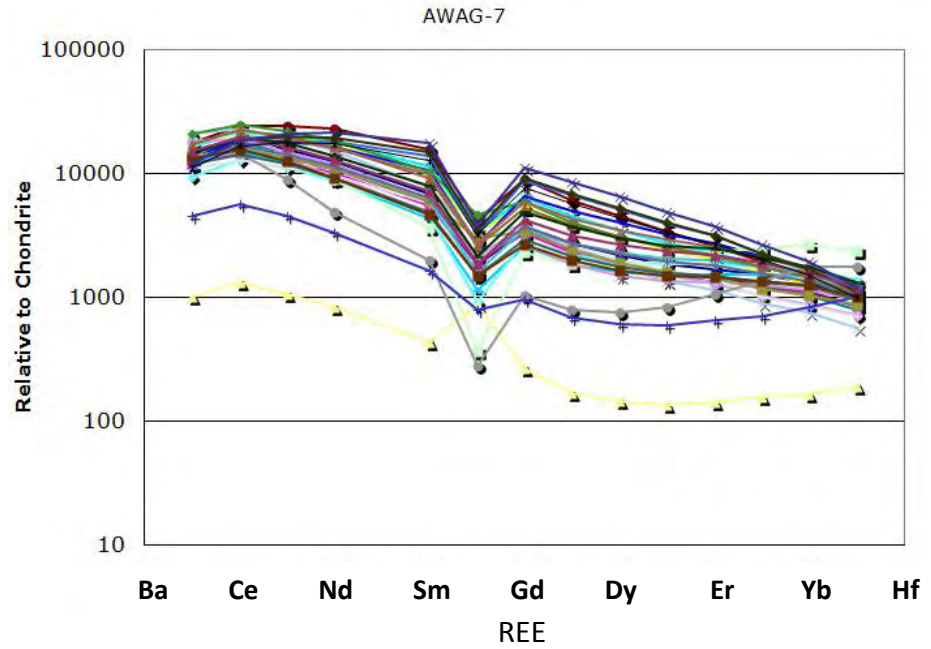

Figure 23 (continued)

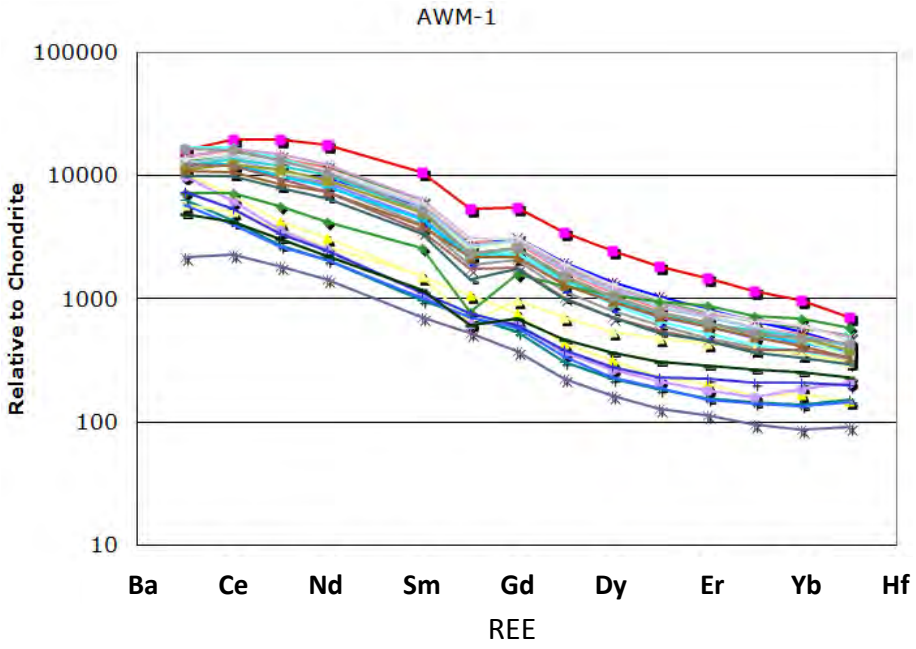

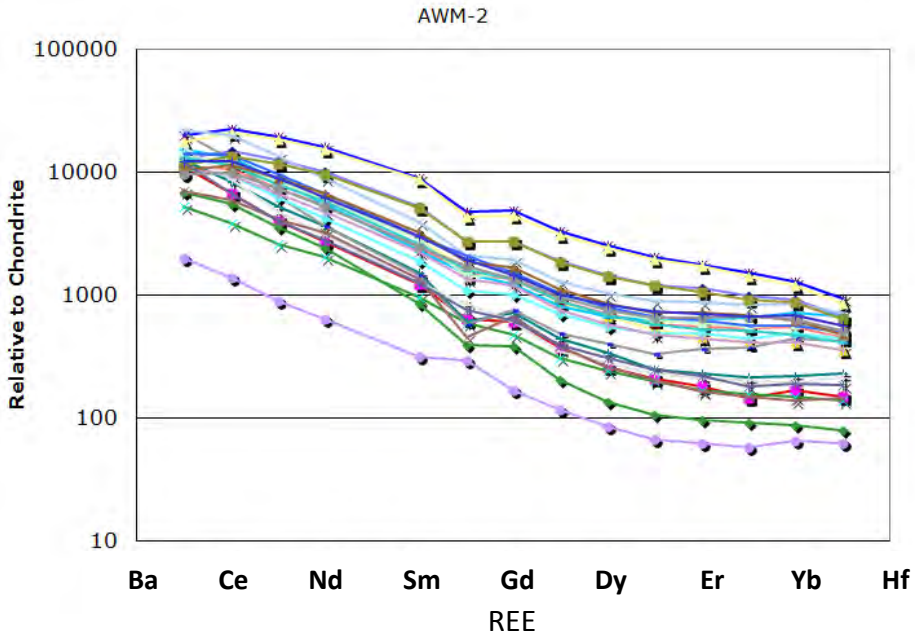

Figure 23 (continued)

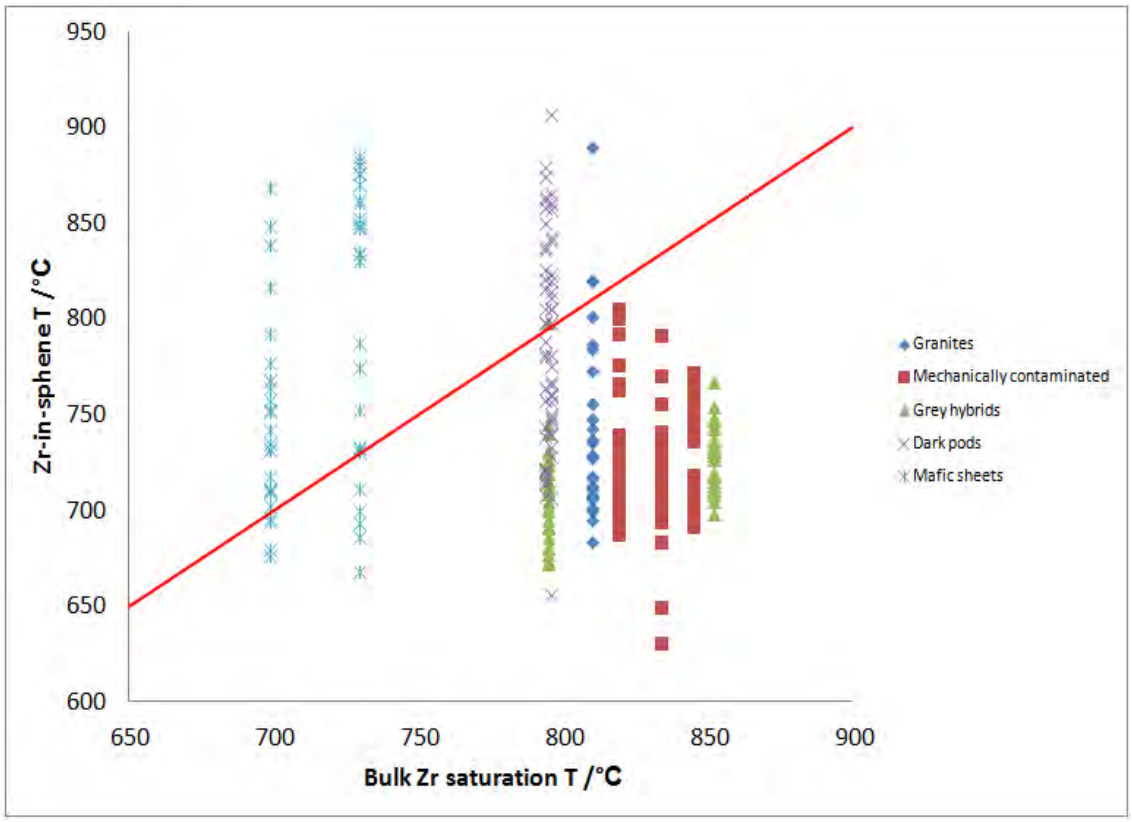

Figure 24. Zr-in-sphene temperature vs. bulk Zr saturation temperatures. Saturation temperatures calculated using data from this study, Ericksen (2006) and Bromley (2008).

Granites

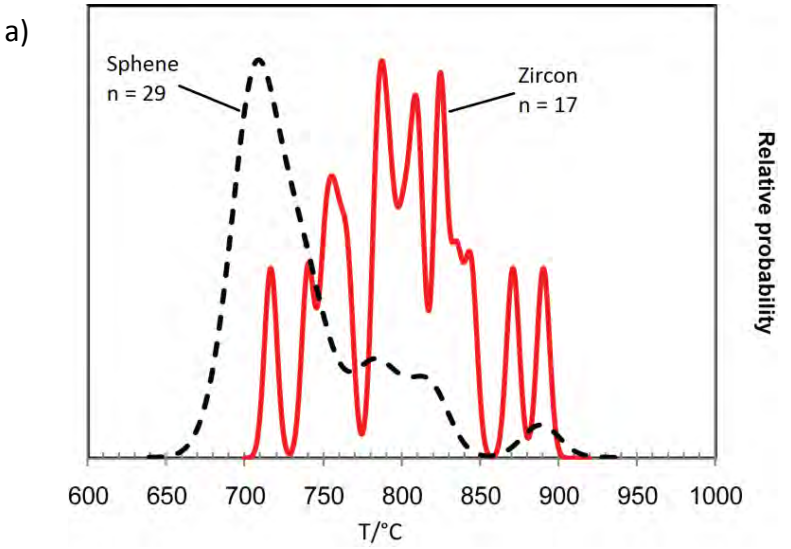

Mechanically Contaminated

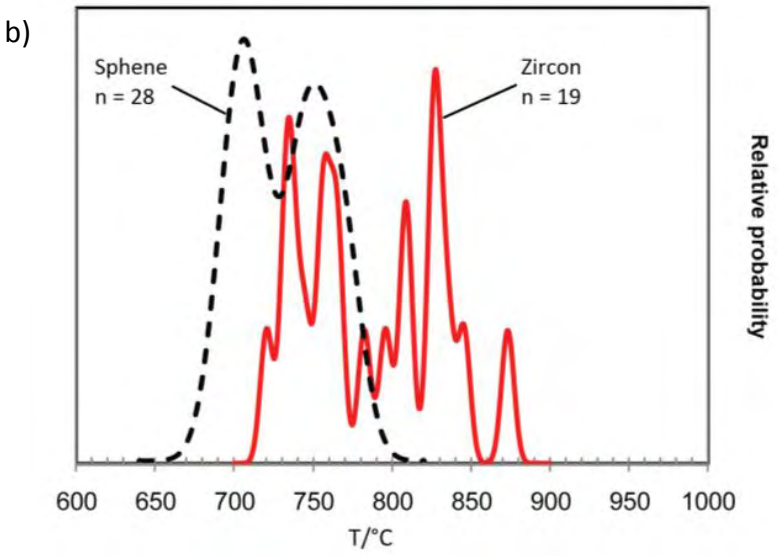

Figure 25. Cumulative probability curves of Zr-in-sphene (dashed black) and Ti-in-zircon (solid red). Temperature data for zircon taken from Bromley (2008). Curves created using Isoplot 3.0 (Ludwig, 2003).

c)

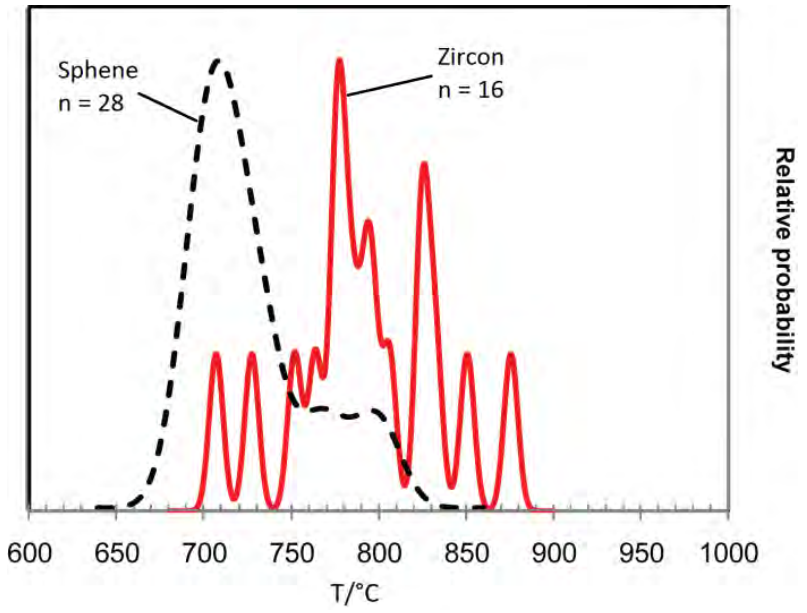

d)

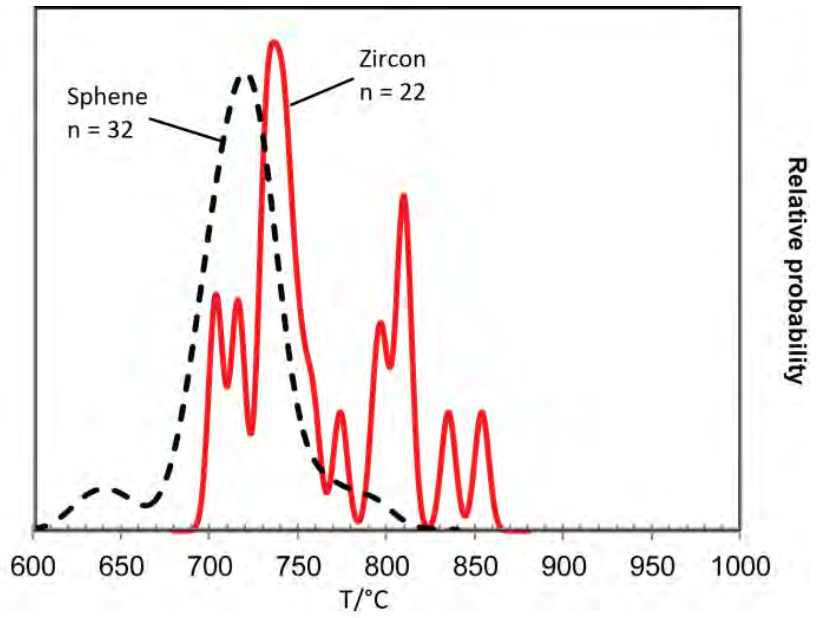

Figure 25 (continued)

Grey Hybrids

e)

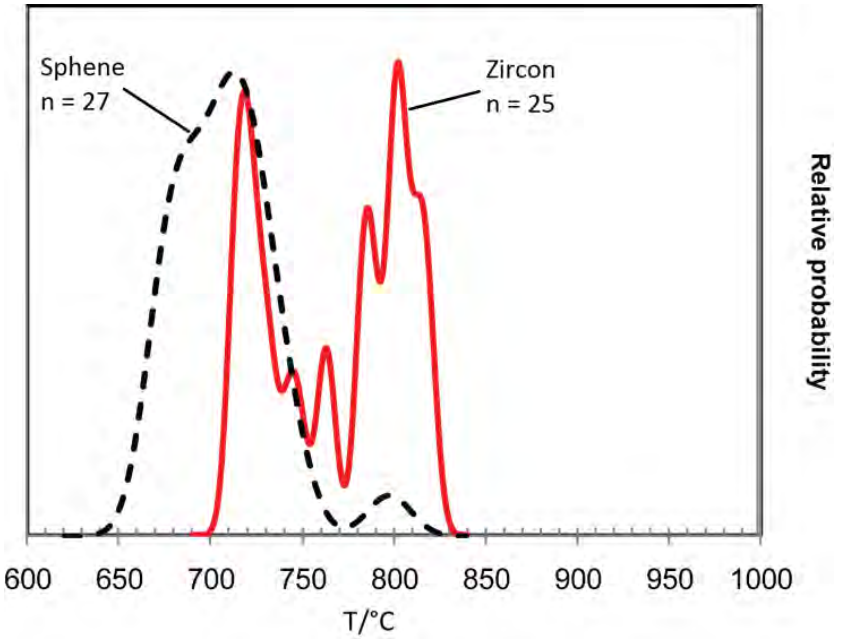

f)

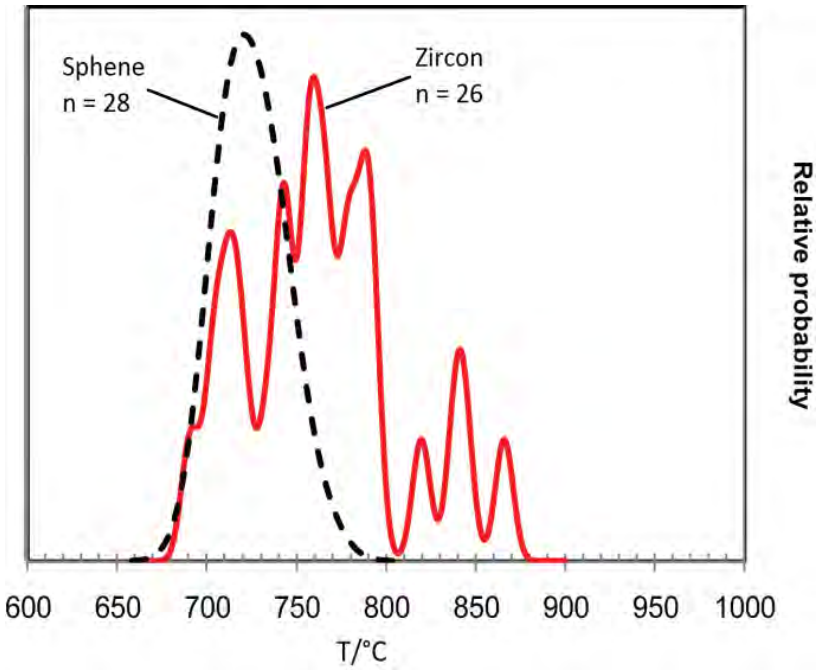

Figure 25 (continued)

Dark Pods

g)

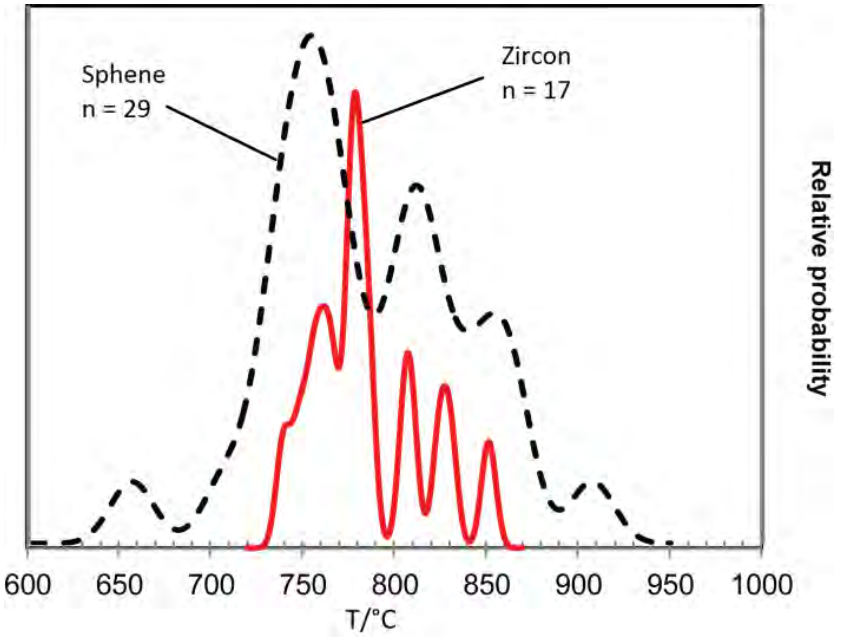

h)

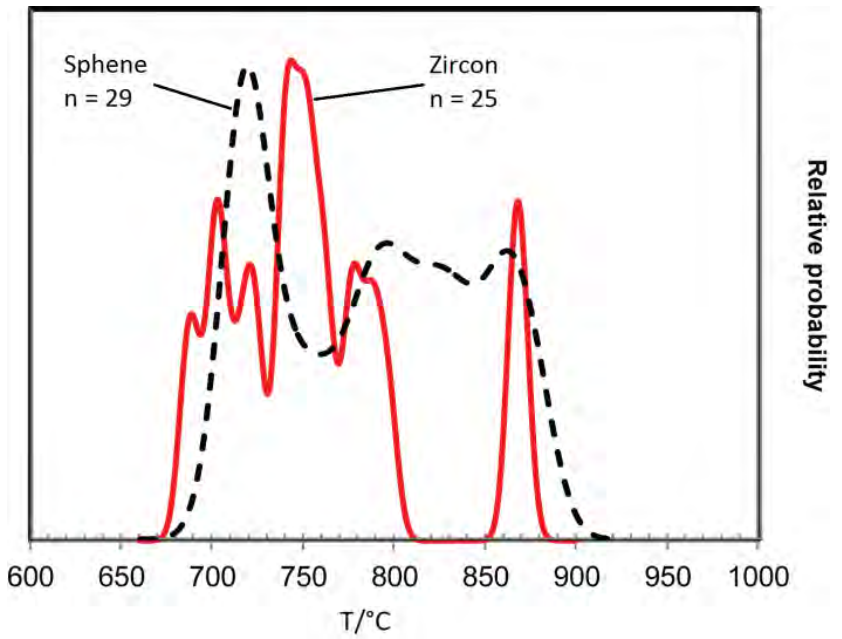

Figure 25 (continued)

Mafic Sheets

i)

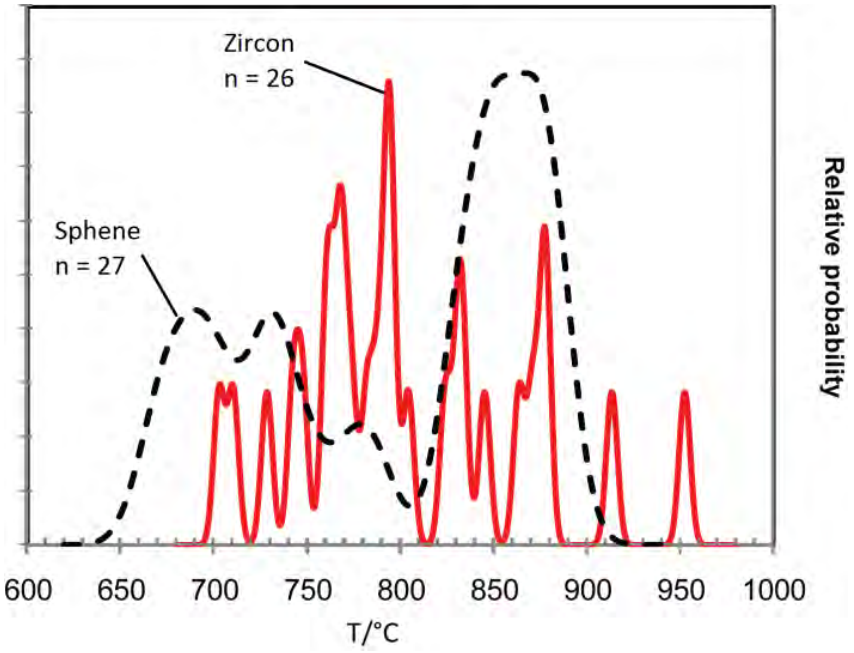

j)

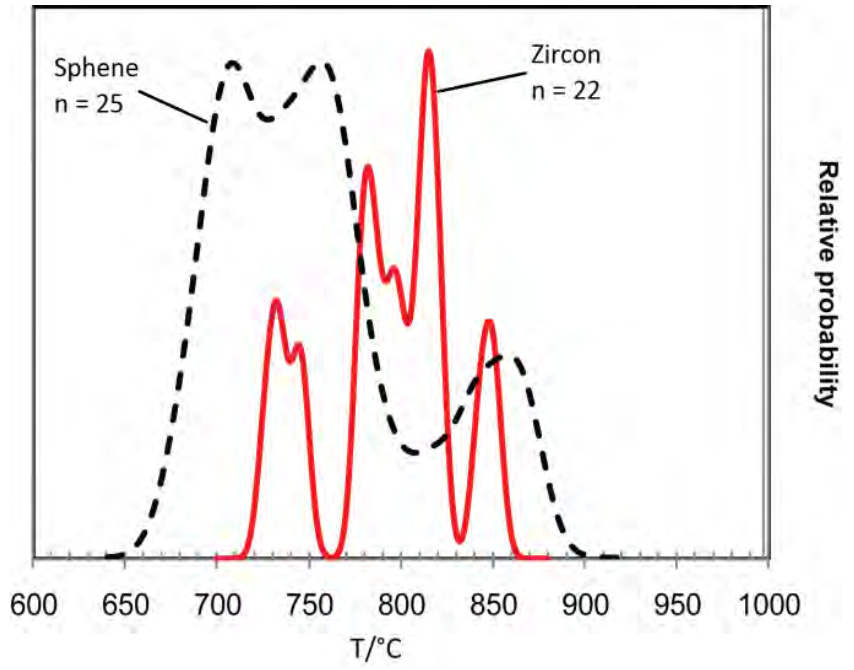

Figure 25 (continued)

DISCUSSION

The Heterogeneous Zone of the Aztec Wash pluton is widely accepted to have grown from repeated injections and mixing of mafic and felsic magmas (Robinson and Miller, 1999; Harper et al., 2004; Ericksen, 2006; Bromley, 2008). Previous whole-rock isotopic studies within the Heterogeneous Zone indicated that mixing involved an enriched mantle source (Falkner et al., 1995; Ericksen, 2006) and Precambrian basement (Ericksen, 2006). Varying degrees and types of interaction between mafic and felsic end-members, including physical mixing of magmas, mixing of crystal-poor magmas and crystal mush, mixing of magma with fully solidified chunks of pluton (autolithic breccias), and more intimate mixing at the scale of chemical diffusion (Ericksen, 2006), led to a spectrum of hybrid materials. This form of incremental pluton construction agrees well with the model proposed by Wiebe (1996). Injection of mafic magmas into felsic units is known to cause widespread *in-situ* diffusion between compositionally distinct melts, which can drastically alter bulk rock geochemistry, particularly for Sr and Nd isotopes (Waight et al., 2001). Ericksen (2006) found, however, that mixing and hybridization of melts in the Heterogeneous Zone is not a simple binary process between two isotopically distinct (e.g., mantle and crust) components, and that the measured isotopic ratios of Sr and Nd are a product of multiple mixing pathways and multiple isotopic components (Fig. 5). The new whole-rock isotopic data in the present study support the operation of widespread open-system processes as suggested in

earlier studies, and the scatter of the data argues for multicomponent mixing (i.e., not binary mixing) (Figs. 10 - 13).

The complex exchange between chemically distinct melts is relatively difficult to monitor in the whole-rock isotope data of the Aztec Wash pluton. Work by Bromley (2008) highlighted the importance of Hf concentrations in zircon as a proxy for the compositional nature of the melt during crystal growth, tracking both positive and negative correlations with temperature from core to rim, which imply new influxes of magma. In addition, CL image analysis provided further evidence of melt rejuvenation and compositional changes with frequent occurrences of resorption textures and sector zoning; both features are common in igneous zircon where the zircon saturation of the melt fluctuates (Robinson and Miller, 1999; Corfu et al., 2003). Extending the isotopic analysis to the crystal scale reveals important new insights concerning mixing processes.

A critical issue not addressed in earlier studies was the degree to which the mixed isotopic signatures were the result mainly of interaction of isotopically distinct magmas prior to emplacement, rather than *in-situ* mixing within the magma chamber. Field evidence would suggest the latter as the dominating mechanism, but not until this study has the problem been broached in such detail.

The zircon εHf and $\delta^{18}O$ zircon spot values reveal isotopic variation that is considerably greater than observed on the hand-sample scale. This is particularly evident when εHf(zirc.) is plotted against εHf(WR) (Fig. 17), where total spread of εHf(WR) is approximately 7 epsilon units yet εHf(zirc.) ranges up to 11 epsilon units in a

single sample (AWAG-1C). Beyond analytical error, εHf(zirc.) values plot above and below the εHf(WR) means, so single-grain analysis is able to 'see through' the bulk rock composition providing evidence for interaction of multiple isotopic components in all samples. In nine of the 15 samples, representing the complete range of bulk compositions in Aztec Wash, whole-rock εHf values are restricted to two epsilon units despite containing zircons in which the range of εHf values is typically 2 to 3 times as great.

Plotting εHf(zirc.) vs. SiO_2 underscores the very complicated mixing processes involved in producing the Hf isotopic signatures of all samples (Fig. 26). Other than the one granite outlier, this plot shows that the Hf isotopic composition of zircon is effectively decoupled from bulk composition. High εHf components indicative of mantle-derived magmas and low εHf components indicative of continental crustal components are present in the most mafic samples and the most felsic samples.

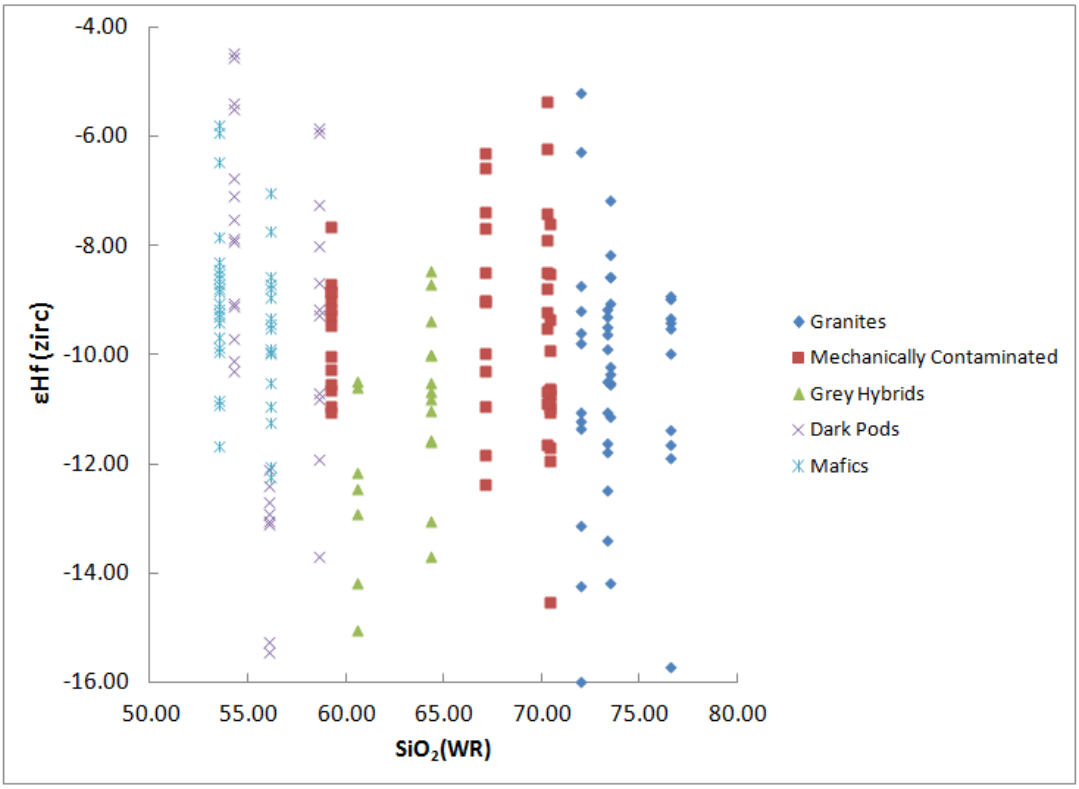

Figure 26. εHf in zircon vs. whole-rock SiO_2.

When $\delta^{18}O$(zirc.) is plotted against whole rock SiO_2, a similar open-system behavior is apparent (Fig. 27). Although the 2‰ range of $\delta^{18}O$ for all spots (exclusive of outliers) is relatively limited it still exceeds the likely shift in $\delta^{18}O$ of a melt undergoing fractional crystallization. An increase in 30 wt% SiO_2 in the melt increases $\delta^{18}O$ by 0.5 to 1‰ at most (Bindeman et al., 2008) but samples AWAG-7 and NAWZ-26 show a 1.2‰ change. Changing the $\delta^{18}O$(zirc.) by this amount requires open system contamination (Valley et al., 2003; Appleby et al., 2008). In addition the samples with highest silica content (73-77 wt% in granites) do not correspond to zircons with the highest $\delta^{18}O$. These values are dominantly in the intermediate units (60 – 64 wt%), which yielded the highest $\delta^{18}O$ values in the data set and suggest incorporation of new material with higher $\delta^{18}O$. The negative correlation between $\delta^{18}O$(zirc.) and SiO_2(WR) from intermediate toward the most felsic samples is more difficult to explain.

One complicating factor in interpreting this trend is the composition-dependent fractionation of O isotopes between zircon and melt (Lackey et al., 2008). Based on their large data set from Sierran plutons, Lackey et al. (2008) found that whole-rock compositions (presumably reflective of melt compositions) are shifted from +0.5‰ at 50 wt% SiO_2 to +2‰ at 70 wt% SiO_2 relative to zircon. Thus zircons in the granite samples would be in O isotopic equilibrium with melts that could have had $\delta^{18}O$ values +2‰ higher.

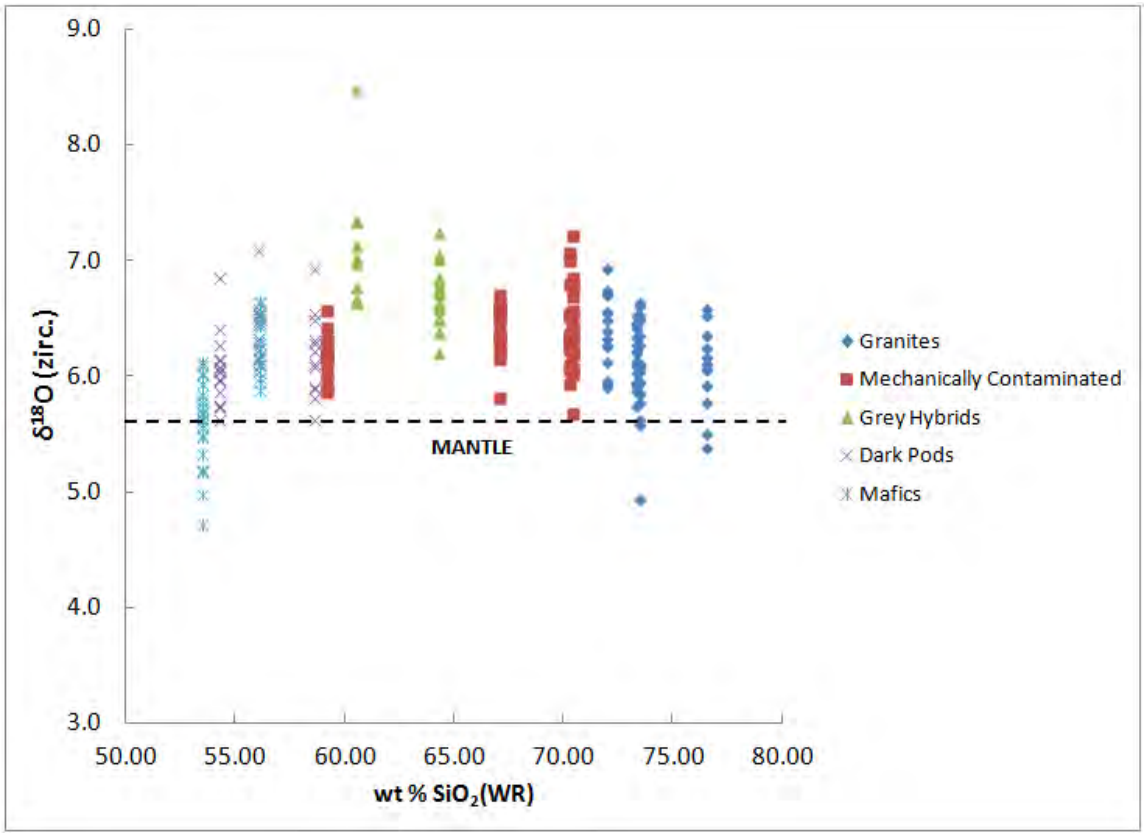

Figure 27. $\delta^{18}O$ of zircon vs. whole-rock SiO_2. Dashed line indicates accepted mantle $\delta^{18}O$ value (Valley et al., 2005).

Zircons from the intermediate samples would be in O isotopic equilibrium with melts that would have $\delta^{18}O$ values on the order of only +1‰ higher, so melt $\delta^{18}O$ values for the intermediate and felsic samples may not have been too dissimilar. No whole rocks were analyzed for O isotopes to better assess possible fractionations between zircon and melt, but the intrasample spread is incompatible with any simple fractionation-controlled O isotopic variation. It is very difficult to assess the O isotope composition of the melt during the growth of any particular zircon (or zone within a zircon) in a pluton like Aztec Wash, where the evidence for open system behavior is overwhelming, but systematic correlations of O isotopes with temperature may be fruitful.

Ion probe spots during measurement of $\delta^{18}O$ in zircon were made as close as possible to previously obtained Ti-in-zircon thermometry spots to look at possible core-to-rim correlations between temperature and O isotopic composition of individual grains (e.g., Appleby et al., 2008; Bindeman, 2008). Bromley (2008) demonstrated common core-to-rim temperature increases in zircon grains from all her samples indicating fresh input of melt, but there appears to be no systematic or correlated core-rim variation between $\delta^{18}O$ and temperature (Fig. 28). The mechanically contaminated units, for example, show evidence for both decreasing $\delta^{18}O$ with decreasing temperature and vice-versa (Fig. 28b). This is common among all samples, which further indicates that no unit in this study of the Heterogeneous Zone experienced simple closed-system fractionation (i.e., where only a minor negative correlation would be expected from core to rim). A similar analysis with εHf and temperature proved

difficult as laser ablation spot sizes and ablation depths were too large to permit correlation with the ion probe spots.

The lack of any obvious temperature-dependent correlation with O isotopes, and the spread in O and Hf isotopes seen within the zircons analyzed suggests that mixing processes were highly efficient in transferring zircon grains between distinctly different melts to produce highly variable εHf and δ^{18}O values in all samples. Such intra- and intersample variability cannot have arisen by simple bimodal mixing of melts as the scatter in whole-rock isotopic variability seen here and in the earlier study of Ericksen (2006) suggests. But the zircon isotopic data also clearly reveal that samples with otherwise very similar or even identical whole-rock isotopic compositions contain crystals that are in strong isotopic disequilibrium. In this light, what were the sources of the multiple batches of melt that mixed together, and at what stage of pluton formation did zircons grow and become mixed together?

a)

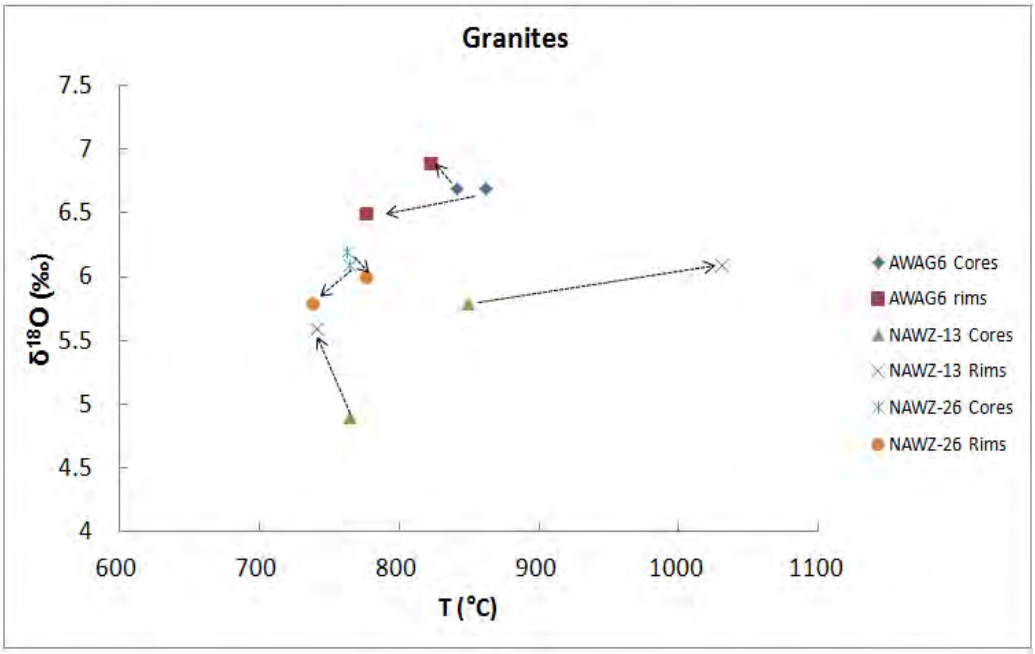

b)

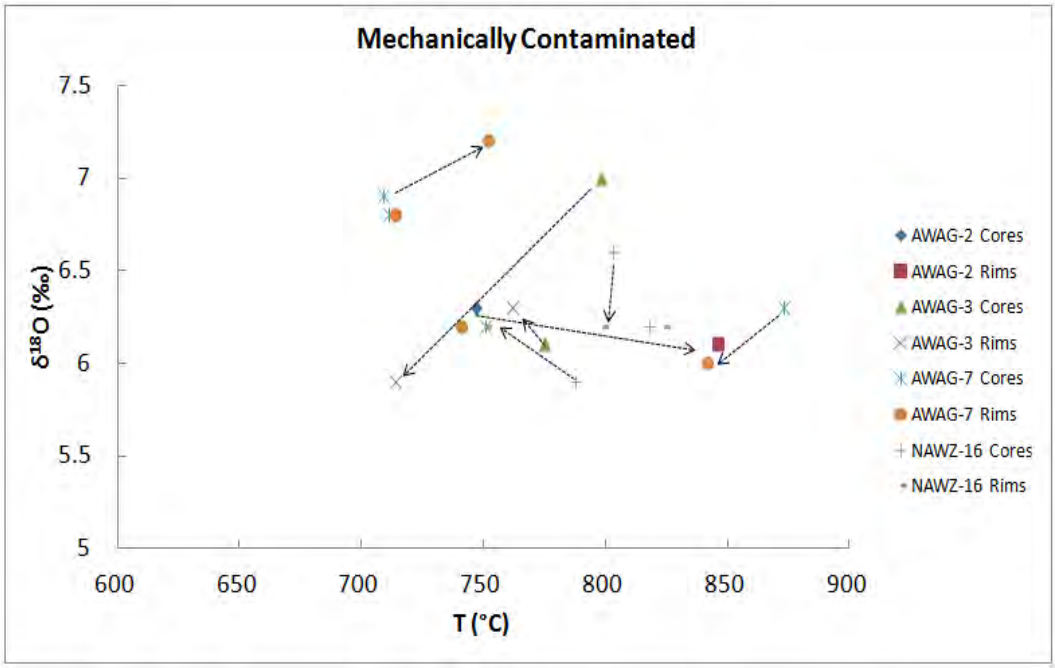

Figure 28. $\delta^{18}O$ vs. Ti-in-zircon temperatures for cores and rims of zircons in units sampled. Arrows indicate crystallization trend from core to rim. Temperatures taken from Bromley (2008).

c)

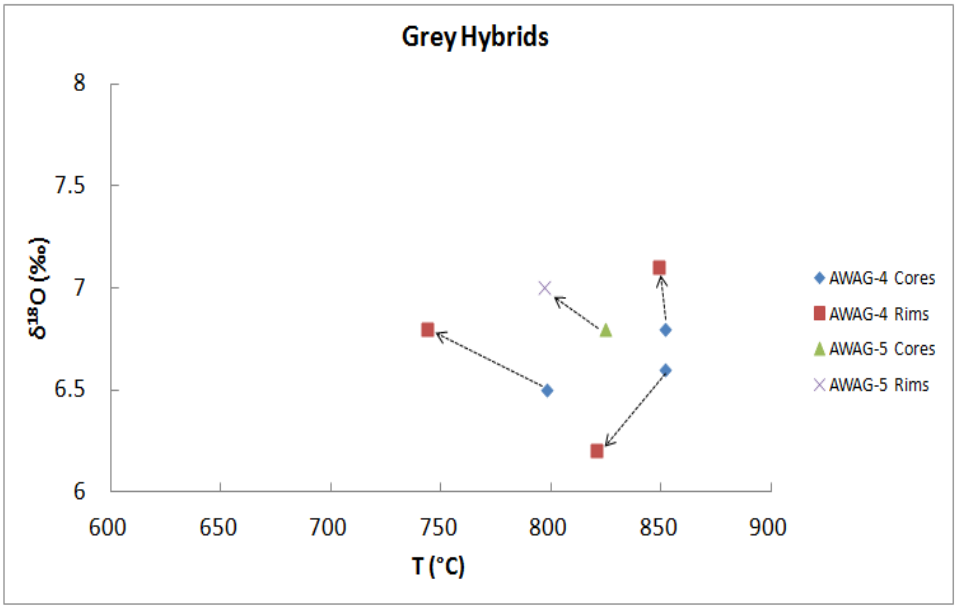

d)

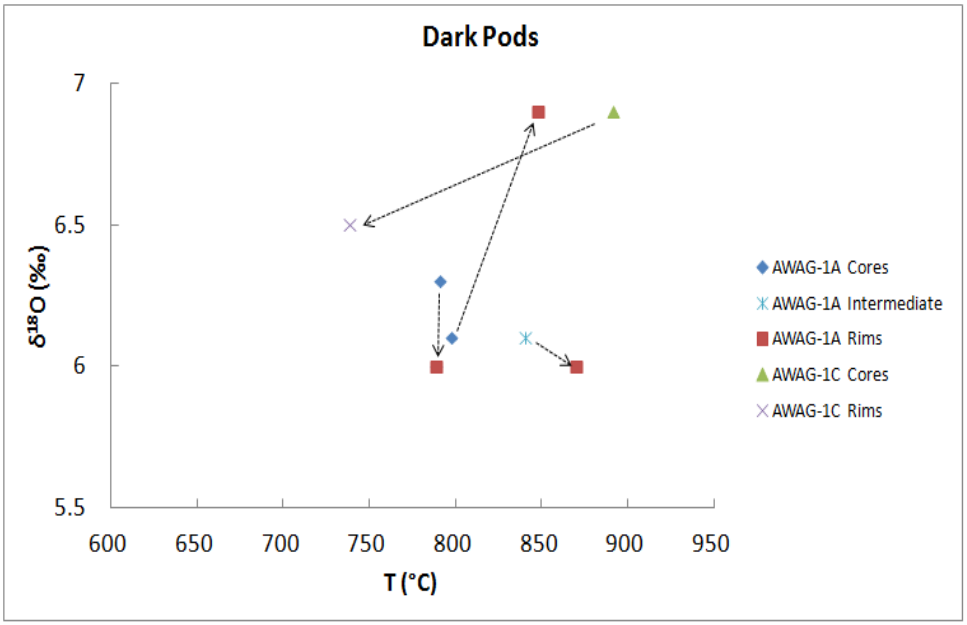

Figure 28 (continued)

Sources of Magmatic Input

Most previous studies have concluded that LIL- and LREE-enriched lithospheric mantle is the primary source of mantle basalts involved in early Tertiary magmatism in the eastern Mojave Desert and the northern Colorado River extensional corridor (Feuerbach et al., 1993; Bradshaw et al., 1993; Metcalf et al., 1995; Miller et al., 2000; Bachl et al., 2001; Metcalf, 2004), and work by Falkner et al. (1995) and Ericksen (2006) concluded that mafic sheets in the Aztec Wash pluton also traced back to this enriched mantle source with $(^{87}Sr/^{86}Sr)_i \approx 0.7075$, $\varepsilon Nd_{(t)} \approx -6$.

Mixing curves of $(^{87}Sr/^{86}Sr)_i$ vs. $\varepsilon Nd_{(t)}$, and εHf vs. $\delta^{18}O$ generated from whole-rock and zircon isotope data from this study reinforce the interpretation that enriched mantle was the major contributor to mafic sheets within the Heterogeneous Zone (Figs. 14 and 22b), and that variation can be ascribed chiefly to contributions from local basement rocks: Ireteba granite and Precambrian basement (e.g., Old Woman Mountains, or overall crustal mean of the Mojave basement). None of the analyzed spots produced εHf values above -4.5. Although it might be plausible to invoke a moderately depleted asthenospheric source that incorporated ancient crustal material prior to zircon saturation, in general a mixing model between these end-members produces a poorer fit (Fig. 22b). Pliocene and younger basalts within the eastern Mojave show asthenospheric Hf isotopic compositions (εHf ≈ +8; Beard and Johnson, 1997), and the mean εHf for the Mojave basement in the study by Goodge and Vervoort (2006) is -30; nearby Spirit Mountain Batholith contains scant inherited zircon cores with

εHf = -35 (Jonathan Miller, pers. comm.). Whole-rock and quartz $\delta^{18}O$ values within Mojave basement rocks and the muscovite-garnet-bearing Cretaceous Ireteba granite are typically between 8-12‰ (Glazner and O'Neil, 1989; Bender et al. 1993; D'Andrea-Kapp et al., 2002). Convergence toward these values would therefore be expected if contamination from local basement crustal melts were to occur. Mixing asthenosperic mantle with Proterozoic crust could plausibly reproduce appropriate isotopic compositions for some of the intermediate rocks (Fig. 22b) but because the Hf concentrations in the mixing end members are not dramatically different, and the O abundances are effectively the same, the mixing curve between asthenospheric mantle and crust cannot reproduce the mantle $\delta^{18}O$ values and also the negative εHf values of the mafic sheet zircons, particularly for AWM-1. The $\delta^{18}O$ values for zircon in the two mafic samples (AWM-1 and AWM-2), average 5.6 and 6.3‰, respectively. For AWM-1 in particular, this value is within error of the mantle value given by Valley et al. (2003) of 5.3 ± 0.3‰ and is inconsistent with a depleted melt that has been severely contaminated by the regional crust. Even if zircons are shifted -0.5‰ relative to mantle-derived mafic melts with which they would have been in equilibrium (e.g., Lackey et al., 2008), mixing between asthenospheric mantle and crust still cannot explain the data, because the proportion of crust required would mean that the mafic rocks would no longer be mafic. Modest variability in Hf at the lowest $\delta^{18}O$ values allows for some mantle heterogeneity with respect to Hf.

An enriched lithospheric mantle as the major source of melt for the mafic units in the Aztec Wash pluton is therefore favored and in accord with previous studies. AWM-2 is compositionally more mafic than AWM-1 but has systematically higher $\delta^{18}O$. Either mafic melts injected into the Aztec Wash pluton experienced varying degrees of modest interaction with the crust, or slightly different sources for mafic melts were tapped during pluton emplacement. AWM-2 is a coarse-grained gabbro and the zircons are large enough to be seen in hand sample with a hand lens. Ericksen (2006) found that the larger, coarser-grained gabbro sheets, which cooled more slowly, showed greater evidence for interaction with resident magma in the magma chamber when they were injected, but were also partly cumulates (hence more mafic but also more contaminated by interaction with melt and mush in the magma chamber). This may explain the contrasting O isotopic data in the zircons for these two samples, especially considering that zircon would have saturated very late in the magmas that formed these rocks. Their Hf isotopic compositions are not appreciably different, so some initial O isotopic variability in the mafic input melts also cannot be ruled out.

As was noted above, apart from the single analysis that has a distinctly lower εHf than all other analyzed spots, the εHf zircon values for the granites show substantial overlap with many of the hybrid rocks and mafic rocks (Fig. 22). Binary mixing between plausible crustal end-members and enriched mantle plotted in a 1:1 ratio would produce εHf values of approximately -15 to -18. Very few of the granite zircons analyzed are this low, which suggests that the zircons in the granites contain an

appreciable fraction of mantle Hf, also in general agreement with whole rock isotope data. The granites also have a limited $\delta^{18}O$ range of 6 – 6.4‰, suggesting a relatively modest shift from mantle values, again bearing in mind felsic melt that would be in O isotope equilibrium with granite zircons could be shifted up to 2‰ higher.

Both Harper et al (2004) and Ericksen (2006) concluded, on the basis of trace element modeling and whole-rock isotopic data, that there was primary felsic input into the Aztec Wash pluton from anatexis of pre-existing crust. However, the large fraction of mantle Hf (> 50%) inferred for nearly all the granite zircons suggests that either: 1) the primary felsic inputs are themselves the products of anatexis of a hybrid source (i.e., Precambrian basement + juvenile mantle component); or 2) that the zircons in the granites are themselves mixtures of crustal and mantle end members.

That isotopic zoning in individual zircons is either absent or very limited for both Hf and O isotopes (essentially at or near the analytical limits of the techniques) indicates that the zircons mostly grew from melts that were already isotopic hybrids of crustal and mantle components (i.e., they do not appear to be inherited Precambrian zircons armored with younger overgrowths; cf. Griffin et al. 2002; Yang et al., 2006). The one zircon with a demonstrably older core has εHf = -25 and also low $\delta^{18}O$, so perhaps the O isotope compositions of basement extend to much lower values than in whole rocks, and O isotope zoning might not be observed easily. But Hf isotopic zoning should be very evident. The ablation check shows that this zircon is not overgrown by more radiogenic, younger zircon with higher εHf. It is instead interpreted as a true xenocryst

that was added to the magma chamber not long before the rock in which it is contained cooled below the solidus. The anomalously low $\delta^{18}O$ suggests a relatively mafic source for this xenocryst, possibly amphibolite xenoliths and dikes, which are found in the basement and in stoped blocks approximately 1 km to the south of where this sample was collected (Smith et al., 2008).

This lack of zircons inherited from possible crustal sources is an important observation because zircon saturation thermometry (e.g., Hanchar and Watson, 2003; Miller et al., 2003), shows that the granites would have been saturated in Zr at 760–790°C (Table 1). If the granites were mostly anatectic melts of Precambrian crust, the low saturating values of Zr suggest that inherited zircons should be abundant, yet they are not preserved. Inherited cores may be so small in volume as to be essentially undetectable by laser ablation analysis, but ion probe U-Pb dating by Cates (2003) also shows that such cores are very rare. Instead, the zircons likely grew from granitoid anatectic melts that were from a mixed source region. A variant on this option is that Precambrian zircons that might have survived initial anatexis were completely or mostly dissolved away by mixing with hot mafic melts to produce hybrids in the magma chamber during its growth, and then zircon saturated later during cooling of the hybrid melts. This would seem fortuitous.

That at least some of the zircons have essentially mantle Hf and O isotope values suggests that a small population of the zircons in the granites were actually derived

from more mafic melts. The granites in this case should contain evidence of zircon growth at higher temperature (in somewhat more mafic magmas and/or hybrids in the Heterogeneous Zone). The granite trace element and Ti-in-zircon temperature data from Bromley (2008) in general show considerable overlap with hybrids (grey hybrids, mechanically contaminated) as well as with the mafic sheets and the mafic pod. For example, Ti-in-zircon temperatures plotted against elemental concentrations (e.g., U, Hf) show that the granite samples contain grains from magmas having temperatures well over 800°C (thus well above bulk zircon saturation for the granites in which the zircons are found), and also with low U and low Hf indicative of less evolved melts. The abundant evidence for hybridization combined with the isotope and trace element data indicates that some of the zircons in the granites grew *in situ* in hybrid magmas and possibly in mafic sheet magmas and were then incorporated or entrained in more felsic differentiates of these hybrids that formed the granites.

Ericksen (2006) suggested that the more mantle-like isotopic signatures in the hybrids and granites might arise via delivery of residual felsic fractionates of coarse-grained very mafic gabbros to troctolitic masses that are modeled as cumulates that had lost felsic melt. These residual melts can "contaminate" and percolate up into granite that overlies the mafic sheets. Ericksen (2006) also showed that intruding mafic sheets assimilated feldspar-rich monzonitic cumulates (that resulted from internal granite magma fractionation; see Harper et al., 2004) on the local floor of the magma chamber to make some of the hybrids. These cumulates also contain abundant zircon, which

could have been relatively easily dissolved in the hot intruding mafic magmas. Thus hybrids formed by mixing of cumulates and intruding mafic sheets would have high resulting Zr, and so subsequent cooling of these hybrids would result in abundant zircon grown at high temperature.

Melt removal and entrainment of the zircon from the hybrids and mafic melts and mixing into the overlying granite part of the magma chamber would then bring together zircons with somewhat variable isotopic compositions (derived ultimately from mixing of melts in the Heterogeneous Zone) with zircon at lower temperature and with somewhat more crustally derived isotopic values from a primary anatectic melt (Fig. 29). If Hf and O isotopic composition of analysis spots could be better linked to the trace element data spots in enough crystals, then it might be possible to better track specifically where zircons formed initially. For example, those zircons in the granites that have $\delta^{18}O$ as low as 5‰, which is essentially a mantle value, are possibly derived from fractionation of more mafic magma. However, because zircon-melt fractionations may be –2‰ (Lackey et al., 2008), zircons with these low $\delta^{18}O$ values might also have grown in a magma that had a more 'crustal' $\delta^{18}O$ value of +7‰. Being able to better link $\delta^{18}O$ with temperature of zircon crystallization might resolve which of these two possibilities is correct.

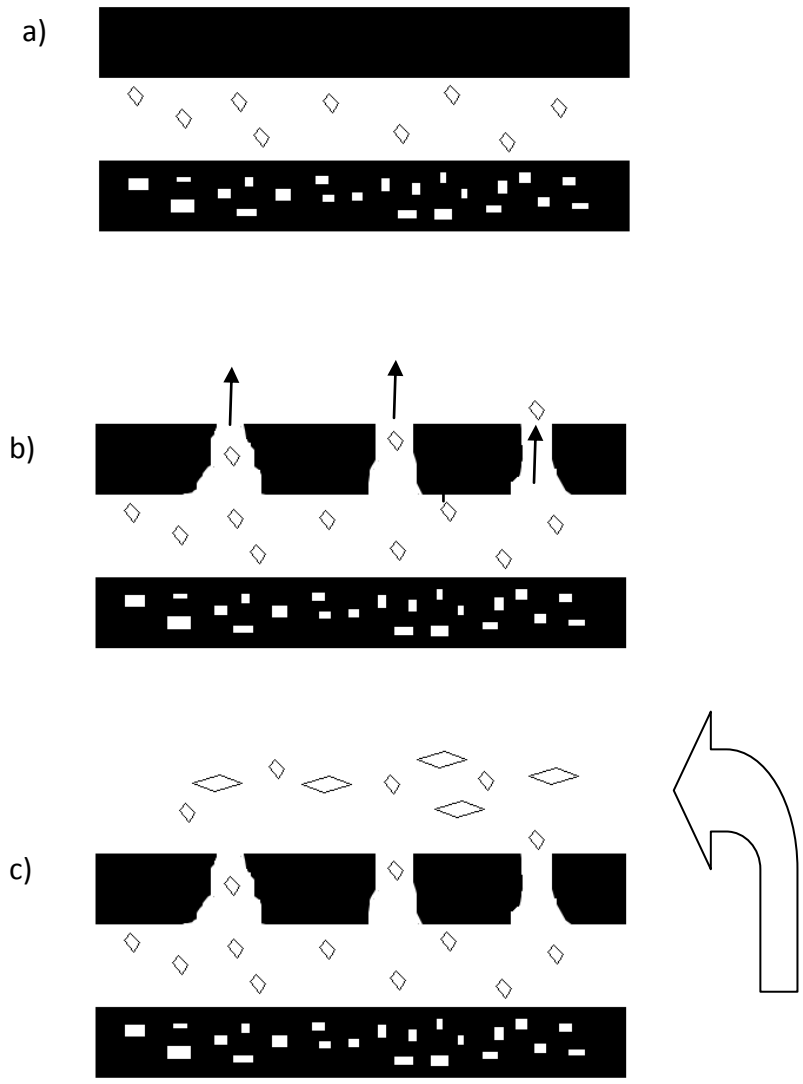

Figure 29. Cartoon for potential mechanism to create heterogeneity in zircon population within felsic units. Zircons grow from a felsic melt fractionally crystallized from mafic sheet intrusion (a). Felsic melt escapes upward through vertical pipes due to filter-pressing (b), previously grown zircons are entrained in pipes. Recharge of chamber with felsic melt may carry new batch of zircons (c). Mixing of these distinct felsic melts occur. Stage (b) may explain granitic zircons with apparent high crystallization temperature as pipes may entrain mafic zircons from sheets.

In any case, it seems inescapable that zircons in the granites must have grown in a variety of different magmas at variable temperatures and with moderately variable O and Hf isotopic compositions, and all with a large fraction of mantle component. The abundance of data from zircon trace elements and isotopes agrees with the general model for derivation of the Granite Zone by fractionation of felsic magmas and crystal mush that had interacted and mixed with mafic magmas in the Hetergeneous Zone (Harper et al., 2004; Ericksen, 2006).

Generalized model for melt derivation and zircon growth in the Aztec Wash pluton

The continental crust clearly supplied material for the Aztec Wash pluton, as indicated by both whole-rock and zircon isotope geochemistry. The range of εHf and $\delta^{18}O$ values in the zircon data must require mixing of magmas with variable Hf and O isotopic compositions, and, as argued earlier, in melts that either lacked old zircons or were mixed under conditions sufficient to mostly eradicate old zircon (strong undersaturation and high temperature). When the melts cooled enough for zircon to saturate, zircons with variable Hf and O isotopic compositions were brought together by mixing processes for which there is abundant field evidence. The scatter of the Hf and O zircon isotopic data also precludes simple binary mixing, and the somewhat scattered but downward-fanning trend on the Sr-Nd isotope diagram (Fig. 12) also suggests that enriched mantle-derived basalts mixed with a somewhat heterogeneous but

nevertheless plausible range of local end members (Mojave Proterozoic and Ireteba granite).

In general the relationships discussed here are compatible with production of crustal anatectic melts in deep crustal "hot zones" (Annen et al. 2006), which are thought to develop by intrusion of sills of mantle-derived hydrous basalt into the deep crust. Sufficient heating of the crust results in partial melting of basement rocks as well as previously intruded sills. Felsic, H_2O-rich residual melts are also generated by differentiation of the basalt sills. However, there can exist a wide compositional variety of residual melts depending on the depth of sill intrusion and the relationship to the local geotherm upon cooling. Melt from local crustal anatexis, residual fractionation of basalt sills, and from freshly intruded material from depth mixes to varying degrees either prior to or during transport to shallower crustal depths. Production and isotopic composition of source melts would be a function of the amount of intruding basalt, level and rate of emplacement, and composition of the lower and middle crust. The degree of mixing and hybridization of these melts depends on the depth and the rate of sill intrusion to maintain a thermal regime agreeable for extended mixing. The final composition of the melt that leaves the hot zone may vary somewhat but is commonly dominated by the mantle component. Following melt generation, ascent will proceed, governed by density, viscosity and pathway taken. Melts will then degas, cool and ultimately begin crystallizing to form plutons (Annen et al., 2006).

This model of a hot zone has been previously used by Appleby et al. (2008) to explain $\delta^{18}O$ heterogeneity in zircon populations of the Caledonian 'I-type' intrusions in the Grampian Highlands of Scotland. Here most $\delta^{18}O$ values from zircons were 6.6 – 7.3 ‰ (i.e., somewhat comparable to that seen in the present study) but some values were mantle-like (5.6‰) and clearly crust-derived (11.7‰). Although $\delta^{18}O$ from Aztec Wash zircons are not quite as high, the typical variation between 5.5 and 7‰ could partly be attributed to the formation of a hot zone. The hot zone presumably would have persistently produced moderately isotopically variable magmas with a large fraction of mantle component that fed the growing Aztec Wash pluton. This also provides a mechanism for the variation of εHf seen in the data, particularly the mafic magmas. The hot zone would have formed and produced initial source melts that either were undersaturated in zircon or were so effectively dominated by the juvenile component that zircons inherited from old Precambrian rocks were essentially absent. The complex interplay between melt channels proposed by Griffin et al. (2002), and especially the mixing processes within the Heterogeneous Zone itself, inevitably created the εHf and $\delta^{18}O$ variability seen across and especially within samples. Figure 30 shows processes that may have been active during construction of the Aztec Wash pluton.

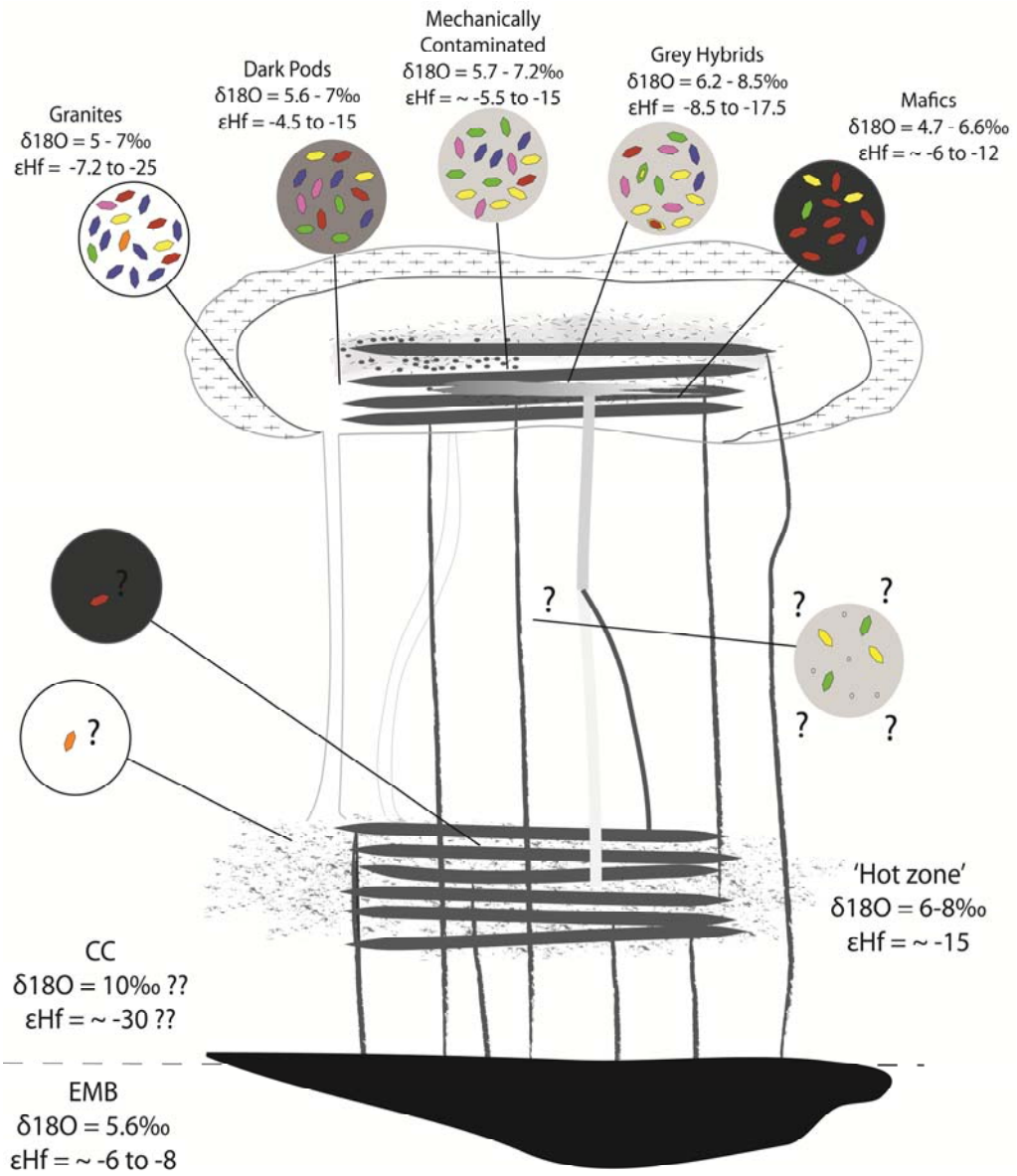

Figure 30. Schematic cartoon of proposed model for construction of the Aztec Wash pluton. Multiple intrusions of basaltic melt from enriched mantle (EMB) create a lower crustal "hot zone" with a limited range of $\delta^{18}O$ and εHf through hybridization. Sources of melt can then be a combination either from the hot zone, direct sampling of the mantle, or through anatexis of the continental crust (CC). The majority of melt hybridization and transfer of zircons takes place within the pluton itself. Minor zircon inheritance and/or mixing at depth prior to emplacement cannot be confirmed but is speculative ("?"). Potential values of εHf and $\delta^{18}O$ for EMB, CC, hot zone and Aztec Wash units are shown here and discussed in text.

Late-stage assimilation and/or hydrothermal alteration?

There is evidence toward the roof of the pluton that stoping of country rock blocks occurred and that these sank through the Aztec Wash magma chamber (Harper et al., 2004; Koteas, 2005; Smith et al., 2008) as it grew. These blocks include mainly Early Proterozoic granitic orthogneiss and Late Cretaceous Ireteba granite. In these block-rich domains of the pluton there is evidence of disaggregation and physical mixing (Smith et al., 2008). This would imply that the magma in which the blocks were incorporated had sufficient melt and heat to allow transport and partial destruction of blocks. Although the model outlined above generally suggests this is not the case, the field relationships observed in the block-rich areas merit considering whether some of the chemical/isotopic signature from these blocks was imparted to magmas in the Aztec Wash magma chamber.

As well as physically incorporating blocks of host material, a pluton can potentially also directly melt and sample the wall-rock. Bulk assimilation of crustal rocks is viewed by some workers as an important factor during growth of plutons and also as a way to impart isotopic variability (Beard et al., 2005), but the enthalpy requirements for large-scale bulk assimilation, particularly at the shallow crustal levels of the Aztec Wash pluton, are formidable (Glazner, 2007).

The zircon data presented here show very little evidence of bulk assimilation of host rock other than the one xenocryst noted earlier with $\varepsilon Hf = -26$. If a significant

proportion of host rock was assimilated at shallow levels, a larger number of ancient xenocrysts would be expected. An argument could be made that all intruding melts were so severely Zr undersaturated that incorporation of any zircon from the host material was dissolved, thereby removing evidence of inheritance. This does not fit the data discussed in previous sections, and saturation of Zr is also thought to have been reached before or relatively soon after intrusion of much of the melt, based on the generally high Zr contents of Aztec Wash rocks. Incorporation of cold host rock into hot melt would also promote crystallization (Glazner, 2007), increasing the rate at which saturation is reached and so driving up the likelihood of xenocrysts being preserved.

Plutons intruded at relatively shallow levels may also either incorporate previously hydrothermally altered material, or become directly altered by hydrothermal activity. The role of meteoric waters in this process has the effect of lowering $\delta^{18}O$ (Valley, 2003; Bindeman, 2008). Zircon, if still growing, has the ability to track this effect via core-to-rim analyses showing a progressive reduction in $\delta^{18}O$. The negative trend seen in the plot of εHf and $\delta^{18}O$ (Fig. 22) precludes any alteration of the melt by hydrothermal processes (Hawkesworth and Kemp, 2006). Additionally, the limited core-to-rim data available from all samples do not show any significant trends toward lower $\delta^{18}O$ that would be consistent with incorporation and/or remelting of hydrothermally altered roof rocks. It is therefore unlikely that these forms of alteration were acting upon the Aztec Wash pluton during zircon crystallization. On the other hand it does not preclude the possibility of hydrothermal alteration occurring after zircon had finished

crystallizing. Whole-rock or quartz $\delta^{18}O$ analysis would be required to see this. The highly extended nature of the Aztec Wash pluton coupled with its late Cenozoic rise through the crust could allow for the opportunity for meteoric water to alter any residual melt in the interstitial spaces. This mechanism, however, appears to only be dominantly related to caldera systems, either during pre- or post-collapse (Valley, 2003).

Further Work Required

Extensive Hf and O isotope analysis was performed on zircon in the Heterogeneous Zone. There is, however, very little zircon data from the Granite Zone, especially at distances away from the Heterogeneous Zone. Similar zircon data like that presented in this and other studies is necessary for the Granite Zone if there is to be complete understanding on the nature of melt involved in the Aztec Wash pluton construction. Magmatic zircon can only record changes in melt environment as long as it is a crystallizing phase. Post-crystallization alteration can still be imprinted on the rocks and is beyond the scope of this study. It is suggested that O isotopes be measured for both whole rock and quartz on samples previously analyzed. This could record any O isotope disequilibria between melt and zircon and allow for a clearer understanding of where zircons grew in the magma system, particularly the granite zircons. Further constraints on the extent of contamination of the melt by host rocks need to be addressed. There is sparse Hf and O isotope data on units within the region of the Aztec

Wash pluton, making it relatively difficult to define precisely which units may have been involved and what role they played during intrusion, although this study has gone far in tackling that issue. Extensive isotope work on host rocks paralleling that performed on zircons in this study needs to be considered. On a broader scale, similar studies should be undertaken on other Miocene intrusions in the northern Colorado River extensional corridor. This would have the benefit of not only updating current models for individual pluton genesis but also of clarifying any inherent links between plutons and the overall controls on melt emplacement. Beyond the particular study performed here there is a current weakness in the techniques used to collect the data. Current spot sizes for laser ablation in measuring εHf are too large for measuring individual zones in zircon. Clarity is reduced when multiple zones are ablated and an average of εHf is recorded. Until beam efficiency is increased and spot sizes reduced, it is difficult to confidently link εHf with respective $\delta^{18}O$ measurements and create a better model of melt evolution.

CONCLUSIONS

The Aztec Wash pluton provides evidence of an intrusive body that experienced widespread open-system behavior throughout bimodal emplacement of mafic and felsic melts, as shown in previous studies. The following are general conclusions from this study.

1) Analysis of combined Sr, Nd and Hf whole-rock data with in-situ Hf and O zircon data reinforce the importance of a relatively large fraction (> 50%) of enriched lithospheric mantle component in all Aztec Wash pluton rocks.
2) Initial isotopic compositions of more felsic magmas feeding the Aztec Wash pluton were acquired from a deep crustal "hot zone" where enriched mantle melts interacted disproportionately with basement crustal rocks. This produced the limited, yet heterogeneous spread in $\delta^{18}O$ data as well as the large spread in εHf values as melts derived from the hot zone were variably sampled. Consequently, the crust experienced both growth and recycling during intrusion of the pluton.
3) Transfer of grains between melts was efficient enough to bring about heterogeneity within small zircon populations across all rock compositions (mafic sheets, intermediate hybrids, and granites).
4) Hf and O isotopic data from zircon also confirm that the Granite Zone was constructed from multiple batches of felsic melt. Likely sources of this felsic melt

include hybridized crust with a large fraction of juvenile component and/or remelting of juvenile mafic sills, and residual liquids from fractionation of intruding mafic melts.

5) A negative correlation between Hf and O isotopes precludes any hydrothermal alteration of melt or incorporation of hydrothermally altered host rock during zircon crystallization. Extensive assimilation of host rock during emplacement did not play an important role in chemical diversification of melts in the Aztec Wash pluton.

REFERENCES

Aleinikoff, J. N., Wintsch, R. P., Tollo, R. P., Unruh, D. M., Fanning, C. M., and Schmitz, M. D., 2007, Ages and origins of rocks of the Killingworth dome, south-central Connecticut: Implications for the tectonic evolution of southern New England: American Journal of Science, v. 307, no. 1, p. 63-118.

Anders, E., and Grevesse, N., 1989, Abundances of the elements – Meteoric and solar: Geochimica Et Cosmochimica Acta, v. 53, no. 1, p. 197-214.

Andersen, T., Andersson, U. B., Graham, S., Aberg, G., and Simonsen, S. L., 2009, Granitic magmatism by melting of juvenile continental crust: new constraints on the source of Palaeoproterozoic granitoids in Fennoscandia from Hf isotopes in zircon: Journal of the Geological Society, v. 166, p. 233-247.

Annen, C., Blundy, J. D., and Sparks, R. S. J., 2006, The genesis of intermediate and silicic magmas in deep crustal hot zones: Journal of Petrology, v. 47, no. 3, p. 505-539.

Appleby, S. K., Graham, C. M., Gillespie, M. R., Hinton, R. W., Oliver, G. J. H., and Eimf, 2008, A cryptic record of magma mixing in diorites revealed by high-precision SIMS oxygen isotope analysis of zircons: Earth and Planetary Science Letters, v. 269, no. 1-2, p. 105-117.

Bachl, C. A., Miller, C. F., Miller, J. S., and Faulds, J. E., 2001, Construction of a pluton: evidence from an exposed cross-section of the Searchlight pluton, Eldorado Mountains, Nevada: Geological Society of America Bulletin, v. 113, p. 1213-1228.

Bachmann, O., and Bergantz, G., 2008, The magma reservoirs that feed supereruptions: Elements, v. 4, no. 1, p. 17-21.

Bachmann, O., Dungan, M. A., and Bussy, F., 2005, Insights into shallow magmatic processes in large silicic magma bodies: the trace element record in the Fish Canyon magma body, Colorado: Contributions to Mineralogy and Petrology, v. 149, no. 3, p. 338-349.

Beard, B. L., and Johnson, C. M., 1997, Hafnium isotope evidence for the origin of Cenozoic basaltic lavas from the southwestern United States: Journal of Geophysical Research-Solid Earth, v. 102, no. B9, p. 20149-20178.

Bender, E. E., Morrison, J., Anderson, J. L., and Wooden, J. L., 1993, Early Proterozoic ties between 2 suspect terranes and the Mojave crustal block of the southwestern US: Journal of Geology, v. 101, no. 6, p. 715-728.

Bindeman, I., 2008, Oxygen Isotopes in mantle and crustal magmas as revealed by single crsyal analysis: Reviews in Mineralogy & Geochemistry, v. 69, p. 445-478.

Bleick, H. A., C. F. Miller, et al., 2005, Production and distribution of hybridized magma in a replenished, open-system magma chamber: Aztec Wash pluton, Eldorado Mountains, Nevada: Geological Society of America Abstracts with Programs, v. 35, no. 4, p. 63.

Bolhar, R., Weaver, S. D., Whitehouse, M. J., Palin, J. M., Woodhead, J. D., and Cole, J. W., 2008, Sources and evolution of arc magmas inferred from coupled O and Hf isotope systematics of plutonic zircons from the Cretaceous Separation Point Suite (New Zealand): Earth and Planetary Science Letters, v. 268, no. 3-4, p. 312-324.

Bromley, S. A., 2008, *In situ* mechanical and diffusive mixing in Aztec Wash Pluton, NV: Evidence from zircon titanium thermometry and elemental zoning. Unpublished senior thesis, Vanderbilt University, 53 p.

Cates, N. L., 2003, Perspectives on the development of an intermediate, open-system magma chamber: Aztec Wash Pluton. Unpublished Master's thesis, Vanderbilt University, Nashville, TN, USA. 162 p.

Claiborne L. L., Miller, C. F., and Wooden, J. L., 2010, Trace element composition of igneous zircon: a thermal and compositional record of the accumulation and evolution of a large silicic batholith, Spirit Mountain, Nevada: Contributions to Mineralogy and Petrology, in press.

Coleman, D. S., Gray, W., and Glazner, A. F., 2004, Rethinking the emplacement and evolution of zoned plutons: Geochronologic evidence for incremental assembly of the Tuolumne Intrusive Suite, California: Geology, v. 32, no. 5, p. 433-436.

Colombini, L. L., Miller, C. F., Gualda, G. A. R., Wooden, J. L., and Miller, J. S., 2011, Sphene and zircon in the Highland Range volcanic sequence (Miocene, southern Nevada, USA): elemental partitioning, phase, relations, and influence on evolution of silicic magma: Mineralogy and Petrology, v. 101. In print.

Corfu, F., Hanchar, J. M., Hoskin, P. W. O., and Kinny, P., 2003, Atlas of zircon textures, *in* Hanchar, J. M., and Hoskin, P. W. O., eds., Zircon: Reviews in Mineralogy & Geochemistry, vol. 53, p. 469-500.

Davidson, J. P., Morgan, D. J., and Charlier, B. L. A., 2007, Isotopic microsampling of magmatic rocks: Elements, v. 3, no. 4, p. 253-259.

Dickin, A. P., 1995, Radiogenic Isotope Geology: Cambridge, Cambridge University Press, 490 p.

Elhlou, S., Belousova, E., Griffin, W. L., Pearson, N. J., and O'Reilly, S. Y., 2006, Trace element and isotopic composition of GJ-red zircon standard by laser ablation: Geochimica Et Cosmochimica Acta, v. 70, no. 18, p. A158-A158.

Ericksen, S. M., Miller, J. S., Harper, B. E., and Aggarwal, J. K., 2004, Isotopic contraints on the evolution of felsic magma in the Aztec Wash pluton, Eldorado Mountains, Nevada: Geological Society of America Abstracts with Programs, v. 36, no. 4, p.8

Ericksen, S. M., 2006, Fractionation, recharge, and hybridization in a shallow, bimodal magma reservoir. San Jose State University. Unpublished Master's thesis, 117 p.

Falkner, C. M., C. F. Miller, et al., 1995, Petrogenesis and tectonic significance of the calc-alkaline, bimodal Aztec Wash pluton, Eldorado Mountains, Colorado River extensional corridor. Journal of Geophysical Research vol. 100, no. B7, p. 10,453-10,476.

Faulds, J. E., Feuerbach, D. L., Reagan, M. K., Metcalf, R. V., Gans, P., and Walker, J. D., 1995, The Mount Perkins Block, Northwestern Arizona – an exposed cross-section of an evolving, preextensional to syextensional magmatic: Journal of Geophysical Research-Solid Earth, v. 100, no. B8, p. 15249-15266.

Faulds, J. E., Olson, E. L., Harlan, S. S., and McIntosh, W. C., 2002, Miocene extension and fault-related folding in the Highland Range, southern Nevada: a three-dimensional perspective: Journal of Structural Geology, v. 24, p. 861-886.

Feuerbach, D. L., Smith, E. I., Walker, J. D., and Tangeman, J. A., 1993, The role of the mantle during crustal extension: Constraints from the geochemistry of volcanic rocks in the Lake Mead area, Nevada and Arizona: Geological Society of America Bulletin, v. 105, p. 1561-1575.

Feuerbach, D. L., Reagan, M. K., Faulds, J. E., and Walker, J. D., 1998, Lead isotopic evidence for synextensional lithospheric ductile flow in the Colorado River extensional corridor, western United States: Journal of Geophysical Research-Solid Earth, v. 103, no. B2, p. 2515-2528.

Gerdes, A., and Zeh, A., 2006, Combined U-Pb and Hf isotope LA-(MC-)ICP-MS analyses of detrital zircons: Comparison with SHRIMP and new constraints for the provenance and age of an Annorican metasediment in Central Germany: Earth and Planetary Science Letters, v. 249, no. 1-2, p. 47-61.

Glazner, A. F., and Oneil, J. R., 1989, Crustal structure of the Mojave Desert, California-inferences from Sr and O isotope studies of Miocene volcanic: Journal of Geophysical Research-Solid Earth and Planets, v. 94, no. B6, p. 7861-7870.

Glazner, A. F., Bartley, J. M., Coleman, D. S., Gray, W., and Taylor, R. Z., 2004, Are plutons assembled over millions of years by amalgamation from small magma chambers?: GSA Today, v. 14, no. 4/5, p. 4-11.

Griffin, W. L., Pearson, N. J., Belousova, E., Jackson, S. E., van Achterbergh, E., O'Reilly, S. Y., and Shee, S. R., 2000, The Hf isotope composition of cratonic mantle: LAM-MC-ICPMS analysis of zircon megacrysts in kimberlites: Geochimica Et Cosmochimica Acta, v. 64, no. 1, p. 133-147.

Griffin, W. L., Wang, X., Jackson, S. E., Pearson, N. J., O'Reilly, S. Y., Xu, X. S., and Zhou, X. M., 2002, Zircon chemistry and magma mixing, SE China: In-situ analysis of Hf isotopes, Tonglu and Pingtan igneous complexes: Lithos, v. 61, no. 3-4, p. 237-269.

Goodge, J. W., and Vervoort, J. D., 2006, Origin of Mesoproterozoic A-type granites in Laurentia: Hf isotope evidence: Earth and Planetary Science Letters, v. 243, no. 3-4, p. 711-731.

Hanchar, J. M., Burakov, B. E., Anderson, E. B., and Zamoryanskaya, M. V., 2003, Investigation of single crystal zircon, (Zr,Pu)SiO4, doped with Pu-238, *in* Finch, R. J., and Bullen, D. B., eds., Scientific Basis for Nuclear Waste Management Xxvi: Materials Research Society Symposium Proceedings, p. 215-225.

Harper, B. E., Miller, C. F., Koteas, C. G., Cates, N. L., Wiebe, R. A., Lazzareschi, D. S., and Cribb, J. W., 2004, Granites, dynamic magma chamber processes and pluton construction: the Aztec Wash pluton, Eldorado Mountains, Nevada, USA: Transactions of the Royal Society of Edinburgh: Earth Sciences, v. 95, p. 277-295

Hawkesworth, C. J., and Kemp, A. I. S., 2006a, The differentiation and rates of generation of the continental crust: Chemical Geology, v. 226, no. 3-4, p. 134-143.

Hawkesworth, C. J., and Kemp, A. I. S., 2006b, Using hafnium and oxygen isotopes in zircons to unravel the record of crustal evolution: Chemical Geology, v. 226, no. 3-4, p. 144-162.

Hayden, L. A., Watson, E. B., and Wark, D. A., 2008, A thermobarometer for sphene (titanite): Contributions to Mineralogy and Petrology, v. 155, no. 4, p. 529-540.

Kapp, J. D., Miller, C. F., and Miller, J. S., 2002, Ireteba pluton, Eldorado Mountains, Nevada: Late, deep-source, peraluminous magmatism in the Cordilleran interior: Journal of Geology, v. 110, no. 6, p. 649-669.

Kemp, A. I. S., Hawkesworth, C. J., Collins, W. J., and Shimura, T., 2007, Tracing the lost arcs: Granitic zircon as a geodynamic indicator?: Geochimica Et Cosmochimica Acta, v. 71, no. 15, p. A476-A476.

Kemp, A.I.S., Hawkesworth, C.J., Foster, G.L., Paterson, B.A., Woodhead, J.D., Hergt, J.M., Gray, C.M., Whitehouse, M.J., 2007. Magmatic and crustal differentiation history of granitic rocks from Hf-O isotopes in zircon. *Science,* Vol. 315, 980-983

Lackey, J. S., Valley, J. W., Chen, J. H., and Stockli, D. F., 2008, Dynamic magma systems, crustal recycling, and alteration in the central Sierra Nevada batholith: the oxygen isotope record: Journal of Petrology, v. 49, no. 7, p. 1397-1426.

Ludwig, K.R., (2003) Isoplot 3.00. Berkeley Geochronology Center, special publication No. 4., 70 p.

Matzel, J. E. P., Bowring, S. A., and Miller, R. B., 2006, Time scales of pluton construction at differing crustal levels: Examples from the Mount Stuart and Tenpeak intrusions, North Cascades, Washington: Geological Society of America Bulletin, v. 118, no. 11-12, p. 1412-1430.

Mazdab, F. K., 2009, Characterization of flux-grown trace-element-doped titanite using the high-mass-resolution ion microprobe (SHRIMP-RG): Canadian Mineralogist, v. 47, no. 4, p. 813-831.

McLeod, G. W., Dempster, T. J., and Faithfull, J. W., Deciphering Magma-Mixing Processes Using Zoned Titanite from the Ross of Mull Granite, Scotland: Journal of Petrology, v. 52, no. 1, p. 55-82.

Metcalf, R. V., and Smith, E. I., 1995, Introduction to special section- Magmatism and extension: Journal of Geophysical Research-Solid Earth, v. 100, no. B6, p. 10249-10253.

Michel, J., Baumgartner, L., Putlitz, B., Schaltegger, U., and Ovtcharova, M., 2008, Incremental growth of the Patagonian Torres del Paine laccolith over 90 k.y.: Geology, v. 36, p. 459-562

Miller, C. F., and Miller, J. S., 2002, Contrasting stratified plutons exposed in tilt blocks, Eldorado Mountains, Colorado River Rift, NV, USA: Lithos, v. 61, p. 209-224.

Miller, C. F., and Wooden, J. L., 1994, Anatexis, hybridization and the modification of ancient crust- Mesozoic plutonism in the Old Woman Mountains area, California: Lithos, v. 32, no. 1-2, p. 111-133.

Miller, R., and Patterson, S., 2001, Construction of mid-crustal sheeted plutons: Example from the North Cascades, Washington: Geological Society of America Bulletin, v. 133, p. 1423-1442.

Moore, J. G., and Sisson, T. W., 2008, Igneous phenocrystic origin of K-feldspar megacrysts in granitic rocks from the Sierra Nevada batholith: Geosphere, v. 4, no. 2, p. 387-400.

Nowell, G. M., Kempton, P. D., Noble, S. R., Fitton, J. G., Saunders, A. D., Mahoney, J. J., and Taylor, R. N., 1998, High precision Hf isotope measurements of MORB and OIB by thermal ionisation mass spectrometry: insights into the depleted mantle: Chemical Geology, v. 149, no. 3-4, p. 211-233.

Patrick, D. W., Miller, C.F., 1997, Processes in a composite, recharging magma chamber: evidence from magmatic structures in the Aztec Wash pluton, Nevada. Proceedings of the 30th International Geological Congress, Igneous Petrology (Research Volume), v. 15, p. 121- 135.

Robinson, D. M., and Miller, C. F., 1999, Record of magma chamber processes preserved in accessory mineral assemblages, Aztec Wash pluton, Nevada: American Mineralogist, v. 84, no. 9, p. 1346-1353.

Russell, W. A., Papanastassiou, D. A., and Tombrello, T. A., 1978, Ca isotope fractionation of Earth and other Solar-System materials: Geochimica Et Cosmochimica Acta, v. 42, p. 1075-1090.

Schaltegger, U., Brack, P., Ovtcharova, M., Peytcheva, I., Schoene, B., Stracke, A., Marocchi, M., and Bargossi, G. M., 2009, Zircon and titanite recording 1.5 million years of magma accretion, crystallization and initial cooling in a composite pluton (southern Adamello batholith, northern Italy): Earth and Planetary Science Letters, v. 286, no. 1-2, p. 208-218.

Smith, J., Miller, J. S., Koteas, C. G., and Miller, C. F., 2008, Incorporation of host rock blocks during growth of the Aztec Wash pluton, Eldorado Mountains, Nevada: Geological Society of America Abstracts with Programs, v. 40, no. 1, p. 92.

Taylor, S. R., and McLennan, S. M., 1995, The Geochemical evolution of the Continental Crust: Reviews of Geophysics, v. 33, no. 2, p. 241-265.

Trail, D., Mojzsis, S. J., Harrison, T. M., Schmitt, A. K., Watson, E. B., and Young, E. D., 2007, Constraints on Hadean zircon protoliths from oxygen isotopes, Ti-thermometry, and rare earth elements: Geochemistry Geophysics Geosystems, v. 8.

Valley, J. W., 2003, Oxygen isotopes in zircon, *in* Hanchar, J. M., and Hoskin, P. W. O., eds., Zircon: Reviews in Mineralogy & Geochemistry, v. 53, p. 343-385.

Valley, J. W., Lackey, J. S., Cavosie, A. J., Clechenko, C. C., Spicuzza, M. J., Basei, M. A. S., Bindeman, I. N., Ferreira, V. P., Sial, A. N., King, E. M., Peck, W. H., Sinha, A. K., and Wei, C. S., 2005, 4.4 billion years of crustal maturation: oxygen isotope ratios of magmatic zircon: Contributions to Mineralogy and Petrology, v. 150, no. 6, p. 561-580.

Vervoort, J. D., Patchett, P. J., Soderlund, U., and Baker, M., 2004, Isotopic composition of Yb and the determination of Lu concentrations and Lu/Hf ratios by isotope dilution using MC-ICPMS: Geochemistry Geophysics Geosystems, v. 5, article number Q11002.

Waight, T. E., Wiebe, R. A., Krogstad, E. J., and Walker, R. J., 2001, Isotopic responses to basaltic injections into silicic magma chambers: a whole-rock and microsampling study of macrorhythmic units in the Pleasant Bay layered gabbro-diorite complex, Maine, USA: Contributions to Mineralogy and Petrology, v. 142, no. 3, p. 323-335.

Walker, B. A., Miller, C. F., Claiborne, L. L., Wooden, J. L., and George, B., 2007, Batholith construction: New insights concerning timescales and physical processes from the Spirit Mountain batholith, southern Nevada: Journal of Volcanol Geotherm Res, v. 167, p. 239-262.

Watson, E. B., and Harrison, T. M., 1983, Zircon saturation revisited- Temperature and composition effects in a variety of crustal magma types: Earth and Planetary Science Letters, v. 64, no. 2, p. 295-304.

Watson, E. B., Wark, D. A., and Thomas, J. B., 2006, Crystallization thermometers for zircon and rutile: Contributions to Mineralogy and Petrology, v. 151, no. 4, p. 413-433.

Wiebe, R. A., 1996, Mafic-silicic layered intrusions: The role of basaltic injections on magmatic processes and the evolution of silicic magma chambers: Transactions of the Royal Society of Edinburgh-Earth Sciences, v. 87, p. 233-242.

Wiebe, R. A., and Collins, W. J., 1998, Depositional features and stratigraphic sections in granitic plutons: implications for the emplacement and crystallization of granitic magma: Journal of Structural Geology, v. 20, no. 9-10, p. 1273-1289.

Wiebe, R. A., Blair, K. D., Hawkins, D. P., and Sabine, C. P., 2002, Mafic injections, in situ hybridization, and crystal accumulation in the Pyramid Peak granite, California: Geological Society of America Bulletin, v. 114, no. 7, p. 909-920.

Woodhead, J., Hergt, J., Shelley, M., Eggins, S., and Kemp, R., 2004, Zircon Hf-isotope analysis with an excimer laser, depth profiling, ablation of complex geometries, and concomitant age estimation: Chemical Geology, v. 209, no. 1-2, p. 121-135.

Zheng, Y. F., Zhang, S. B., and Wu, R. X., 2007, Zircon U-Pb age, Hf and O isotope insight into origin of Neoproterozoic granitoids in South China: Geochimica Et Cosmochimica Acta, v. 71, no. 15, p. A1168-A1168.

Appendix A

Whole rock major and trace element data

and

whole rock Sr, Nd and Hf isotope data

Table A1 Whole-rock major element analysis

Sample	SiO_2	Al_2O_3	Fe_2O_3	MnO	MgO	CaO	Na_2O	K_2O	TiO_2	P_2O_5
NAWZ13	73.89	14.31	1.31	0.03	0.47	1.55	3.83	4.37	0.19	0.06
NAWZ16	60.03	19.07	5.18	0.06	1.79	4.33	5.34	2.85	1.02	0.32
NAWZ26	76.70	12.76	0.78	0.03	0.18	0.56	3.69	5.14	0.14	0.02
NAWZ50	73.93	13.66	1.57	0.03	0.45	1.05	3.39	5.57	0.27	0.07
AWAG1A	55.16	16.91	7.96	0.17	3.70	5.57	4.16	3.55	1.87	0.95
AWAG1B	56.16	16.58	7.89	0.11	3.60	5.42	3.96	3.54	1.81	0.93
AWAG1C	58.99	17.40	6.05	0.08	2.51	4.82	4.27	3.76	1.44	0.68
AWAG2	68.09	16.15	2.86	0.05	1.00	2.36	4.60	4.15	0.55	0.19
AWAG3	71.36	14.84	2.18	0.02	0.61	1.75	3.82	4.96	0.33	0.13
AWAG4	64.86	16.11	4.52	0.08	2.28	3.59	3.64	3.87	0.79	0.27
AWAG5	60.72	17.24	5.67	0.09	2.63	4.64	3.96	3.63	0.94	0.48
AWAG6	71.97	14.50	1.85	0.02	0.61	1.39	3.35	5.88	0.33	0.10
AWAG7	70.82	15.06	2.25	0.04	0.69	1.71	3.70	5.21	0.39	0.13

Table A2 Whole-rock trace element analysis

Sample	La	Ce	Pr	Nd	Sm	Eu	Gd	Tb	Dy	Ho	Er	Tm	Yb	Lu
NAWZ13	36.5	62.8	6.82	22.4	3.62	0.694	2.75	0.44	2.38	0.48	1.46	0.250	1.68	0.250
NAWZ16	124	304	33.6	125	23.6	3.58	18.3	2.86	14.2	2.46	6.09	0.801	4.56	0.581
NAWZ26	41.6	63.8	5.66	14.7	1.96	0.214	1.34	0.25	1.57	0.35	1.19	0.234	1.64	0.258
NAWZ50	61.3	96.3	9.49	28.5	4.05	0.672	2.88	0.43	2.40	0.47	1.41	0.231	1.59	0.252
AWAG1A	102	200	23.8	87	13	3.36	9.25	1.18	5.69	1.02	2.8	0.383	2.37	0.335
AWAG1B	92.4	181	21.2	78.7	11.6	3.21	8.33	1.05	4.92	0.92	2.55	0.347	2.05	0.288
AWAG1C	101	205	23.7	80.7	12.3	3.34	8.84	1.09	5.42	0.96	2.63	0.367	2.22	0.331
AWAG2	66.8	135	15.3	52.4	8.08	1.85	5.73	0.84	4.37	0.82	2.42	0.362	2.29	0.325
AWAG3	66.6	113	11.4	35.9	5.17	1.14	3.37	0.53	2.9	0.54	1.67	0.257	1.72	0.277
AWAG4	48.1	84	8.83	30.9	5	1.35	3.74	0.54	2.92	0.53	1.54	0.229	1.49	0.223
AWAG5	84	164	18.6	66.9	10.8	2.39	7.83	1.15	6.13	1.13	3.31	0.480	2.94	0.426
AWAG6	60.9	108	11.2	35.6	5.19	0.967	3.48	0.54	2.97	0.58	1.75	0.273	1.78	0.275
AWAG7	72.4	128	13.2	42.4	6.3	1.2	4.23	0.65	3.55	0.68	2.11	0.331	2.17	0.32

Table A2 (continued)

Sample	Ba	Sr	Y	Zr	Be	V	Ga	Ge	Rb	Nb	Sn	Cs
NAWZ13	1284	417	14	114	3	12	17	1.3	129	12.8	25	1.9
NAWZ16	1146	880	59	675	3	76	25	1.3	58	28.1	3	0.8
NAWZ26	121	45	12	129	5	6	18	1.5	206	26.5	2	3.4
NAWZ50	540	180	13	179	5	20	20	1.4	206	26.2	12	3.1
AWAG1A	1891	1226	25	417	4	169	28	1.8	101	22	2	2.5
AWAG1B	2025	1328	25	386	3	180	25	1.5	63	20.1	4	1.8
AWAG1C	2051	1413	26	368	2	123	24	1.4	68	22.5	2	1.7
AWAG2	1395	703	25	365	3	31	22	1.2	106	20.1	1	1.1
AWAG3	1196	379	14	251	3	28	20	1.3	109	17.5	< 1	1.3
AWAG4	1281	616	14	233	2	88	23	1.4	93	12.4	< 1	1.7
AWAG5	1651	895	31	517	2	99	25	1.5	84	22.1	2	1.5
AWAG6	835	283	15	224	3	27	20	1.1	140	19.1	1	1.2
AWAG7	1035	381	18	292	3	33	21	1.3	128	21.9	2	1.2

Table A3 Whole-rock major element analysis of AWM-1 and 2

Sample	SiO2	TiO2	Al2O3	FeO*	MnO	MgO	CaO	Na2O	K2O	P2O5
AWM-1	56.13	1.289	15.90	6.58	0.157	4.45	7.18	3.52	3.96	0.826
AWM-2	53.53	1.206	15.18	8.51	0.131	6.32	8.70	3.30	2.63	0.500

Table A4 Whole-rock trace element analysis of AWM1 and 2

Sample	Ni	Cr	Sc	V	Ba	Rb	Sr	Zr	Y	Nb	Ga	Cu	Zn	Pb	La	Ce	Th	Nd	U
AWM-1	31	36	18	172	1872	117	1227	265	42	29.8	22	80	88	18	91	216	13	98	4
AWM-2	82	176	24	213	1322	64	1096	246	25	13.8	19	103	81	13	61	117	9	56	2

Table A5 Whole-rock Sr, Hf and Nd isotope analysis

Sample Name	$^{87}Sr/^{86}Sr$	$^{87}Sr/^{86}Sr_i$	2SE	$^{176}Hf/^{177}Hf$	2SE	εHf	$\varepsilon Hf_{(t)}$	$^{143}Nd/^{144}Nd$	2SE	εNd	$\varepsilon Nd_{(t)}$
AWAG 1A	0.709428	0.709375	16	0.282438	12	-11.81	-11.5	0.512042	6	-11.62	-11.40
AWAG 1B	0.709341	0.70931	15	0.282411	6	-12.75	-12.44	0.512062	6	-11.23	-11.00
AWAG 1C	0.709360	0.709329	14	0.282417	5	-12.56	-12.3	0.512065	7	-11.17	-10.95
AWAG 2	0.709713	0.709616	17	0.282488	10	-10.05	-9.75	NA	NA	NA	NA
AWAG 3	0.710249	0.710064	12	0.282455	12	-11.22	-10.93	0.512142	7	-9.68	-9.44
AWAG 4	0.709981	0.709884	11	0.282447	8	-11.49	-11.19	NA	NA	NA	NA
AWAG 5	0.710115	0.710054	19	0.282407	10	-12.92	-12.62	0.512076	5	-10.97	-10.75
AWAG 6	0.710430	0.710112	15	0.282473	11	-10.58	-10.3	0.512112	7	-10.26	-10.03
AWAG 7	0.710220	0.710005	15	0.282498	11	-9.70	-9.41	0.512169	6	-9.15	-8.92
AWM-1	0.708002	0.708002	19	0.282581	10	-6.75	-6.74	0.512263	8	-7.32	-7.32
AWM-2	0.708490	0.708458	16	0.282500	7	-9.61	-9.33	0.512227	5	-8.02	-7.83
BCR.2	0.705041	NA	15	0.282867	7	3.37	NA	0.512695	4	1.11	NA
G.2	0.708296	NA	13	0.282523	5	-8.79	NA	0.512544	7	-1.84	NA
NAW 13	0.712085	0.711887	17	0.282394	7	-13.36	-13.11	0.512100	8	-10.49	-10.28
NAW 16	0.708894	0.708852	11	0.282541	8	-8.15	-7.85	0.512163	7	-9.27	-9.08
NAW 26	0.714425	0.711488	13	0.282485	6	-10.14	-9.87	0.512096	8	-10.57	-10.33
NAW 50	0.711100	0.710366	13	0.282468	7	-10.76	-10.48	0.512106	6	-10.37	-10.14

All initial ratios were calculated using an age of 15.6 Ma for the Aztec Wash pluton

Appendix B

Zircon SHRIMP trace element analysis

Sample AWM-1

Table B1: Zircon *in-situ* compositions from SHRIMP-RG

	Li Rel.	Be9 ppm	B11 ppm	F19 ppm	Na Rel	Al27 Rel.	P31 ppm	K39 Rel.	Ca40 Rel.	Sc45 ppm	48/49
AWM1-1.1	0.0	0.01	0.2	11	14	29	164	4	42	136	12.6
AWM1-1.2	0.0	0.00	0.1	4	20	26	64	4	36	90	13.4
AWM1-2.1	0.2	0.03	0.3	12	26	31	378	5	95	257	14.1
AWM1-2.2	0.0	0.01	0.1	28	27	45	478	4	1546	57	14.7
AWM1-3.1	0.0	0.00	0.5	11	28	31	44	5	44	35	13.0
AWM1-3.2	0.0	0.01	0.2	9	23	26	254	5	47	229	12.3
AWM1-4.1	0.0	0.01	0.3	10	34	34	301	6	49	381	13.4
AWM1-4.2	0.1	0.01	0.2	9	32	28	159	6	47	187	14.0
AWM1-4.3	3.2	0.17	82.2	20	12062	4765	49	4352	1072	31	12.0
AWM1-5.1	0.0	0.01	0.2	9	27	25	263	5	49	205	13.1
AWM1-5.2	0.0	0.01	0.3	11	33	29	212	4	65	231	12.0
AWM1-5.3	0.0	0.00	0.4	10	43	53	42	11	80	34	12.7
AWM1-6.1	0.1	0.00	0.2	11	27	104	48	45	59	38	14.3
AWM1-6.2	0.0	0.01	0.1	6	30	28	223	5	49	215	13.5
AWM1-7.1	0.1	0.08	0.2	15	26	22	534	5	49	125	12.7
AWM1-7.2	0.0	0.01	0.2	12	29	26	59	6	55	48	14.2
AWM1-8.1	0.0	0.07	0.3	8	31	24	260	6	62	295	11.7
AWM1-8.2	0.1	0.01	0.3	7	41	32	299	7	58	293	13.2
AWM1-8.3	0.2	0.00	0.7	13	105	196	75	32	1068	60	12.3
AWM1-9.1	0.2	0.22	0.2	14	43	32	384	7	81	214	13.3
AWM1-9.2	0.3	0.05	0.7	10	5061	7280	36	28923	138	37	12.9
AWM1-10.1	0.1	0.24	0.3	10	33	25	296	6	57	293	13.6
AWM1-10.2	0.1	0.05	0.4	12	38	32	140	7	80	242	13.5
AWM1-11.1	0.1	0.04	0.1	10	37	30	296	6	57	260	12.9
AWM1-11.2	0.0	0.00	0.1	3	10	17	44	3	31	57	10.6
AWM1-12.1	0.1	0.06	0.3	8	23	21	286	5	38	217	12.3
AWM1-12.2	0.1	0.10	0.1	9	22	21	295	5	41	366	13.7

Table B1 (cont): Zircon *in-situ* compositions from SHRIMP-RG

	Ti48 ppm	Ti49 ppm	Fe56 ppm	Y89 ppm	Nb93 ppm	Zr94H Rel.	Zr96/Si30	La139 ppm	Ce140 ppm	Nd146 ppm	Sm147 ppm
AWM1-1.1	22.8	24.2	1.1	1806	19	3.5	3.65	0.122	662	18.01	20.78
AWM1-1.2	4.7	4.7	1.7	531	4	3.2	3.45	0.033	56	0.89	1.74
AWM1-2.1	15.9	15.1	1.1	4155	15	3.4	3.51	1.814	535	73.35	67.16
AWM1-2.2	7.4	6.7	20.3	414	4	3.6	3.43	1.344	79	1.48	1.98
AWM1-3.1	6.9	7.1	0.9	566	2	3.3	3.53	0.035	44	3.22	3.89
AWM1-3.2	9.3	10.1	1.0	3443	10	3.3	3.34	0.637	431	37.26	37.71
AWM1-4.1	11.5	11.5	1.1	2914	13	3.3	3.42	0.045	331	5.82	10.13
AWM1-4.2	25.3	24.1	1.3	2228	30	3.3	3.30	0.139	774	18.97	22.93
AWM1-4.3	9.6	10.7	50.6	311	6	8.7	3.45	0.967	47	1.10	1.30
AWM1-5.1	12.3	12.6	1.0	2054	9	3.7	3.59	0.059	205	4.53	7.48
AWM1-5.2	7.9	8.8	1.3	2117	8	3.3	3.46	0.049	207	3.33	6.90
AWM1-5.3	5.5	5.8	41.0	226	2	2.8	3.32	0.051	23	0.19	0.52
AWM1-6.1	8.8	8.3	30.3	335	3	3.6	3.26	0.178	43	0.66	1.20
AWM1-6.2	32.5	32.3	1.2	3081	35	3.5	3.40	0.179	942	24.35	31.40
AWM1-7.1	41.3	43.4	1.0	4889	19	3.3	3.20	0.415	515	71.02	88.90
AWM1-7.2	8.6	8.1	0.9	814	4	3.1	3.20	0.074	74	4.09	5.58
AWM1-8.1	7.7	8.8	1.5	4341	15	3.9	3.67	0.664	474	34.58	41.55
AWM1-8.2	11.2	11.4	1.2	2907	15	3.7	3.60	0.066	304	5.67	10.57
AWM1-8.3	93.8	102.2	34.3	647	4	5.0	3.37	0.251	69	1.79	2.87
AWM1-9.1	22.6	22.8	1.6	5287	25	3.8	3.37	1.697	669	91.95	93.69
AWM1-9.2	9.0	9.3	24.7	319	3	2.6	3.04	0.566	30	1.36	2.03
AWM1-10.1	16.7	16.5	1.0	4159	15	3.7	3.61	1.316	535	51.71	51.83
AWM1-10.2	21.7	21.5	2.9	2326	25	4.4	3.87	0.245	725	15.28	20.48
AWM1-11.1	15.5	16.1	1.2	4482	16	3.6	3.65	1.062	540	54.28	56.12
AWM1-11.2	3.4	4.3	1.5	336	3	4.2	4.01	0.033	43	0.42	0.96
AWM1-12.1	16.8	18.3	0.9	4872	19	3.2	3.79	0.852	537	56.54	62.48
AWM1-12.2	11.5	11.3	0.9	3930	13	3.1	3.56	0.822	499	46.26	49.76

Table B1 (cont): Zircon *in-situ* compositions from SHRIMP-RG

	Eu153 ppm	GdO173 ppm	DyO179 ppm	ErO182 ppm	YbO188 ppm	LuO191 ppm	Zr96/Zr2O	196/Si30	Hf ppm	Pb7/6 est	Th ppm	U ppm
AWM1-1.1	9.804	97	176	236	410	80	103	0.0355	6727	0.0000	16096	2572
AWM1-1.2	1.241	16	50	91	181	39	96	0.0361	7641	0.0000	1031	803
AWM1-2.1	27.597	288	483	587	934	174	104	0.0338	6840	0.0516	4181	734
AWM1-2.2	0.963	13	30	55	123	27	94	0.0363	7676	0.0000	769	315
AWM1-3.1	2.014	21	51	83	166	36	102	0.0347	6993	0.0000	184	99
AWM1-3.2	19.978	184	354	468	847	167	102	0.0326	6377	0.0000	5266	1045
AWM1-4.1	5.032	71	217	464	962	201	102	0.0334	7468	0.0376	3397	1452
AWM1-4.2	11.521	117	246	322	534	98	102	0.0323	7615	0.0000	22498	3735
AWM1-4.3	0.669	7	23	51	121	27	71	0.0484	9922	0.0000	425	423
AWM1-5.1	3.987	54	157	320	695	147	101	0.0357	6863	0.0724	1920	906
AWM1-5.2	4.206	56	195	366	647	124	104	0.0335	7218	0.0000	5790	3480
AWM1-5.3	0.260	5	18	40	98	22	109	0.0306	8980	0.0000	236	252
AWM1-6.1	0.673	9	31	57	128	27	104	0.0314	8075	0.0000	270	194
AWM1-6.2	13.519	157	345	465	807	146	103	0.0330	6630	0.0000	14132	2826
AWM1-7.1	43.292	363	728	805	1112	177	106	0.0303	6737	0.0000	2736	637
AWM1-7.2	2.745	30	74	119	239	48	106	0.0300	7483	0.0000	340	160
AWM1-8.1	22.247	214	475	674	1151	217	104	0.0353	8592	0.0000	9185	2335
AWM1-8.2	5.310	80	242	459	857	172	103	0.0351	8053	0.0000	2177	926
AWM1-8.3	1.391	21	56	88	171	34	89	0.0378	8580	0.0000	243	150
AWM1-9.1	35.829	366	626	663	1041	180	106	0.0317	7802	0.0000	2138	355
AWM1-9.2	1.000	11	31	51	112	23	109	0.0279	8492	0.0000	127	92
AWM1-10.1	23.005	234	450	581	1005	188	112	0.0324	7486	0.0000	4569	982
AWM1-10.2	12.016	113	255	359	615	112	103	0.0377	8505	0.0000	26688	6244
AWM1-11.1	25.557	262	497	627	1077	195	108	0.0337	7569	0.0000	4730	1007
AWM1-11.2	0.729	8	25	53	123	26	91	0.0439	9260	0.0000	461	431
AWM1-12.1	24.492	280	512	617	1037	189	108	0.0351	8337	0.0000	2066	368
AWM1-12.2	23.896	228	447	565	956	180	108	0.0330	7229	0.0167	5768	1078

Table B1 (cont): Zircon *in-situ* compositions from SHRIMP-RG

	Y/Nb	Th/U	Yb/Gd	Yb/Nd	U/Yb	Th/Yb	Ce/Sm	Ce/Lu	U/Ce	Y/Yb	Y/Nb
AWM1-1.1	96	6.26	4.2	23	6.3	39.2	31.9	8.3	3.9	4.4	96
AWM1-1.2	133	1.28	11.5	202	4.4	5.7	32.2	1.4	14.3	2.9	133
AWM1-2.1	269	5.70	3.2	13	0.8	4.5	8.0	3.1	1.4	4.4	269
AWM1-2.2	95	2.44	9.7	83	2.6	6.2	40.0	2.9	4.0	3.4	95
AWM1-3.1	232	1.85	7.9	51	0.6	1.1	11.2	1.2	2.3	3.4	232
AWM1-3.2	362	5.04	4.6	23	1.2	6.2	11.4	2.6	2.4	4.1	362
AWM1-4.1	224	2.34	13.5	165	1.5	3.5	32.7	1.6	4.4	3.0	224
AWM1-4.2	75	6.02	4.5	28	7.0	42.1	33.7	7.9	4.8	4.2	75
AWM1-4.3	50	1.01	16.6	110	3.5	3.5	35.9	1.7	9.0	2.6	50
AWM1-5.1	228	2.12	13.0	154	1.3	2.8	27.4	1.4	4.4	3.0	228
AWM1-5.2	254	1.66	11.6	194	5.4	8.9	30.0	1.7	16.8	3.3	254
AWM1-5.3	104	0.94	18.2	507	2.6	2.4	44.2	1.0	10.8	2.3	104
AWM1-6.1	114	1.39	13.9	194	1.5	2.1	35.8	1.6	4.5	2.6	114
AWM1-6.2	89	5.00	5.2	33	3.5	17.5	30.0	6.4	3.0	3.8	89
AWM1-7.1	256	4.29	3.1	16	0.6	2.5	5.8	2.9	1.2	4.4	256
AWM1-7.2	211	2.12	8.0	59	0.7	1.4	13.3	1.5	2.2	3.4	211
AWM1-8.1	293	3.93	5.4	33	2.0	8.0	11.4	2.2	4.9	3.8	293
AWM1-8.2	195	2.35	10.7	151	1.1	2.5	28.7	1.8	3.0	3.4	195
AWM1-8.3	155	1.62	8.2	96	0.9	1.4	24.2	2.1	2.2	3.8	155
AWM1-9.1	209	6.03	2.8	11	0.3	2.1	7.1	3.7	0.5	5.1	209
AWM1-9.2	126	1.39	10.4	82	0.8	1.1	14.9	1.3	3.0	2.9	126
AWM1-10.1	271	4.65	4.3	19	1.0	4.5	10.3	2.8	1.8	4.1	271
AWM1-10.2	93	4.27	5.4	40	10.2	43.4	35.4	6.5	8.6	3.8	93
AWM1-11.1	285	4.70	4.1	20	0.9	4.4	9.6	2.8	1.9	4.2	285
AWM1-11.2	128	1.07	16.0	294	3.5	3.8	44.6	1.6	10.0	2.7	128
AWM1-12.1	263	5.62	3.7	18	0.4	2.0	8.6	2.8	0.7	4.7	263
AWM1-12.2	297	5.35	4.2	21	1.1	6.0	10.0	2.8	2.2	4.1	297

Table B1 (cont): Zircon *in-situ* compositions from SHRIMP-RG

	Yb / Nb	Yb / Sc	Yb / Dy	Dy / Sm	Yb / Nd	Sm / Nd
AWM1-1.1	96	6.26	4.2	23	6.3	39.2
AWM1-1.2	133	1.28	11.5	202	4.4	5.7
AWM1-2.1	269	5.70	3.2	13	0.8	4.5
AWM1-2.2	95	2.44	9.7	83	2.6	6.2
AWM1-3.1	232	1.85	7.9	51	0.6	1.1
AWM1-3.2	362	5.04	4.6	23	1.2	6.2
AWM1-4.1	224	2.34	13.5	165	1.5	3.5
AWM1-4.2	75	6.02	4.5	28	7.0	42.1
AWM1-4.3	50	1.01	16.6	110	3.5	3.5
AWM1-5.1	228	2.12	13.0	154	1.3	2.8
AWM1-5.2	254	1.66	11.6	194	5.4	8.9
AWM1-5.3	104	0.94	18.2	507	2.6	2.4
AWM1-6.1	114	1.39	13.9	194	1.5	2.1
AWM1-6.2	89	5.00	5.2	33	3.5	17.5
AWM1-7.1	256	4.29	3.1	16	0.6	2.5
AWM1-7.2	211	2.12	8.0	59	0.7	1.4
AWM1-8.1	293	3.93	5.4	33	2.0	8.0
AWM1-8.2	195	2.35	10.7	151	1.1	2.5
AWM1-8.3	155	1.62	8.2	96	0.9	1.4
AWM1-9.1	209	6.03	2.8	11	0.3	2.1
AWM1-9.2	126	1.39	10.4	82	0.8	1.1
AWM1-10.1	271	4.65	4.3	19	1.0	4.5
AWM1-10.2	93	4.27	5.4	40	10.2	43.4
AWM1-11.1	285	4.70	4.1	20	0.9	4.4
AWM1-11.2	128	1.07	16.0	294	3.5	3.8
AWM1-12.1	263	5.62	3.7	18	0.4	2.0
AWM1-12.2	297	5.35	4.2	21	1.1	6.0

Appendix C

Zircon age data

Samples AWM-1 and AWM-2

Table C1. SHRIMP U/Pb age data for AWM-1

Spot Name	% comm 206	ppm U	ppm Th	232Th /238U	204corr 206Pb /238U Age	1σ err	207corr 206Pb /238U Age	1σ err
AWM1-1.1	**2.50**	**773**	**3356**	4.49	**13.9**	**0.3**	**14.0**	**0.2**
AWM1-2.1	**5.59**	**335**	**1036**	3.20	**13.7**	**0.5**	**13.9**	**0.3**
AWM1-3.1	**0.79**	**3531**	**16994**	4.97	**15.2**	**0.1**	**15.2**	**0.1**
AWM1-4.1	**0.87**	**2521**	**13518**	5.54	**15.4**	**0.1**	**15.5**	**0.1**
AWM1-5.1	**1.94**	**750**	**3877**	5.34	**16.0**	**0.2**	**15.5**	**0.2**
AWM1-6.1	**0.55**	**1837**	**4008**	2.25	**15.7**	**0.1**	**15.7**	**0.1**
AWM1-7.1	**3.90**	**876**	**3282**	3.87	**15.4**	**0.2**	**15.0**	**0.2**
AWM1-8.1	**1.36**	**2533**	**6892**	2.81	**15.5**	**0.1**	**15.5**	**0.1**
AWM1-9.1	**3.24**	**638**	**2624**	4.25	**15.3**	**0.3**	**15.3**	**0.2**
AWM1-10.1	**2.11**	**914**	**3867**	4.37	**15.1**	**0.2**	**15.3**	**0.2**
AWM1-11.1	**0.37**	**4733**	**26192**	5.72	**16.1**	**0.1**	**16.1**	**0.1**
AWM1-12.1	**1.04**	**1941**	**10714**	5.70	**15.8**	**0.1**	**15.7**	**0.1**
AWM1-13.1	**1.87**	**867**	**2767**	3.30	**16.1**	**0.2**	**15.8**	**0.2**
AWM1-14.1	**0.78**	**1894**	**10922**	5.96	**15.8**	**0.1**	**15.8**	**0.1**
AWM1-15.1	**0.76**	**2252**	**6720**	3.08	**15.6**	**0.1**	**15.7**	**0.1**
AWM1-16.1	**2.25**	**685**	**1305**	1.97	**15.5**	**0.3**	**15.6**	**0.2**
AWM1-17.1	**0.86**	**956**	**3065**	3.31	**15.3**	**0.3**	**15.9**	**0.2**
AWM1-18.1	**0.70**	**1333**	**2964**	2.30	**15.7**	**0.2**	**15.9**	**0.1**
AWM1-19.1	**1.16**	**823**	**3752**	4.71	**15.2**	**0.2**	**15.6**	**0.2**
AWM1-20.1	**0.51**	**1444**	**6648**	4.76	**16.1**	**0.1**	**16.0**	**0.1**
AWM1-21.1	**0.87**	**1583**	**6060**	3.96	**15.8**	**0.2**	**15.8**	**0.1**
AWM1-22.1	**1.29**	**816**	**4018**	5.08	**16.0**	**0.2**	**16.0**	**0.2**

Table C2. SHRIMP U/Pb age data for AWM-2

Spot Name	% comm 206	ppm U	ppm Th	232Th /238U	204corr 206Pb /238U Age	1σ err	207corr 206Pb /238U Age	1σ err
AWM2-1.1	**4.55**	**228**	**396**	1.80	**17.8**	**0.4**	**16.5**	**0.3**
AWM2-2.1	**3.95**	**329**	**587**	1.84	**14.7**	**0.5**	**15.4**	**0.3**
AWM2-3.1	**3.50**	**366**	**747**	2.11	**14.8**	**0.4**	**15.0**	**0.3**
AWM2-4.1	**1.94**	**517**	**1288**	2.57	**15.4**	**0.3**	**15.8**	**0.2**
AWM2-5.1	**1.46**	**636**	**1925**	3.13	**15.7**	**0.2**	**15.8**	**0.2**
AWM2-6.1	**3.71**	**396**	**756**	1.97	**15.5**	**0.3**	**15.1**	**0.3**
AWM2-7.1	**2.75**	**537**	**1124**	2.16	**15.2**	**0.3**	**15.3**	**0.2**
AWM2-8.1	**1.93**	**507**	**1015**	2.07	**15.7**	**0.3**	**15.8**	**0.2**
AWM2-9.1	**2.53**	**382**	**695**	1.88	**14.9**	**0.4**	**15.4**	**0.3**
AWM2-10.1	**2.87**	**336**	**529**	1.63	**15.2**	**0.4**	**15.5**	**0.3**
AWM2-11.1	**1.83**	**395**	**910**	2.38	**15.4**	**0.3**	**15.6**	**0.3**
AWM2-12.1	**3.22**	**395**	**558**	1.46	**15.8**	**0.4**	**15.8**	**0.3**
AWM2-13.1	**3.47**	**397**	**685**	1.78	**15.5**	**0.3**	**15.3**	**0.3**
AWM2-14.1	**3.56**	**396**	**820**	2.14	**14.9**	**0.4**	**15.0**	**0.3**
AWM2-15.1	**4.26**	**261**	**388**	1.54	**16.0**	**0.4**	**15.9**	**0.4**
AWM2-16.1	**2.07**	**569**	**1816**	3.30	**15.7**	**0.3**	**15.7**	**0.2**
AWM2-17.1	**1.87**	**585**	**2138**	3.78	**15.5**	**0.3**	**15.6**	**0.2**
AWM2-18.1	**4.64**	**284**	**251**	0.91	**15.1**	**0.4**	**15.0**	**0.3**
AWM2-19.1	**3.18**	**437**	**941**	2.22	**15.4**	**0.3**	**15.2**	**0.2**
AWM2-20.1	**1.62**	**509**	**1325**	2.69	**14.9**	**0.3**	**15.3**	**0.2**

Appendix D

LA-ICP-MS in-situ zircon Hf isotopic data

Table D1. LA-ICP-MS in-situ zircon data

Sample Name	Mean	Std.Dev.	Std.Dev.%	εHf[#]	Std.Err.	Std.Err.%
AWM-1 6	0.28244	0.00025	0.00089	-11.7	0.00003	0.00011
8	0.28247	0.00024	0.00083	-10.8	0.00003	0.00010
12	0.28251	0.00029	0.00102	-9.3	0.00004	0.00014
13	0.28248	0.00024	0.00087	-10.3	0.00003	0.00011
14	0.28253	0.00025	0.00089	-8.4	0.00004	0.00012
15	0.28255	0.00022	0.00078	-7.8	0.00003	0.00012
16	0.28253	0.00029	0.00102	-8.7	0.00004	0.00016
17	0.28260	0.00021	0.00075	-6.1	0.00003	0.00011
18	0.28251	0.00022	0.00079	-9.4	0.00003	0.00010
19	0.28261	0.00022	0.00079	-5.8	0.00003	0.00012
20	0.28253	0.00029	0.00101	-8.6	0.00004	0.00014
21	0.28251	0.00024	0.00084	-9.2	0.00004	0.00014
22	0.28259	0.00020	0.00072	-6.5	0.00003	0.00010
25	0.28249	0.00022	0.00077	-10.1	0.00003	0.00012
26	0.28241	0.00024	0.00086	-12.7	0.00004	0.00014
27	0.28254	0.00022	0.00078	-8.3	0.00003	0.00011
28	0.28251	0.00020	0.00069	-9.2	0.00003	0.00009
29	0.28250	0.00026	0.00092	-9.7	0.00004	0.00014
30	0.28246	0.00021	0.00075	-10.9	0.00004	0.00013
31	0.28249	0.00022	0.00079	-9.9	0.00003	0.00012

εHf calculated using CHUR value = 0.282772 (Blichert-Toft and Alberéde, 1997)
Sample names indicate individual ablation spots
Errors are reported to 1SD and 1SE
Data not age corrected owing to low Lu/Hf. Measured values not affected beyond reported errors.

Table D1 (continued)

Sample Name	Mean	Std.Dev.	Std.Dev.%	εHf#	Std.Err.	Std.Err.%
32	0.28252	0.00021	0.00074	-9.1	0.00003	0.00012
33	0.28249	0.00028	0.00098	-9.9	0.00004	0.00015
34	0.28252	0.00022	0.00078	-8.8	0.00003	0.00012
35	0.28252	0.00023	0.00083	-8.8	0.00003	0.00011
36	0.28253	0.00022	0.00078	-8.5	0.00003	0.00012
37	0.28260	0.00027	0.00097	-5.9	0.00004	0.00014
AWM-2 44	0.28250	0.00017	0.00061	-9.4	0.00002	0.00009
45	0.28249	0.00023	0.00080	-10.0	0.00004	0.00013
46	0.28253	0.00026	0.00093	-8.6	0.00003	0.00012
47	0.28253	0.00020	0.00069	-8.4	0.00003	0.00010
48	0.28255	0.00029	0.00104	-7.7	0.00005	0.00017
49	0.28257	0.00029	0.00104	-7.0	0.00005	0.00016
50	0.28245	0.00027	0.00096	-11.3	0.00003	0.00012
51	0.28247	0.00022	0.00077	-10.5	0.00003	0.00010
52	0.28249	0.00023	0.00082	-10.0	0.00003	0.00011
56	0.28243	0.00020	0.00071	-12.2	0.00003	0.00010
57	0.28251	0.00026	0.00091	-9.3	0.00004	0.00013
58	0.28249	0.00034	0.00120	-9.9	0.00005	0.00018

εHf calculated using CHUR value = 0.282772 (Blichert-Toft and Alberéde, 1997)
Sample names indicate individual ablation spots
Errors are reported to 1SD and 1SE
Data not age corrected owing to low Lu/Hf. Measured values not affected beyond reported errors.

Table D1 (continued)

Sample Name	Mean	Std.Dev.	Std.Dev.%	εHf[#]	Std.Err.	Std.Err.%
59	0.28253	0.00030	0.00108	-8.7	0.00005	0.00019
60	0.28252	0.00024	0.00084	-8.9	0.00003	0.00010
61	0.28243	0.00027	0.00096	-12.1	0.00003	0.00012
62	0.28252	0.00025	0.00089	-8.8	0.00003	0.00011
63	0.28246	0.00026	0.00091	-11.0	0.00003	0.00012
64	0.28250	0.00020	0.00072	-9.5	0.00002	0.00008
NAWZ-13 75	0.28248	0.00021	0.00076	-10.2	0.00002	0.00008
76	0.28246	0.00018	0.00065	-11.2	0.00003	0.00009
77	0.28246	0.00019	0.00067	-11.1	0.00002	0.00007
78	0.28248	0.00019	0.00067	-10.5	0.00002	0.00007
79	0.28254	0.00020	0.00071	-8.2	0.00003	0.00009
80	0.28253	0.00020	0.00072	-8.6	0.00003	0.00011
81	0.28237	0.00020	0.00071	-14.2	0.00003	0.00009
82	0.28248	0.00020	0.00072	-10.3	0.00003	0.00009
83	0.28252	0.00018	0.00065	-9.1	0.00002	0.00007
84	0.28205	0.00022	0.00076	-25.7	0.00002	0.00008
85	0.28257	0.00022	0.00078	-7.2	0.00002	0.00009
86	0.28253	0.00020	0.00071	-8.6	0.00002	0.00008
87	0.28247	0.00019	0.00068	-10.6	0.00002	0.00009
88	0.28230	0.00013	0.00047	-16.8	0.00002	0.00008

εHf calculated using CHUR value = 0.282772 (Blichert-Toft and Alberéde, 1997)
Sample names indicate individual ablation spots
Errors are reported to 1SD and 1SE
Data not age corrected owing to low Lu/Hf. Measured values not affected beyond reported errors.

Table D1 (continued)

Sample Name	Mean	Std.Dev.	Std.Dev.%	εHf#	Std.Err.	Std.Err.%
NAWZ-50 92	0.28248	0.00018	0.00063	-10.5	0.00002	0.00008
93	0.28244	0.00020	0.00071	-11.8	0.00003	0.00010
94	0.28239	0.00021	0.00076	-13.4	0.00002	0.00009
95	0.28246	0.00025	0.00087	-11.0	0.00003	0.00010
96	0.28242	0.00025	0.00088	-12.5	0.00002	0.00009
97	0.28251	0.00017	0.00061	-9.2	0.00003	0.00011
98	0.28249	0.00024	0.00085	-9.9	0.00003	0.00011
99	0.28250	0.00024	0.00086	-9.5	0.00003	0.00010
100	0.28251	0.00024	0.00083	-9.3	0.00002	0.00009
101	0.28250	0.00019	0.00067	-9.6	0.00002	0.00008
102	0.28243	0.00026	0.00094	-11.9	0.00004	0.00014
103	0.28244	0.00031	0.00109	-11.6	0.00004	0.00013
NAWZ-16 106	0.28250	0.00023	0.00080	-9.7	0.00002	0.00008
107	0.28251	0.00025	0.00087	-9.3	0.00003	0.00010
108	0.28248	0.00024	0.00084	-10.3	0.00002	0.00009
109	0.28252	0.00021	0.00074	-9.0	0.00002	0.00007
110	0.28247	0.00021	0.00074	-10.7	0.00002	0.00007
111	0.28253	0.00022	0.00077	-8.7	0.00002	0.00008
112	0.28246	0.00021	0.00076	-11.1	0.00002	0.00007
113	0.28246	0.00026	0.00091	-10.9	0.00003	0.00011

εHf calculated using CHUR value = 0.282772 (Blichert-Toft and Alberéde, 1997)
Sample names indicate individual ablation spots
Errors are reported to 1SD and 1SE
Data not age corrected owing to low Lu/Hf. Measured values not affected beyond reported errors.

Table D1 (continued)

Sample Name	Mean	Std.Dev.	Std.Dev.%	εHf#	Std.Err.	Std.Err.%
114	0.28256	0.00021	0.00074	-7.7	0.00002	0.00007
115	0.28252	0.00020	0.00072	-8.8	0.00002	0.00009
116	0.28247	0.00020	0.00072	-10.5	0.00002	0.00007
117	0.28252	0.00023	0.00082	-8.8	0.00002	0.00009
118	0.28251	0.00022	0.00077	-9.2	0.00002	0.00009
119	0.28249	0.00021	0.00073	-10.0	0.00002	0.00007
120	0.28250	0.00020	0.00072	-9.5	0.00003	0.00010
NAWZ-26 123	0.28245	0.00022	0.00077	-11.4	0.00002	0.00009
124	0.28244	0.00023	0.00083	-11.9	0.00003	0.00009
125	0.28251	0.00028	0.00098	-9.3	0.00004	0.00014
126	0.28233	0.00024	0.00086	-15.7	0.00003	0.00012
127	0.28252	0.00028	0.00099	-9.0	0.00005	0.00018
128	0.28244	0.00025	0.00089	-11.7	0.00003	0.00012
129	0.28251	0.00022	0.00077	-9.4	0.00002	0.00008
130	0.28252	0.00019	0.00065	-8.9	0.00003	0.00012
131	0.28249	0.00016	0.00056	-10.0	0.00003	0.00010
132	0.28250	0.00015	0.00052	-9.5	0.00002	0.00007
133	0.28248	0.00022	0.00079	-10.4	0.00003	0.00009
134	0.28243	0.00021	0.00074	-12.1	0.00002	0.00007
135	0.28255	0.00020	0.00070	-7.8	0.00002	0.00008

εHf calculated using CHUR value = 0.282772 (Blichert-Toft and Alberéde, 1997)
Sample names indicate individual ablation spots
Errors are reported to 1SD and 1SE
Data not age corrected owing to low Lu/Hf. Measured values not affected beyond reported errors.

Table D1 (continued)

Sample Name	Mean	Std.Dev.	Std.Dev.%	εHf[#]	Std.Err.	Std.Err.%
136	0.28248	0.00021	0.00074	-10.4	0.00005	0.00018
137	0.28250	0.00022	0.00080	-9.7	0.00003	0.00010
138	0.28249	0.00020	0.00072	-10.0	0.00003	0.00009
139	0.28249	0.00022	0.00077	-10.0	0.00002	0.00009
140	0.28245	0.00018	0.00064	-11.4	0.00002	0.00008
AWAG7 148	0.28243	0.00032	0.00113	-12.0	0.00004	0.00014
149	0.28236	0.00026	0.00090	-14.5	0.00003	0.00011
150	0.28240	0.00024	0.00084	-13.3	0.00003	0.00012
151	0.28246	0.00025	0.00090	-11.0	0.00003	0.00010
152	0.28247	0.00023	0.00080	-10.6	0.00003	0.00010
153	0.28249	0.00019	0.00066	-9.9	0.00002	0.00008
154	0.28256	0.00024	0.00083	-7.6	0.00003	0.00010
155	0.28244	0.00018	0.00063	-11.7	0.00002	0.00007
156	0.28246	0.00022	0.00080	-11.1	0.00002	0.00008
157	0.28253	0.00023	0.00082	-8.5	0.00002	0.00008
158	0.28247	0.00026	0.00092	-10.7	0.00003	0.00010
159	0.28251	0.00019	0.00068	-9.3	0.00003	0.00009
160	0.28246	0.00020	0.00069	-10.9	0.00002	0.00008
161	0.28247	0.00018	0.00065	-10.7	0.00002	0.00007
AWAG-6 166	0.28250	0.00020	0.00070	-9.8	0.00002	0.00008

εHf calculated using CHUR value = 0.282772 (Blichert-Toft and Alberéde, 1997)
Sample names indicate individual ablation spots
Errors are reported to 1SD and 1SE
Data not age corrected owing to low Lu/Hf. Measured values not affected beyond reported errors.

Table D1 (continued)

Sample Name	Mean	Std.Dev.	Std.Dev.%	εHf[#]	Std.Err.	Std.Err.%
167	0.28252	0.00026	0.00093	-8.7	0.00003	0.00010
168	0.28262	0.00029	0.00102	-5.2	0.00003	0.00011
169	0.28259	0.00028	0.00099	-6.3	0.00003	0.00010
170	0.28245	0.00023	0.00080	-11.2	0.00003	0.00009
171	0.28245	0.00025	0.00088	-11.4	0.00003	0.00009
172	0.28232	0.00019	0.00068	-16.0	0.00002	0.00008
173	0.28237	0.00026	0.00091	-14.2	0.00003	0.00009
174	0.28250	0.00020	0.00070	-9.6	0.00003	0.00009
175	0.28246	0.00033	0.00117	-11.1	0.00003	0.00012
176	0.28251	0.00032	0.00113	-9.2	0.00003	0.00011
177	0.28240	0.00028	0.00099	-13.1	0.00003	0.00010
178	0.28245	0.00022	0.00079	-11.3	0.00002	0.00008
AWAG-3 183	0.28260	0.00027	0.00095	-6.2	0.00003	0.00010
184	0.28255	0.00025	0.00087	-7.9	0.00002	0.00008
185	0.28262	0.00028	0.00100	-5.4	0.00003	0.00011
186	0.28244	0.00026	0.00092	-11.6	0.00002	0.00008
187	0.28256	0.00025	0.00087	-7.4	0.00002	0.00008
188	0.28253	0.00030	0.00107	-8.5	0.00003	0.00010
189	0.28250	0.00019	0.00067	-9.5	0.00002	0.00007
190	0.28252	0.00021	0.00075	-8.8	0.00002	0.00008

εHf calculated using CHUR value = 0.282772 (Blichert-Toft and Alberéde, 1997)
Sample names indicate individual ablation spots
Errors are reported to 1SD and 1SE
Data not age corrected owing to low Lu/Hf. Measured values not affected beyond reported errors.

Table D1 (continued)

Sample Name	Mean	Std.Dev.	Std.Dev.%	εHf#	Std.Err.	Std.Err.%
199	0.28246	0.00025	0.00090	-11.0	0.00004	0.00013
200	0.28242	0.00025	0.00087	-12.4	0.00003	0.00009
201	0.28259	0.00031	0.00111	-6.3	0.00003	0.00011
202	0.28253	0.00027	0.00097	-8.5	0.00003	0.00010
203	0.28249	0.00027	0.00096	-10.0	0.00003	0.00009
204	0.28252	0.00027	0.00095	-9.0	0.00004	0.00013
205	0.28248	0.00025	0.00088	-10.3	0.00003	0.00011
206	0.28255	0.00021	0.00074	-7.7	0.00003	0.00011
207	0.28244	0.00019	0.00068	-11.8	0.00002	0.00008
208	0.28256	0.00022	0.00077	-7.4	0.00003	0.00011
209	0.28259	0.00024	0.00086	-6.6	0.00003	0.00011
AWAG-1C 212	0.28255	0.00029	0.00101	-8.0	0.00004	0.00016
213	0.28251	0.00025	0.00090	-9.3	0.00002	0.00009
214	0.28243	0.00036	0.00126	-11.9	0.00005	0.00017
215	0.28251	0.00030	0.00107	-9.2	0.00004	0.00014
216	0.28247	0.00020	0.00072	-10.7	0.00003	0.00011
217	0.28253	0.00035	0.00126	-8.7	0.00004	0.00013
218	0.28257	0.00030	0.00105	-7.3	0.00005	0.00017
219	0.28260	0.00035	0.00123	-5.9	0.00004	0.00015
220	0.28247	0.00034	0.00119	-10.8	0.00005	0.00018

εHf calculated using CHUR value = 0.282772 (Blichert-Toft and Alberéde, 1997)
Sample names indicate individual ablation spots
Errors are reported to 1SD and 1SE
Data not age corrected owing to low Lu/Hf. Measured values not affected beyond reported errors.

Table D1 (continued)

Sample Name	Mean	Std.Dev.	Std.Dev.%	εHf[#]	Std.Err.	Std.Err.%
221	0.28238	0.00023	0.00083	-13.7	0.00003	0.00011
222	0.28261	0.00038	0.00133	-5.8	0.00007	0.00025
AWAG-1A 225	0.28248	0.00032	0.00115	-10.3	0.00005	0.00016
226	0.28264	0.00028	0.00100	-4.5	0.00005	0.00016
227	0.28265	0.00036	0.00127	-4.5	0.00004	0.00016
228	0.28255	0.00024	0.00085	-7.9	0.00004	0.00013
229	0.28258	0.00030	0.00107	-6.8	0.00004	0.00014
230	0.28262	0.00026	0.00093	-5.4	0.00003	0.00012
231	0.28249	0.00023	0.00081	-10.1	0.00004	0.00013
232	0.28255	0.00023	0.00083	-7.9	0.00004	0.00013
233	0.28256	0.00032	0.00114	-7.5	0.00004	0.00014
234	0.28251	0.00040	0.00142	-9.1	0.00004	0.00015
235	0.28262	0.00030	0.00104	-5.5	0.00003	0.00011
236	0.28252	0.00027	0.00094	-9.1	0.00002	0.00009
237	0.28250	0.00032	0.00114	-9.7	0.00003	0.00010
238	0.28257	0.00038	0.00133	-7.1	0.00004	0.00014
AWAG-4 244	0.28251	0.00031	0.00111	-9.4	0.00004	0.00015
245	0.28249	0.00030	0.00106	-10.0	0.00005	0.00017
246	0.28253	0.00022	0.00078	-8.7	0.00003	0.00012
247	0.28244	0.00023	0.00081	-11.6	0.00004	0.00015
248	0.28246	0.00022	0.00077	-11.0	0.00004	0.00013

εHf calculated using CHUR value = 0.282772 (Blichert-Toft and Alberéde, 1997)
Sample names indicate individual ablation spots
Errors are reported to 1SD and 1SE
Data not age corrected owing to low Lu/Hf. Measured values not affected beyond reported errors.

Table D1 (continued)

Sample Name	Mean	Std.Dev.	Std.Dev.%	εHf#	Std.Err.	Std.Err.%
249	0.28247	0.00021	0.00076	-10.5	0.00003	0.00010
250	0.28253	0.00022	0.00078	-8.5	0.00003	0.00011
251	0.28244	0.00023	0.00080	-11.6	0.00003	0.00011
252	0.28249	0.00026	0.00093	-10.0	0.00003	0.00011
253	0.28247	0.00028	0.00098	-10.8	0.00004	0.00014
254	0.28247	0.00026	0.00091	-10.7	0.00003	0.00012
255	0.28247	0.00023	0.00080	-10.5	0.00002	0.00008
256	0.28238	0.00023	0.00081	-13.7	0.00003	0.00011
257	0.28240	0.00025	0.00089	-13.0	0.00003	0.00012
AWAG-5 260	0.28228	0.00027	0.00094	-17.5	0.00003	0.00012
261	0.28242	0.00022	0.00079	-12.5	0.00002	0.00007
262	0.28243	0.00020	0.00072	-12.2	0.00002	0.00008
263	0.28247	0.00024	0.00086	-10.6	0.00003	0.00010
264	0.28237	0.00022	0.00079	-14.2	0.00003	0.00010
265	0.28248	0.00028	0.00098	-10.5	0.00002	0.00008
266	0.28235	0.00030	0.00106	-15.0	0.00006	0.00020
267	0.28241	0.00033	0.00117	-12.9	0.00005	0.00019
AWAG-1B 268	0.28234	0.00029	0.00104	-15.4	0.00002	0.00009
269	0.28233	0.00034	0.00120	-15.6	0.00005	0.00016
270	0.28243	0.00019	0.00069	-12.1	0.00003	0.00009
271	0.28240	0.00029	0.00103	-13.1	0.00005	0.00017

εHf calculated using CHUR value = 0.282772 (Blichert-Toft and Alberéde, 1997)
Sample names indicate individual ablation spots
Errors are reported to 1SD and 1SE
Data not age corrected owing to low Lu/Hf. Measured values not affected beyond reported errors.

Table D1 (continued)

Sample Name	Mean	Std.Dev.	Std.Dev.%	εHf#	Std.Err.	Std.Err.%
272	0.28241	0.00022	0.00078	-12.9	0.00003	0.00009
273	0.28240	0.00021	0.00074	-13.1	0.00003	0.00009
274	0.28234	0.00030	0.00104	-15.3	0.00004	0.00013
275	0.28234	0.00026	0.00093	-15.3	0.00003	0.00011
276	0.28241	0.00024	0.00084	-12.7	0.00003	0.00012
277	0.28242	0.00025	0.00089	-12.4	0.00003	0.00012
GJ-1 1	0.28196	0.00037	0.00130	-28.7	0.00003	0.00012
2	0.28205	0.00021	0.00074	-25.4	0.00002	0.00007
3	0.28201	0.00024	0.00083	-27.0	0.00002	0.00008
4	0.28202	0.00025	0.00088	-26.5	0.00002	0.00009
5	0.28205	0.00026	0.00091	-25.5	0.00002	0.00009
9	0.28188	0.00027	0.00095	-31.4	0.00003	0.00009
10	0.28196	0.00023	0.00082	-28.7	0.00003	0.00009
11	0.28202	0.00017	0.00060	-26.4	0.00002	0.00007
23	0.28208	0.00022	0.00078	-24.6	0.00002	0.00008
24	0.28211	0.00019	0.00066	-23.5	0.00002	0.00007
38	0.28203	0.00017	0.00060	-26.2	0.00002	0.00007
39	0.28206	0.00015	0.00052	-25.0	0.00002	0.00007
40	0.28207	0.00020	0.00070	-25.0	0.00003	0.00009
41	0.28199	0.00016	0.00057	-27.7	0.00002	0.00007
42	0.28205	0.00017	0.00061	-25.6	0.00002	0.00006

εHf calculated using CHUR value = 0.282772 (Blichert-Toft and Alberéde, 1997)
Sample names indicate individual ablation spots
Errors are reported to 1SD and 1SE
Data not age corrected owing to low Lu/Hf. Measured values not affected beyond reported errors.

Table D1 (continued)

Sample Name	Mean	Std.Dev.	Std.Dev.%	εHf[#]	Std.Err.	Std.Err.%
43	0.28208	0.00018	0.00065	-24.3	0.00002	0.00007
53	0.28198	0.00017	0.00060	-28.1	0.00002	0.00007
54	0.28198	0.00022	0.00078	-28.0	0.00002	0.00007
55	0.28210	0.00023	0.00083	-23.7	0.00003	0.00009
65	0.28209	0.00023	0.00083	-24.0	0.00003	0.00010
66	0.28204	0.00019	0.00068	-25.7	0.00002	0.00008
67	0.28200	0.00021	0.00073	-27.2	0.00002	0.00008
68	0.28203	0.00019	0.00069	-26.3	0.00002	0.00008
69	0.28198	0.00026	0.00093	-28.2	0.00002	0.00008
70	0.28199	0.00021	0.00075	-27.5	0.00002	0.00009
71	0.28210	0.00023	0.00080	-23.7	0.00002	0.00008
72	0.28206	0.00020	0.00070	-25.2	0.00002	0.00008
73	0.28203	0.00018	0.00065	-26.1	0.00002	0.00007
74	0.28204	0.00021	0.00076	-25.7	0.00002	0.00008
89	0.28201	0.00028	0.00098	-27.0	0.00003	0.00009
90	0.28198	0.00019	0.00066	-27.9	0.00002	0.00007
91	0.28203	0.00021	0.00074	-26.1	0.00002	0.00008
104	0.28206	0.00023	0.00081	-25.3	0.00002	0.00008
105	0.28197	0.00022	0.00079	-28.4	0.00003	0.00009

εHf calculated using CHUR value = 0.282772 (Blichert-Toft and Alberéde, 1997)
Sample names indicate individual ablation spots
Errors are reported to 1SD and 1SE
Data not age corrected owing to low Lu/Hf. Measured values not affected beyond reported errors.

Table D1 (continued)

Sample Name	Mean	Std.Dev.	Std.Dev.%	εHf[#]	Std.Err.	Std.Err.%
121	0.28203	0.00025	0.00088	-26.4	0.00003	0.00009
122	0.28204	0.00028	0.00098	-25.7	0.00003	0.00012
141	0.28205	0.00024	0.00084	-25.6	0.00002	0.00009
142	0.28197	0.00023	0.00083	-28.4	0.00002	0.00008
143	0.28205	0.00020	0.00071	-25.5	0.00002	0.00008
144	0.28202	0.00015	0.00054	-26.5	0.00002	0.00007
145	0.28200	0.00020	0.00069	-27.1	0.00002	0.00008
146	0.28204	0.00019	0.00069	-25.9	0.00002	0.00007
147	0.28213	0.00019	0.00066	-22.7	0.00002	0.00008
163	0.28199	0.00020	0.00070	-27.8	0.00002	0.00008
164	0.28205	0.00018	0.00065	-25.7	0.00002	0.00007
165	0.28205	0.00019	0.00069	-25.5	0.00002	0.00007
179	0.28202	0.00017	0.00062	-26.6	0.00002	0.00007
180	0.28209	0.00022	0.00078	-24.2	0.00002	0.00009
181	0.28200	0.00018	0.00063	-27.3	0.00002	0.00007
182	0.28206	0.00019	0.00066	-25.2	0.00002	0.00007
194	0.28209	0.00021	0.00075	-24.1	0.00002	0.00007
195	0.28205	0.00018	0.00063	-25.5	0.00002	0.00007
196	0.28208	0.00018	0.00064	-24.6	0.00002	0.00006
197	0.28208	0.00023	0.00080	-24.3	0.00002	0.00008
210	0.28197	0.00024	0.00086	-28.3	0.00002	0.00008

εHf calculated using CHUR value = 0.282772 (Blichert-Toft and Alberéde, 1997)
Sample names indicate individual ablation spots
Errors are reported to 1SD and 1SE
Data not age corrected owing to low Lu/Hf. Measured values not affected beyond reported errors.

Table D1 (continued)

Sample Name	Mean	Std.Dev.	Std.Dev.%	εHf[#]	Std.Err.	Std.Err.%
211	0.28199	0.00022	0.00077	-27.8	0.00002	0.00008
223	0.28208	0.00028	0.00099	-24.6	0.00002	0.00008
224	0.28201	0.00023	0.00083	-27.0	0.00002	0.00008
239	0.28201	0.00025	0.00089	-26.9	0.00003	0.00009
240	0.28203	0.00021	0.00074	-26.4	0.00002	0.00009
241	0.28207	0.00019	0.00067	-24.9	0.00002	0.00008
242	0.28205	0.00029	0.00102	-25.5	0.00002	0.00009
243	0.28206	0.00028	0.00098	-25.0	0.00002	0.00009
258	0.28203	0.00021	0.00074	-26.4	0.00002	0.00009
259	0.28207	0.00019	0.00067	-24.9	0.00002	0.00008
278	0.28205	0.00029	0.00102	-25.5	0.00002	0.00009
279	0.28206	0.00028	0.00098	-25.0	0.00002	0.00009

εHf calculated using CHUR value = 0.282772 (Blichert-Toft and Alberéde, 1997)
Sample names indicate individual ablation spots
Errors are reported to 1SD and 1SE
Data not age corrected owing to low Lu/Hf. Measured values not affected beyond reported errors.

Appendix E

Zircon *in-situ* Oxygen isotope data

Table E1. Micro ionprobe in-situ zircon oxygen isotope data

Sample name	^{16}O	^{18}O	$^{18}O/^{16}O$	$^{18}O/^{16}O$ 1 s.e.	$\delta^{18}O$ /‰ (SMOW[#])	$\delta^{18}O$ (SMOW) 1 s.e.	IMF[##] Corrected	Corrected δ18O /‰	External 1 s.e.
NAWZ16_3_1.ais	2.37E+09	4.78E+06	2.02E-03	1.55E-07	6.18	0.08	1.5503E-07	6.0	0.2
NAWZ16_1_1.ais	2.38E+09	4.80E+06	2.02E-03	1.46E-07	6.29	0.07	1.4629E-07	6.1	0.2
NAWZ16_4_1.ais	2.39E+09	4.82E+06	2.02E-03	1.92E-07	6.30	0.09	1.9164E-07	6.2	0.2
NAWZ16_4_2.ais	2.37E+09	4.78E+06	2.02E-03	1.32E-07	6.44	0.07	1.3149E-07	6.2	0.2
NAWZ16_5_1.ais	2.42E+09	4.88E+06	2.02E-03	8.82E-08	6.31	0.04	8.8171E-08	6.3	0.2
NAWZ16_5_2.ais	2.38E+09	4.80E+06	2.02E-03	1.22E-07	6.34	0.06	1.2162E-07	6.2	0.2
NAWZ16_6_1.ais	2.42E+09	4.88E+06	2.02E-03	1.77E-07	6.22	0.09	1.7744E-07	6.2	0.2
NAWZ16_6_2.ais	2.39E+09	4.83E+06	2.02E-03	1.56E-07	6.68	0.08	1.5596E-07	6.6	0.2
NAWZ16_7_1.ais	2.34E+09	4.73E+06	2.02E-03	1.42E-07	6.50	0.07	1.4206E-07	6.2	0.2
NAWZ16_7_2.ais	2.40E+09	4.84E+06	2.02E-03	1.71E-07	6.13	0.08	1.7098E-07	6.0	0.2
NAWZ16_8_1.ais	2.39E+09	4.83E+06	2.02E-03	1.23E-07	6.28	0.06	1.2291E-07	6.2	0.2
NAWZ16_9_1.ais	2.39E+09	4.82E+06	2.02E-03	1.60E-07	6.30	0.08	1.6047E-07	6.2	0.2
NAWZ16_9_2.ais	2.38E+09	4.81E+06	2.02E-03	1.39E-07	6.03	0.07	1.3896E-07	5.9	0.2
NAWZ16_10_1.ais	2.43E+09	4.90E+06	2.02E-03	8.07E-08	5.86	0.04	8.0750E-08	5.9	0.2
NAWZ16_11_1.ais	2.38E+09	4.81E+06	2.02E-03	1.78E-07	6.47	0.09	1.7786E-07	6.3	0.2
NAWZ16_12_1.ais	2.37E+09	4.78E+06	2.02E-03	1.91E-07	6.65	0.09	1.9073E-07	6.4	0.2
NAWZ26_1_1.ais	2.38E+09	4.80E+06	2.02E-03	1.24E-07	6.52	0.06	1.2442E-07	6.3	0.2
NAWZ26_1_2.ais	2.39E+09	4.83E+06	2.02E-03	7.53E-08	6.28	0.04	7.5297E-08	6.2	0.2
NAWZ26_2_1.ais	2.35E+09	4.74E+06	2.02E-03	1.27E-07	6.88	0.06	1.2676E-07	6.6	0.2
NAWZ26_3_1.ais	2.37E+09	4.79E+06	2.02E-03	1.25E-07	6.73	0.06	1.2493E-07	6.5	0.2
NAWZ26_4_1.ais	2.37E+09	4.78E+06	2.02E-03	1.15E-07	5.72	0.06	1.1522E-07	5.5	0.2
NAWZ26_5_1.ais	2.35E+09	4.74E+06	2.02E-03	1.97E-07	6.42	0.10	1.9684E-07	6.1	0.2
NAWZ26_6_1.ais	2.37E+09	4.79E+06	2.02E-03	1.76E-07	6.12	0.09	1.7582E-07	5.9	0.2
NAWZ26_8_2.ais	2.40E+09	4.84E+06	2.02E-03	1.29E-07	6.15	0.06	1.2907E-07	6.0	0.2

Standard R33 used. Accepted ratio for standard = 5.55 ‰ ± 0.04 (Valley, 2003)

[#]Ratios relative to standard mean ocean water (SMOW) = 2.0052×10^{-3}

[##]IMF = Instrumental mass fractionation

Table E1 continued

Sample name	^{16}O	^{18}O	$^{18}O/^{16}O$	$^{18}O/^{16}O$ 1 s.e.	$\delta^{18}O$ /‰ (SMOW[#])	$\delta^{18}O$ (SMOW) 1 s.e.	IMF[##] Corrected	Corrected δ18O /‰	External 1 s.e.
NAWZ26_8_1.ais	2.35E+09	4.74E+06	2.02E-03	1.59E-07	6.54	0.08	1.585E-07	6.2	0.2
NAWZ26_7_1.ais	2.39E+09	4.83E+06	2.02E-03	1.68E-07	5.88	0.08	1.683E-07	5.8	0.2
NAWZ26_7_2.ais	2.38E+09	4.81E+06	2.02E-03	1.80E-07	6.22	0.09	1.802E-07	6.1	0.2
NAWZ26_9_1.ais	2.38E+09	4.80E+06	2.02E-03	1.51E-07	5.56	0.07	1.505E-07	5.4	0.2
NAWZ13_1_3.ais	2.36E+09	4.76E+06	2.02E-03	1.54E-07	6.75	0.08	1.539E-07	6.5	0.2
NAWZ13_1_1.ais	2.40E+09	4.84E+06	2.02E-03	1.78E-07	5.86	0.09	1.781E-07	5.8	0.2
NAWZ13_1_2.ais	2.35E+09	4.74E+06	2.02E-03	1.75E-07	6.41	0.09	1.748E-07	6.1	0.2
NAWZ13_2_1.ais	2.35E+09	4.75E+06	2.02E-03	1.45E-07	6.91	0.07	1.447E-07	6.6	0.2
NAWZ13_3_1.ais	2.34E+09	4.72E+06	2.02E-03	1.10E-07	6.29	0.05	1.097E-07	5.9	0.2
NAWZ13_4_2.ais	2.38E+09	4.80E+06	2.02E-03	1.48E-07	6.29	0.07	1.485E-07	6.1	0.2
NAWZ13_4_1.ais	2.31E+09	4.66E+06	2.02E-03	1.74E-07	6.73	0.09	1.744E-07	6.3	0.2
NAWZ13_5_1.ais	2.33E+09	4.71E+06	2.02E-03	2.03E-07	5.95	0.10	2.030E-07	5.6	0.2
NAWZ13_5_2.ais	2.39E+09	4.82E+06	2.02E-03	1.89E-07	5.07	0.09	1.892E-07	4.9	0.2
NAWZ13_6_1.ais	2.33E+09	4.70E+06	2.02E-03	1.66E-07	6.42	0.08	1.657E-07	6.0	0.2
NAWZ13_7_2.ais	2.40E+09	4.84E+06	2.02E-03	1.05E-07	6.18	0.05	1.053E-07	6.1	0.2
NAWZ13_7_1.ais	2.35E+09	4.74E+06	2.02E-03	1.43E-07	6.65	0.07	1.432E-07	6.3	0.2
NAWZ13_8_1.ais	2.34E+09	4.73E+06	2.02E-03	1.09E-07	5.96	0.05	1.094E-07	5.6	0.2
NAWZ13_9_1.ais	2.31E+09	4.67E+06	2.02E-03	9.57E-08	6.30	0.05	9.564E-08	5.8	0.2
NAWZ13_9_2.ais	2.35E+09	4.74E+06	2.02E-03	1.25E-07	6.91	0.06	1.252E-07	6.6	0.2
NAWZ13_10_1.ais	2.35E+09	4.75E+06	2.02E-03	2.01E-07	6.82	0.10	2.012E-07	6.5	0.2
NAWZ13_11_1.ais	2.32E+09	4.68E+06	2.02E-03	1.68E-07	6.38	0.08	1.683E-07	5.9	0.2
NAWZ50_1_2.ais	2.32E+09	4.69E+06	2.02E-03	9.20E-08	6.52	0.05	9.196E-08	6.1	0.2

Standard R33 used. Accepted ratio for standard = 5.55 ‰ ± 0.04 (Valley, 2003)
[#]Ratios relative to standard mean ocean water (SMOW) = 2.0052×10^{-3}
[##]IMF = Instrumental mass fractionation

Table E1 continued

Sample name	^{16}O	^{18}O	$^{18}O/^{16}O$	$^{18}O/^{16}O$ 1 s.e.	$\delta^{18}O$ /‰ (SMOW[#])	$\delta^{18}O$ (SMOW) 1 s.e.	IMF[##] Corrected	Corrected δ18O /‰	External 1 s.e.
NAWZ50_1_1.ais	2.35E+09	4.75E+06	2.02E-03	1.04E-07	6.75	0.05	1.040E-07	6.5	0.2
NAWZ50_9_2.ais	2.35E+09	4.75E+06	2.02E-03	1.48E-07	6.42	0.07	1.483E-07	6.1	0.2
NAWZ50_9_1.ais	2.34E+09	4.72E+06	2.02E-03	9.46E-08	6.63	0.05	9.453E-08	6.3	0.2
NAWZ50_2_1.ais	2.32E+09	4.69E+06	2.02E-03	1.69E-07	6.83	0.08	1.687E-07	6.4	0.2
NAWZ50_2_2.ais	2.33E+09	4.70E+06	2.02E-03	1.82E-07	6.73	0.09	1.817E-07	6.3	0.2
NAWZ50_8_1.ais	2.31E+09	4.66E+06	2.02E-03	1.44E-07	6.34	0.07	1.435E-07	5.9	0.2
NAWZ50_8_2.ais	2.31E+09	4.66E+06	2.02E-03	1.16E-07	6.94	0.06	1.163E-07	6.5	0.2
NAWZ50_10_1.ais	2.34E+09	4.71E+06	2.02E-03	1.35E-07	6.39	0.07	1.347E-07	6.0	0.2
NAWZ50_10_2.ais	2.35E+09	4.74E+06	2.02E-03	1.65E-07	6.51	0.08	1.649E-07	6.2	0.2
NAWZ50_4_1.ais	2.32E+09	4.68E+06	2.02E-03	1.49E-07	6.32	0.07	1.491E-07	5.9	0.2
NAWZ50_4_2.ais	2.36E+09	4.75E+06	2.02E-03	1.76E-07	6.01	0.09	1.762E-07	5.7	0.2
NAWZ50_3_2.ais	2.39E+09	4.83E+06	2.02E-03	1.79E-07	6.64	0.09	1.794E-07	6.5	0.2
NAWZ50_3_1.ais	2.33E+09	4.70E+06	2.02E-03	2.19E-07	6.61	0.11	2.194E-07	6.2	0.2
NAWZ50_7_1.ais	2.34E+09	4.71E+06	2.02E-03	1.35E-07	6.30	0.07	1.348E-07	5.9	0.2
NAWZ50_7_2.ais	2.36E+09	4.76E+06	2.02E-03	1.82E-07	6.60	0.09	1.818E-07	6.3	0.2
NAWZ50_6_2.ais	2.34E+09	4.72E+06	2.02E-03	1.69E-07	6.28	0.08	1.693E-07	5.9	0.2
NAWZ50_5_1.ais	2.34E+09	4.72E+06	2.02E-03	1.65E-07	6.30	0.08	1.653E-07	6.0	0.2
NAWZ50_5_2.ais	2.32E+09	4.69E+06	2.02E-03	2.18E-07	6.51	0.11	2.180E-07	6.1	0.2
AWAG1A_1_1.ais	2.35E+09	4.74E+06	2.02E-03	1.47E-07	6.07	0.07	1.4730E-07	5.7	0.2
AWAG1A_3_2.ais	2.36E+09	4.77E+06	2.02E-03	1.12E-07	6.61	0.06	1.1159E-07	6.3	0.2

Standard R33 used. Accepted ratio for standard = 5.55 ‰ ± 0.04 (Valley, 2003)
[#]Ratios relative to standard mean ocean water (SMOW) = 2.0052×10^{-3}
[##]IMF = Instrumental mass fractionation

Table E1 continued

Sample name	^{16}O	^{18}O	$^{18}O/^{16}O$	$^{18}O/^{16}O$ 1 s.e.	$\delta^{18}O$ /‰ (SMOW[#])	$\delta^{18}O$ (SMOW) 1 s.e.	IMF[##] Corrected	Corrected δ18O /‰	External 1 s.e.
AWAG1A_3_1.ais	2.33E+09	4.71E+06	2.02E-03	1.13E-07	6.32	0.06	1.1268E-07	6.0	0.2
AWAG1A_4_2.ais	2.24E+09	4.52E+06	2.02E-03	2.35E-07	7.27	0.12	2.3524E-07	6.9	0.2
AWAG1A_4_1.ais	2.35E+09	4.74E+06	2.02E-03	1.77E-07	6.49	0.09	1.7682E-07	6.1	0.2
AWAG1A_5_1.ais	2.38E+09	4.80E+06	2.02E-03	1.52E-07	6.20	0.08	1.5172E-07	5.9	0.2
AWAG1A_6_1.ais	2.37E+09	4.77E+06	2.02E-03	1.31E-07	6.40	0.07	1.3130E-07	6.1	0.2
AWAG1A_12_1.ais	2.36E+09	4.75E+06	2.02E-03	1.42E-07	5.96	0.07	1.4152E-07	5.6	0.2
AWAG1A_12_2.ais	2.31E+09	4.66E+06	2.02E-03	1.36E-07	6.78	0.07	1.3592E-07	6.4	0.2
AWAG1A_7_1.ais	2.34E+09	4.73E+06	2.02E-03	1.65E-07	6.43	0.08	1.6498E-07	6.1	0.2
AWAG1A_8_1.ais	2.35E+09	4.75E+06	2.02E-03	1.60E-07	6.31	0.08	1.5978E-07	6.0	0.2
AWAG1A_8_2.ais	2.34E+09	4.72E+06	2.02E-03	1.42E-07	6.49	0.07	1.4164E-07	6.1	0.2
AWAG1A_8_3.ais	2.37E+09	4.78E+06	2.02E-03	1.13E-07	6.38	0.06	1.1332E-07	6.0	0.2
AWAG1A_11_1.ais	2.36E+09	4.77E+06	2.02E-03	1.61E-07	6.08	0.08	1.6086E-07	5.7	0.2
AWAG1A_M_1.ais	2.37E+09	4.79E+06	2.02E-03	1.22E-07	6.08	0.06	1.2194E-07	5.7	0.2
AWAG1A_M_2.ais	2.35E+09	4.74E+06	2.02E-03	1.75E-07	6.38	0.09	1.7454E-07	6.0	0.2
AWAG1C_1_1.ais	2.35E+09	4.74E+06	2.02E-03	1.21E-07	6.43	0.06	1.2052E-07	6.1	0.2
AWAG1C_3_1.ais	2.36E+09	4.77E+06	2.02E-03	1.82E-07	6.87	0.09	1.8217E-07	6.5	0.2
AWAG1C_3_2.ais	2.32E+09	4.68E+06	2.02E-03	1.43E-07	7.30	0.07	1.4300E-07	6.9	0.2
AWAG1C_5_1.ais	2.36E+09	4.77E+06	2.02E-03	1.07E-07	6.44	0.05	1.0660E-07	6.1	0.2
AWAG1C_7_1.ais	2.37E+09	4.78E+06	2.02E-03	1.60E-07	5.96	0.08	1.6042E-07	5.6	0.2
AWAG1C_8_1.ais	2.36E+09	4.77E+06	2.02E-03	1.25E-07	6.23	0.06	1.253E-07	5.9	0.2
AWAG1C_9_1.ais	2.37E+09	4.79E+06	2.02E-03	2.04E-07	6.14	0.10	2.038E-07	5.8	0.2
AWAG1C_10_1.ais	2.38E+09	4.81E+06	2.02E-03	1.28E-07	6.54	0.06	1.282E-07	6.2	0.2
AWAG1C_11_1.ais	2.35E+09	4.75E+06	2.02E-03	1.06E-07	6.83	0.05	1.061E-07	6.5	0.2
AWAG1C_M_1.ais	2.37E+09	4.79E+06	2.02E-03	1.64E-07	6.61	0.08	1.643E-07	6.3	0.2

Standard R33 used. Accepted ratio for standard = 5.55 ‰ ± 0.04 (Valley, 2003)

[#]Ratios relative to standard mean ocean water (SMOW) = 2.0052×10^{-3}

[##]IMF = Instrumental mass fractionation

Table E1 continued

Sample name	^{16}O	^{18}O	$^{18}O/^{16}O$	$^{18}O/^{16}O$ 1 s.e.	$\delta^{18}O$ /‰ (SMOW[#])	$\delta^{18}O$ (SMOW) 1 s.e.	IMF[##] Corrected	Corrected δ18O /‰	External 1 s.e.
AWAG1C_M_2.ais	2.40E+09	4.85E+06	2.02E-03	1.58E-07	6.62	0.08	1.584E-07	6.3	0.2
AWAG1C_M_3.ais	2.41E+09	4.87E+06	2.02E-03	2.07E-07	6.22	0.10	2.065E-07	5.9	0.2
AWAG2_1_3.ais	2.40E+09	4.85E+06	2.02E-03	1.87E-07	6.60	0.09	1.868E-07	6.3	0.2
AWAG2_1_1.ais	2.41E+09	4.86E+06	2.02E-03	1.08E-07	6.52	0.05	1.083E-07	6.2	0.2
AWAG2_3_2.ais	2.43E+09	4.90E+06	2.02E-03	1.52E-07	6.10	0.08	1.520E-07	5.8	0.2
AWAG2_3_1.ais	2.39E+09	4.82E+06	2.02E-03	1.75E-07	6.90	0.09	1.750E-07	6.6	0.2
AWAG2_4_1.ais	2.41E+09	4.88E+06	2.02E-03	1.12E-07	6.94	0.06	1.123E-07	6.6	0.2
AWAG2_4_2.ais	2.39E+09	4.83E+06	2.02E-03	9.58E-08	7.02	0.05	9.577E-08	6.7	0.2
AWAG2_5_1.ais	2.39E+09	4.82E+06	2.02E-03	1.83E-07	6.82	0.09	1.833E-07	6.5	0.2
AWAG2_5_2.ais	2.42E+09	4.88E+06	2.02E-03	1.47E-07	6.65	0.07	1.472E-07	6.3	0.2
AWAG2_6_1.ais	2.39E+09	4.83E+06	2.02E-03	1.55E-07	6.86	0.08	1.549E-07	6.5	0.2
AWAG2_8_2.ais	2.38E+09	4.81E+06	2.02E-03	1.59E-07	6.90	0.08	1.591E-07	6.6	0.2
AWAG2_9_1.ais	2.39E+09	4.83E+06	2.02E-03	1.37E-07	6.66	0.07	1.374E-07	6.3	0.2
AWAG2_9_2.ais	2.39E+09	4.83E+06	2.02E-03	1.84E-07	6.47	0.09	1.840E-07	6.1	0.2
AWAG2_10_2.ais	2.43E+09	4.91E+06	2.02E-03	4.40E-07	6.62	0.22	4.395E-07	6.3	0.2
AWAG2_M_1.ais	2.40E+09	4.84E+06	2.02E-03	1.72E-07	6.52	0.09	1.722E-07	6.2	0.2
AWAG2_M_2.ais	2.40E+09	4.84E+06	2.02E-03	1.34E-07	6.91	0.07	1.341E-07	6.6	0.2
AWAG2_M_3.ais	2.37E+09	4.79E+06	2.02E-03	1.39E-07	6.78	0.07	1.386E-07	6.4	0.2
AWAG3_1_1.ais	2.40E+09	4.84E+06	2.02E-03	1.59E-07	6.40	0.08	1.586E-07	6.1	0.2
AWAG3_1_2.ais	2.37E+09	4.79E+06	2.02E-03	9.21E-08	6.65	0.05	9.207E-08	6.3	0.2
AWAG3_2_1.ais	2.40E+09	4.85E+06	2.02E-03	1.76E-07	6.37	0.09	1.761E-07	6.1	0.2
AWAG3_2_2.ais	2.38E+09	4.81E+06	2.02E-03	1.46E-07	6.83	0.07	1.456E-07	6.5	0.2

Standard R33 used. Accepted ratio for standard = 5.55 ‰ ± 0.04 (Valley, 2003)

[#]Ratios relative to standard mean ocean water (SMOW) = 2.0052×10^{-3}

[##]IMF = Instrumental mass fractionation

Table E1 continued

Sample name	^{16}O	^{18}O	$^{18}O/^{16}O$	$^{18}O/^{16}O$ 1 s.e.	$\delta^{18}O$ /‰ (SMOW[#])	$\delta^{18}O$ (SMOW) 1 s.e.	IMF[##] Corrected	Corrected δ18O /‰	External 1 s.e.
AWAG3_2_3.ais	2.42E+09	4.88E+06	2.02E-03	1.34E-07	6.55	0.07	1.335E-07	6.2	0.2
AWAG3_3_1.ais	2.41E+09	4.87E+06	2.02E-03	1.16E-07	6.84	0.06	1.162E-07	6.5	0.2
AWAG3_3_2.ais	2.46E+09	4.96E+06	2.02E-03	1.26E-07	6.57	0.06	1.257E-07	6.3	0.2
AWAG3_4_1.ais	2.41E+09	4.86E+06	2.02E-03	1.01E-07	7.30	0.05	1.011E-07	7.0	0.2
AWAG3_4_2.ais	2.39E+09	4.83E+06	2.02E-03	1.98E-07	6.25	0.10	1.980E-07	5.9	0.2
AWAG3_6_1.ais	2.41E+09	4.87E+06	2.02E-03	1.73E-07	7.37	0.09	1.734E-07	7.1	0.2
AWAG3_7_3.ais	2.41E+09	4.87E+06	2.02E-03	1.63E-07	6.83	0.08	1.628E-07	6.5	0.2
AWAG3_7_1.ais	2.40E+09	4.84E+06	2.02E-03	1.04E-07	6.64	0.05	1.041E-07	6.3	0.2
AWAG3_M_1.ais	2.45E+09	4.94E+06	2.02E-03	1.11E-07	7.07	0.05	1.105E-07	6.8	0.2
AWAG3_M_2.ais	2.38E+09	4.80E+06	2.02E-03	1.38E-07	6.69	0.07	1.382E-07	6.4	0.2
AWAG3_M_3.ais	2.43E+09	4.90E+06	2.02E-03	1.51E-07	6.53	0.07	1.509E-07	6.2	0.2
AWAG3_M_4.ais	2.39E+09	4.83E+06	2.02E-03	1.63E-07	6.67	0.08	1.633E-07	6.4	0.2
AWAG6_1_2.ais	2.42E+09	4.89E+06	2.02E-03	1.55E-07	6.62	0.08	1.547E-07	6.3	0.2
AWAG6_1_1.ais	2.43E+09	4.90E+06	2.02E-03	1.30E-07	7.22	0.06	1.300E-07	6.9	0.2
AWAG6_3_1.ais	2.40E+09	4.84E+06	2.02E-03	1.29E-07	7.03	0.06	1.285E-07	6.7	0.2
AWAG6_3_2.ais	2.40E+09	4.85E+06	2.02E-03	1.53E-07	7.01	0.08	1.532E-07	6.7	0.2
AWAG6_4_2.ais	2.44E+09	4.92E+06	2.02E-03	1.24E-07	6.23	0.06	1.240E-07	5.9	0.2
AWAG6_4_1.ais	2.42E+09	4.88E+06	2.02E-03	2.08E-07	6.42	0.10	2.081E-07	6.1	0.2
AWAG6_6_3.ais	2.41E+09	4.86E+06	2.02E-03	1.87E-07	7.04	0.09	1.871E-07	6.7	0.2
AWAG6_6_2.ais	2.43E+09	4.91E+06	2.02E-03	1.39E-07	6.68	0.07	1.392E-07	6.4	0.2
AWAG6_6_1.ais	2.44E+09	4.93E+06	2.02E-03	1.58E-07	6.83	0.08	1.584E-07	6.5	0.2
AWAG6_7_1.ais	2.42E+09	4.89E+06	2.02E-03	1.42E-07	7.03	0.07	1.419E-07	6.7	0.2
AWAG6_M_1.ais	2.42E+09	4.88E+06	2.02E-03	2.05E-07	6.56	0.10	2.046E-07	6.3	0.2
AWAG6_M_2.ais	2.44E+09	4.93E+06	2.02E-03	1.80E-07	6.24	0.09	1.803E-07	6.0	0.2

Standard R33 used. Accepted ratio for standard = 5.55 ‰ ± 0.04 (Valley, 2003)

[#]Ratios relative to standard mean ocean water (SMOW) = 2.0052×10^{-3}

[##]IMF = Instrumental mass fractionation

Table E1 continued

Sample name	^{16}O	^{18}O	$^{18}O/^{16}O$	$^{18}O/^{16}O$ 1 s.e.	$\delta^{18}O$ /‰ (SMOW[#])	$\delta^{18}O$ (SMOW) 1 s.e.	IMF[##] Corrected	Corrected δ18O /‰	External 1 s.e.
AWAG6_M_3.ais	2.43E+09	4.91E+06	2.02E-03	1.12E-07	6.78	0.06	1.124E-07	6.5	0.2
AWAG6_M_4.ais	2.46E+09	4.96E+06	2.02E-03	9.09E-08	6.18	0.05	9.084E-08	5.9	0.2
AWAG6_M_5.ais	2.42E+09	4.88E+06	2.02E-03	1.63E-07	6.58	0.08	1.626E-07	6.3	0.2
AWAG6_M_6.ais	2.42E+09	4.88E+06	2.02E-03	1.69E-07	6.85	0.08	1.685E-07	6.6	0.2
AWAG7_2_2.ais	2.43E+09	4.90E+06	2.02E-03	1.42E-07	7.14	0.07	1.420E-07	6.9	0.2
AWAG7_2_1.ais	2.42E+09	4.89E+06	2.02E-03	1.94E-07	7.52	0.10	1.943E-07	7.2	0.2
AWAG7_3_1.ais	2.43E+09	4.91E+06	2.02E-03	1.27E-07	6.50	0.06	1.269E-07	6.2	0.2
AWAG7_3_2.ais	2.42E+09	4.88E+06	2.02E-03	1.24E-07	6.52	0.06	1.235E-07	6.2	0.2
AWAG7_4_2.ais	2.37E+09	4.78E+06	2.02E-03	1.19E-07	7.13	0.06	1.188E-07	6.8	0.2
AWAG7_4_1.ais	2.41E+09	4.88E+06	2.02E-03	7.66E-08	7.09	0.04	7.653E-08	6.8	0.2
AWAG7_6_1.ais	2.44E+09	4.93E+06	2.02E-03	6.87E-08	6.63	0.03	6.872E-08	6.3	0.2
AWAG7_6_2.ais	2.40E+09	4.85E+06	2.02E-03	1.72E-07	6.32	0.09	1.718E-07	6.0	0.2
AWAG7_8_2.ais	2.43E+09	4.91E+06	2.02E-03	9.15E-08	6.63	0.05	9.147E-08	6.3	0.2
AWAG7_8_1.ais	2.46E+09	4.96E+06	2.02E-03	1.38E-07	5.95	0.07	1.377E-07	5.7	0.2
AWAG7_9_2.ais	2.42E+09	4.89E+06	2.02E-03	1.33E-07	6.72	0.07	1.329E-07	6.4	0.2
AWAG7_9_1.ais	2.44E+09	4.93E+06	2.02E-03	1.51E-07	6.34	0.07	1.505E-07	6.1	0.2
AWAG7_10_2.ais	2.43E+09	4.91E+06	2.02E-03	1.27E-07	6.86	0.06	1.272E-07	6.6	0.2
AWAG7_10_1.ais	2.44E+09	4.93E+06	2.02E-03	1.64E-07	6.72	0.08	1.641E-07	6.4	0.2
AWAG7_M_1.ais	2.43E+09	4.91E+06	2.02E-03	1.89E-07	6.98	0.09	1.891E-07	6.7	0.2
AWAG7_M_2.ais	2.45E+09	4.95E+06	2.02E-03	1.95E-07	6.47	0.10	1.946E-07	6.2	0.2
AWAG7_M_3.ais	2.44E+09	4.91E+06	2.02E-03	1.35E-07	6.48	0.07	1.348E-07	6.2	0.2
AWAG7_M_4.ais	2.41E+09	4.87E+06	2.02E-03	1.36E-07	6.58	0.07	1.360E-07	6.3	0.2
AWAG7_M_5.ais	2.44E+09	4.93E+06	2.02E-03	9.24E-08	6.82	0.05	9.238E-08	6.5	0.2
AWAG7_M_6.ais	2.45E+09	4.95E+06	2.02E-03	1.15E-07	6.35	0.06	1.153E-07	6.1	0.2
AWAG4_1_1.ais	2.33E+09	4.71E+06	2.02E-03	1.51E-07	7.30	0.07	1.5070E-07	7.2	0.3

Standard R33 used. Accepted ratio for standard = 5.55 ‰ ± 0.04 (Valley, 2003)
[#]Ratios relative to standard mean ocean water (SMOW) = 2.0052×10^{-3}
[##]IMF = Instrumental mass fractionation

Table E1 continued

Sample name	^{16}O	^{18}O	$^{18}O/^{16}O$	$^{18}O/^{16}O$ 1 s.e.	$\delta^{18}O$ /‰ (SMOW[#])	$\delta^{18}O$ (SMOW) 1 s.e.	IMF[##] Corrected	Corrected δ18O /‰	External 1 s.e.
AWAG4_M_1.ais	2.31E+09	4.67E+06	2.02E-03	1.51E-07	7.13	0.07	1.5075E-07	7.0	0.3
AWAG4_2_2.ais	2.31E+09	4.66E+06	2.02E-03	2.08E-07	7.20	0.10	2.0765E-07	7.1	0.3
AWAG4_2_1.ais	2.33E+09	4.71E+06	2.02E-03	1.40E-07	6.90	0.07	1.3976E-07	6.8	0.3
AWAG4_M_2.ais	2.34E+09	4.72E+06	2.02E-03	1.42E-07	6.82	0.07	1.4185E-07	6.8	0.3
AWAG4_4_2.ais	2.30E+09	4.65E+06	2.02E-03	1.93E-07	6.74	0.10	1.9248E-07	6.6	0.3
AWAG4_4_1.ais	2.33E+09	4.70E+06	2.02E-03	1.64E-07	6.27	0.08	1.6410E-07	6.2	0.3
AWAG4_5_2.ais	2.33E+09	4.70E+06	2.02E-03	1.29E-07	6.69	0.06	1.2939E-07	6.6	0.3
AWAG4_8_1.ais	2.33E+09	4.70E+06	2.02E-03	1.79E-07	6.57	0.09	1.7860E-07	6.5	0.3
AWAG4_8_2.ais	2.31E+09	4.65E+06	2.02E-03	1.21E-07	7.00	0.06	1.2078E-07	6.8	0.3
AWAG4_10_1.ais	2.33E+09	4.70E+06	2.02E-03	1.09E-07	6.71	0.05	1.0911E-07	6.6	0.3
AWAG4_11_1.ais	2.31E+09	4.67E+06	2.02E-03	1.38E-07	6.87	0.07	1.3811E-07	6.7	0.3
AWAG4_M_3.ais	2.31E+09	4.66E+06	2.02E-03	1.18E-07	6.88	0.06	1.1764E-07	6.7	0.3
AWAG4_M_4.ais	2.31E+09	4.66E+06	2.02E-03	1.02E-07	6.86	0.05	1.0199E-07	6.7	0.3
AWAG4_12_1.ais	2.32E+09	4.68E+06	2.02E-03	1.51E-07	6.59	0.08	1.5142E-07	6.5	0.3
AWAG4_M_5.ais	2.33E+09	4.71E+06	2.02E-03	1.85E-07	6.56	0.09	1.8508E-07	6.5	0.3
AWAG4_M_6.ais	2.29E+09	4.62E+06	2.02E-03	1.22E-07	6.60	0.06	1.2176E-07	6.4	0.3
AWAG5_7_1.ais	2.26E+09	4.57E+06	2.02E-03	1.41E-07	7.08	0.07	1.4075E-07	6.8	0.3
AWAG5_7_2.ais	2.28E+09	4.60E+06	2.02E-03	1.58E-07	7.29	0.08	1.5774E-07	7.0	0.3
AWAG5_M_1.ais	2.30E+09	4.64E+06	2.02E-03	9.71E-08	7.15	0.05	9.7097E-08	7.0	0.3
AWAG5_M_2.ais	2.27E+09	4.59E+06	2.02E-03	1.41E-07	7.61	0.07	1.4072E-07	7.3	0.3
AWAG5_8_2.ais	2.29E+09	4.62E+06	2.02E-03	1.26E-07	7.35	0.06	1.2566E-07	7.1	0.3
AWAG5_M_3.ais	2.23E+09	4.51E+06	2.02E-03	1.08E-07	8.89	0.05	1.0830E-07	8.5	0.3
AWAG5_M_4.ais	2.34E+09	4.72E+06	2.02E-03	1.48E-07	7.37	0.07	1.475E-07	7.3	0.3
AWAG5_M_5.ais	2.31E+09	4.66E+06	2.02E-03	1.60E-07	6.78	0.08	1.603E-07	6.6	0.3
AWAG5_M_6.ais	2.32E+09	4.67E+06	2.02E-03	1.48E-07	6.78	0.07	1.484E-07	6.7	0.3

Standard R33 used. Accepted ratio for standard = 5.55 ‰ ± 0.04 (Valley, 2003)

[#]Ratios relative to standard mean ocean water (SMOW) = 2.0052×10^{-3}

[##]IMF = Instrumental mass fractionation

Table E1 continued

Sample name	^{16}O	^{18}O	$^{18}O/^{16}O$	$^{18}O/^{16}O$ 1 s.e.	$\delta^{18}O$ /‰ (SMOW[#])	$\delta^{18}O$ (SMOW) 1 s.e.	IMF[##] Corrected	Corrected δ18O /‰	External 1 s.e.
AWAG5_M_7.ais	2.32E+09	4.68E+06	2.02E-03	1.67E-07	6.77	0.08	1.668E-07	6.7	0.3
AWAG1B_1_4.ais	2.31E+09	4.66E+06	2.02E-03	1.71E-07	6.59	0.08	1.706E-07	6.4	0.3
AWAG1B_1_2.ais	2.23E+09	4.51E+06	2.02E-03	1.23E-07	7.00	0.06	1.232E-07	6.6	0.3
AWAG1B_2_2.ais	2.27E+09	4.59E+06	2.02E-03	1.08E-07	6.75	0.05	1.077E-07	6.5	0.3
AWAG1B_M_1.ais	2.26E+09	4.57E+06	2.02E-03	1.41E-07	7.40	0.07	1.413E-07	7.1	0.3
AWAG1B_M_2.ais	2.18E+09	4.40E+06	2.02E-03	1.21E-07	6.78	0.06	1.209E-07	6.2	0.3
AWAG1B_M_3.ais	2.28E+09	4.60E+06	2.02E-03	1.43E-07	6.77	0.07	1.433E-07	6.5	0.3
AWAG1B_8_1.ais	2.25E+09	4.54E+06	2.02E-03	1.81E-07	6.89	0.09	1.814E-07	6.5	0.3
AWAG1B_M_4.ais	2.32E+09	4.68E+06	2.02E-03	2.10E-07	6.24	0.10	2.103E-07	6.1	0.3
AWAG1B_10_3.ais	2.31E+09	4.67E+06	2.02E-03	2.02E-07	6.16	0.10	2.018E-07	6.0	0.3
AWAG1B_11_1.ais	2.32E+09	4.68E+06	2.02E-03	1.60E-07	6.33	0.08	1.597E-07	6.2	0.3
AWAG1B_M_5.ais	2.29E+09	4.61E+06	2.02E-03	1.43E-07	6.56	0.07	1.429E-07	6.3	0.3
AWAG1B_M_6.ais	2.24E+09	4.53E+06	2.02E-03	1.75E-07	6.68	0.09	1.754E-07	6.3	0.3
AWSC2_M_1.ais	2.35E+09	4.74E+06	2.02E-03	1.80E-07	5.70	0.09	1.801E-07	5.9	0.3
AWSC2_M_2.ais	2.35E+09	4.75E+06	2.02E-03	1.16E-07	5.97	0.06	1.162E-07	6.2	0.3
AWSC2_M_3.ais	2.30E+09	4.63E+06	2.02E-03	1.26E-07	6.01	0.06	1.262E-07	6.2	0.3
AWSC2_M_4.ais	2.29E+09	4.63E+06	2.02E-03	2.23E-07	6.28	0.11	2.235E-07	6.5	0.3
AWSC2_M_5.ais	2.34E+09	4.71E+06	2.02E-03	1.01E-07	5.81	0.05	1.012E-07	6.0	0.3
AWSC2_M_6.ais	2.35E+09	4.73E+06	2.02E-03	1.46E-07	5.77	0.07	1.455E-07	5.9	0.3
AWSC2_M_7.ais	2.32E+09	4.69E+06	2.02E-03	1.16E-07	6.36	0.06	1.160E-07	6.5	0.3
AWSC2_M_8.ais	2.31E+09	4.66E+06	2.02E-03	8.43E-08	5.93	0.04	8.429E-08	6.1	0.3
AWSC2_M_9.ais	2.32E+09	4.69E+06	2.02E-03	1.37E-07	6.25	0.07	1.368E-07	6.4	0.3
AWSC2_M_10.ais	2.33E+09	4.70E+06	2.02E-03	1.87E-07	5.92	0.09	1.874E-07	6.1	0.3

Standard R33 used. Accepted ratio for standard = 5.55 ‰ ± 0.04 (Valley, 2003)

[#]Ratios relative to standard mean ocean water (SMOW) = 2.0052×10^{-3}

[##]IMF = Instrumental mass fractionation

Table E1 continued

Sample name	^{16}O	^{18}O	$^{18}O/^{16}O$	$^{18}O/^{16}O$ 1 s.e.	$\delta^{18}O$ /‰ (SMOW[#])	$\delta^{18}O$ (SMOW) 1 s.e.	IMF[##] Corrected	Corrected δ18O /‰	External 1 s.e.
AWSC2_M_11.ais	2.27E+09	4.58E+06	2.02E-03	1.02E-07	6.47	0.05	1.016E-07	6.6	0.3
AWSC2_M_12.ais	2.27E+09	4.58E+06	2.02E-03	8.85E-08	6.35	0.04	8.853E-08	6.5	0.3
AWSC2_M_13.ais	2.27E+09	4.58E+06	2.02E-03	1.82E-07	6.33	0.09	1.819E-07	6.5	0.3
AWSC2_M_14.ais	2.28E+09	4.60E+06	2.02E-03	1.05E-07	6.47	0.05	1.048E-07	6.6	0.3
AWSC2_M_15.ais	2.31E+09	4.66E+06	2.02E-03	1.31E-07	5.93	0.06	1.306E-07	6.1	0.3
AWSC2_M_16.ais	2.31E+09	4.67E+06	2.02E-03	1.07E-07	6.32	0.05	1.068E-07	6.5	0.3
AWSC2_M_17.ais	2.32E+09	4.68E+06	2.02E-03	1.62E-07	6.06	0.08	1.617E-07	6.2	0.3
AWSC2_M_18.ais	2.32E+09	4.68E+06	2.02E-03	1.16E-07	6.10	0.06	1.163E-07	6.3	0.3
AWM1_1.ais	2.35E+09	4.74E+06	2.02E-03	1.57E-07	6.26	0.08	1.573E-07	6.0	0.5
AWM1_2.ais	2.33E+09	4.69E+06	2.02E-03	1.58E-07	5.71	0.08	1.582E-07	5.2	0.5
AWM1_3.ais	2.35E+09	4.74E+06	2.02E-03	1.33E-07	5.40	0.07	1.328E-07	5.2	0.5
AWM1_4.ais	2.39E+09	4.82E+06	2.02E-03	1.17E-07	5.75	0.06	1.167E-07	6.0	0.5
AWM1_5.ais	2.34E+09	4.71E+06	2.02E-03	1.24E-07	5.14	0.06	1.235E-07	4.7	0.5
AWM1_6.ais	2.36E+09	4.76E+06	2.02E-03	1.28E-07	5.29	0.06	1.281E-07	5.2	0.5
AWM1_7.ais	2.38E+09	4.79E+06	2.02E-03	9.83E-08	5.59	0.05	9.830E-08	5.7	0.5
AWM1_8.ais	2.37E+09	4.79E+06	2.02E-03	2.15E-07	6.05	0.11	2.152E-07	6.1	0.5
AWM1_9.ais	2.34E+09	4.72E+06	2.02E-03	1.55E-07	5.83	0.08	1.550E-07	5.5	0.5
AWM1_10.ais	2.37E+09	4.77E+06	2.02E-03	1.78E-07	5.89	0.09	1.780E-07	5.8	0.5
AWM1_11.ais	2.35E+09	4.73E+06	2.02E-03	1.87E-07	5.61	0.09	1.865E-07	5.3	0.5
AWM1_12.ais	2.34E+09	4.72E+06	2.02E-03	1.30E-07	5.94	0.06	1.304E-07	5.6	0.5
AWM1_13.ais	2.37E+09	4.78E+06	2.02E-03	1.64E-07	5.95	0.08	1.640E-07	5.9	0.5
AWM1_14.ais	2.36E+09	4.75E+06	2.02E-03	1.04E-07	5.15	0.05	1.044E-07	5.0	0.5
AWM1_15.ais	2.35E+09	4.75E+06	2.02E-03	1.42E-07	5.94	0.07	1.419E-07	5.7	0.5
AWM1_16.ais	2.35E+09	4.74E+06	2.02E-03	1.24E-07	5.40	0.06	1.239E-07	5.2	0.5
AWM1_17.ais	2.34E+09	4.71E+06	2.02E-03	1.75E-07	5.91	0.09	1.749E-07	5.5	0.5

Standard R33 used. Accepted ratio for standard = 5.55 ‰ ± 0.04 (Valley, 2003)
[#]Ratios relative to standard mean ocean water (SMOW) = 2.0052×10^{-3}
[##]IMF = Instrumental mass fractionation

Table E1 continued

Sample name	^{16}O	^{18}O	$^{18}O/^{16}O$	$^{18}O/^{16}O$ 1 s.e.	$\delta^{18}O$ /‰ (SMOW[#])	$\delta^{18}O$ (SMOW) 1 s.e.	IMF[##] Corrected	Corrected δ18O /‰	External 1 s.e.
AWM1_18.ais	2.38E+09	4.80E+06	2.02E-03	1.74E-07	5.68	0.09	1.738E-07	5.8	0.5
AWM1_19.ais	2.36E+09	4.76E+06	2.02E-03	1.30E-07	5.84	0.06	1.297E-07	5.7	0.5
AWM1_20.ais	2.37E+09	4.77E+06	2.02E-03	1.59E-07	5.65	0.08	1.593E-07	5.6	0.5
AWM1_21.ais	2.36E+09	4.77E+06	2.02E-03	1.24E-07	5.71	0.06	1.241E-07	5.6	0.5
AWM1_22.ais	2.33E+09	4.70E+06	2.02E-03	1.39E-07	6.25	0.07	1.391E-07	5.8	0.5
AWM1_23.ais	2.35E+09	4.74E+06	2.02E-03	1.59E-07	5.90	0.08	1.593E-07	5.6	0.5
AWM1_24.ais	2.32E+09	4.69E+06	2.02E-03	1.44E-07	6.71	0.07	1.435E-07	6.1	0.5
R33_JW109@21.ais	2.36E+09	4.75E+06	2.02E-03	1.32E-07	6.03	0.07	1.318E-07	5.8	0.2
R33_JW109@22.ais	2.34E+09	4.72E+06	2.02E-03	1.56E-07	6.31	0.08	1.560E-07	6.0	0.2
R33_JW109@23.ais	2.35E+09	4.73E+06	2.02E-03	1.17E-07	5.82	0.06	1.166E-07	5.5	0.2
R33_JW109@24.ais	2.34E+09	4.71E+06	2.02E-03	1.54E-07	5.77	0.08	1.542E-07	5.4	0.2
R33_JW109@25.ais	2.35E+09	4.74E+06	2.02E-03	1.75E-07	5.30	0.09	1.748E-07	5.0	0.2
R33_JW109@26.ais	2.34E+09	4.72E+06	2.02E-03	1.35E-07	5.86	0.07	1.353E-07	5.5	0.2
R33_JW109@27.ais	2.33E+09	4.70E+06	2.02E-03	1.14E-07	5.92	0.06	1.140E-07	5.5	0.2
R33_JW109@28.ais	2.35E+09	4.74E+06	2.02E-03	1.42E-07	6.16	0.07	1.424E-07	5.9	0.2
R33_JW109@29.ais	2.35E+09	4.74E+06	2.02E-03	1.61E-07	5.97	0.08	1.611E-07	5.7	0.2
R33_JW109@30.ais	2.35E+09	4.73E+06	2.02E-03	1.70E-07	5.56	0.08	1.701E-07	5.2	0.2
R33_JW109@31.ais	2.35E+09	4.73E+06	2.02E-03	1.69E-07	5.93	0.08	1.686E-07	5.6	0.2
R33_JW109@32.ais	2.35E+09	4.75E+06	2.02E-03	1.25E-07	6.16	0.06	1.254E-07	5.9	0.2
R33_JW109@33.ais	2.33E+09	4.70E+06	2.02E-03	1.07E-07	5.72	0.05	1.072E-07	5.3	0.2
R33_JW109@34.ais	2.34E+09	4.72E+06	2.02E-03	2.14E-07	5.86	0.11	2.137E-07	5.5	0.2
R33_JW109@35.ais	2.35E+09	4.74E+06	2.02E-03	1.04E-07	5.82	0.05	1.043E-07	5.5	0.2
R33_JW109@36.ais	2.35E+09	4.74E+06	2.02E-03	1.53E-07	6.09	0.08	1.526E-07	5.8	0.2
R33_JW109@37.ais	2.33E+09	4.70E+06	2.02E-03	1.26E-07	5.87	0.06	1.255E-07	5.5	0.2

Standard R33 used. Accepted ratio for standard = 5.55 ‰ ± 0.04 (Valley, 2003)

[#]Ratios relative to standard mean ocean water (SMOW) = 2.0052×10^{-3}

[##]IMF = Instrumental mass fractionation

Table E1 continued

Sample name	^{16}O	^{18}O	$^{18}O/^{16}O$	$^{18}O/^{16}O$ 1 s.e.	$\delta^{18}O$ /‰ (SMOW[#])	$\delta^{18}O$ (SMOW) 1 s.e.	IMF[##] Corrected	Corrected δ18O /‰	External 1 s.e.
R33_JW109@38.ais	2.32E+09	4.69E+06	2.02E-03	1.91E-07	6.02	0.09	1.912E-07	5.6	0.2
R33_JW366@7.ais	2.35E+09	4.75E+06	2.02E-03	1.28E-07	5.79	0.06	1.2844E-07	5.5	0.2
R33_JW366@8.ais	2.37E+09	4.78E+06	2.02E-03	1.49E-07	5.74	0.07	1.4930E-07	5.4	0.2
R33_JW366@9.ais	2.34E+09	4.72E+06	2.02E-03	2.47E-07	5.86	0.12	2.4646E-07	5.5	0.2
R33_JW366@10.ais	2.35E+09	4.75E+06	2.02E-03	1.28E-07	5.89	0.06	1.2791E-07	5.5	0.2
R33_JW366@11.ais	2.39E+09	4.81E+06	2.02E-03	1.20E-07	5.54	0.06	1.2042E-07	5.2	0.2
R33_JW366@12.ais	2.34E+09	4.73E+06	2.02E-03	1.47E-07	6.07	0.07	1.4688E-07	5.7	0.2
R33_JW366@13.ais	2.36E+09	4.75E+06	2.02E-03	1.69E-07	5.74	0.08	1.6918E-07	5.4	0.2
R33_JW366@14.ais	2.36E+09	4.77E+06	2.02E-03	1.25E-07	5.67	0.06	1.2519E-07	5.3	0.2
R33_JW366@15.ais	2.38E+09	4.79E+06	2.02E-03	1.14E-07	5.64	0.06	1.1436E-07	5.3	0.2
R33_JW366@16.ais	2.39E+09	4.81E+06	2.02E-03	1.59E-07	5.78	0.08	1.5940E-07	5.5	0.2
R33_JW366@17.ais	2.38E+09	4.80E+06	2.02E-03	1.51E-07	5.69	0.07	1.5055E-07	5.4	0.2
R33_JW366@18.ais	2.36E+09	4.75E+06	2.02E-03	1.27E-07	5.78	0.06	1.2736E-07	5.4	0.2
R33_JW366@19.ais	2.33E+09	4.70E+06	2.02E-03	1.45E-07	6.37	0.07	1.4520E-07	6.0	0.2
R33_JW366@20.ais	2.38E+09	4.80E+06	2.02E-03	1.56E-07	5.88	0.08	1.5584E-07	5.6	0.2
R33_JW366@21.ais	2.40E+09	4.85E+06	2.02E-03	1.53E-07	5.93	0.08	1.530E-07	5.6	0.2
R33_JW366@22.ais	2.37E+09	4.78E+06	2.02E-03	1.60E-07	5.87	0.08	1.595E-07	5.5	0.2
R33_JW366@23.ais	2.42E+09	4.88E+06	2.02E-03	9.96E-08	5.64	0.05	9.957E-08	5.3	0.2
R33_JW366@24.ais	2.40E+09	4.84E+06	2.02E-03	1.38E-07	5.74	0.07	1.383E-07	5.4	0.2
R33_JW366@25.ais	2.40E+09	4.85E+06	2.02E-03	1.29E-07	5.81	0.06	1.291E-07	5.5	0.2
R33_JW366@26.ais	2.37E+09	4.79E+06	2.02E-03	1.06E-07	6.14	0.05	1.059E-07	5.8	0.2
R33_JW366@27.ais	2.44E+09	4.92E+06	2.02E-03	1.74E-07	5.74	0.09	1.741E-07	5.4	0.2
R33_JW366@28.ais	2.42E+09	4.87E+06	2.02E-03	8.17E-08	5.72	0.04	8.171E-08	5.4	0.2
R33_JW366@29.ais	2.44E+09	4.92E+06	2.02E-03	1.67E-07	5.64	0.08	1.669E-07	5.4	0.2
R33_JW366@30.ais	2.43E+09	4.91E+06	2.02E-03	1.77E-07	5.73	0.09	1.772E-07	5.4	0.2

Standard R33 used. Accepted ratio for standard = 5.55 ‰ ± 0.04 (Valley, 2003)

[#]Ratios relative to standard mean ocean water (SMOW) = 2.0052×10^{-3}

[##]IMF = Instrumental mass fractionation

Table E1 continued

Sample name	^{16}O	^{18}O	$^{18}O/^{16}O$	$^{18}O/^{16}O$ 1 s.e.	$\delta^{18}O$ /‰ (SMOW[#])	$\delta^{18}O$ (SMOW) 1 s.e.	IMF[##] Corrected	Corrected δ18O /‰	External 1 s.e.
R33_JW366@31.ais	2.41E+09	4.86E+06	2.02E-03	1.52E-07	6.01	0.08	1.518E-07	5.7	0.2
R33_JW366@32.ais	2.40E+09	4.84E+06	2.02E-03	1.15E-07	6.09	0.06	1.149E-07	5.8	0.2
R33_JW366@33.ais	2.39E+09	4.83E+06	2.02E-03	1.74E-07	5.99	0.09	1.743E-07	5.7	0.2
R33_JW366@34.ais	2.44E+09	4.92E+06	2.02E-03	1.32E-07	5.67	0.07	1.322E-07	5.4	0.2
R33_JW366@35.ais	2.43E+09	4.89E+06	2.02E-03	1.58E-07	5.76	0.08	1.581E-07	5.5	0.2
R33_JW366@36.ais	2.42E+09	4.89E+06	2.02E-03	1.18E-07	5.94	0.06	1.180E-07	5.6	0.2
R33_JW366@37.ais	2.42E+09	4.88E+06	2.02E-03	1.82E-07	6.36	0.09	1.822E-07	6.1	0.2
R33_JW366@38.ais	2.39E+09	4.82E+06	2.02E-03	1.46E-07	5.66	0.07	1.463E-07	5.3	0.2
R33_JW366@39.ais	2.40E+09	4.83E+06	2.02E-03	2.03E-07	6.04	0.10	2.025E-07	5.7	0.2
R33_JW366@40.ais	2.43E+09	4.91E+06	2.02E-03	1.28E-07	5.75	0.06	1.276E-07	5.5	0.2
R33_JW366@41.ais	2.42E+09	4.88E+06	2.02E-03	1.41E-07	5.79	0.07	1.409E-07	5.5	0.2
R33_JW366@42.ais	2.44E+09	4.93E+06	2.02E-03	1.88E-07	5.77	0.09	1.883E-07	5.5	0.2
R33_JW366@43.ais	2.45E+09	4.94E+06	2.02E-03	9.93E-08	5.77	0.05	9.929E-08	5.5	0.2
R33_JW366@44.ais	2.45E+09	4.93E+06	2.02E-03	2.21E-07	5.95	0.11	2.207E-07	5.7	0.2
R33_JW366@45.ais	2.42E+09	4.87E+06	2.02E-03	1.18E-07	6.10	0.06	1.175E-07	5.8	0.2
R33_JW366@46.ais	2.43E+09	4.90E+06	2.02E-03	1.25E-07	6.06	0.06	1.246E-07	5.8	0.2
R33_JW366@47.ais	2.43E+09	4.90E+06	2.02E-03	1.86E-07	5.87	0.09	1.860E-07	5.6	0.2
R33_JW366@48.ais	2.41E+09	4.87E+06	2.02E-03	1.43E-07	6.04	0.07	1.426E-07	5.7	0.2
R33_JW366@49.ais	2.45E+09	4.94E+06	2.02E-03	2.06E-07	5.78	0.10	2.055E-07	5.5	0.2
R33_JW366@50.ais	2.43E+09	4.90E+06	2.02E-03	1.92E-07	6.03	0.10	1.916E-07	5.7	0.2
R33_JW366@51.ais	2.44E+09	4.91E+06	2.02E-03	1.26E-07	5.96	0.06	1.258E-07	5.7	0.2
R33_JW366@52.ais	2.42E+09	4.89E+06	2.02E-03	1.43E-07	5.88	0.07	1.429E-07	5.6	0.2
R33_JW309@9.ais	2.32E+09	4.68E+06	2.02E-03	1.60E-07	6.15	0.08	1.5953E-07	6.0	0.3
R33_JW309@10.ais	2.31E+09	4.65E+06	2.02E-03	1.30E-07	6.00	0.06	1.2963E-07	5.8	0.3

Standard R33 used. Accepted ratio for standard = 5.55 ‰ ± 0.04 (Valley, 2003)

[#]Ratios relative to standard mean ocean water (SMOW) = 2.0052×10^{-3}

[##]IMF = Instrumental mass fractionation

Table E1 continued

Sample name	^{16}O	^{18}O	$^{18}O/^{16}O$	$^{18}O/^{16}O$ 1 s.e.	$\delta^{18}O$ /‰ (SMOW[#])	$\delta^{18}O$ (SMOW) 1 s.e.	IMF[##] Corrected	Corrected δ18O /‰	External 1 s.e.
R33_JW309@11.ais	2.30E+09	4.64E+06	2.02E-03	1.68E-07	6.06	0.08	1.6830E-07	5.9	0.3
R33_JW309@12.ais	2.33E+09	4.69E+06	2.02E-03	1.38E-07	5.38	0.07	1.3848E-07	5.3	0.3
R33_JW309@13.ais	2.34E+09	4.72E+06	2.02E-03	1.73E-07	5.56	0.09	1.7343E-07	5.5	0.3
R33_JW309@14.ais	2.29E+09	4.62E+06	2.02E-03	1.21E-07	5.82	0.06	1.2060E-07	5.6	0.3
R33_JW309@15.ais	2.29E+09	4.62E+06	2.02E-03	1.41E-07	6.23	0.07	1.4130E-07	6.0	0.3
R33_JW309@16.ais	2.33E+09	4.69E+06	2.02E-03	1.67E-07	5.68	0.08	1.6720E-07	5.6	0.3
R33_JW309@17.ais	2.32E+09	4.68E+06	2.02E-03	1.22E-07	5.79	0.06	1.2210E-07	5.7	0.3
R33_JW309@18.ais	2.33E+09	4.70E+06	2.02E-03	9.18E-08	5.62	0.05	9.176E-08	5.6	0.3
R33_JW309@19.ais	2.31E+09	4.66E+06	2.02E-03	9.75E-08	5.59	0.05	9.748E-08	5.4	0.3
R33_JW309@20.ais	2.34E+09	4.71E+06	2.02E-03	1.06E-07	5.50	0.05	1.061E-07	5.5	0.3
R33_JW309@21.ais	2.30E+09	4.64E+06	2.02E-03	1.47E-07	5.47	0.07	1.468E-07	5.3	0.3
R33_JW309@22.ais	2.30E+09	4.64E+06	2.02E-03	1.60E-07	5.24	0.08	1.601E-07	5.1	0.3
R33_JW309@23.ais	2.33E+09	4.70E+06	2.02E-03	1.63E-07	5.17	0.08	1.626E-07	5.1	0.3
R33_JW309@24.ais	2.30E+09	4.64E+06	2.02E-03	1.67E-07	5.39	0.08	1.672E-07	5.2	0.3
R33_JW368@27.ais	2.32E+09	4.68E+06	2.02E-03	1.25E-07	5.26	0.06	1.255E-07	5.4	0.3
R33_JW368@28.ais	2.32E+09	4.68E+06	2.02E-03	1.50E-07	5.31	0.07	1.502E-07	5.5	0.3
R33_JW368@29.ais	2.31E+09	4.67E+06	2.02E-03	1.20E-07	5.63	0.06	1.196E-07	5.8	0.3
R33_JW368@30.ais	2.29E+09	4.61E+06	2.02E-03	2.23E-07	5.78	0.11	2.229E-07	5.9	0.3
R33_JW368@31.ais	2.30E+09	4.63E+06	2.02E-03	1.18E-07	5.73	0.06	1.182E-07	5.9	0.3
R33_JW368@32.ais	2.30E+09	4.64E+06	2.02E-03	1.43E-07	5.56	0.07	1.425E-07	5.7	0.3
R33_JW438@44.ais	2.37E+09	4.78E+06	2.02E-03	1.30E-07	5.60	0.06	1.303E-07	5.6	0.5
R33_JW438@45.ais	2.35E+09	4.75E+06	2.02E-03	1.24E-07	6.43	0.06	1.244E-07	6.2	0.5
R33_JW438@46.ais	2.36E+09	4.75E+06	2.02E-03	2.28E-07	5.96	0.11	2.276E-07	5.8	0.5

Standard R33 used. Accepted ratio for standard = 5.55 ‰ ± 0.04 (Valley, 2003)

[#]Ratios relative to standard mean ocean water (SMOW) = 2.0052×10^{-3}

[##]IMF = Instrumental mass fractionation

Table E1 continued

Sample name	^{16}O	^{18}O	$^{18}O/^{16}O$	$^{18}O/^{16}O$ 1 s.e.	$\delta^{18}O$ /‰ (SMOW#)	$\delta^{18}O$ (SMOW) 1 s.e.	IMF## Corrected	Corrected δ18O /‰	External 1 s.e.
R33_JW438@47.ais	2.36E+09	4.76E+06	2.02E-03	1.59E-07	5.63	0.08	1.589E-07	5.5	0.5
R33_JW438@48.ais	2.33E+09	4.70E+06	2.02E-03	1.06E-07	5.97	0.05	1.055E-07	5.5	0.5
R33_JW438@49.ais	2.35E+09	4.73E+06	2.02E-03	1.58E-07	5.28	0.08	1.579E-07	5.0	0.5
R33_JW438@50.ais	2.34E+09	4.73E+06	2.02E-03	1.03E-07	6.72	0.05	1.029E-07	6.4	0.5
R33_JW438@51.ais	2.34E+09	4.72E+06	2.02E-03	2.09E-07	5.25	0.10	2.091E-07	4.9	0.5

Standard R33 used. Accepted ratio for standard = 5.55 ‰ ± 0.04 (Valley, 2003)
#Ratios relative to standard mean ocean water (SMOW) = 2.0052×10^{-3}
##IMF = Instrumental mass fractionation

Appendix F

Sphene SHRIMP trace element

and

Zr-in-sphene thermometry analyses

Table F1. Sphene SHRIMP trace element data

	F ppm	Na ppm	Mg ppm	Si ppm	P ppm	K ppm	Ca ppm	Al ppm	Ti ppm	V ppm
AWM1.1	4169	239	183	127109	201	0.9	199469	4941	221528	603.8
AWM1-2.1	4191	402	380	122204	344	1.0	206763	7405	218331	631.1
AWM1-2.2	4513	103	87	118605	232	1.1	214079	4786	240504	607.2
AWM1-3.1	5542	290	283	120882	183	0.9	212599	7105	224503	698.7
AWM1-3.2	4886	183	174	119811	226	0.9	209237	6114	238506	639.1
AWM1-4.1	4394	305	225	123095	232	0.8	210759	5855	233843	714.6
AWM1-4.2	5616	102	100	132324	122	0.9	207163	5426	226339	607.2
AWM1-5.1	5068	244	186	131497	158	0.9	204954	5383	223075	638.9
AWM1-5.2	4243	202	138	126927	210	0.7	206057	5185	230510	630.8
AWM1-6.1	4047	312	222	129604	172	0.9	204700	6237	225165	681.8
AWM1-6.2	4795	195	173	125231	230	1.3	208646	6009	234485	631.5
AWM1-7.1	4647	125	119	117522	149	1.0	219206	5577	243853	653.6
AWM1-7.2	4549	312	233	124788	323	0.9	213259	5877	230310	696.4
AWM1-8.1	4938	301	279	121993	248	0.8	215430	6614	233202	682.0
AWM1-8.2	5450	122	113	116591	129	1.0	217671	5873	236559	629.3
AWM1-9.1	4838	238	215	124917	207	28.6	211121	6163	232231	648.3
AWM1-9.2	5732	102	99	125900	124	1.0	211312	5721	231177	581.4
AWM1-10.1	6717	235	227	126234	114	1.2	209434	6847	224682	694.0
AWM1-10.2	6241	151	133	127089	130	1.1	214297	5975	232430	646.3
AWM1-11.1	6289	228	207	129245	211	3.8	208887	6337	223413	676.8
AWM1-11.2	4974	179	151	125920	124	0.7	211150	5843	234754	627.6
AWM1-12.1	4750	247	182	131649	188	1.4	206140	5107	221972	562.6
AWM1-12.2	3745	45	42	108549	30	0.9	230780	6260	257960	996.2
AWM1-13.1	3670	272	192	118866	204	1.0	214453	5380	238109	663.5

Table F1 (continued) Sphene SHRIMP trace element data

	F ppm	Na ppm	Mg ppm	Si ppm	P ppm	K ppm	Ca ppm	Al ppm	Ti ppm	V ppm
AWM1-13.2	4902	123	110	136700	245	1.0	203838	4572	229636	573.3
AWM1-14.1	5954	191	173	148024	158	0.8	198202	5642	215960	657.4
AWM1-14.2	5755	99	104	154092	82	0.8	191937	5238	217428	562.4
AMW2-1.1	1500	152	103	115694	258	0.6	201808	5561	231081	451.9
AMW2-1.2	1182	141	114	125218	155	0.8	205352	4428	229213	524.5
AMW2-2.1	2580	129	80	117234	252	0.9	220147	4997	253522	619.8
AMW2-2.2	1667	104	76	124467	164	0.8	209600	4830	238971	596.5
AWM2-3.1	1167	278	134	117801	349	0.8	215456	6182	240142	755.1
AWM2-3.2	2968	164	176	123162	166	1.4	214266	5417	236312	597.3
AWM2-4.1	1446	186	117	128520	143	0.8	215261	4378	238702	539.5
AWM2-4.2	1319	321	119	120221	213	0.9	220408	4447	237935	427.9
AWM2-5.1	1953	253	157	129300	1452	1.0	214390	5332	230539	677.1
AWM2-5.2	1662	138	124	126196	165	1.0	215796	5694	232490	562.5
AWM2-6.1	2435	137	86	120909	124	0.8	217212	5276	240575	690.6
AWM2-6.2	1197	277	137	134164	292	0.8	200763	5971	225804	590.2
AWM2-7.1	1424	268	129	121048	778	12.5	216395	5512	241543	618.5
AWM2-7.2	2495	151	112	138936	195	0.7	205613	4706	228042	563.4
AWM2-8.1	2291	84	51	148541	117	0.9	191661	3824	211287	513.9
AWM2-8.2	2252	166	114	124133	1133	1.1	217416	4448	245065	542.5
AWM2-9.1	1853	172	88	128862	215	1.2	212058	4439	237132	657.9
AWM2-9.2	1917	175	74	131491	202	0.8	209648	3764	240272	677.8
AWM2-9.3	1800	68	31	113489	66	5.5	227924	4594	260530	781.9
AWM2-10.1	1785	164	76	132554	226	0.9	207979	4705	225642	452.3

Table F1 (continued) Sphene SHRIMP trace element data for samples

	F ppm	Na ppm	Mg ppm	Si ppm	P ppm	K ppm	Ca ppm	Al ppm	Ti ppm	V ppm
AWM2-10.2	2380	139	93	139203	132	0.8	200599	5135	222213	594.1
AWM2-11.1	3138	99	55	138370	134	0.7	205782	4648	231417	625.5
AWM2-11.2	2643	138	90	133511	754	0.9	209953	4188	235758	550.7
AWM2-12.1	1332	213	130	120699	153	34.7	216211	6032	233598	492.2
AWM2-12.2	1245	293	131	137893	359	0.7	202817	4805	218381	416.9
AWAG_1A-1.1	2436	433	347	134223	324	3.6	193071	6105	214587	477.0
AWAG_1A-1.2	4272	240	293	118144	176	1.0	215597	7328	235013	601.0
AWAG_1A-2.1	3051	316	205	117494	465	1.2	222025	5983	245793	524.7
AWAG_1A-2.2	4744	169	175	116754	141	5.9	219414	6500	243491	645.8
AWAG_1A-3.1	2990	345	249	132154	498	0.8	204603	5987	230128	414.9
AWAG_1A-3.2	5923	212	207	127229	127	1.2	213746	6334	233821	469.9
AWAG_1A-4.1	5735	138	215	124299	111	53.6	215086	6393	242921	500.8
AWAG_1A-4.2	5725	190	192	114824	79	0.8	222792	6928	244671	655.7
AWAG_1A-4.3	5210	289	322	133748	185	1.0	201602	6870	219330	569.4
AWAG_1A-5.1	5361	228	228	117632	193	0.7	221184	7279	244845	648.9
AWAG_1A-5.2	2397	393	326	109718	356	1.2	221280	7023	242694	578.5
AWAG_1A-6.1	3010	300	207	130396	275	3.3	206552	5612	230842	574.1
AWAG_1A-6.2	3424	217	203	138754	127	8.6	204765	4990	216637	386.6
AWAG_1A-7.1	2639	271	221	120125	634	0.7	210509	5918	241687	573.1
AWAG_1A-7.2	2650	276	226	124183	398	0.7	208809	6040	239567	558.5
AWAG_1A-8.1	3644	152	133	130925	83	0.7	210220	4761	236715	466.4
AWAG_1A-8.2	6848	169	176	132757	366	0.8	208363	5177	233558	389.7

Table F1 (continued) Sphene SHRIMP trace element data for samples

	F ppm	Na ppm	Mg ppm	Si ppm	P ppm	K ppm	Ca ppm	Al ppm	Ti ppm	V ppm
AWAG_1A-9.1	3198	191	201	121174	186	0.7	212664	6286	238380	516.4
AWAG_1A-9.2	3113	306	217	128635	286	9.4	208084	5736	229536	441.9
AWAG_1A-10.1	5472	194	200	143091	152	0.8	198360	5984	217487	535.7
AWAG_1A-10.2	3237	236	187	133466	440	0.9	202520	5698	229378	513.6
AWAG_1A-11.1	4648	206	241	126950	224	0.6	210480	6824	234444	620.4
AWAG_1A-11.2	3228	323	288	138604	822	0.7	197349	6058	221723	499.6
AWAG_1A-12.1	3208	199	215	121319	139	0.7	217725	5381	239657	441.2
AWAG_1A-12.2	3069	375	270	120238	1491	0.7	215114	5397	241581	504.0
AWAG_1A-13.1	4769	179	196	137590	194	0.6	205708	6149	224014	499.9
AWAG_1A-13.2	3606	271	226	129048	583	0.9	207279	5807	233730	570.8
AWAG_1A-14.1	3268	290	335	115172	448	0.7	210129	6943	241422	595.0
AWAG_1A-14.2	4084	277	343	136379	236	0.7	202218	6817	222653	581.7
AWAG_1B-1.1	3265	134	110	146948	104	0.9	200116	4030	221493	445.3
AWAG_1B-1.2	2812	130	105	129617	86	1.7	212180	4509	240777	453.8
AWAG_1B-2.1	3287	169	109	145061	155	0.7	204445	4039	227688	413.2
AWAG_1B-2.2	3751	261	167	138271	191	0.7	208175	4538	231338	531.9
AWAG_1B-3.1	5704	144	141	133600	113	45.6	207944	5498	233342	562.9
AWAG_1B-3.2	4227	275	227	123567	271	0.7	214848	6140	237538	576.7
AWAG_1B-4.1	4718	267	350	131508	215	1.0	209115	6779	222980	573.7
AWAG_1B-4.2	3305	154	137	147006	143	22.3	204704	4460	226238	460.2
AWAG_1B-5.1	3191	196	105	142264	186	47.8	204570	3569	233604	455.6
AWAG_1B-5.2	2935	322	150	134401	169	30.5	203563	4560	232183	551.7
AWAG_1B-6.1	4340	218	207	125781	163	1.1	211013	6149	236353	579.1
AWAG_1B-6.2	3218	171	129	142672	191	1.8	207161	4332	229644	408.7

Table F1 (continued) Sphene SHRIMP trace element data for samples

	F ppm	Na ppm	Mg ppm	Si ppm	P ppm	K ppm	Ca ppm	Al ppm	Ti ppm	V ppm
AWAG_1B-7.1	2779	249	185	122396	588	0.8	210185	5469	240738	552.5
AWAG_1B-7.2	2864	242	170	124339	186	0.6	214011	5455	241523	601.5
AWAG_1B-8.1	5454	230	220	130405	159	1.9	209393	6495	232228	559.5
AWAG_1B-8.2	3575	306	209	129513	386	0.8	208862	5734	232210	473.0
AWAG_1B-9.1	4224	278	290	131935	110	98.6	203572	8040	224793	466.1
AWAG_1B-9.2	5504	156	149	131733	172	8.0	206828	5963	234998	580.3
AWAG_1B-9.3	3021	122	109	135928	122	1.0	211523	4562	233071	472.1
AWAG_1B-10.1	2818	264	213	116406	404	0.6	205750	6093	240195	533.9
AWAG_1B-10.2	3387	135	95	123758	211	7.5	209878	3817	246217	477.6
AWAG_1B-11.1	2889	175	199	125087	202	0.7	203516	6093	236004	556.3
AWAG_1B-11.2	2732	271	232	125495	940	0.7	205576	6047	238512	548.2
AWAG_1B-12.1	2839	124	97	122297	347	14.1	203821	3745	245600	481.1
AWAG_1B-12.2	3113	210	260	119552	238	5.4	205212	6405	233657	518.3
AWAG_1B-13.1	3019	246	224	131097	259	0.6	204459	5837	227405	453.4
AWAG_1B-13.2	3147	285	248	136198	252	0.7	203343	5984	228339	508.4
AWAG_1B-13.3	3392	262	212	117949	471	0.8	208993	6555	243991	576.3
AWAG_1B-13.4	5155	179	163	139150	161	0.5	203488	5467	228144	568.8
AWAG_2-1.1	3114	235	169	131218	212	1.2	202575	5661	237381	369.5
AWAG_2-1.2	2503	432	396	138501	267	1.1	199372	7318	224854	397.9
AWAG_2-2.1	6023	181	209	142565	148	0.8	199518	6563	227463	393.6
AWAG_2-2.2	3766	328	271	145948	286	7.5	197674	6594	224154	344.6
AWAG_2-3.1	2174	412	322	133004	255	1.1	200968	7651	232558	419.2
AWAG_2-3.2	6147	179	197	139357	138	1.0	201187	6167	225365	380.7
AWAG_2-4.1	2519	380	291	132528	356	1.3	203987	7717	231035	418.6

Table F1 (continued) Sphene SHRIMP trace element data for samples

	F ppm	Na ppm	Mg ppm	Si ppm	P ppm	K ppm	Ca ppm	Al ppm	Ti ppm	V ppm
AWAG_2-4.2	6461	184	208	141530	164	1.0	203101	6209	225574	373.8
AWAG_2-5.1	3524	378	329	134085	373	1.7	205407	7292	229564	358.6
AWAG_2-5.2	6579	186	179	139336	167	1.2	205742	6090	227408	376.1
AWAG_2-6.1	2376	367	270	126659	326	1.1	205518	6941	237896	396.0
AWAG_2-6.2	4557	266	180	150371	122	56.6	195394	5870	214365	317.1
AWAG_2-7.1	2684	379	265	138229	313	1.0	201868	5970	227131	369.8
AWAG_2-7.2	4564	343	592	109218	199	150.8	216748	9865	250482	355.3
AWAG_2-8.1	4911	297	366	121646	214	0.9	216929	8093	238283	424.8
AWAG_2-8.2	3807	293	215	148178	188	8.6	192965	5216	217047	352.9
AWAG_2-9.1	2027	510	453	131507	362	49.4	200955	7467	227304	399.3
AWAG_2-9.2	6593	213	225	144431	179	1.0	199075	6535	215871	357.8
AWAG_2-10.1	4595	278	504	123993	271	71.8	204650	6454	261785	475.7
AWAG_2-10.2	6439	229	204	127137	115	1.1	212033	6367	237244	342.9
AWAG_2-11.1	4652	305	274	143591	263	1.0	196103	6603	215808	367.9
AWAG_2-11.2	4373	334	385	140497	192	7.8	195754	7098	219260	407.5
AWAG_2-12.1	2117	393	336	122838	256	1.7	207671	7358	240591	430.0
AWAG_2-12.2	6647	179	172	145298	171	1.2	199490	5956	218023	352.4
AWAG_2-13.1	2700	343	265	126056	219	0.9	206091	6479	235312	454.6
AWAG_2-13.2	6067	169	162	122986	151	22.8	213485	6444	238058	420.5
AWAG_2-14.1	2415	347	331	126486	235	258.7	199286	9430	228948	418.4
AWAG_2-14.2	5358	169	167	123239	122	1.2	208938	6227	239207	403.4
AWAG3-1.1	3673	374	346	130562	212	1.8	201965	6827	225488	423.2

Table F1 (continued) Sphene SHRIMP trace element data for samples

	F ppm	Na ppm	Mg ppm	Si ppm	P ppm	K ppm	Ca ppm	Al ppm	Ti ppm	V ppm
AWAG3-1.2	3900	205	186	125556	165	2.6	204145	6113	234257	331.6
AWAG3-2.1	3035	360	257	130760	319	9.5	206193	6648	232097	379.2
AWAG3-2.2	4199	182	206	141211	107	2.6	198759	6234	222353	385.1
AWAG3-2.2	4028	186	200	133164	220	2.4	200254	6024	220822	388.1
AWAG3-3.1	5820	205	243	104144	101	6.0	229111	7759	255343	372.5
AWAG3-3.2	6145	215	245	127839	159	12.6	205158	7327	223646	259.8
AWAG3-4.1	3608	453	302	133057	346	18.7	199873	5938	216090	347.6
AWAG3-4.2	4455	311	274	137659	176	5.9	200934	5825	224432	355.3
AWAG3-5.1	5461	197	215	121542	91	2.9	217652	6874	238837	371.9
AWAG3-5.2	5319	230	263	137537	111	3.5	198675	6514	218933	349.1
AWAG3-6.1	4430	279	301	141099	192	6.2	196950	6367	219629	330.5
AWAG3-6.2	5970	199	218	143289	114	3.1	197740	6533	216751	316.8
AWAG3-7.1	3110	444	375	132526	415	2.2	205173	7216	223812	380.5
AWAG3-7.2	2502	256	164	127948	186	3.0	207223	5726	238840	331.3
AWAG3-7.3	3668	1005	157	166939	115	1288.3	164316	12201	174040	181.0
AWAG3-8.1	4108	242	323	130193	218	2.1	207812	8114	234750	400.4
AWAG3-8.2	5574	192	226	148265	94	1.6	185571	6418	219046	311.8
AWAG3-9.1	3268	251	329	123110	256	1.8	212421	7935	241641	415.0
AWAG3-9.2	5952	185	206	142428	120	1.7	205818	7212	225707	328.1
AWAG3-10.1	3188	500	200	141816	160	22.0	205130	5818	229878	219.0
AWAG3-10.2	3294	180	171	142887	296	1.8	202575	6977	222745	373.6
AWAG3-11.1	6346	177	247	137740	163	1.7	205167	7763	225797	423.2
AWAG3-11.2	5612	222	261	152347	163	1.7	192443	6716	211784	382.0

Table F1 (continued) Sphene SHRIMP trace element data for samples

	F ppm	Na ppm	Mg ppm	Si ppm	P ppm	K ppm	Ca ppm	Al ppm	Ti ppm	V ppm
AWAG3-12.1	2080	345	319	133083	326	1.8	204602	7224	236173	370.0
AWAG3-12.2	4997	219	272	153644	159	1.8	194107	6752	217704	334.2
AWAG3-13.1	1680	255	187	149296	392	2.3	176154	6214	228647	411.7
AWAG3-13.2	4713	134	194	156087	171	2.0	194099	6898	211412	417.0
AWAG4-1.1	2030	154	138	121179	403	28.2	202595	5440	242201	452.4
AWAG4-1.2	1963	107	104	120650	80	5.7	211230	5533	232988	509.4
AWAG4-2.1	2151	191	108	129617	393	2.9	205892	5026	238641	393.1
AWAG4-2.2	1896	126	80	147604	98	3.0	204626	4662	229035	376.1
AWAG4-3.1	2584	197	112	133980	734	2.2	211665	5021	241249	444.4
AWAG4-3.2	1839	106	69	130980	90	1.8	217411	5141	247261	437.2
AWAG4-4.1	2184	197	103	142635	321	2.1	204646	4860	234797	393.1
AWAG4-4.2	2103	156	109	141706	64	2.7	209222	4978	235525	459.2
AWAG4-5.1	2315	146	94	139335	109	2.0	209707	5052	236527	476.5
AWAG4-5.2	2484	200	105	142346	271	3.3	208125	4845	235244	369.8
AWAG4-6.1	3797	136	152	148676	167	2.1	201090	6460	226076	518.4
AWAG4-6.2	2410	200	128	152691	134	2.2	199310	4860	223039	420.4
AWAG4-7.1	1684	196	94	135744	160	15.1	211078	4708	241401	328.4
AWAG4-7.2	2547	134	117	147203	117	11.1	205960	5344	230734	501.3
AWAG4-8.1	2300	173	139	138385	157	1.6	204890	5986	233548	491.0
AWAG4-8.2	2300	201	165	134441	404	5.5	207761	7014	238483	465.7
AWAG4-8.3	1859	211	113	142208	152	3.0	206302	5073	235635	424.3
AWAG4-9.1	2114	288	158	149824	453	2.9	199017	5327	223346	382.0
AWAG4-9.2	2109	233	119	152520	94	1.9	202684	4680	228798	403.9
AWAG4-10.1	1286	242	167	143220	348	1.8	200676	6364	229122	488.3

Table F1 (continued) Sphene SHRIMP trace element data for samples

	F ppm	Na ppm	Mg ppm	Si ppm	P ppm	K ppm	Ca ppm	Al ppm	Ti ppm	V ppm
AWAG4-10.2	3023	139	149	132036	181	1.6	208299	7219	238830	550.9
AWAG4-11.1	1278	229	146	134380	339	1.9	207201	6133	240712	524.1
AWAG4-11.2	3079	132	151	130538	137	1.6	208871	6697	240211	555.9
AWAG4-12.1	1745	149	120	146715	137	1.8	203899	4949	230602	382.8
AWAG4-12.2	2159	173	123	138472	147	1.8	211656	5378	238593	487.6
AWAG4-13.1	1979	140	97	148560	28	2.0	206199	4928	234752	417.5
AWAG4-13.2	1648	136	236	140857	78	84.7	202817	5481	232806	373.5
AWAG5-1.1	1572	286	255	123741	291	1.5	211639	7087	242535	418.8
AWAG5-1.2	3650	153	164	128320	193	3.4	210694	6961	240109	424.6
AWAG5-2.1	4153	181	268	139372	201	3.0	198435	7583	220223	405.3
AWAG5-2.2	3540	127	292	133656	83	275.5	208735	7485	237002	440.8
AWAG5-3.1	3156	230	265	149228	325	1.8	198683	7273	224294	375.9
AWAG5-3.2	3596	148	188	142769	176	2.0	204218	6863	229300	437.2
AWAG5-4.1	1427	278	208	137722	368	2.1	206762	6366	235983	430.7
AWAG5-4.2	2557	220	135	143547	108	2.2	204719	5120	231958	345.8
AWAG5-5.1	1223	287	268	129931	333	1.5	203649	7245	239476	397.9
AWAG5-5.2	3720	153	247	136616	157	1.5	204022	7939	233143	417.8
AWAG5-6.1	2162	266	194	150884	350	1.6	200025	6252	226182	390.2
AWAG5-6.2	2883	214	125	151988	166	1.9	199708	4608	231498	363.4
AWAG5-7.1	1426	298	230	138762	344	1.8	205839	6653	237931	415.0
AWAG5-7.2	3594	131	172	137760	175	1.8	206673	7039	236954	436.6
AWAG5-8.1	2428	203	207	134070	253	14.9	204134	6739	238815	409.5
AWAG5-8.2	4326	155	160	153280	170	2.1	199266	6461	223613	390.7
AWAG5-9.1	3906	121	164	144551	182	1.7	199824	7013	230105	418.9

Table F1 (continued) Sphene SHRIMP trace element data for samples

	F ppm	Na ppm	Mg ppm	Si ppm	P ppm	K ppm	Ca ppm	Al ppm	Ti ppm	V ppm
AWAG5-9.2	1461	257	169	150197	246	1.7	196845	6246	228516	404.7
AWAG5-10.1	1585	253	194	149801	313	1.6	197525	6516	228611	370.3
AWAG5-10.2	3585	143	160	146590	198	1.6	200000	6524	229939	420.8
AWAG5-11.1	1368	249	185	139161	378	1.7	201960	6259	235331	402.4
AWAG5-11.2	3992	151	183	153292	193	1.9	196769	6666	222932	403.4
AWAG5-12.1	1692	307	265	150946	410	2.7	197439	6418	228085	384.7
AWAG5-12.2	3119	112	155	131072	179	1.2	199415	6893	235685	428.6
AWAG5-13.1	1389	255	207	129429	367	1.8	204745	7024	240606	407.1
AWAG5-13.2	4008	121	165	144358	187	16.3	198876	7093	226719	409.0
AWAG5-14.1	1193	255	218	131122	299	1.5	203588	6634	240506	416.7
AWAG5-14.2	3181	139	161	141213	195	1.5	201266	6532	232224	412.5
AWAG6-1.1	2000	350	261	124702	308	4.9	204051	6549	241444	331.1
AWAG6-1.2	5096	248	251	140801	112	3.3	200441	6561	226969	296.6
AWAG6-1.3	3247	234	317	124272	155	3.1	205931	7751	241040	391.5
AWAG6-1.4	4818	181	252	152988	183	14.5	195633	6838	226484	359.0
AWAG6-2.1	4784	204	603	161978	196	37.9	186605	8828	213753	327.8
AWAG6-2.2	3837	232	303	156447	149	2.6	195400	7172	224131	357.7
AWAG6-2.3	6826	322	309	151549	143	8.2	198810	6849	223486	284.6
AWAG6-3.1	4575	207	205	155812	109	1.9	198947	6337	225009	342.1
AWAG6-3.2	2794	261	251	139681	262	6.1	201519	6663	238221	386.1
AWAG6-4.1	3416	396	460	130915	198	6.4	205251	7767	234360	598.5
AWAG6-4.2	4619	229	207	153532	213	2.3	200284	5956	228170	331.1
AWAG6-5.1	5198	453	537	150723	336	2.3	203599	7323	214723	327.0
AWAG6-5.2	3975	218	211	153376	169	2.1	199331	6000	230765	345.6

Table F1 (continued) Sphene SHRIMP trace element data for samples

	F ppm	Na ppm	Mg ppm	Si ppm	P ppm	K ppm	Ca ppm	Al ppm	Ti ppm	V ppm
AWAG6-6.1	3874	220	320	152124	258	1.9	197914	7422	226452	380.8
AWAG6-6.2	5947	176	201	142376	125	2.2	206176	7126	234541	350.0
AWAG6-7.1	3347	271	314	140232	262	2.2	201711	7081	234156	384.1
AWAG6-7.2	4363	157	189	146890	119	1.8	199160	6576	231257	333.8
AWAG6-8.1	2197	393	360	140339	373	2.1	204010	7016	234014	469.4
AWAG6-8.2	4701	197	215	136463	139	1.7	205439	6281	238298	366.3
AWAG6-9.1	2122	449	422	138233	344	2.3	206321	7401	238227	425.2
AWAG6-9.2	4855	243	251	146996	179	2.8	203972	6782	227772	364.7
AWAG6-10.1	2748	509	465	143565	498	2.0	206248	7517	235297	609.5
AWAG6-10.2	2683	284	191	159375	198	1.9	196793	6137	226969	323.7
AWAG6-11.1	1295	324	333	132266	340	1.6	195502	6829	236868	397.5
AWAG6-11.2	5423	183	230	156120	98	1.5	199214	6788	225722	352.4
AWAG6-12.1	2703	389	440	140757	390	2.9	203438	6982	233939	420.7
AWAG6-12.2	4559	306	301	143494	258	1.8	204618	6918	233252	403.4
AWAG6-13.1	1977	345	304	151035	282	1.8	195495	6612	223790	363.9
AWAG6-13.2	4865	194	339	151846	198	93.4	196448	7136	228184	339.7
AWAG7-1.1	3734	202	219	155308	207	1.4	194189	6180	231955	343.8
AWAG7-1.2	5790	165	207	169212	162	1.6	193650	6749	218388	358.6
AWAG7-2.1	4189	261	303	142031	225	1.4	205473	7282	236745	465.5
AWAG7-3.1	2845	347	333	158282	366	48.1	196742	6660	226628	366.2
AWAG7-3.2	5982	198	272	163804	151	1.9	193759	6478	215816	344.1
AWAG7-4.1	3888	523	472	142600	416	2.3	212413	7618	236262	509.1
AWAG7-4.2	5258	218	255	152436	130	2.4	204587	6797	216836	414.7
AWAG7-5.1	3581	268	288	150611	192	3.0	200695	6758	228572	364.8

Table F1 (continued) Sphene SHRIMP trace element data for samples

	F ppm	Na ppm	Mg ppm	Si ppm	P ppm	K ppm	Ca ppm	Al ppm	Ti ppm	V ppm
AWAG7-5.2	6666	242	225	147993	127	3.3	207852	7180	226994	331.6
AWAG7-6.1	5296	309	189	155855	83	2.7	202667	6089	223429	291.6
AWAG7-6.2	5207	603	321	143401	174	2.4	209491	7199	225982	304.9
AWAG7-6.3	14487	69	89	150920	19	3.9	208262	17915	212324	444.8
AWAG7-7.1	2976	438	391	151439	466	2.7	200498	6225	228776	477.6
AWAG7-7.2	5048	231	206	146553	191	2.7	214084	6205	239790	334.9
AWAG7-9.1	2354	204	167	151312	305	2.4	203658	5977	229314	454.8
AWAG7-9.2	4354	159	199	137938	201	2.2	219107	7356	238354	507.0
AWAG7-8.1	3851	267	340	161152	241	12.7	192811	7145	213999	349.4
AWAG7-8.2	5869	200	247	154548	193	3.7	202280	6793	224460	297.4
AWAG7-10.1	1784	262	210	136015	365	2.9	215012	6982	242106	411.6
AWAG7-10.2	3528	185	170	159838	198	2.4	195818	6119	219709	366.5
AWAG7-11.1	2638	392	299	149646	341	1.9	205342	6416	230539	375.2
AWAG7-11.2	4638	224	284	136137	149	2.9	218950	7534	242710	387.9
AWAG7-11.3	6125	191	255	155941	153	1.6	197231	7343	221833	354.0
AWA67-12.1	4021	759	281	157082	213	2.4	199253	6648	210292	284.4
AWA67-12.2	7256	204	119	162647	78	2.0	199429	5600	223333	277.3
AWAG7-13.1	5912	194	231	162062	139	2.5	193604	6504	215076	300.7
AWAG7-13.2	4229	219	249	135099	234	4.1	211967	7239	241854	367.9
AWAG7-13.3	3872	287	333	155080	199	3.4	199643	7376	224529	380.5
AWAG7-14.1	5424	206	217	149466	184	3.4	202429	6561	228289	327.0
AWAG7-14.2	3485	340	262	157888	217	2.6	198350	6208	221454	295.3
AWA67-15.1	2860	393	382	142555	257	2.7	203437	7203	233281	371.6
AWA67-15.2	4807	290	344	147939	237	19.0	194716	7128	214291	392.7

Table F1 (continued) Sphene SHRIMP trace element data for samples

	Cr ppm	Mn ppm	Fe ppm	Sr ppm	Y ppm	Zr90 ppm	Zr91 ppm	Nb ppm	Ba ppm	La ppm
AWM1.1	1.6	857	13266	66.0	1343	7426	7561	1438	16.5	3980
AWM1-2.1	15.4	802	19238	97.0	3070	11743	11850	2790	17.6	5074
AWM1-2.2	89.3	1864	9562	61.3	447	843	829	631	17.1	3339
AWM1-3.1	1.2	872	19632	69.9	1885	9809	10033	2152	19.0	4071
AWM1-3.2	2.7	865	15225	73.1	1695	2033	2048	1380	19.1	3987
AWM1-4.1	1.2	831	15432	72.7	1773	7250	7330	2035	17.1	4486
AWM1-4.2	13.9	1269	13406	53.2	360	464	454	348	16.5	2005
AWM1-5.1	2.7	895	14551	60.9	1225	8497	8706	1560	17.4	3674
AWM1-5.2	1.0	935	13552	60.5	1333	5544	5649	1548	17.2	4027
AWM1-6.1	2.1	882	13597	78.1	1338	8738	8911	2409	16.9	5408
AWM1-6.2	2.5	860	14841	68.6	1548	1604	1658	1319	18.2	4097
AWM1-7.1	17.5	1121	15012	55.2	966	563	558	798	19.2	1826
AWM1-7.2	1.6	955	15799	74.6	1741	10413	10801	2276	16.6	3972
AWM1-8.1	1.0	875	18535	72.6	1927	11154	11384	2432	17.6	4579
AWM1-8.2	45.8	984	16231	55.0	409	1148	1152	992	19.5	3143
AWM1-9.1	6.3	881	15787	78.0	1841	5891	6031	2013	17.8	4338
AWM1-9.2	6.1	1473	12487	56.3	347	498	493	313	17.5	1838
AWM1-10.1	58.7	954	17328	64.4	1467	7686	7811	1118	17.4	3870
AWM1-10.2	85.3	995	16187	50.1	2069	574	570	1327	16.9	2263
AWM1-11.1	2.0	1030	16257	59.9	1521	7212	7377	1226	16.6	3527
AWM1-11.2	2.0	867	13782	72.0	1252	806	792	1187	17.3	3500
AWM1-12.1	0.7	915	13901	60.2	1081	11972	12159	1435	16.8	3939
AWM1-12.2	6.3	839	12086	62.0	270	241	240	117	21.0	692
AWM1-13.1	6.1	967	14754	75.3	1508	10444	10760	1991	19.0	5197

Table F1 (continued) Sphene SHRIMP trace element data for samples

	Cr ppm	Mn ppm	Fe ppm	Sr ppm	Y ppm	Zr90 ppm	Zr91 ppm	Nb ppm	Ba ppm	La ppm
AWM1-13.2	14.3	1502	10165	54.8	493	819	819	777	16.6	2366
AWM1-14.1	3.3	888	16102	52.2	1044	5926	6002	905	12.9	3173
AWM1-14.2	32.1	1438	12587	44.3	693	417	409	407	12.3	1536
AMW2-1.1	19.8	704	15995	66.3	2300	6284	6415	4904	18.4	4135
AMW2-1.2	56.2	736	14650	50.9	375	1710	1736	733	17.9	3532
AMW2-2.1	58.8	732	12386	56.7	1017	562	541	914	19.8	4121
AMW2-2.2	195.4	704	13003	54.0	354	832	843	318	19.3	1672
AWM2-3.1	116.2	745	16376	79.7	3641	1456	1499	5740	18.3	6398
AWM2-3.2	38.6	743	14635	59.0	1188	1392	1405	2338	18.3	3595
AWM2-4.1	81.1	793	15164	51.5	460	1510	1498	512	18.0	3974
AWM2-4.2	68.5	927	15920	53.1	814	9604	9761	5154	19.3	6640
AWM2-5.1	155.0	838	16273	52.5	1334	1233	1249	3318	17.0	4900
AWM2-5.2	165.9	745	17320	52.8	959	3200	3196	1687	18.1	3360
AWM2-6.1	258.7	732	13789	55.5	1240	663	665	1584	19.4	4274
AWM2-6.2	50.5	686	16078	67.1	3478	1627	1628	6060	16.7	5592
AWM2-7.1	77.2	770	16250	56.7	1815	1648	1657	7145	19.3	7079
AWM2-7.2	365.7	694	13877	48.7	924	1320	1366	1285	16.2	3467
AWM2-8.1	143.2	555	9326	43.4	131	397	400	189	12.7	642
AWM2-8.2	78.4	840	12952	53.9	403	1114	1137	2060	18.9	5124
AWM2-9.1	82.8	681	11320	57.2	1342	755	773	2185	18.0	4570
AWM2-9.2	82.4	680	9988	51.2	1130	1161	1168	1510	17.8	4184
AWM2-9.3	96.5	572	11150	60.3	204	343	312	156	20.7	2202
AWM2-10.1	260.9	637	14035	53.0	2216	7292	7349	5030	17.0	3673
AWM2-10.2	29.0	623	14601	50.5	1418	620	622	1535	16.9	3337

Table F1 (continued) Sphene SHRIMP trace element data for samples

	Cr ppm	Mn ppm	Fe ppm	Sr ppm	Y ppm	Zr90 ppm	Zr91 ppm	Nb ppm	Ba ppm	La ppm
AWM2-11.1	92.1	619	12489	49.9	361	421	415	131	17.0	2262
AWM2-11.2	54.7	771	11229	51.5	431	783	786	1471	17.1	3778
AWM2-12.1	241.7	753	17688	62.4	1365	4584	4625	2421	18.9	3043
AWM2-12.2	183.7	740	15024	65.1	1493	9254	9399	6316	16.4	3955
AWAG_1A-1.1	3.1	1112	18827	66.7	3762	6618	6639	3676	14.1	6391
AWAG_1A-1.2	6.7	1205	21519	65.1	3389	4114	4221	1362	19.2	4450
AWAG_1A-2.1	5.2	1070	18478	74.5	3370	9565	9423	3222	19.2	5015
AWAG_1A-2.2	8.6	999	19148	65.4	1834	2589	2646	1044	18.8	3028
AWAG_1A-3.1	21.5	1249	17492	59.3	2739	1548	1553	5293	17.2	6951
AWAG_1A-3.2	45.2	1276	18438	55.5	1655	751	732	2102	18.1	4306
AWAG_1A-4.1	1.2	1396	11954	57.5	352	295	274	334	18.5	1803
AWAG_1A-4.2	1.5	1025	19995	67.5	3260	3786	3871	1338	19.6	3915
AWAG_1A-4.3	4.1	946	19574	64.5	3860	8539	8734	1289	15.7	4368
AWAG_1A-5.1	6.7	1049	20392	73.9	3388	4980	5073	1300	18.8	4251
AWAG_1A-5.2	3.2	1049	21015	99.6	4729	16120	16379	3247	20.0	7457
AWAG_1A-6.1	36.1	1036	17037	64.2	3417	6672	6811	3253	17.5	5035
AWAG_1A-6.2	1.5	1569	17317	49.6	511	3369	3447	769	16.8	3470
AWAG_1A-7.1	6.3	1065	17917	72.8	2689	1973	2039	3471	19.6	6533
AWAG_1A-7.2	3.6	1053	17984	76.6	2834	2048	2091	3310	18.6	6509
AWAG_1A-8.1	1.1	1646	14968	54.4	280	1050	1070	342	18.7	1648
AWAG_1A-8.2	1.3	1860	14495	55.2	593	1349	1332	1120	17.7	2811
AWAG_1A-9.1	2.7	1027	18454	65.5	2055	4728	4823	1518	18.6	3479
AWAG_1A-9.2	2.0	1046	17088	74.9	2471	8391	8394	2637	18.3	4389

Table F1 (continued) Sphene SHRIMP trace element data for samples

	Cr ppm	Mn ppm	Fe ppm	Sr ppm	Y ppm	Zr90 ppm	Zr91 ppm	Nb ppm	Ba ppm	La ppm
AWAG_1A-10.1	9.8	912	17172	54.1	1587	1314	1323	1128	15.5	2720
AWAG_1A-10.2	3.2	985	15864	63.4	2247	1873	1889	3213	17.5	5473
AWAG_1A-11.1	3.2	1088	19476	58.0	2728	1184	1183	1250	18.8	3582
AWAG_1A-11.2	1.0	1075	17318	65.0	2784	1787	1784	3320	15.7	5509
AWAG_1A-12.1	0.9	1229	20880	54.1	1303	3937	3916	2035	19.3	3644
AWAG_1A-12.2	0.4	1338	19360	54.5	1907	1560	1587	7940	20.0	6321
AWAG_1A-13.1	4.9	929	17576	58.3	1466	1522	1513	1092	17.4	2944
AWAG_1A-13.2	3.4	1032	16653	66.9	2413	1794	1852	2449	17.4	4649
AWAG_1A-14.1	5.8	1076	20957	89.2	3819	4398	4472	2901	20.0	7220
AWAG_1A-14.2	6.5	1016	19432	67.6	2836	2406	2414	1370	16.5	4429
AWAG_1B-1.1	3.6	997	12788	46.7	255	731	739	159	14.6	854
AWAG_1B-1.2	1.7	1098	13484	53.7	364	851	835	228	18.6	1202
AWAG_1B-2.1	2.3	1063	12783	49.2	188	1423	1419	306	16.1	980
AWAG_1B-2.2	2.1	1130	16723	50.2	571	2992	2993	978	17.8	3864
AWAG_1B-3.1	5.0	933	16400	53.3	742	939	906	683	17.8	3521
AWAG_1B-3.2	3.1	1012	17390	75.1	3367	10924	11262	1864	18.7	4042
AWAG_1B-4.1	46.4	973	19129	71.4	3265	8190	8440	1386	17.4	3564
AWAG_1B-4.2	2.3	1052	13674	48.3	224	994	971	218	15.9	968
AWAG_1B-5.1	4.3	1003	9856	51.2	1170	3387	3465	691	16.9	2075
AWAG_1B-5.2	3.4	1040	16028	50.6	2621	4811	4901	2118	17.5	4659
AWAG_1B-6.1	14.0	973	17857	73.5	2154	5194	5293	1313	18.8	3702
AWAG_1B-6.2	2.9	1138	13005	49.3	201	1804	1796	301	16.3	960
AWAG_1B-7.1	0.8	1063	16012	79.6	1502	2622	2673	3357	19.0	7196

Table F1 (continued) Sphene SHRIMP trace element data for samples

	Cr ppm	Mn ppm	Fe ppm	Sr ppm	Y ppm	Zr90 ppm	Zr91 ppm	Nb ppm	Ba ppm	La ppm
AWAG_1B-7.2	1.2	1168	16238	70.7	843	1316	1308	1015	19.6	3395
AWAG_1B-8.1	36.2	957	18272	71.8	2435	6217	6321	1156	18.1	3240
AWAG_1B-8.2	5.8	955	15752	78.1	2527	9123	9215	2331	17.9	4824
AWAG_1B-9.1	0.2	965	20410	177.6	3811	7443	7551	1483	17.9	4580
AWAG_1B-9.2	4.2	891	16435	66.6	1486	2001	2012	930	17.5	4059
AWAG_1B-9.3	0.5	1085	13674	53.4	208	1005	970	200	18.3	869
AWAG_1B-10.1	9.2	984	16863	82.5	3880	10301	10537	2303	19.2	4778
AWAG_1B-10.2	4.8	1107	9825	59.3	577	954	949	520	18.6	2198
AWAG_1B-11.1	5.5	946	17398	70.6	1468	2615	2622	1142	18.3	3570
AWAG_1B-11.2	5.7	1019	16905	88.6	2269	3476	3480	3555	18.4	6657
AWAG_1B-12.1	3.2	1088	10344	59.4	659	967	939	539	17.6	2542
AWAG_1B-12.2	4.5	992	18340	75.6	2670	8706	8924	1369	17.5	3858
AWAG_1B-13.1	1.6	989	15897	74.1	2054	6082	6184	1609	18.0	3771
AWAG_1B-13.2	2.0	1053	15869	68.8	1612	3810	3898	1051	17.7	2947
AWAG_1B-13.3	1.4	936	16532	100.0	2638	4478	4577	2033	18.9	6068
AWAG_1B-13.4	3.9	938	15672	65.3	800	855	851	774	17.6	3192
AWAG_2-1.1	30.7	1475	15193	54.5	2384	855	808	3437	18.5	5981
AWAG_2-1.2	17.5	1264	21061	60.3	5717	2045	2057	3623	17.0	6550
AWAG_2-2.1	25.8	1501	18021	51.3	2376	846	832	2426	17.2	4237
AWAG_2-2.2	7.2	1401	17606	49.9	4538	1518	1532	3499	16.8	4986
AWAG_2-3.1	13.6	1356	18369	57.6	5780	2117	2129	3731	18.1	6906
AWAG_2-3.2	10.3	1475	17794	48.9	2193	791	793	2403	17.1	4259
AWAG_2-4.1	2.5	1417	17736	55.7	6044	2226	2239	4182	17.7	5616

Table F1 (continued) Sphene SHRIMP trace element data for samples

	Cr ppm	Mn ppm	Fe ppm	Sr ppm	Y ppm	Zr90 ppm	Zr91 ppm	Nb ppm	Ba ppm	La ppm
AWAG_2-4.2	7.3	1483	17521	48.8	1919	734	713	2213	16.2	4048
AWAG_2-5.1	26.3	1367	19560	53.1	5920	2276	2281	3801	17.0	5147
AWAG_2-5.2	24.8	1532	17711	50.5	1463	655	635	2386	17.4	4234
AWAG_2-6.1	3.7	1421	17433	56.9	5624	1788	1823	4262	18.6	5835
AWAG_2-6.2	35.8	1635	15261	43.9	932	649	635	2438	14.5	3426
AWAG_2-7.1	4.4	1429	17319	49.6	4443	1433	1411	4724	16.3	5604
AWAG_2-7.2	8.8	2178	18489	55.9	1485	952	919	4033	20.7	8238
AWAG_2-8.1	2.5	1487	23452	55.7	6230	2184	2216	2336	18.7	3725
AWAG_2-8.2	11.0	1383	14321	44.7	2204	739	725	3013	14.3	4676
AWAG_2-9.1	21.6	1351	20925	52.3	6494	1613	1652	3102	16.5	6812
AWAG_2-9.2	9.2	1404	18162	46.0	2607	849	850	1978	15.2	4053
AWAG_2-10.1	75.1	8161	44220	54.6	2620	1231	1239	2694	17.6	4619
AWAG_2-10.2	34.2	1840	17402	52.9	1537	561	548	1769	18.5	5245
AWAG_2-11.1	7.0	1367	18024	48.6	4963	1434	1432	2589	15.5	3536
AWAG_2-11.2	22.4	1287	20065	47.8	5364	1476	1478	1978	15.7	4452
AWAG_2-12.1	41.3	1326	19224	62.2	5883	1411	1431	2668	19.3	6449
AWAG_2-12.2	36.9	1391	17595	46.1	1409	645	626	1965	15.9	4015
AWAG_2-13.1	13.9	1469	17866	57.3	6001	1746	1742	3782	19.2	4669
AWAG_2-13.2	21.5	1575	19216	54.9	1471	695	677	2235	19.5	4585
AWAG_2-14.1	29.5	1413	15725	54.3	4418	1303	1288	4075	17.7	5955
AWAG_2-14.2	87.6	1593	17934	54.7	1200	687	691	2191	19.8	4974
AWAG3-1.1	1.0	1353	19937	51.5	6252	2072	2090	2564	17.4	4574

Table F1 (continued) Sphene SHRIMP trace element data for samples

	Cr ppm	Mn ppm	Fe ppm	Sr ppm	Y ppm	Zr90 ppm	Zr91 ppm	Nb ppm	Ba ppm	La ppm
AWAG3-1.2	2.6	1691	17063	54.2	3108	945	924	2685	18.2	5243
AWAG3-2.1	10.2	1024	18395	75.3	3800	2426	2452	3053	18.4	5999
AWAG3-2.2	27.0	1156	15014	57.8	2805	956	976	2156	16.5	4098
AWAG3-2.2	27.4	1158	14725	57.6	2903	919	938	2121	13.6	3960
AWAG3-3.1	22.2	1821	20130	58.1	3214	770	797	2606	21.2	5326
AWAG3-3.2	10.7	1918	19231	47.5	5526	561	553	2335	16.4	2963
AWAG3-4.1	1.9	1421	16492	57.0	3007	3131	3168	2455	15.6	5533
AWAG3-4.2	2.4	1378	14435	58.4	2367	1993	1976	1647	15.1	3971
AWAG3-5.1	22.2	1641	18245	52.8	2813	720	691	2771	18.7	4808
AWAG3-5.2	17.6	1482	16356	47.1	2820	715	704	2432	15.1	4112
AWAG3-6.1	20.4	1374	16795	48.1	4071	1012	1007	2319	14.9	4154
AWAG3-6.2	15.6	1516	16444	46.5	2699	607	598	2391	15.4	3823
AWAG3-7.1	0.4	1321	20360	69.1	5399	3767	3872	2693	16.3	5605
AWAG3-7.2	11.5	1780	13891	54.5	2696	725	743	2652	18.2	5962
AWAG3-7.3	1.7	1738	13536	37.4	3788	514	508	3016	12.4	2409
AWAG3-8.1	27.2	1377	19722	53.8	6866	1143	1149	2050	18.1	4030
AWAG3-8.2	20.0	1443	16485	45.7	3099	681	688	2292	14.8	4070
AWAG3-9.1	25.4	1378	19994	58.8	7332	1315	1327	2519	20.2	4649
AWAG3-9.2	18.1	1728	18560	48.8	4386	647	628	2181	16.6	3764
AWAG3-10.1	1.6	2618	17193	48.8	4739	655	625	10652	16.7	3738
AWAG3-10.2	5.9	1166	15671	52.0	4507	3566	3613	2259	16.6	3789
AWAG3-11.1	90.9	1488	19541	51.9	4260	716	728	1343	17.8	3722

Table F1 (continued) Sphene SHRIMP trace element data for samples

	Cr ppm	Mn ppm	Fe ppm	Sr ppm	Y ppm	Zr90 ppm	Zr91 ppm	Nb ppm	Ba ppm	La ppm
AWAG3-11.2	60.1	1246	17689	47.2	4498	828	842	1386	13.8	2879
AWAG3-12.1	21.5	1342	18423	56.6	7650	1241	1223	3186	18.6	5010
AWAG3-12.2	26.0	1388	16882	47.3	3958	807	832	2185	15.2	4043
AWAG3-13.1	14.6	1058	15664	65.4	4078	1287	1305	4433	15.9	5850
AWAG3-13.2	47.4	1039	17693	56.9	3604	762	763	1424	14.3	3506
AWAG4-1.1	34.2	1347	16805	55.7	2003	726	711	1735	18.6	7568
AWAG4-1.2	59.1	1158	15245	55.6	804	459	445	462	19.8	4164
AWAG4-2.1	13.1	1244	15669	51.7	1996	975	935	3003	18.7	9156
AWAG4-2.2	17.9	1050	13378	50.4	868	858	859	508	17.5	3181
AWAG4-3.1	23.5	1347	16702	52.6	1946	790	767	1751	18.7	7196
AWAG4-3.2	17.0	1101	14285	54.5	792	515	496	362	19.5	3525
AWAG4-4.1	19.3	1192	14578	50.1	1825	934	936	2678	18.1	8662
AWAG4-4.2	53.7	1095	15998	50.4	1002	437	394	439	18.5	4079
AWAG4-5.1	23.0	1161	15001	51.0	1154	455	423	677	18.9	4109
AWAG4-5.2	12.3	1183	15232	50.8	1714	1016	1038	2878	18.0	8701
AWAG4-6.1	19.9	901	16568	51.2	3574	680	650	1607	16.4	3468
AWAG4-6.2	33.5	1114	15390	46.3	1920	467	449	1479	16.5	3661
AWAG4-7.1	36.3	1140	14040	53.6	1660	3398	3457	2023	18.4	6764
AWAG4-7.2	60.3	1036	14090	49.3	981	378	372	482	17.1	3710
AWAG4-8.1	18.9	923	15633	58.5	4202	825	804	2055	17.8	4436
AWAG4-8.2	15.0	956	17203	64.5	4885	1304	1334	3107	18.1	5282
AWAG4-8.3	41.1	1162	14382	52.0	2822	579	551	2178	18.3	4771
AWAG4-9.1	7.7	1196	16556	46.8	3025	1113	1122	5008	16.4	7435
AWAG4-9.2	15.9	1259	14436	48.5	1559	415	388	1086	16.4	3136

Table F1 (continued) Sphene SHRIMP trace element data for samples

	Cr ppm	Mn ppm	Fe ppm	Sr ppm	Y ppm	Zr90 ppm	Zr91 ppm	Nb ppm	Ba ppm	La ppm
AWAG4-10.1	14.9	914	16928	66.0	4954	1426	1458	4578	17.5	6033
AWAG4-10.2	21.5	950	18372	60.9	4450	884	861	1685	18.7	4409
AWAG4-11.1	3.4	936	16139	63.9	4776	1078	1133	3854	18.2	6020
AWAG4-11.2	4.3	958	18515	62.0	4001	804	810	1809	18.8	4137
AWAG4-12.1	41.7	1098	15800	51.3	1620	658	658	937	17.8	3971
AWAG4-12.2	57.5	1177	16504	53.9	1704	591	585	1039	19.0	4713
AWAG4-13.1	36.4	1135	14592	51.2	971	552	548	523	17.4	3738
AWAG4-13.2	36.3	1075	14278	51.8	997	1021	1007	791	18.0	3896
AWAG5-1.1	24.7	1231	17222	80.1	6549	1180	1188	2931	18.8	5197
AWAG5-1.2	35.6	1217	17070	64.4	4091	804	799	2186	19.0	4489
AWAG5-2.1	41.6	1141	19402	65.5	5798	1045	1018	1648	16.4	3808
AWAG5-2.2	57.6	1199	18388	61.6	4527	902	869	2002	18.3	4564
AWAG5-3.1	35.8	1150	17504	66.7	5734	1249	1253	2298	16.6	4055
AWAG5-3.2	21.3	1172	17024	64.0	4253	918	920	2362	17.6	4198
AWAG5-4.1	32.2	1162	16402	74.2	5643	1122	1126	3925	18.2	5943
AWAG5-4.2	48.7	1402	17249	51.0	1193	1537	1515	4633	18.7	5201
AWAG5-5.1	38.0	1203	18041	88.3	6490	2074	2098	5564	18.8	6445
AWAG5-5.2	56.1	1213	19419	72.8	5595	1126	1130	1736	18.7	4309
AWAG5-6.1	66.1	1205	16160	62.9	4796	1534	1542	4884	16.6	5019
AWAG5-6.2	84.0	1241	13217	49.7	2279	653	630	1566	16.7	5354
AWAG5-7.1	23.1	1154	16401	75.9	5626	1158	1175	3558	18.2	5910
AWAG5-7.2	36.1	1184	17261	65.5	4348	901	894	2465	18.0	4315
AWAG5-8.1	27.7	1157	17320	70.3	5430	1111	1099	2714	19.0	4921
AWAG5-8.2	32.9	1118	16065	52.4	3227	710	702	1793	15.9	3983

Table F1 (continued) Sphene SHRIMP trace element data for samples

	Cr ppm	Mn ppm	Fe ppm	Sr ppm	Y ppm	Zr90 ppm	Zr91 ppm	Nb ppm	Ba ppm	La ppm
AWAG5-9.1	71.2	1171	17478	59.9	4352	794	811	1853	17.5	4341
AWAG5-9.2	28.2	1098	13177	74.4	3660	805	795	3689	17.1	6156
AWAG5-10.1	37.1	1164	13623	74.8	4277	920	916	3529	16.9	5975
AWAG5-10.2	30.9	1150	16183	59.1	4016	773	748	2377	17.5	4021
AWAG5-11.1	30.8	1130	15651	69.6	5108	1057	1057	3782	18.0	6054
AWAG5-11.2	44.9	1117	16422	60.7	3787	809	814	2117	16.4	3840
AWAG5-12.1	33.1	1118	15538	71.6	5816	1247	1264	3115	16.9	4616
AWAG5-12.2	44.4	1193	17517	64.1	4781	910	897	2010	17.7	4567
AWAG5-13.1	38.5	1181	16270	82.1	5196	1375	1397	4742	18.5	6610
AWAG5-13.2	47.0	1141	18043	58.8	4262	797	776	1837	17.9	4234
AWAG5-14.1	37.1	1163	16516	72.6	5862	1244	1214	3909	18.8	6222
AWAG5-14.2	46.2	1159	16130	63.7	4117	842	823	2478	17.8	4311
AWAG6-1.1	6.3	1660	15779	54.9	6211	833	878	3986	18.8	5630
AWAG6-1.2	3.2	1730	17871	49.3	4677	757	752	3148	16.4	3777
AWAG6-1.3	41.9	1418	18822	56.3	7741	1091	1071	2551	19.5	4222
AWAG6-1.4	22.2	1403	16934	50.1	4043	847	823	2354	16.6	4218
AWAG6-2.1	15.2	1400	17523	46.7	3619	720	727	2822	15.2	3881
AWAG6-2.2	29.6	1369	17281	54.9	5055	1239	1259	1933	15.8	4355
AWAG6-2.3	13.4	2174	19815	50.7	2359	459	468	8513	16.3	3315
AWAG6-3.1	13.5	1479	15930	50.0	2998	727	722	2850	16.5	4502
AWAG6-3.2	11.8	1489	17106	56.2	3661	1085	1082	3685	18.2	6238
AWAG6-4.1	4.6	1365	23864	54.5	4639	4705	4818	3187	17.9	8262
AWAG6-4.2	13.2	1533	15572	48.9	2554	691	650	2973	16.8	4598
AWAG6-5.1	14.8	1338	21431	47.7	4794	12727	12974	9999	16.4	2964

Table F1 (continued) Sphene SHRIMP trace element data for samples

	Cr ppm	Mn ppm	Fe ppm	Sr ppm	Y ppm	Zr90 ppm	Zr91 ppm	Nb ppm	Ba ppm	La ppm
AWAG6-5.2	17.2	1491	15866	52.4	3158	727	721	2837	17.0	4866
AWAG6-6.1	32.4	1270	18553	54.8	7152	1108	1105	2171	16.8	3996
AWAG6-6.2	15.0	1695	18264	52.9	2738	671	662	2581	17.4	4542
AWAG6-7.1	26.6	1399	18763	57.4	5449	1559	1534	2729	18.2	5186
AWAG6-7.2	26.1	1496	16569	53.3	3245	676	649	2731	17.8	4803
AWAG6-8.1	3.5	1525	16560	61.2	2492	2755	2802	3109	18.1	8964
AWAG6-8.2	8.5	1767	17660	52.8	1555	1412	1403	3848	18.3	5539
AWAG6-9.1	3.9	1311	19773	56.2	5552	2813	2888	3192	18.5	7012
AWAG6-9.2	13.7	1503	17797	51.6	2820	860	878	2657	17.1	5086
AWAG6-10.1	11.7	1152	19048	63.2	4739	4677	4816	4904	17.3	6342
AWAG6-10.2	12.9	1504	13030	49.8	2440	600	588	3805	17.0	6378
AWAG6-11.1	16.8	1280	18806	63.4	8314	1736	1747	3719	17.6	5996
AWAG6-11.2	13.0	1513	17222	50.4	3036	774	785	2310	17.0	4732
AWAG6-12.1	4.4	1369	21138	53.3	5942	3620	3673	3439	17.7	6459
AWAG6-12.2	6.6	1479	18849	51.9	4008	2268	2309	2626	18.3	5107
AWAG6-13.1	18.6	1246	16936	56.4	6592	1211	1228	3257	16.7	5135
AWAG6-13.2	18.0	1506	17428	50.4	3863	810	815	2864	17.0	4253
AWAG7-1.1	16.2	1489	15887	54.0	3773	794	797	2987	15.7	4853
AWAG7-1.2	16.5	1371	16150	46.7	2827	809	835	2034	15.7	3841
AWAG7-2.1	4.4	1399	19280	55.2	4473	2180	2213	2244	17.5	5344
AWAG7-3.1	17.0	1310	16573	55.0	4827	1155	1182	2912	15.6	5177
AWAG7-3.2	17.6	1434	17117	46.3	2983	771	791	2202	14.4	4173
AWAG7-4.1	6.6	1429	20931	58.4	5576	3035	3126	3828	16.9	5626

Table F1 (continued) Sphene SHRIMP trace element data for samples

	Cr ppm	Mn ppm	Fe ppm	Sr ppm	Y ppm	Zr90 ppm	Zr91 ppm	Nb ppm	Ba ppm	La ppm
AWAG7-4.2	7.3	1394	18311	51.8	2913	1132	1128	2323	16.3	4795
AWAG7-5.1	20.7	1323	17406	50.4	5485	996	1002	2607	15.7	4292
AWAG7-5.2	14.1	1940	19671	49.1	3164	696	673	4211	16.4	4097
AWAG7-6.1	8.0	2143	16410	47.5	3919	492	472	4653	16.5	2975
AWAG7-6.2	7.7	2570	22063	48.9	5120	1366	1359	13193	17.2	5747
AWAG7-6.3	6.8	758	10829	46.9	352	172	160	658	14.5	321
AWAG7-7.1	20.1	1117	16989	62.4	2557	1733	1748	3304	15.2	6740
AWAG7-7.2	18.3	1641	15823	51.1	2656	572	576	3134	16.9	4466
AWAG7-9.1	2.1	1059	14052	54.0	2848	948	952	3008	16.2	5823
AWAG7-9.2	18.0	1172	18653	57.5	2855	1108	1109	1791	17.5	3463
AWAG7-8.1	35.0	1239	17391	49.3	6550	967	953	2149	14.2	3578
AWAG7-8.2	27.1	1646	17668	47.9	3984	663	666	2389	15.6	4052
AWAG7-10.1	16.9	1250	16658	77.0	4500	1259	1262	4264	18.1	6613
AWAG7-10.2	18.6	1147	14399	56.4	3065	767	763	2185	14.8	4256
AWAG7-11.1	14.5	1407	16901	52.6	4698	1059	1056	3697	16.7	5549
AWAG7-11.2	24.6	1548	19552	55.9	5083	954	950	2532	19.3	4777
AWAG7-11.3	14.9	1498	18377	47.5	3695	855	862	2035	15.9	4313
AWA67-12.1	11.5	2703	20711	44.6	2579	669	665	22843	16.0	4557
AWA67-12.2	12.6	1891	13085	46.6	1379	274	242	2786	15.8	1458
AWAG7-13.1	18.6	1479	15854	45.3	3031	598	583	2402	15.4	3792
AWAG7-13.2	13.2	1576	18149	55.6	4940	907	910	3083	20.0	4648
AWAG7-13.3	22.9	1276	18380	53.5	6834	1022	1031	2234	15.9	3877
AWAG7-14.1	17.0	1594	15995	50.4	3045	638	636	2843	16.1	4202
AWAG7-14.2	11.5	1665	16227	48.3	4694	750	747	3953	16.6	4869

Table F1 (continued) Sphene SHRIMP trace element data for samples

	Ce ppm	Pr ppm	Nd ppm	Sm ppm	Eu ppm	Gd ppm	Tb ppm	Dy ppm	Ho ppm	Er ppm
AWM1.1	10786	1321	5410	905	164	631	68	314	54	129
AWM1-2.1	16205	2337	10782	2145	409	1479	171	810	138	319
AWM1-2.2	5638	508	1914	298	81	203	21	104	17	44
AWM1-3.1	12389	1657	7177	1232	208	837	90	413	72	167
AWM1-3.2	10409	1291	5738	1131	205	833	96	456	78	175
AWM1-4.1	13046	1693	7093	1179	222	766	82	373	63	155
AWM1-4.2	3565	329	1266	194	53	145	15	74	14	34
AWM1-5.1	10024	1240	5051	796	144	553	57	263	46	104
AWM1-5.2	10098	1194	4968	884	161	621	69	330	56	139
AWM1-6.1	13916	1661	6463	997	173	631	68	296	50	113
AWM1-6.2	10498	1289	5613	1072	196	785	89	407	70	160
AWM1-7.1	4160	442	1637	306	48	257	35	180	36	94
AWM1-7.2	11622	1542	6618	1138	204	794	83	385	66	152
AWM1-8.1	13579	1798	7575	1272	232	818	89	406	70	162
AWM1-8.2	5035	434	1559	219	48	167	18	87	16	39
AWM1-9.1	12172	1577	6794	1211	227	830	94	425	75	172
AWM1-9.2	3301	318	1272	203	53	154	17	76	14	33
AWM1-10.1	11095	1441	6139	1027	165	684	72	326	56	135
AWM1-10.2	5908	676	2600	515	60	418	62	353	71	189
AWM1-11.1	10187	1333	5673	999	177	686	74	347	58	140
AWM1-11.2	8747	1028	4495	786	167	585	65	315	55	129
AWM1-12.1	9867	1136	4489	711	134	478	50	233	41	99
AWM1-12.2	1867	220	873	141	40	100	11	54	10	24
AWM1-13.1	13327	1599	6546	1054	175	695	75	342	58	137

Table F1 (continued) Sphene SHRIMP trace element data for samples

	Ce ppm	Pr ppm	Nd ppm	Sm ppm	Eu ppm	Gd ppm	Tb ppm	Dy ppm	Ho ppm	Er ppm
AWM1-13.2	4426	410	1510	224	58	162	19	93	17	48
AWM1-14.1	8128	960	3983	666	109	462	49	234	40	99
AWM1-14.2	3462	366	1374	238	46	186	23	120	23	62
AMW2-1.1	12346	1534	6246	1062	207	732	95	478	91	244
AMW2-1.2	5524	482	1680	244	48	163	18	86	16	40
AMW2-2.1	9696	1025	3793	580	124	358	43	219	40	99
AMW2-2.2	3132	316	1250	195	45	127	15	79	15	36
AWM2-3.1	18667	2370	9946	1792	359	1290	163	831	154	381
AWM2-3.2	8638	902	3297	499	113	358	45	231	43	120
AWM2-4.1	6872	630	2244	302	47	192	22	113	19	50
AWM2-4.2	10319	763	2233	290	44	201	24	133	25	78
AWM2-5.1	10734	1021	3379	465	114	327	40	220	47	138
AWM2-5.2	7678	748	2613	381	82	270	35	182	37	105
AWM2-6.1	9887	1013	3644	571	109	391	50	252	47	129
AWM2-6.2	16991	2230	9382	1729	330	1196	153	795	146	376
AWM2-7.1	16465	1633	5498	786	159	521	64	339	67	190
AWM2-7.2	7753	812	2952	449	103	322	37	191	36	95
AWM2-8.1	1131	108	396	63	23	45	6	28	5	14
AWM2-8.2	7099	574	1891	250	65	161	17	92	18	46
AWM2-9.1	11244	1152	4086	598	158	410	51	263	50	136
AWM2-9.2	9360	963	3537	522	123	358	44	225	44	114
AWM2-9.3	4495	434	1503	172	30	103	10	45	8	21
AWM2-10.1	11155	1424	5909	1033	207	729	92	469	90	231
AWM2-10.2	9320	1071	4079	644	140	447	55	285	54	156

Table F1 (continued) Sphene SHRIMP trace element data for samples

	Ce ppm	Pr ppm	Nd ppm	Sm ppm	Eu ppm	Gd ppm	Tb ppm	Dy ppm	Ho ppm	Er ppm
AWM2-11.1	4809	497	1971	274	35	179	19	85	15	36
AWM2-11.2	5522	485	1706	251	58	168	19	101	19	47
AWM2-12.1	8179	903	3236	498	130	357	48	248	50	142
AWM2-12.2	10014	1073	3853	599	147	392	50	273	55	153
AWAG_1A-1.1	19966	2754	12234	2207	329	1469	185	910	166	406
AWAG_1A-1.2	14910	2147	9877	1883	293	1328	166	835	151	372
AWAG_1A-2.1	16405	2293	10308	1926	391	1342	166	828	145	337
AWAG_1A-2.2	9980	1359	5865	1010	266	718	87	433	77	183
AWAG_1A-3.1	18225	2058	7740	1163	239	797	99	519	104	279
AWAG_1A-3.2	11119	1215	4574	674	156	490	57	306	60	165
AWAG_1A-4.1	3831	394	1523	221	52	144	15	77	14	34
AWAG_1A-4.2	13870	2049	9576	1943	358	1414	172	860	149	341
AWAG_1A-4.3	15172	2263	10761	2152	400	1550	196	970	176	419
AWAG_1A-5.1	14401	2116	9921	1942	368	1427	175	856	149	347
AWAG_1A-5.2	24318	3440	15685	2981	565	2068	256	1252	224	529
AWAG_1A-6.1	16557	2337	10631	2022	315	1409	173	847	152	350
AWAG_1A-6.2	6823	688	2554	355	43	224	24	116	21	54
AWAG_1A-7.1	19800	2560	10454	1693	464	1093	131	649	111	270
AWAG_1A-7.2	20080	2636	10761	1824	461	1177	141	690	121	267
AWAG_1A-8.1	3006	291	1034	143	32	99	11	58	11	30
AWAG_1A-8.2	5398	539	2057	306	63	228	27	131	24	59
AWAG_1A-9.1	11375	1548	6736	1214	292	840	101	498	89	201
AWAG_1A-9.2	14010	1920	8311	1445	347	1023	123	611	104	239

Table F1 (continued) Sphene SHRIMP trace element data for samples

	Ce ppm	Pr ppm	Nd ppm	Sm ppm	Eu ppm	Gd ppm	Tb ppm	Dy ppm	Ho ppm	Er ppm
AWAG_1A-10.1	8871	1216	5226	908	239	624	74	371	68	152
AWAG_1A-10.2	16644	2137	8656	1380	378	924	111	547	94	225
AWAG_1A-11.1	11880	1636	7258	1303	299	986	124	635	115	284
AWAG_1A-11.2	16930	2228	9346	1567	349	1063	130	650	116	286
AWAG_1A-12.1	8922	1061	4411	744	88	534	63	305	55	131
AWAG_1A-12.2	14770	1704	6894	1103	151	738	90	439	80	199
AWAG_1A-13.1	9097	1208	5002	849	257	583	70	348	61	144
AWAG_1A-13.2	14658	1931	8032	1361	414	907	110	560	98	232
AWAG_1A-14.1	23271	3240	14266	2652	538	1779	215	1056	180	415
AWAG_1A-14.2	14525	2037	9024	1657	373	1177	146	708	126	294
AWAG_1B-1.1	1561	167	687	124	23	98	12	64	11	28
AWAG_1B-1.2	2404	265	1082	191	38	149	18	87	16	41
AWAG_1B-2.1	1513	139	547	96	17	68	8	42	8	21
AWAG_1B-2.2	6618	604	2180	306	40	228	26	125	23	56
AWAG_1B-3.1	8026	838	3116	427	85	301	33	156	30	75
AWAG_1B-3.2	13626	1954	9190	1794	346	1314	162	815	147	359
AWAG_1B-4.1	12274	1809	8524	1709	319	1298	159	805	141	345
AWAG_1B-4.2	1617	152	609	101	19	75	9	47	9	24
AWAG_1B-5.1	5581	816	4061	875	113	617	73	351	54	113
AWAG_1B-5.2	15574	2102	9013	1530	378	1025	125	631	115	283
AWAG_1B-6.1	11405	1518	6717	1220	234	888	105	521	93	216
AWAG_1B-6.2	1591	156	577	91	18	72	8	43	8	21
AWAG_1B-7.1	16928	1819	6945	961	165	643	69	327	58	138

Table F1 (continued) Sphene SHRIMP trace element data for samples

	Ce ppm	Pr ppm	Nd ppm	Sm ppm	Eu ppm	Gd ppm	Tb ppm	Dy ppm	Ho ppm	Er ppm
AWAG_1B-7.2	8580	949	3761	523	93	356	39	186	34	77
AWAG_1B-8.1	10581	1496	6849	1293	240	998	118	601	105	250
AWAG_1B-8.2	14304	1855	8234	1462	262	1084	128	615	108	251
AWAG_1B-9.1	16031	2403	11388	2184	423	1585	199	980	175	412
AWAG_1B-9.2	11080	1331	5513	916	139	663	75	353	64	149
AWAG_1B-9.3	1489	144	592	100	20	75	9	45	9	24
AWAG_1B-10.1	15934	2259	10610	2100	389	1561	192	941	172	414
AWAG_1B-10.2	4473	480	1960	321	69	241	28	137	24	59
AWAG_1B-11.1	10477	1330	5685	949	215	637	75	359	62	142
AWAG_1B-11.2	18696	2272	9314	1466	341	988	113	542	93	219
AWAG_1B-12.1	5350	576	2331	383	73	263	30	152	28	69
AWAG_1B-12.2	12477	1699	7496	1399	361	1024	126	636	115	278
AWAG_1B-13.1	11376	1492	6509	1146	295	868	102	502	87	209
AWAG_1B-13.2	9041	1187	5165	925	231	667	81	393	70	165
AWAG_1B-13.3	16810	2075	8716	1492	385	1097	134	649	114	270
AWAG_1B-13.4	7805	849	3266	457	104	324	36	173	31	76
AWAG_2-1.1	15753	1680	5865	829	125	626	80	434	88	255
AWAG_2-1.2	22222	3265	15255	3209	361	2474	315	1567	271	617
AWAG_2-2.1	11818	1316	4916	770	107	600	75	420	89	247
AWAG_2-2.2	15704	2026	8579	1653	183	1354	181	971	192	490
AWAG_2-3.1	23084	3338	15274	3270	330	2485	319	1595	274	610
AWAG_2-3.2	11663	1302	4845	722	101	576	74	401	83	236
AWAG_2-4.1	18748	2790	12862	2980	291	2391	320	1670	291	645
AWAG_2-4.2	10850	1189	4285	637	92	481	61	333	70	204

Table F1 (continued) Sphene SHRIMP trace element data for samples

	Ce ppm	Pr ppm	Nd ppm	Sm ppm	Eu ppm	Gd ppm	Tb ppm	Dy ppm	Ho ppm	Er ppm
AWAG_2-5.1	17285	2441	11033	2402	262	2010	274	1448	266	637
AWAG_2-5.2	10202	995	3321	438	72	340	43	236	51	157
AWAG_2-6.1	19165	2610	11690	2408	244	1953	265	1390	253	610
AWAG_2-6.2	7587	684	2097	272	36	199	26	142	32	93
AWAG_2-7.1	17165	2197	9018	1638	188	1295	176	957	186	472
AWAG_2-7.2	17096	1624	5640	761	73	502	58	291	58	153
AWAG_2-8.1	13671	2161	10661	2601	254	2278	309	1649	298	690
AWAG_2-8.2	12643	1388	4958	729	103	527	67	373	76	220
AWAG_2-9.1	23804	3587	17034	3651	372	2721	351	1753	306	694
AWAG_2-9.2	11677	1364	5230	844	111	651	84	474	97	263
AWAG_2-10.1	13606	1590	5860	906	228	652	90	483	98	273
AWAG_2-10.2	11906	1159	3928	536	77	419	51	278	56	161
AWAG_2-11.1	12282	1780	8212	1828	186	1558	216	1163	215	534
AWAG_2-11.2	16141	2469	11908	2721	280	2161	283	1441	252	582
AWAG_2-12.1	22375	3401	16025	3329	395	2517	323	1619	279	640
AWAG_2-12.2	9652	949	3209	439	65	332	42	236	50	149
AWAG_2-13.1	16035	2337	11053	2511	225	2145	289	1534	279	679
AWAG_2-13.2	10764	1020	3326	429	67	336	41	236	51	154
AWAG_2-14.1	18549	2427	10193	1968	198	1503	200	1049	187	455
AWAG_2-14.2	10896	1001	3222	452	59	346	40	218	45	128
AWAG3-1.1	16644	2516	11815	2707	269	2232	308	1620	293	677
AWAG3-1.2	13992	1602	6258	1111	146	921	122	647	125	324
AWAG3-2.1	17766	2239	9035	1556	239	1189	157	837	161	415
AWAG3-2.2	11900	1444	5871	1021	156	806	109	593	118	317

Table F1 (continued) Sphene SHRIMP trace element data for samples

	Ce ppm	Pr ppm	Nd ppm	Sm ppm	Eu ppm	Gd ppm	Tb ppm	Dy ppm	Ho ppm	Er ppm
AWAG3-3.1	15755	1857	7120	1196	148	924	120	660	131	360
AWAG3-3.2	11242	1744	8311	1982	210	1772	247	1331	242	573
AWAG3-4.1	15639	1900	7623	1235	181	947	123	647	122	317
AWAG3-4.2	11025	1319	5297	891	160	679	88	463	91	242
AWAG3-5.1	13829	1594	6004	956	125	747	99	541	109	306
AWAG3-5.2	12281	1509	6012	1043	132	822	111	595	115	298
AWAG3-6.1	13860	1887	8236	1588	184	1276	171	912	171	431
AWAG3-6.2	11595	1394	5412	942	115	747	100	535	108	295
AWAG3-7.1	18716	2740	12863	2703	334	2097	275	1410	250	573
AWAG3-7.2	14976	1638	6522	1176	205	886	115	606	113	274
AWAG3-7.3	9132	1323	5990	1226	117	1037	142	792	153	392
AWAG3-8.1	15565	2427	12017	2993	285	2553	356	1873	329	763
AWAG3-8.2	12488	1532	6033	1030	125	809	109	600	117	323
AWAG3-9.1	17579	2791	13814	3392	318	2883	400	2053	354	815
AWAG3-9.2	12565	1713	7694	1625	181	1400	197	1049	191	473
AWAG3-10.1	13316	1713	6698	1143	79	896	123	727	157	453
AWAG3-10.2	13069	1897	8765	1846	239	1524	208	1107	205	496
AWAG3-11.1	12961	1889	9067	2000	178	1717	220	1138	197	460
AWAG3-11.2	11162	1777	9012	2202	203	1813	240	1204	202	452
AWAG3-12.1	18762	2924	14252	3473	308	2966	411	2160	383	860
AWAG3-12.2	13477	1822	7696	1465	165	1177	158	862	164	421
AWAG3-13.1	17726	2275	9707	1784	296	1460	186	975	179	442
AWAG3-13.2	11547	1606	7274	1490	220	1227	158	832	155	382

Table F1 (continued) Sphene SHRIMP trace element data for samples

	Ce ppm	Pr ppm	Nd ppm	Sm ppm	Eu ppm	Gd ppm	Tb ppm	Dy ppm	Ho ppm	Er ppm
AWAG4-1.1	14870	1401	5101	816	119	654	83	442	86	218
AWAG4-1.2	6950	599	2102	321	53	247	33	168	33	87
AWAG4-2.1	17873	1659	5905	897	124	682	86	429	84	212
AWAG4-2.2	6498	641	2311	357	56	290	36	183	35	91
AWAG4-3.1	14392	1386	5095	800	115	630	79	423	81	210
AWAG4-3.2	6669	629	2298	344	51	281	34	183	34	86
AWAG4-4.1	16414	1521	5457	835	112	654	78	416	78	198
AWAG4-4.2	8238	783	2841	437	62	336	42	215	41	104
AWAG4-5.1	8063	767	2839	437	72	374	47	255	50	127
AWAG4-5.2	16267	1490	5172	767	112	585	72	371	71	183
AWAG4-6.1	11910	1678	7668	1595	262	1283	170	874	161	382
AWAG4-6.2	9334	1059	4250	770	106	624	79	416	81	202
AWAG4-7.1	13559	1279	4713	724	103	564	68	357	71	172
AWAG4-7.2	7023	675	2475	396	56	319	41	215	41	107
AWAG4-8.1	15018	2124	9548	1943	315	1535	204	1060	189	456
AWAG4-8.2	17381	2420	11029	2269	346	1801	236	1231	223	521
AWAG4-8.3	12764	1496	6087	1101	166	873	118	602	113	299
AWAG4-9.1	16987	1796	7012	1239	156	1006	126	662	126	326
AWAG4-9.2	7604	839	3362	604	82	510	66	342	66	162
AWAG4-10.1	19676	2762	12410	2469	388	1932	254	1281	226	535
AWAG4-10.2	15045	2157	9983	2116	328	1636	214	1096	198	476
AWAG4-11.1	19713	2693	11992	2384	386	1819	237	1199	214	503
AWAG4-11.2	13996	1977	9085	1915	306	1523	200	1029	185	438

Table F1 (continued) Sphene SHRIMP trace element data for samples

	Ce ppm	Pr ppm	Nd ppm	Sm ppm	Eu ppm	Gd ppm	Tb ppm	Dy ppm	Ho ppm	Er ppm
AWAG4-12.1	9143	965	3692	638	93	509	64	340	65	164
AWAG4-12.2	10154	1017	3854	637	94	518	66	345	70	173
AWAG4-13.1	7712	751	2724	419	59	323	40	204	40	99
AWAG4-13.2	7950	768	2812	451	62	348	43	220	42	109
AWAG5-1.1	18543	2815	13706	3156	439	2554	341	1758	305	690
AWAG5-1.2	14507	1939	8030	1405	237	1111	149	835	166	429
AWAG5-2.1	13817	2163	10743	2588	358	2180	299	1560	273	627
AWAG5-2.2	15273	2050	8805	1605	257	1260	169	943	187	482
AWAG5-3.1	14664	2227	11026	2640	352	2180	295	1522	268	608
AWAG5-3.2	13929	1893	8448	1663	260	1335	177	918	174	443
AWAG5-4.1	19814	2688	11808	2310	363	1753	232	1260	235	579
AWAG5-4.2	10734	987	3314	419	43	308	37	199	40	122
AWAG5-5.1	21511	3185	14875	3264	473	2510	333	1704	304	692
AWAG5-5.2	15395	2320	11309	2535	386	2033	275	1434	258	610
AWAG5-6.1	15822	2054	8570	1572	249	1242	175	972	193	504
AWAG5-6.2	12065	1275	4898	809	97	614	84	454	90	224
AWAG5-7.1	19428	2764	12779	2710	396	2124	280	1431	254	585
AWAG5-7.2	14256	1915	8200	1493	242	1194	162	909	178	464
AWAG5-8.1	16832	2439	11372	2425	352	1960	260	1327	243	579
AWAG5-8.2	12387	1574	6475	1141	184	923	119	655	130	341
AWAG5-9.1	14224	1909	8241	1526	232	1205	169	929	182	463
AWAG5-9.2	18466	2320	9422	1591	236	1137	149	790	152	377
AWAG5-10.1	18814	2458	10357	1916	286	1419	184	981	179	447

Table F1 (continued) Sphene SHRIMP trace element data for samples

	Ce ppm	Pr ppm	Nd ppm	Sm ppm	Eu ppm	Gd ppm	Tb ppm	Dy ppm	Ho ppm	Er ppm
AWAG5-10.2	13140	1778	7589	1411	209	1153	156	858	164	429
AWAG5-11.1	19160	2578	11269	2169	321	1739	227	1197	221	541
AWAG5-11.2	12408	1696	7526	1456	216	1219	161	858	161	406
AWAG5-12.1	16345	2464	11945	2743	378	2187	294	1511	265	606
AWAG5-12.2	15363	2101	9168	1723	261	1371	190	1040	205	518
AWAG5-13.1	21128	2841	12768	2535	360	1992	252	1268	228	549
AWAG5-13.2	13810	1865	8014	1510	213	1267	173	941	184	461
AWAG5-14.1	20327	2874	13309	2866	406	2225	293	1495	266	612
AWAG5-14.2	14112	1864	7933	1433	229	1141	156	868	171	445
AWAG6-1.1	19236	2656	11459	2404	205	1971	277	1519	279	663
AWAG6-1.2	12448	1620	6437	1253	120	1059	157	913	186	492
AWAG6-1.3	16576	2671	13470	3397	300	2906	406	2138	374	852
AWAG6-1.4	14036	1848	7701	1422	160	1129	155	834	165	433
AWAG6-2.1	12531	1606	6338	1120	115	869	121	689	138	382
AWAG6-2.2	15472	2319	10968	2424	299	1949	255	1323	236	557
AWAG6-2.3	10707	1181	4158	635	41	468	59	327	72	238
AWAG6-3.1	13716	1639	6190	1035	129	776	104	570	116	317
AWAG6-3.2	18836	2337	9425	1623	201	1184	152	784	148	374
AWAG6-4.1	28489	4140	18803	3494	357	2238	261	1227	203	461
AWAG6-4.2	13336	1561	5939	948	125	705	92	493	99	270
AWAG6-5.1	11757	1798	8160	1798	107	1386	197	1063	196	493
AWAG6-5.2	14813	1798	7137	1222	153	906	120	644	126	332
AWAG6-6.1	15681	2490	12602	3162	285	2634	362	1879	332	745
AWAG6-6.2	13988	1614	6053	956	109	679	88	481	97	279

Table F1 (continued) Sphene SHRIMP trace element data for samples

	Ce ppm	Pr ppm	Nd ppm	Sm ppm	Eu ppm	Gd ppm	Tb ppm	Dy ppm	Ho ppm	Er ppm
AWAG6-7.1	18185	2600	11856	2473	258	1890	251	1321	238	558
AWAG6-7.2	14480	1738	6746	1138	137	892	120	661	129	344
AWAG6-8.1	25077	3073	12507	1965	256	1240	137	623	105	239
AWAG6-8.2	13058	1239	4019	532	63	367	48	258	54	160
AWAG6-9.1	23520	3342	15133	3052	305	2231	282	1422	247	570
AWAG6-9.2	14802	1765	6812	1132	138	859	110	593	114	300
AWAG6-10.1	21198	3055	14187	2922	330	2108	261	1256	214	481
AWAG6-10.2	17243	1864	6713	974	119	690	88	471	92	251
AWAG6-11.1	22174	3438	17198	4197	384	3354	459	2331	402	872
AWAG6-11.2	14181	1697	6494	1084	136	834	111	592	119	314
AWAG6-12.1	22097	3206	14654	3027	291	2280	295	1512	262	621
AWAG6-12.2	16335	2137	8644	1504	152	1155	157	833	163	422
AWAG6-13.1	18331	2740	12860	2894	273	2366	323	1687	306	717
AWAG6-13.2	13701	1729	6934	1235	134	950	130	739	147	391
AWAG7-1.1	15363	1894	7679	1363	161	1001	133	722	139	362
AWAG7-1.2	12006	1507	6206	1107	142	876	113	605	116	302
AWAG7-2.1	17609	2447	10884	2088	252	1547	200	1025	183	445
AWAG7-3.1	17416	2449	11018	2270	257	1685	222	1139	207	500
AWAG7-3.2	12817	1617	6628	1197	142	914	118	635	122	311
AWAG7-4.1	19750	2958	14136	3152	325	2400	303	1511	256	564
AWAG7-4.2	14356	1796	7352	1253	164	970	121	649	122	302
AWAG7-5.1	15253	2214	10072	2134	205	1748	244	1313	244	590
AWAG7-5.2	12541	1460	5427	866	87	688	92	535	113	326

Table F1 (continued) Sphene SHRIMP trace element data for samples

	Ce ppm	Pr ppm	Nd ppm	Sm ppm	Eu ppm	Gd ppm	Tb ppm	Dy ppm	Ho ppm	Er ppm
AWAG7-6.1	10493	1364	5414	936	70	758	109	640	141	405
AWAG7-6.2	16852	1748	5492	738	28	613	92	604	151	512
AWAG7-6.3	1094	128	513	87	67	70	8	48	10	31
AWAG7-7.1	18915	2339	9445	1543	221	1042	122	577	102	244
AWAG7-7.2	13290	1546	5891	945	118	708	91	498	101	284
AWAG7-9.1	15481	1802	7303	1244	165	1000	121	608	117	280
AWAG7-9.2	10445	1336	5920	1161	152	1023	129	656	123	299
AWAG7-8.1	13800	2201	11067	2804	249	2338	327	1705	295	682
AWAG7-8.2	13171	1651	6612	1197	123	956	134	767	156	431
AWAG7-10.1	20405	2683	11415	2080	355	1573	200	1026	191	467
AWAG7-10.2	12972	1624	6766	1186	230	916	119	633	120	314
AWAG7-11.1	18373	2414	10052	1843	198	1407	190	1009	191	480
AWAG7-11.2	16419	2271	9926	1989	207	1578	215	1158	220	549
AWAG7-11.3	13680	1732	7009	1280	143	1005	134	748	148	391
AWA67-12.1	12014	1076	3038	398	21	275	39	252	64	230
AWA67-12.2	4659	551	2021	330	60	260	34	202	45	142
AWAG7-13.1	11783	1435	5648	975	113	784	105	588	119	322
AWAG7-13.2	15825	2113	8601	1591	163	1307	183	1005	198	532
AWAG7-13.3	15040	2393	11961	2949	267	2430	336	1739	300	686
AWAG7-14.1	12767	1506	5656	942	113	721	98	546	113	317
AWAG7-14.2	15881	2009	7937	1437	139	1130	156	880	177	476
AWA67-15.1	15351	2534	13230	3525	293	2983	418	2175	372	811
AWA67-15.2	13716	2144	10639	2536	245	2040	280	1458	257	582

Table F1 (continued) Sphene SHRIMP trace element data for samples

	Yb ppm	Lu ppm	Hf ppm	Ta ppm	Pb206 ppm	Pb208 ppm	Th ppm	U ppm
AWM1.1	97	13	232	104	0	0.0	264	22
AWM1-2.1	212	24	254	207	0	0.0	446	48
AWM1-2.2	37	5	29	18	0	0.0	567	335
AWM1-3.1	129	16	443	199	1	0.0	241	22
AWM1-3.2	119	13	73	121	0	0.0	505	54
AWM1-4.1	113	14	191	116	0	0.0	310	24
AWM1-4.2	30	5	13	7	0	0.0	338	188
AWM1-5.1	80	10	287	116	0	0.0	150	13
AWM1-5.2	99	12	190	107	0	0.0	554	50
AWM1-6.1	84	10	259	153	1	0.0	333	22
AWM1-6.2	104	11	65	105	0	0.0	451	48
AWM1-7.1	80	10	25	16	0	0.0	484	209
AWM1-7.2	112	14	344	157	0	0.0	164	12
AWM1-8.1	131	16	349	201	0	0.0	272	21
AWM1-8.2	41	7	115	76	1	0.0	594	336
AWM1-9.1	134	15	221	145	0	0.0	340	34
AWM1-9.2	30	5	17	11	0	0.0	367	114
AWM1-10.1	107	14	237	61	0	0.0	192	13
AWM1-10.2	154	19	40	115	0	0.0	348	149
AWM1-11.1	105	13	202	96	0	0.0	153	15
AWM1-11.2	92	11	37	75	0	0.0	505	57
AWM1-12.1	85	11	380	75	0	0.0	289	31
AWM1-12.2	19	3	3	9	0	0.0	47	9
AWM1-13.1	105	14	325	114	0	0.0	322	21

Table F1 (continued) Sphene SHRIMP trace element data for samples

	Yb ppm	Lu ppm	Hf ppm	Ta ppm	Pb206 ppm	Pb208 ppm	Th ppm	U ppm
AWM1-13.2	46	7	21	12	1	0.0	563	244
AWM1-14.1	73	10	174	52	0	0.0	194	15
AWM1-14.2	56	8	15	10	0	0.0	283	158
AMW2-1.1	202	22	469	1257	0	0.0	933	86
AMW2-1.2	37	5	62	57	1	0.0	615	313
AMW2-2.1	90	12	24	56	0	0.0	584	40
AMW2-2.2	33	5	33	17	0	0.0	339	98
AWM2-3.1	288	31	92	805	1	0.0	1369	119
AWM2-3.2	122	15	130	581	0	0.0	756	86
AWM2-4.1	48	8	67	20	1	0.0	378	224
AWM2-4.2	99	14	785	880	1	0.0	1949	268
AWM2-5.1	158	22	64	343	1	0.0	1470	155
AWM2-5.2	109	15	252	275	0	0.0	609	63
AWM2-6.1	127	16	38	150	0	0.0	782	72
AWM2-6.2	265	28	86	735	0	0.0	1186	100
AWM2-7.1	190	24	90	1067	1	0.0	1998	218
AWM2-7.2	92	12	119	137	0	0.0	606	57
AWM2-8.1	15	2	13	8	0	0.0	203	15
AWM2-8.2	44	7	10	62	1	0.0	1828	923
AWM2-9.1	126	17	36	229	0	0.0	1098	119
AWM2-9.2	106	14	98	264	1	0.0	792	101
AWM2-9.3	19	3	6	13	0	0.0	198	18
AWM2-10.1	192	21	421	1173	0	0.0	660	88
AWM2-10.2	137	16	45	231	0	0.0	554	59

Table F1 (continued) Sphene SHRIMP trace element data for samples

	Yb ppm	Lu ppm	Hf ppm	Ta ppm	Pb206 ppm	Pb208 ppm	Th ppm	U ppm
AWM2-11.1	31	5	43	18	0	0.0	253	28
AWM2-11.2	42	6	9	48	1	0.0	1565	653
AWM2-12.1	140	17	261	410	1	0.0	596	81
AWM2-12.2	152	19	540	1486	1	0.0	1017	175
AWAG_1A-1.1	288	31	188	313	0	0.0	607	62
AWAG_1A-1.2	271	31	226	118	0	0.0	337	34
AWAG_1A-2.1	205	21	549	353	0	0.0	342	26
AWAG_1A-2.2	114	12	209	79	0	0.0	179	18
AWAG_1A-3.1	245	29	81	542	0	0.0	907	68
AWAG_1A-3.2	155	22	44	139	0	0.0	565	46
AWAG_1A-4.1	24	4	5	11	0	0.0	201	41
AWAG_1A-4.2	206	20	143	119	0	0.0	203	18
AWAG_1A-4.3	299	32	249	137	0	0.0	196	17
AWAG_1A-5.1	221	22	165	140	0	0.0	181	14
AWAG_1A-5.2	350	39	441	295	0	0.0	366	27
AWAG_1A-6.1	232	24	263	318	0	0.0	540	45
AWAG_1A-6.2	48	8	145	31	1	0.0	319	163
AWAG_1A-7.1	176	18	70	138	0	0.0	363	31
AWAG_1A-7.2	187	18	75	154	0	0.0	327	26
AWAG_1A-8.1	25	4	37	11	0	0.0	316	83
AWAG_1A-8.2	47	7	31	39	0	0.0	633	208
AWAG_1A-9.1	132	12	268	109	0	0.0	163	13
AWAG_1A-9.2	152	15	383	301	0	0.0	266	20
AWAG_1A-10.1	103	11	152	45	0	0.0	100	9

Table F1 (continued) Sphene SHRIMP trace element data for samples

	Yb ppm	Lu ppm	Hf ppm	Ta ppm	Pb206 ppm	Pb208 ppm	Th ppm	U ppm
AWAG_1A-10.2	151	15	65	130	0	0.0	352	30
AWAG_1A-11.1	199	23	53	65	0	0.0	446	40
AWAG_1A-11.2	211	23	52	146	0	0.0	617	75
AWAG_1A-12.1	104	14	193	128	1	0.0	393	291
AWAG_1A-12.2	171	25	69	236	2	0.0	1393	739
AWAG_1A-13.1	94	9	139	53	0	0.0	135	13
AWAG_1A-13.2	158	17	72	85	0	0.0	310	28
AWAG_1A-14.1	266	26	150	280	1	0.0	355	28
AWAG_1A-14.2	192	22	92	93	0	0.0	213	14
AWAG_1B-1.1	22	4	25	4	0	0.0	108	14
AWAG_1B-1.2	31	5	25	11	0	0.0	64	10
AWAG_1B-2.1	18	3	60	9	0	0.0	231	34
AWAG_1B-2.2	47	6	209	52	1	0.0	1175	139
AWAG_1B-3.1	55	6	57	45	0	0.0	203	18
AWAG_1B-3.2	241	27	377	174	0	0.0	218	21
AWAG_1B-4.1	239	26	336	146	0	0.0	165	17
AWAG_1B-4.2	23	4	33	6	0	0.0	268	36
AWAG_1B-5.1	58	5	148	102	0	0.0	41	14
AWAG_1B-5.2	197	22	247	165	1	0.0	206	19
AWAG_1B-6.1	140	15	239	102	0	0.0	183	17
AWAG_1B-6.2	21	3	59	12	0	0.0	251	33
AWAG_1B-7.1	101	12	129	196	0	0.0	538	48
AWAG_1B-7.2	57	7	92	55	0	0.0	157	12
AWAG_1B-8.1	159	17	236	98	0	0.0	149	15

Table F1 (continued) Sphene SHRIMP trace element data for samples

	Yb ppm	Lu ppm	Hf ppm	Ta ppm	Pb206 ppm	Pb208 ppm	Th ppm	U ppm
AWAG_1B-8.2	156	15	429	294	0	0.0	265	21
AWAG_1B-9.1	268	30	205	101	0	0.0	151	13
AWAG_1B-9.2	90	10	84	71	0	0.0	194	16
AWAG_1B-9.3	21	3	43	10	0	0.0	229	22
AWAG_1B-10.1	267	27	307	247	0	0.0	269	22
AWAG_1B-10.2	44	7	38	27	1	0.0	251	33
AWAG_1B-11.1	94	10	157	76	0	0.0	140	14
AWAG_1B-11.2	139	14	97	178	0	0.0	411	45
AWAG_1B-12.1	53	7	33	41	0	0.0	243	30
AWAG_1B-12.2	191	21	530	95	0	0.0	165	14
AWAG_1B-13.1	128	15	307	180	0	0.0	192	16
AWAG_1B-13.2	100	11	198	89	1	0.0	124	11
AWAG_1B-13.3	162	17	146	156	1	0.0	363	35
AWAG_1B-13.4	51	7	47	32	0	0.0	179	16
AWAG_2-1.1	237	29	50	278	0	0.0	708	51
AWAG_2-1.2	357	36	84	406	0	0.0	461	33
AWAG_2-2.1	235	27	41	195	0	0.0	454	45
AWAG_2-2.2	339	37	94	508	0	0.0	560	40
AWAG_2-3.1	339	32	79	348	0	0.0	500	33
AWAG_2-3.2	227	26	44	209	0	0.0	456	43
AWAG_2-4.1	359	35	100	417	1	0.0	530	38
AWAG_2-4.2	196	25	34	176	0	0.0	438	43
AWAG_2-5.1	402	43	127	567	0	0.0	542	40
AWAG_2-5.2	169	22	41	165	0	0.0	554	48

Table F1 (continued) Sphene SHRIMP trace element data for samples

	Yb ppm	Lu ppm	Hf ppm	Ta ppm	Pb206 ppm	Pb208 ppm	Th ppm	U ppm
AWAG_2-6.1	369	38	81	503	0	0.0	577	41
AWAG_2-6.2	103	15	66	196	0	0.0	419	43
AWAG_2-7.1	340	38	63	612	0	0.0	632	47
AWAG_2-7.2	160	22	85	261	1	0.0	661	329
AWAG_2-8.1	414	42	210	274	0	0.0	314	32
AWAG_2-8.2	209	25	40	247	0	0.0	503	40
AWAG_2-9.1	406	40	62	330	0	0.0	480	29
AWAG_2-9.2	236	27	42	219	0	0.0	387	39
AWAG_2-10.1	229	26	41	108	1	0.0	536	72
AWAG_2-10.2	175	26	49	89	1	0.0	411	268
AWAG_2-11.1	328	35	74	317	0	0.0	346	32
AWAG_2-11.2	336	34	56	167	0	0.0	314	28
AWAG_2-12.1	370	36	67	259	0	0.0	441	30
AWAG_2-12.2	160	21	53	190	0	0.0	427	42
AWAG_2-13.1	410	43	78	397	0	0.0	505	40
AWAG_2-13.2	166	25	70	234	0	0.0	487	47
AWAG_2-14.1	290	30	59	441	0	0.0	530	38
AWAG_2-14.2	140	21	43	115	0	0.0	653	59
AWAG3-1.1	407	41	89	352	0	0.0	328	29
AWAG3-1.2	262	31	59	268	0	0.0	530	44
AWAG3-2.1	302	33	131	500	0	0.0	490	36
AWAG3-2.2	259	31	44	221	0	0.0	381	41
AWAG3-2.2	258	30	44	224	0	0.0	363	36
AWAG3-3.1	300	37	44	250	0	0.0	618	56

Table F1 (continued) Sphene SHRIMP trace element data for samples

	Yb ppm	Lu ppm	Hf ppm	Ta ppm	Pb206 ppm	Pb208 ppm	Th ppm	U ppm
AWAG3-3.2	374	38	38	250	0	0.0	316	34
AWAG3-4.1	235	26	114	322	0	0.0	353	23
AWAG3-4.2	200	24	65	139	0	0.0	244	23
AWAG3-5.1	276	34	37	271	0	0.0	510	52
AWAG3-5.2	243	30	40	225	0	0.0	444	43
AWAG3-6.1	291	32	51	245	0	0.0	363	34
AWAG3-6.2	248	31	31	208	0	0.0	443	46
AWAG3-7.1	336	35	208	511	0	0.0	357	26
AWAG3-7.2	227	29	46	234	0	0.0	723	51
AWAG3-7.3	285	31	40	325	0	0.0	344	33
AWAG3-8.1	436	44	54	234	0	0.0	384	33
AWAG3-8.2	267	31	36	196	0	0.0	419	39
AWAG3-9.1	469	47	59	310	0	0.0	438	41
AWAG3-9.2	326	34	37	198	0	0.0	406	41
AWAG3-10.1	464	55	79	1410	1	0.0	742	104
AWAG3-10.2	320	36	160	289	0	0.0	363	21
AWAG3-11.1	280	28	39	151	0	0.0	229	23
AWAG3-11.2	260	26	39	147	0	0.0	184	18
AWAG3-12.1	452	46	63	512	0	0.0	578	36
AWAG3-12.2	312	34	37	220	0	0.0	411	40
AWAG3-13.1	301	34	83	546	0	0.0	561	28
AWAG3-13.2	255	28	40	165	0	0.0	256	17
AWAG4-1.1	191	28	20	58	0	0.0	846	186
AWAG4-1.2	74	12	21	28	0	0.0	280	47

Table F1 (continued) Sphene SHRIMP trace element data for samples

	Yb ppm	Lu ppm	Hf ppm	Ta ppm	Pb206 ppm	Pb208 ppm	Th ppm	U ppm
AWAG4-2.1	177	25	40	93	1	0.0	959	300
AWAG4-2.2	73	11	56	32	0	0.0	155	27
AWAG4-3.1	182	26	29	50	0	0.0	771	177
AWAG4-3.2	71	10	28	28	0	0.0	170	28
AWAG4-4.1	164	23	50	109	1	0.0	905	254
AWAG4-4.2	94	13	21	18	0	0.0	259	51
AWAG4-5.1	117	16	23	26	0	0.0	327	53
AWAG4-5.2	151	21	40	144	1	0.0	920	288
AWAG4-6.1	249	25	37	178	0	0.0	234	17
AWAG4-6.2	171	22	23	39	0	0.0	344	107
AWAG4-7.1	148	22	245	192	0	0.0	595	88
AWAG4-7.2	96	13	19	16	0	0.0	292	38
AWAG4-8.1	298	29	38	232	0	0.0	333	19
AWAG4-8.2	322	33	98	582	0	0.0	423	22
AWAG4-8.3	235	30	35	97	0	0.0	397	133
AWAG4-9.1	270	36	55	164	1	0.0	931	405
AWAG4-9.2	126	17	42	63	0	0.0	199	55
AWAG4-10.1	328	33	81	624	0	0.0	473	27
AWAG4-10.2	292	30	49	200	0	0.0	284	20
AWAG4-11.1	310	31	66	530	0	0.0	469	22
AWAG4-11.2	266	27	47	211	0	0.0	290	19
AWAG4-12.1	143	19	53	53	0	0.0	284	74
AWAG4-12.2	153	22	38	40	0	0.0	441	81
AWAG4-13.1	89	12	34	30	0	0.0	218	42

Table F1 (continued) Sphene SHRIMP trace element data for samples

	Yb ppm	Lu ppm	Hf ppm	Ta ppm	Pb206 ppm	Pb208 ppm	Th ppm	U ppm
AWAG4-13.2	94	13	83	46	0	0.0	235	40
AWAG5-1.1	381	40	57	406	0	0.0	389	21
AWAG5-1.2	316	36	45	184	0	0.0	358	25
AWAG5-2.1	349	37	47	213	0	0.0	266	20
AWAG5-2.2	345	37	51	193	0	0.0	361	23
AWAG5-3.1	362	36	66	331	0	0.0	294	19
AWAG5-3.2	327	37	48	244	0	0.0	308	25
AWAG5-4.1	387	40	50	544	0	0.0	471	27
AWAG5-4.2	149	23	167	237	1	0.0	692	286
AWAG5-5.1	405	42	96	715	0	0.0	532	29
AWAG5-5.2	369	39	53	186	0	0.0	309	23
AWAG5-6.1	380	41	84	508	0	0.0	575	35
AWAG5-6.2	187	22	48	185	1	0.0	547	163
AWAG5-7.1	353	36	57	528	0	0.0	468	24
AWAG5-7.2	351	39	42	242	0	0.0	342	26
AWAG5-8.1	356	39	52	308	0	0.0	370	25
AWAG5-8.2	266	31	40	146	0	0.0	342	24
AWAG5-9.1	346	39	46	181	0	0.0	350	24
AWAG5-9.2	256	28	43	399	0	0.0	400	20
AWAG5-10.1	296	29	50	405	0	0.0	399	23
AWAG5-10.2	322	35	42	209	0	0.0	333	26
AWAG5-11.1	367	40	56	522	0	0.0	532	26
AWAG5-11.2	308	33	46	206	0	0.0	296	26
AWAG5-12.1	340	34	68	463	0	0.0	357	20

Table F1 (continued) Sphene SHRIMP trace element data for samples

	Yb ppm	Lu ppm	Hf ppm	Ta ppm	Pb206 ppm	Pb208 ppm	Th ppm	U ppm
AWAG5-12.2	362	40	50	214	0	0.0	366	27
AWAG5-13.1	352	35	69	609	0	0.0	458	23
AWAG5-13.2	341	39	41	185	0	0.0	354	24
AWAG5-14.1	373	40	58	573	0	0.0	505	28
AWAG5-14.2	338	36	47	236	0	0.0	335	25
AWAG6-1.1	418	43	60	487	0	0.0	477	31
AWAG6-1.2	385	42	44	270	0	0.0	394	38
AWAG6-1.3	468	45	49	302	0	0.0	416	38
AWAG6-1.4	319	35	44	233	0	0.0	440	41
AWAG6-2.1	297	33	39	261	1	0.0	425	42
AWAG6-2.2	334	35	54	212	0	0.0	289	24
AWAG6-2.3	377	64	51	407	1	0.0	245	210
AWAG6-3.1	253	31	39	267	0	0.0	439	42
AWAG6-3.2	273	32	56	464	0	0.0	595	48
AWAG6-4.1	279	29	137	199	0	0.0	409	47
AWAG6-4.2	230	28	42	293	0	0.0	566	51
AWAG6-5.1	350	38	209	377	0	0.0	1200	178
AWAG6-5.2	261	31	43	261	0	0.0	501	46
AWAG6-6.1	411	40	44	260	0	0.0	375	34
AWAG6-6.2	245	31	36	209	0	0.0	547	56
AWAG6-7.1	338	37	69	375	0	0.0	449	40
AWAG6-7.2	284	33	39	256	0	0.0	541	48
AWAG6-8.1	154	16	101	324	0	0.0	460	32
AWAG6-8.2	163	22	62	254	0	0.0	639	65

Table F1 (continued) Sphene SHRIMP trace element data for samples

	Yb ppm	Lu ppm	Hf ppm	Ta ppm	Pb206 ppm	Pb208 ppm	Th ppm	U ppm
AWAG6-9.1	337	33	112	478	0	0.0	494	35
AWAG6-9.2	239	27	43	243	0	0.0	491	50
AWAG6-10.1	260	27	184	699	0	0.0	670	52
AWAG6-10.2	214	26	38	410	0	0.0	638	43
AWAG6-11.1	470	44	77	610	0	0.0	593	35
AWAG6-11.2	256	30	40	207	0	0.0	493	45
AWAG6-12.1	357	36	135	503	1	0.0	488	35
AWAG6-12.2	298	32	90	267	0	0.0	419	40
AWAG6-13.1	396	40	61	544	0	0.0	550	34
AWAG6-13.2	321	39	41	270	0	0.0	457	48
AWAG7-1.1	290	32	46	298	0	0.0	506	45
AWAG7-1.2	236	28	41	172	0	0.0	436	43
AWAG7-2.1	280	31	79	237	0	0.0	371	33
AWAG7-3.1	313	31	57	424	0	0.0	477	32
AWAG7-3.2	246	28	38	203	0	0.0	416	40
AWAG7-4.1	330	33	144	588	0	0.0	444	37
AWAG7-4.2	229	26	52	186	0	0.0	439	46
AWAG7-5.1	380	39	49	293	0	0.0	430	36
AWAG7-5.2	330	42	57	355	0	0.0	538	82
AWAG7-6.1	383	46	43	393	0	0.0	369	60
AWAG7-6.2	591	78	121	1282	1	0.0	1090	206
AWAG7-6.3	36	6	10	17	0	0.0	21	26
AWAG7-7.1	167	19	80	336	0	0.0	684	46
AWAG7-7.2	253	32	35	295	0	0.0	535	50

Table F1 (continued) Sphene SHRIMP trace element data for samples

	Yb ppm	Lu ppm	Hf ppm	Ta ppm	Pb206 ppm	Pb208 ppm	Th ppm	U ppm
AWAG7-9.1	196	24	56	264	0	0.0	707	38
AWAG7-9.2	191	23	162	153	0	0.0	319	24
AWAG7-8.1	383	39	41	245	0	0.0	326	28
AWAG7-8.2	345	37	39	198	0	0.0	460	43
AWAG7-10.1	325	35	64	516	0	0.0	527	26
AWAG7-10.2	230	29	45	207	0	0.0	314	23
AWAG7-11.1	325	36	50	489	0	0.0	647	42
AWAG7-11.2	370	42	45	276	0	0.0	484	42
AWAG7-11.3	302	35	46	201	0	0.0	450	44
AWA67-12.1	388	59	101	2043	1	0.0	482	295
AWA67-12.2	186	33	23	91	0	0.0	134	165
AWAG7-13.1	268	32	31	200	0	0.0	418	42
AWAG7-13.2	386	43	48	307	0	0.0	490	46
AWAG7-13.3	370	37	46	252	0	0.0	350	29
AWAG7-14.1	280	33	33	241	0	0.0	474	46
AWAG7-14.2	347	40	44	501	0	0.0	604	43
AWA67-15.1	427	40	46	329	0	0.0	375	32
AWA67-15.2	331	33	42	202	0	0.0	294	28

Table F2 Sphene SHRIMP trace element data for standard BLR

	F ppm	Na ppm	Mg ppm	Si ppm	P ppm	K ppm	Ca ppm	Al ppm	Ti ppm	V ppm
BLR-1.1	22838	1219	712	154769	78	5.2	191810	16451	194598	99.6
BLR-2.1	22900	1524	662	156072	58	2.7	191111	16106	191502	100.6
BLR-3.1	20140	1425	608	139527	72	3.2	194917	16874	205949	102.4
BLR-4.1	22307	1517	639	162099	33	2.4	190192	15455	194641	94.4
BRL-5.1	20350	981	679	136350	66	2.6	203068	17807	206369	105.7
BRL-6.1	20556	1881	412	161591	65	16.6	186314	15707	196651	99.7
BRL-7.1	22280	1067	733	166049	63	7.5	189177	16738	192915	99.2
BRL-8.1	22347	1290	686	166387	82	2.2	189892	16132	194459	96.5
BRL-9.1	17809	1142	646	149888	68	2.1	190531	16234	200660	102.5
BRL-10.1	22739	1473	639	171288	52	2.3	188675	15867	193538	98.2
BRL-11.1	22331	1547	653	107079	80	8.1	188587	16003	191904	102.8
BLR-5.2	24273	1120	747	163384	42	0.7	186932	16550	186857	95.6
BLR-6.2	19854	1376	612	135375	76	1.1	200234	16710	205629	104.4
BLR-7.2	21483	1347	619	149217	80	1.2	192816	15682	197480	99.4
BLR-10.1	18863	1217	630	133100	68	0.8	196063	17133	204336	108.5
BLR-11.1	20386	1378	662	140748	70	0.8	195913	15772	201583	95.0
BLR-12.1	22335	1528	621	150150	56	0.9	192017	14773	197790	91.6
BLR-13.1	24038	1557	640	153345	76	0.8	190869	16059	189898	93.0
BLR-14.1	24667	1670	670	131287	61	1.0	207172	17727	206409	104.2
BLR-15.1	26250	1293	758	138449	50	1.0	193541	16970	186380	99.5
BLR-8.1	22730	1481	640	133319	55	0.9	192402	15981	194325	97.1

Table F2 (continued) Sphene SHRIMP trace element data for standard BLR

	F ppm	Na ppm	Mg ppm	Si ppm	P ppm	K ppm	Ca ppm	Al ppm	Ti ppm	V ppm
BLR-8.2	18309	1221	617	128329	77	0.8	200185	16420	210215	103.3
BLR-9.1	19750	1267	633	148226	76	0.9	198096	16730	204183	103.4
BLR-9.2	20298	1246	642	151406	62	1.1	195116	16703	199540	99.8
BLR-2.1	19548	1396	593	145269	46	0.7	200101	15480	209718	100.1
BLR-5.1	22850	1097	744	125056	63	0.6	203327	17909	201297	112.7
BLR-6.1	24018	1565	656	131979	69	0.9	190205	15850	192655	94.5
BLR-7.1	23283	1535	644	134873	77	0.9	187670	15838	190671	96.2
BLR-2.1	19548	1396	593	133319	46	0.7	200101	15480	209718	100.1
BLR-5.1	22850	1097	744	128329	63	0.6	203327	17909	201297	112.7
BLR-6.1	24018	1565	656	148226	69	0.9	190205	15850	192655	94.5
BLR-7.1	23283	1535	644	151406	77	0.9	187670	15838	190671	96.2
BLR-8.1	22730	1481	640	145269	55	0.9	192402	15981	194325	97.1
BLR-8.2	18309	1221	617	125056	77	0.8	200185	16420	210215	103.3
BLR-9.1	19750	1267	633	131979	76	0.9	198096	16730	204183	103.4
BLR-9.2	20298	1246	642	134873	62	1.1	195116	16703	199540	99.8
BLR-10.1	18863	1217	630	133100	68	0.8	196063	17133	204336	108.5
BLR-11.1	20386	1378	662	140748	70	0.8	195913	15772	201583	95.0
BLR-12.1	22335	1528	621	150150	56	0.9	192017	14773	197790	91.6
BLR-13.1	24038	1557	640	153345	76	0.8	190869	16059	189898	93.0
BLR-14.1	24667	1670	670	131287	61	1.0	207172	17727	206409	104.2
BLR-15.1	26250	1293	758	138449	50	1.0	193541	16970	186380	99.5
BLR-5.2	24273	1120	747	163384	42	0.7	186932	16550	186857	95.6
BLR-6.2	19854	1376	612	135375	76	1.1	200234	16710	205629	104.4

Table F2 (continued) Sphene SHRIMP trace element data for standard BLR

	F ppm	Na ppm	Mg ppm	Si ppm	P ppm	K ppm	Ca ppm	Al ppm	Ti ppm	V ppm
BLR-7.2	21483	1347	619	149217	80	1.2	192816	15682	197480	99.4
BLR-1.1	22838	1219	712	154769	78	5.2	191810	16451	194598	99.6
BLR-2.1	22900	1524	662	156072	58	2.7	191111	16106	191502	100.6
BLR-3.1	20140	1425	608	139527	72	3.2	194917	16874	205949	102.4
BLR-4.1	22307	1517	639	162099	33	2.4	190192	15455	194641	94.4
BRL-5.1	20350	981	679	136350	66	2.6	203068	17807	206369	105.7
BRL-6.1	20556	1881	412	161591	65	16.6	186314	15707	196651	99.7
BRL-7.1	22280	1067	733	166049	63	7.5	189177	16738	192915	99.2
BRL-8.1	22347	1290	686	166387	82	2.2	189892	16132	194459	96.5
BRL-9.1	17809	1142	646	149888	68	2.1	190531	16234	200660	102.5
BRL-10.1	22739	1473	639	171288	52	2.3	188675	15867	193538	98.2
BRL-11.1	22331	1547	653	107079	80	8.1	188587	16003	191904	102.8
BRL-12.1	17255	1172	605	152162	62	1.8	189281	15537	202904	103.0
BRL-13.1	24193	1529	682	174748	54	1.7	184768	15292	188541	94.3

Table F2 (continued) Sphene SHRIMP trace element data for standard BLR

	Cr ppm	Mn ppm	Fe ppm	Sr ppm	Y ppm	Zr90 ppm	Zr91 ppm	Nb ppm	Ba ppm	La ppm
BLR-1.1	105.3	887	17949	53.4	3214	1296	1287	3488	13.8	468
BLR-2.1	106.2	1028	19306	48.0	3396	1325	1331	3489	13.8	344
BLR-3.1	110.5	1091	20065	50.0	3565	1369	1359	3852	15.6	367
BLR-4.1	99.6	987	18733	46.0	3048	1290	1291	3592	13.2	308
BRL-5.1	111.6	930	19964	55.3	3698	1474	1440	3975	16.4	521
BRL-6.1	102.6	986	16481	51.9	3364	1239	1256	3581	14.0	338
BRL-7.1	101.9	835	18539	53.3	3203	1283	1271	3464	13.8	452
BRL-8.1	102.5	912	18424	48.3	3246	1293	1299	3517	13.7	347
BRL-9.1	108.6	1002	19192	53.7	3658	1453	1444	3929	14.5	394
BRL-10.1	103.2	1018	18684	43.7	3239	1275	1253	3499	13.8	331
BRL-11.1	105.6	996	18695	46.6	3346	1324	1346	3574	12.9	338
BLR-5.2	99.6	826	18097	46.7	2963	1211	1202	3286	12.7	409
BLR-6.2	110.4	1101	20580	53.4	3598	1408	1390	3867	15.4	375
BLR-7.2	106.8	1060	19297	49.0	3375	1277	1288	3591	13.9	350
BLR-10.1	110.6	1067	20058	51.7	3748	1473	1495	3828	15.1	391
BLR-11.1	98.1	1053	19759	52.4	3486	1353	1339	3945	14.2	371
BLR-12.1	93.0	1007	18812	49.4	2981	1320	1330	3740	13.4	318
BLR-13.1	102.4	1025	18751	46.2	3267	1230	1217	3403	12.8	333
BLR-14.1	111.7	1125	20564	50.7	3667	1316	1347	3712	14.6	379
BLR-15.1	102.4	883	18402	49.2	3012	1212	1218	3193	11.7	416
BLR-8.1	105.0	1037	19106	46.4	3261	1277	1271	3504	13.7	333
BLR-8.2	109.4	1082	20363	52.9	3726	1445	1469	4019	15.3	390
BLR-9.1	108.5	1073	19979	51.0	3603	1424	1420	3824	14.8	376

Table F2 (continued) Sphene SHRIMP trace element data for standard BLR

	Cr ppm	Mn ppm	Fe ppm	Sr ppm	Y ppm	Zr90 ppm	Zr91 ppm	Nb ppm	Ba ppm	La ppm
BLR-9.2	108.2	1026	19860	51.3	3499	1405	1403	3733	15.2	372
BLR-2.1	99.7	1041	19844	51.9	3260	1454	1416	4156	14.1	354
BLR-5.1	112.2	888	19199	55.9	3380	1362	1365	3731	14.2	479
BLR-6.1	102.4	1018	18682	46.7	3157	1216	1235	3411	12.7	324
BLR-7.1	101.8	1016	18229	45.1	3178	1209	1229	3352	12.5	321
BLR-2.1	99.7	1041	19844	51.9	3260	1454	1416	4156	14.1	354
BLR-5.1	112.2	888	19199	55.9	3380	1362	1365	3731	14.2	479
BLR-6.1	102.4	1018	18682	46.7	3157	1216	1235	3411	12.7	324
BLR-7.1	101.8	1016	18229	45.1	3178	1209	1229	3352	12.5	321
BLR-8.1	105.0	1037	19106	46.4	3261	1277	1271	3504	13.7	333
BLR-8.2	109.4	1082	20363	52.9	3726	1445	1469	4019	15.3	390
BLR-9.1	108.5	1073	19979	51.0	3603	1424	1420	3824	14.8	376
BLR-9.2	108.2	1026	19860	51.3	3499	1405	1403	3733	15.2	372
BLR-10.1	110.6	1067	20058	51.7	3748	1473	1495	3828	15.1	391
BLR-11.1	98.1	1053	19759	52.4	3486	1353	1339	3945	14.2	371
BLR-12.1	93.0	1007	18812	49.4	2981	1320	1330	3740	13.4	318
BLR-13.1	102.4	1025	18751	46.2	3267	1230	1217	3403	12.8	333
BLR-14.1	111.7	1125	20564	50.7	3667	1316	1347	3712	14.6	379
BLR-15.1	102.4	883	18402	49.2	3012	1212	1218	3193	11.7	416
BLR-5.2	99.6	826	18097	46.7	2963	1211	1202	3286	12.7	409
BLR-6.2	110.4	1101	20580	53.4	3598	1408	1390	3867	15.4	375
BLR-7.2	106.8	1060	19297	49.0	3375	1277	1288	3591	13.9	350

Table F2 (continued) Sphene SHRIMP trace element data for standard BLR

	Cr ppm	Mn ppm	Fe ppm	Sr ppm	Y ppm	Zr90 ppm	Zr91 ppm	Nb ppm	Ba ppm	La ppm
BLR-1.1	105.3	887	17949	53.4	3214	1296	1287	3488	13.8	468
BLR-2.1	106.2	1028	19306	48.0	3396	1325	1331	3489	13.8	344
BLR-3.1	110.5	1091	20065	50.0	3565	1369	1359	3852	15.6	367
BLR-4.1	99.6	987	18733	46.0	3048	1290	1291	3592	13.2	308
BRL-5.1	111.6	930	19964	55.3	3698	1474	1440	3975	16.4	521
BRL-6.1	102.6	986	16481	51.9	3364	1239	1256	3581	14.0	338
BRL-7.1	101.9	835	18539	53.3	3203	1283	1271	3464	13.8	452
BRL-8.1	102.5	912	18424	48.3	3246	1293	1299	3517	13.7	347
BRL-9.1	108.6	1002	19192	53.7	3658	1453	1444	3929	14.5	394
BRL-10.1	103.2	1018	18684	43.7	3239	1275	1253	3499	13.8	331
BRL-11.1	105.6	996	18695	46.6	3346	1324	1346	3574	12.9	338
BRL-12.1	106.9	1037	19228	51.5	3611	1463	1442	3951	14.2	373
BRL-13.1	99.9	951	18175	44.9	3080	1220	1210	3313	11.9	314

Table F2 (continued) Sphene SHRIMP trace element data for standard BLR

	Ce ppm	Pr ppm	Nd ppm	Sm ppm	Eu ppm	Gd ppm	Tb ppm	Dy ppm	Ho ppm	Er ppm
BLR-1.1	1966	317	1630	509	74	638	115	765	173	480
BLR-2.1	1525	270	1423	498	71	656	122	820	190	532
BLR-3.1	1646	293	1558	529	79	702	132	890	203	579
BLR-4.1	1413	247	1312	452	68	606	114	767	173	493
BRL-5.1	2225	366	1896	597	84	742	135	895	208	579
BRL-6.1	1519	271	1415	481	72	645	122	822	187	521
BRL-7.1	1912	321	1627	513	73	645	116	778	178	490
BRL-8.1	1534	260	1396	482	71	622	117	788	179	505
BRL-9.1	1735	297	1616	530	79	693	131	877	201	572
BRL-10.1	1496	264	1407	471	70	623	115	781	177	496
BRL-11.1	1588	270	1434	493	74	608	114	752	171	478
BLR-5.2	1714	291	1494	479	67	590	107	713	161	449
BLR-6.2	1672	293	1574	526	79	714	133	893	208	585
BLR-7.2	1543	271	1469	490	73	662	123	853	190	546
BLR-10.1	1757	305	1598	571	81	721	136	914	211	581
BLR-11.1	1634	287	1504	513	77	679	126	849	192	543
BLR-12.1	1433	248	1316	453	68	590	111	746	169	476
BLR-13.1	1467	258	1337	467	68	611	114	783	175	503
BLR-14.1	1696	296	1557	503	78	686	128	874	204	568
BLR-15.1	1754	286	1478	456	67	578	106	693	158	440
BLR-8.1	1515	265	1401	484	72	635	119	810	185	518
BLR-8.2	1754	308	1623	555	82	745	140	948	216	611
BLR-9.1	1671	291	1569	532	79	711	135	909	209	589

Table F2 (continued) Sphene SHRIMP trace element data for standard BLR

	Ce ppm	Pr ppm	Nd ppm	Sm ppm	Eu ppm	Gd ppm	Tb ppm	Dy ppm	Ho ppm	Er ppm
BLR-9.2	1645	282	1518	523	78	704	134	890	203	577
BLR-2.1	1589	275	1504	519	77	647	120	806	184	500
BLR-5.1	2069	341	1763	540	81	667	120	790	180	491
BLR-6.1	1433	252	1364	453	69	611	115	779	177	497
BLR-7.1	1438	252	1357	466	68	610	115	774	177	500
BLR-2.1	1589	275	1504	519	77	647	120	806	184	500
BLR-5.1	2069	341	1763	540	81	667	120	790	180	491
BLR-6.1	1433	252	1364	453	69	611	115	779	177	497
BLR-7.1	1438	252	1357	466	68	610	115	774	177	500
BLR-8.1	1515	265	1401	484	72	635	119	810	185	518
BLR-8.2	1754	308	1623	555	82	745	140	948	216	611
BLR-9.1	1671	291	1569	532	79	711	135	909	209	589
BLR-9.2	1645	282	1518	523	78	704	134	890	203	577
BLR-10.1	1757	305	1598	571	81	721	136	914	211	581
BLR-11.1	1634	287	1504	513	77	679	126	849	192	543
BLR-12.1	1433	248	1316	453	68	590	111	746	169	476
BLR-13.1	1467	258	1337	467	68	611	114	783	175	503
BLR-14.1	1696	296	1557	503	78	686	128	874	204	568
BLR-15.1	1754	286	1478	456	67	578	106	693	158	440
BLR-5.2	1714	291	1494	479	67	590	107	713	161	449
BLR-6.2	1672	293	1574	526	79	714	133	893	208	585
BLR-7.2	1543	271	1469	490	73	662	123	853	190	546
BLR-1.1	1966	317	1630	509	74	638	115	765	173	480

Table F2 (continued) Sphene SHRIMP trace element data for standard BLR

	Ce ppm	Pr ppm	Nd ppm	Sm ppm	Eu ppm	Gd ppm	Tb ppm	Dy ppm	Ho ppm	Er ppm
BLR-2.1	1525	270	1423	498	71	656	122	820	190	532
BLR-3.1	1646	293	1558	529	79	702	132	890	203	579
BLR-4.1	1413	247	1312	452	68	606	114	767	173	493
BRL-5.1	2225	366	1896	597	84	742	135	895	208	579
BRL-6.1	1519	271	1415	481	72	645	122	822	187	521
BRL-7.1	1912	321	1627	513	73	645	116	778	178	490
BRL-8.1	1534	260	1396	482	71	622	117	788	179	505
BRL-9.1	1735	297	1616	530	79	693	131	877	201	572
BRL-10.1	1496	264	1407	471	70	623	115	781	177	496
BRL-11.1	1588	270	1434	493	74	608	114	752	171	478
BRL-12.1	1697	296	1605	530	78	688	129	858	200	557
BRL-13.1	1400	246	1303	444	65	585	108	741	168	477

Table F2 (continued) Sphene SHRIMP trace element data for standard BLR

	Yb ppm	Lu ppm	Hf ppm	Ta ppm	Pb206 ppm	Pb208 ppm	Th ppm	U ppm
BLR-1.1	336	34	61	183	16	0.0	193	256
BLR-2.1	349	35	54	211	21	0.0	185	312
BLR-3.1	375	38	48	245	22	0.0	197	331
BLR-4.1	325	33	54	244	18	0.0	147	274
BRL-5.1	388	41	69	255	20	0.0	214	301
BRL-6.1	353	34	44	222	20	0.0	182	306
BRL-7.1	335	35	62	202	16	0.0	199	267
BRL-8.1	326	33	50	213	19	0.0	183	297
BRL-9.1	378	38	52	253	21	0.0	205	333
BRL-10.1	332	34	46	194	18	0.0	171	294
BRL-11.1	311	32	45	195	18	0.0	172	290
BLR-5.2	299	31	60	198	16	0.0	177	236
BLR-6.2	386	38	51	246	23	0.0	200	346
BLR-7.2	360	35	47	226	21	0.0	191	313
BLR-10.1	394	40	55	235	23	0.0	212	359
BLR-11.1	361	36	58	297	20	0.0	181	316
BLR-12.1	314	31	54	274	18	0.0	145	264
BLR-13.1	336	33	46	199	19	0.0	175	278
BLR-14.1	385	36	49	217	22	0.0	186	311
BLR-15.1	303	30	57	209	16	0.0	175	231
BLR-8.1	345	35	42	213	20	0.0	180	301
BLR-8.2	390	39	54	250	24	0.0	215	352
BLR-9.1	387	39	52	244	23	0.0	210	346
BLR-9.2	377	39	60	233	23	0.0	208	338

Table F2 (continued) Sphene SHRIMP trace element data for standard BLR

	Yb ppm	Lu ppm	Hf ppm	Ta ppm	Pb206 ppm	Pb208 ppm	Th ppm	U ppm
BLR-2.1	336	32	43	225	19	0.0	154	286
BLR-5.1	340	34	65	216	18	0.0	210	279
BLR-6.1	333	33	46	196	19	0.0	172	294
BLR-7.1	345	32	47	204	19	0.0	170	288
BLR-2.1	336	32	43	225	19	0.0	154	286
BLR-5.1	340	34	65	216	18	0.0	210	279
BLR-6.1	333	33	46	196	19	0.0	172	294
BLR-7.1	345	32	47	204	19	0.0	170	288
BLR-8.1	345	35	42	213	20	0.0	180	301
BLR-8.2	390	39	54	250	24	0.0	215	352
BLR-9.1	387	39	52	244	23	0.0	210	346
BLR-9.2	377	39	60	233	23	0.0	208	338
BLR-10.1	394	40	55	235	23	0.0	212	359
BLR-11.1	361	36	58	297	20	0.0	181	316
BLR-12.1	314	31	54	274	18	0.0	145	264
BLR-13.1	336	33	46	199	19	0.0	175	278
BLR-14.1	385	36	49	217	22	0.0	186	311
BLR-15.1	303	30	57	209	16	0.0	175	231
BLR-5.2	299	31	60	198	16	0.0	177	236
BLR-6.2	386	38	51	246	23	0.0	200	346
BLR-7.2	360	35	47	226	21	0.0	191	313
BLR-1.1	336	34	61	183	16	0.0	193	256
BLR-2.1	349	35	54	211	21	0.0	185	312
BLR-3.1	375	38	48	245	22	0.0	197	331

Table F2 (continued) Sphene SHRIMP trace element data for standard BLR

	Yb ppm	Lu ppm	Hf ppm	Ta ppm	Pb206 ppm	Pb208 ppm	Th ppm	U ppm
BLR-4.1	325	33	54	244	18	0.0	147	274
BRL-5.1	388	41	69	255	20	0.0	214	301
BRL-6.1	353	34	44	222	20	0.0	182	306
BRL-7.1	335	35	62	202	16	0.0	199	267
BRL-8.1	326	33	50	213	19	0.0	183	297
BRL-9.1	378	38	52	253	21	0.0	205	333
BRL-10.1	332	34	46	194	18	0.0	171	294
BRL-11.1	311	32	45	195	18	0.0	172	290
BRL-12.1	360	36	51	231	20	0.0	197	328
BRL-13.1	309	31	42	193	18	0.0	162	267

Table F3 SHRIMP titanium in sphene temperatures

	^{90}Zr/ppm	Act. SiO_2	Act. TiO_2	Temp/°C#
AWM1.1	7608	0.7	0.7	850
AWM1-2.1	11891	0.7	0.7	882
AWM1-2.2	826	1.0	0.7	733
AWM1-3.1	10110	0.7	0.7	870
AWM1-3.2	2054	1.0	0.7	787
AWM1-4.1	7360	0.7	0.7	848
AWM1-4.2	451	1.0	0.7	700
AWM1-5.1	8777	0.7	0.7	860
AWM1-5.2	5686	0.7	0.7	830
AWM1-6.1	8971	0.7	0.7	862
AWM1-6.2	1676	1.0	0.7	774
AWM1-7.1	557	1.0	0.7	711
AWM1-7.2	10929	0.7	0.7	876
AWM1-8.1	11464	0.7	0.7	880
AWM1-8.2	1154	1.0	0.7	752
AWM1-9.1	6079	0.7	0.7	835
AWM1-9.2	492	0.7	0.7	686
AWM1-10.1	7856	0.7	0.7	852
AWM1-10.2	568	0.7	0.7	693
AWM1-11.1	7434	0.7	0.7	848
AWM1-11.2	789	1.0	0.7	730

Ti-in-sphene temperatures calculated using given ^{90}Zr concentration and SiO_2 and TiO_2 activities following Hayden et al., (2008)

Table F3 (continued) SHRIMP titanium in sphene temperatures

	^{90}Zr/ppm	Act. SiO_2	Act. TiO_2	Temp/°C#
AWM1-12.1	12225	0.7	0.7	884
AWM1-12.2	240	1.0	0.7	668
AWM1-13.1	10865	0.7	0.7	876
AWM1-13.2	819	1.0	0.7	732
AWM1-14.1	6029	0.7	0.7	834
AWM1-14.2	406	0.7	0.7	676
AMW2-1.1	6460	0.7	0.7	839
AMW2-1.2	1745	1.0	0.7	777
AMW2-2.1	535	1.0	0.7	709
AMW2-2.2	846	1.0	0.7	734
AWM2-3.1	1514	1.0	0.7	768
AWM2-3.2	1410	1.0	0.7	764
AWM2-4.1	1496	1.0	0.7	768
AWM2-4.2	9816	0.7	0.7	868
AWM2-5.1	1254	1.0	0.7	757
AWM2-5.2	3197	0.7	0.7	792
AWM2-6.1	666	0.7	0.7	702
AWM2-6.2	1629	0.7	0.7	751
AWM2-7.1	1660	0.7	0.7	753
AWM2-7.2	1382	0.7	0.7	742
AWM2-8.1	402	1.0	0.7	694

Ti-in-sphene temperatures calculated using given ^{90}Zr concentration and SiO_2 and TiO_2 activities following Hayden et al., (2008)

Table F3 (continued) SHRIMP titanium in sphene temperatures

	^{90}Zr/ppm	Act. SiO_2	Act. TiO_2	Temp/°C#
AWM2-8.2	1144	0.7	0.7	731
AWM2-9.1	779	0.7	0.7	710
AWM2-9.2	1170	0.7	0.7	732
AWM2-9.3	303	1.0	0.7	679
AWM2-10.1	7371	0.7	0.7	848
AWM2-10.2	623	1.0	0.7	717
AWM2-11.1	413	1.0	0.7	695
AWM2-11.2	788	0.7	0.7	711
AWM2-12.1	4642	0.7	0.7	816
AWM2-12.2	9451	0.7	0.7	866
AWAG_1A-1.1	6650	0.7	0.7	841
AWAG_1A-1.2	4257	0.7	0.7	811
AWAG_1A-2.1	9384	0.7	0.7	865
AWAG_1A-2.2	2666	0.7	0.7	781
AWAG_1A-3.1	1556	0.7	0.7	749
AWAG_1A-3.2	726	0.7	0.7	706
AWAG_1A-4.1	267	0.7	0.7	656
AWAG_1A-4.2	3900	0.7	0.7	805
AWAG_1A-4.3	8800	0.7	0.7	860
AWAG_1A-5.1	5105	0.7	0.7	823
AWAG_1A-5.2	16470	0.7	0.7	907

Ti-in-sphene temperatures calculated using given ^{90}Zr concentration and SiO_2 and TiO_2 activities following Hayden et al., (2008)

Table F3 (continued) SHRIMP titanium in sphene temperatures

	^{90}Zr/ppm	Act. SiO_2	Act. TiO_2	Temp/°C#
AWAG_1A-6.1	6859	0.7	0.7	843
AWAG_1A-6.2	3473	0.7	0.7	798
AWAG_1A-7.1	2060	0.7	0.7	765
AWAG_1A-7.2	2106	0.7	0.7	767
AWAG_1A-8.1	1077	0.7	0.7	728
AWAG_1A-8.2	1327	0.7	0.7	740
AWAG_1A-9.1	4855	0.7	0.7	819
AWAG_1A-9.2	8400	0.7	0.7	857
AWAG_1A-10.1	1326	0.7	0.7	740
AWAG_1A-10.2	1896	0.7	0.7	760
AWAG_1A-11.1	1183	0.7	0.7	733
AWAG_1A-11.2	1785	0.7	0.7	757
AWAG_1A-12.1	3912	0.7	0.7	805
AWAG_1A-12.2	1596	0.7	0.7	750
AWAG_1A-13.1	1511	0.7	0.7	747
AWAG_1A-13.2	1871	0.7	0.7	760
AWAG_1A-14.1	4498	0.7	0.7	814
AWAG_1A-14.2	2418	0.7	0.7	775
AWAG_1B-1.1	742	0.7	0.7	707
AWAG_1B-1.2	830	0.7	0.7	714
AWAG_1B-2.1	1419	0.7	0.7	743

Ti-in-sphene temperatures calculated using given ^{90}Zr concentration and SiO_2 and TiO_2 activities following Hayden et al., (2008)

Table F3 (continued) SHRIMP titanium in sphene temperatures

	^{90}Zr/ppm	Act. SiO_2	Act. TiO_2	Temp/°C#
AWAG_1B-2.2	2996	0.7	0.7	788
AWAG_1B-3.1	896	0.7	0.7	718
AWAG_1B-3.2	11376	0.7	0.7	879
AWAG_1B-4.1	8524	0.7	0.7	858
AWAG_1B-4.2	965	0.7	0.7	722
AWAG_1B-5.1	3491	0.7	0.7	798
AWAG_1B-5.2	4932	0.7	0.7	820
AWAG_1B-6.1	5328	0.7	0.7	826
AWAG_1B-6.2	1795	0.7	0.7	757
AWAG_1B-7.1	2691	0.7	0.7	782
AWAG_1B-7.2	1307	0.7	0.7	739
AWAG_1B-8.1	6358	0.7	0.7	838
AWAG_1B-8.2	9250	0.7	0.7	864
AWAG_1B-9.1	7589	0.7	0.7	850
AWAG_1B-9.2	2017	0.7	0.7	764
AWAG_1B-9.3	959	0.7	0.7	721
AWAG_1B-10.1	10618	0.7	0.7	874
AWAG_1B-10.2	948	0.7	0.7	721
AWAG_1B-11.1	2626	0.7	0.7	780
AWAG_1B-11.2	3484	0.7	0.7	798
AWAG_1B-12.1	932	0.7	0.7	720

Ti-in-sphene temperatures calculated using given ^{90}Zr concentration and SiO_2 and TiO_2 activities following Hayden et al., (2008)

Table F3 (continued) SHRIMP titanium in sphene temperatures

	^{90}Zr/ppm	Act. SiO_2	Act. TiO_2	Temp/°C#
AWAG_1B-12.2	8998	0.7	0.7	862
AWAG_1B-13.1	6219	0.7	0.7	836
AWAG_1B-13.2	3928	0.7	0.7	806
AWAG_1B-13.3	4611	0.7	0.7	816
AWAG_1B-13.4	851	0.7	0.7	715
AWAG_2-1.1	794	0.7	0.7	711
AWAG_2-1.2	2062	0.7	0.7	765
AWAG_2-2.1	829	0.7	0.7	713
AWAG_2-2.2	1537	0.7	0.7	748
AWAG_2-3.1	2134	0.7	0.7	767
AWAG_2-3.2	794	0.7	0.7	711
AWAG_2-4.1	2245	0.7	0.7	771
AWAG_2-4.2	708	0.7	0.7	705
AWAG_2-5.1	2284	0.7	0.7	772
AWAG_2-5.2	630	0.7	0.7	699
AWAG_2-6.1	1835	0.7	0.7	758
AWAG_2-6.2	631	0.7	0.7	699
AWAG_2-7.1	1404	0.7	0.7	743
AWAG_2-7.2	909	0.7	0.7	718
AWAG_2-8.1	2227	0.7	0.7	770
AWAG_2-8.2	720	0.7	0.7	706

Ti-in-sphene temperatures calculated using given ^{90}Zr concentration and SiO_2 and TiO_2 activities following Hayden et al., (2008)

Table F3 (continued) SHRIMP titanium in sphene temperatures

	^{90}Zr/ppm	Act. SiO_2	Act. TiO_2	Temp/°C#
AWAG_2-9.1	1665	0.7	0.7	753
AWAG_2-9.2	851	0.7	0.7	715
AWAG_2-10.1	1242	0.7	0.7	736
AWAG_2-10.2	544	0.7	0.7	691
AWAG_2-11.1	1432	0.7	0.7	744
AWAG_2-11.2	1479	0.7	0.7	746
AWAG_2-12.1	1438	0.7	0.7	744
AWAG_2-12.2	621	0.7	0.7	698
AWAG_2-13.1	1742	0.7	0.7	755
AWAG_2-13.2	672	0.7	0.7	702
AWAG_2-14.1	1285	0.7	0.7	738
AWAG_2-14.2	692	0.7	0.7	704
AWAG3-1.1	2096	0.7	0.7	766
AWAG3-1.2	918	0.7	0.7	719
AWAG3-2.1	2461	0.7	0.7	776
AWAG3-2.2	983	0.7	0.7	723
AWAG3-2.2	944	0.7	0.7	721
AWAG3-3.1	807	0.7	0.7	712
AWAG3-3.2	551	0.7	0.7	692
AWAG3-4.1	3182	0.7	0.7	792
AWAG3-4.2	1972	0.7	0.7	763

Ti-in-sphene temperatures calculated using given ^{90}Zr concentration and SiO_2 and TiO_2 activities following Hayden et al., (2008)

Table F3 (continued) SHRIMP titanium in sphene temperatures

	^{90}Zr/ppm	Act. SiO_2	Act. TiO_2	Temp/°C#
AWAG3-5.1	683	0.7	0.7	703
AWAG3-5.2	701	0.7	0.7	704
AWAG3-6.1	1006	0.7	0.7	724
AWAG3-6.2	595	0.7	0.7	696
AWAG3-7.1	3908	0.7	0.7	805
AWAG3-7.2	749	0.7	0.7	708
AWAG3-7.3	506	0.7	0.7	687
AWAG3-8.1	1151	0.7	0.7	732
AWAG3-8.2	690	0.7	0.7	704
AWAG3-9.1	1332	0.7	0.7	740
AWAG3-9.2	622	0.7	0.7	698
AWAG3-10.1	616	0.7	0.7	698
AWAG3-10.2	3629	0.7	0.7	800
AWAG3-11.1	732	0.7	0.7	707
AWAG3-11.2	847	0.7	0.7	715
AWAG3-12.1	1218	0.7	0.7	735
AWAG3-12.2	841	0.7	0.7	714
AWAG3-13.1	1311	0.7	0.7	739
AWAG3-13.2	764	0.7	0.7	709
AWAG4-1.1	706	0.7	0.7	705
AWAG4-1.2	441	0.7	0.7	680

Ti-in-sphene temperatures calculated using given ^{90}Zr concentration and SiO_2 and TiO_2 activities following Hayden et al., (2008)

Table F3 (continued) SHRIMP titanium in sphene temperatures

	^{90}Zr/ppm	Act. SiO_2	Act. TiO_2	Temp/°C#
AWAG4-2.1	923	0.7	0.7	719
AWAG4-2.2	860	0.7	0.7	715
AWAG4-3.1	761	0.7	0.7	709
AWAG4-3.2	491	0.7	0.7	686
AWAG4-4.1	937	0.7	0.7	720
AWAG4-4.2	380	0.7	0.7	673
AWAG4-5.1	413	0.7	0.7	677
AWAG4-5.2	1046	0.7	0.7	726
AWAG4-6.1	641	0.7	0.7	700
AWAG4-6.2	443	0.7	0.7	681
AWAG4-7.1	3478	0.7	0.7	798
AWAG4-7.2	371	0.7	0.7	672
AWAG4-8.1	798	0.7	0.7	711
AWAG4-8.2	1344	0.7	0.7	740
AWAG4-8.3	542	0.7	0.7	691
AWAG4-9.1	1126	0.7	0.7	730
AWAG4-9.2	380	0.7	0.7	673
AWAG4-10.1	1470	0.7	0.7	745
AWAG4-10.2	855	0.7	0.7	715
AWAG4-11.1	1151	0.7	0.7	732
AWAG4-11.2	813	0.7	0.7	712

Ti-in-sphene temperatures calculated using given ^{90}Zr concentration and SiO_2 and TiO_2 activities following Hayden et al., (2008)

Table F3 (continued) SHRIMP titanium in sphene temperatures

	^{90}Zr/ppm	Act. SiO_2	Act. TiO_2	Temp/°C#
AWAG4-12.1	658	0.7	0.7	701
AWAG4-12.2	583	0.7	0.7	695
AWAG4-13.1	548	0.7	0.7	691
AWAG4-13.2	1003	0.7	0.7	724
AWAG5-1.1	1191	0.7	0.7	754
AWAG5-1.2	797	0.7	0.7	731
AWAG5-2.1	1010	0.7	0.7	744
AWAG5-2.2	859	0.7	0.7	715
AWAG5-3.1	1255	0.7	0.7	736
AWAG5-3.2	922	0.7	0.7	719
AWAG5-4.1	1128	0.7	0.7	730
AWAG5-4.2	1509	0.7	0.7	747
AWAG5-5.1	2106	0.7	0.7	767
AWAG5-5.2	1131	0.7	0.7	731
AWAG5-6.1	1545	0.7	0.7	748
AWAG5-6.2	623	0.7	0.7	698
AWAG5-7.1	1181	0.7	0.7	733
AWAG5-7.2	892	0.7	0.7	717
AWAG5-8.1	1096	0.7	0.7	729
AWAG5-8.2	700	0.7	0.7	704
AWAG5-9.1	816	0.7	0.7	713

Ti-in-sphene temperatures calculated using given ^{90}Zr concentration and SiO_2 and TiO_2 activities following Hayden et al., (2008)

Table F3 (continued) SHRIMP titanium in sphene temperatures

	^{90}Zr/ppm	Act. SiO_2	Act. TiO_2	Temp/°C#
AWAG5-9.2	793	0.7	0.7	711
AWAG5-10.1	915	0.7	0.7	719
AWAG5-10.2	741	0.7	0.7	707
AWAG5-11.1	1057	0.7	0.7	727
AWAG5-11.2	816	0.7	0.7	713
AWAG5-12.1	1270	0.7	0.7	737
AWAG5-12.2	894	0.7	0.7	718
AWAG5-13.1	1404	0.7	0.7	743
AWAG5-13.2	770	0.7	0.7	709
AWAG5-14.1	1206	0.7	0.7	734
AWAG5-14.2	817	0.7	0.7	713
AWAG6-1.1	893	0.7	0.7	717
AWAG6-1.2	751	0.7	0.7	708
AWAG6-1.3	1066	0.7	0.7	727
AWAG6-1.4	817	0.7	0.7	713
AWAG6-2.1	730	0.7	0.7	707
AWAG6-2.2	1266	0.7	0.7	737
AWAG6-2.3	471	0.7	0.7	684
AWAG6-3.1	722	0.7	0.7	706
AWAG6-3.2	1081	0.7	0.7	728
AWAG6-4.1	4857	0.7	0.7	819

Ti-in-sphene temperatures calculated using given ^{90}Zr concentration and SiO_2 and TiO_2 activities following Hayden et al., (2008)

Table F3 (continued) SHRIMP titanium in sphene temperatures

	^{90}Zr/ppm	Act. SiO_2	Act. TiO_2	Temp/°C#
AWAG6-4.2	638	0.7	0.7	699
AWAG6-5.1	13060	0.7	0.7	889
AWAG6-5.2	720	0.7	0.7	706
AWAG6-6.1	1105	0.7	0.7	729
AWAG6-6.2	660	0.7	0.7	701
AWAG6-7.1	1528	0.7	0.7	748
AWAG6-7.2	641	0.7	0.7	700
AWAG6-8.1	2819	0.7	0.7	784
AWAG6-8.2	1402	0.7	0.7	743
AWAG6-9.1	2914	0.7	0.7	787
AWAG6-9.2	884	0.7	0.7	717
AWAG6-10.1	4862	0.7	0.7	820
AWAG6-10.2	584	0.7	0.7	695
AWAG6-11.1	1752	0.7	0.7	756
AWAG6-11.2	789	0.7	0.7	711
AWAG6-12.1	3691	0.7	0.7	802
AWAG6-12.2	2323	0.7	0.7	773
AWAG6-13.1	1234	0.7	0.7	735
AWAG6-13.2	817	0.7	0.7	713
AWAG7-1.1	798	0.7	0.7	711
AWAG7-1.2	844	0.7	0.7	714

Ti-in-sphene temperatures calculated using given ^{90}Zr concentration and SiO_2 and TiO_2 activities following Hayden et al., (2008)

Table F3 (continued) SHRIMP titanium in sphene temperatures

	^{90}Zr/ppm	Act. SiO_2	Act. TiO_2	Temp/°C#
AWAG7-2.1	2224	0.7	0.7	770
AWAG7-3.1	1191	0.7	0.7	733
AWAG7-3.2	798	0.7	0.7	711
AWAG7-4.1	3156	0.7	0.7	792
AWAG7-4.2	1127	0.7	0.7	730
AWAG7-5.1	1005	0.7	0.7	724
AWAG7-5.2	667	0.7	0.7	702
AWAG7-6.1	466	0.7	0.7	683
AWAG7-6.2	1357	0.7	0.7	741
AWAG7-6.3	156	0.7	0.7	631
AWAG7-7.1	1754	0.7	0.7	756
AWAG7-7.2	577	0.7	0.7	694
AWAG7-9.1	954	0.7	0.7	721
AWAG7-9.2	1111	0.7	0.7	730
AWAG7-8.1	949	0.7	0.7	721
AWAG7-8.2	667	0.7	0.7	702
AWAG7-10.1	1263	0.7	0.7	737
AWAG7-10.2	762	0.7	0.7	709
AWAG7-11.1	1055	0.7	0.7	727
AWAG7-11.2	950	0.7	0.7	721
AWAG7-11.3	865	0.7	0.7	716

Ti-in-sphene temperatures calculated using given ^{90}Zr concentration and SiO_2 and TiO_2 activities following Hayden et al., (2008)

Table F3 (continued) SHRIMP titanium in sphene temperatures

	^{90}Zr/ppm	Act. SiO_2	Act. TiO_2	Temp/°C#
AWA67-12.1	664	0.7	0.7	702
AWA67-12.2	232	0.7	0.7	649
AWAG7-13.1	579	0.7	0.7	694
AWAG7-13.2	912	0.7	0.7	719
AWAG7-13.3	1035	0.7	0.7	726
AWAG7-14.1	635	0.7	0.7	699
AWAG7-14.2	747	0.7	0.7	708
AWA67-15.1	1118	0.7	0.7	730
AWA67-15.2	1036	0.7	0.7	726
BLR-1.1	1285	1.0	0.7	758
BLR-2.1	1334	1.0	0.7	761
BLR-3.1	1356	1.0	0.7	762
BLR-4.1	1293	1.0	0.7	759
BRL-5.1	1431	1.0	0.7	765
BRL-6.1	1262	1.0	0.7	757
BRL-7.1	1268	1.0	0.7	758
BRL-8.1	1301	1.0	0.7	759
BRL-9.1	1442	1.0	0.7	765
BRL-10.1	1247	1.0	0.7	757
BRL-11.1	1354	1.0	0.7	762
BLR-5.2	1200	1.0	0.7	754

Ti-in-sphene temperatures calculated using given ^{90}Zr concentration and SiO_2 and TiO_2 activities following Hayden et al., (2008)

Table F3 (continued) SHRIMP titanium in sphene temperatures

	^{90}Zr/ppm	Act. SiO_2	Act. TiO_2	Temp/°C#
BLR-6.2	1385	1.0	0.7	763
BLR-7.2	1293	1.0	0.7	759
BLR-10.1	1503	1.0	1.0	790
BLR-11.1	1335	1.0	1.0	782
BLR-12.1	1334	1.0	1.0	782
BLR-13.1	1213	1.0	1.0	776
BLR-14.1	1358	1.0	1.0	783
BLR-15.1	1221	1.0	1.0	777
BLR-8.1	1270	1.0	1.0	779
BLR-8.2	1478	1.0	1.0	789
BLR-9.1	1420	1.0	1.0	786
BLR-9.2	1404	1.0	1.0	785
BLR-2.1	1406	1.0	1.0	786
BLR-5.1	1367	1.0	1.0	784
BLR-6.1	1242	1.0	1.0	778
BLR-7.1	1236	1.0	1.0	778
BLR-2.1	1406	1.0	1.0	786
BLR-5.1	1367	1.0	1.0	784
BLR-6.1	1242	1.0	1.0	778
BLR-7.1	1236	1.0	1.0	778
BLR-8.1	1270	1.0	1.0	779

Ti-in-sphene temperatures calculated using given ^{90}Zr concentration and SiO_2 and TiO_2 activities following Hayden et al., (2008)

Table F3 (continued) SHRIMP titanium in sphene temperatures

	^{90}Zr/ppm	Act. SiO_2	Act. TiO_2	Temp/°C#
BLR-8.2	1478	1.0	1.0	789
BLR-9.1	1420	1.0	1.0	786
BLR-9.2	1404	1.0	1.0	785
BLR-10.1	1503	1.0	1.0	790
BLR-11.1	1335	1.0	1.0	782
BLR-12.1	1334	1.0	1.0	782
BLR-13.1	1213	1.0	1.0	776
BLR-14.1	1358	1.0	1.0	783
BLR-15.1	1221	1.0	1.0	777
BLR-5.2	1200	1.0	0.7	754
BLR-6.2	1385	1.0	0.7	763
BLR-7.2	1293	1.0	0.7	759
BLR-1.1	1285	1.0	0.7	758
BLR-2.1	1334	1.0	0.7	761
BLR-3.1	1356	1.0	0.7	762
BLR-4.1	1293	1.0	0.7	759
BRL-5.1	1431	1.0	0.7	765
BRL-6.1	1262	1.0	0.7	757
BRL-7.1	1268	1.0	0.7	758
BRL-8.1	1301	1.0	0.7	759
BRL-9.1	1442	1.0	0.7	765

Ti-in-sphene temperatures calculated using given ^{90}Zr concentration and SiO_2 and TiO_2 activities following Hayden et al., (2008)

Appendix G

Cathodoluminescence images of zircon grains

Figure G1: Zircon images for sample NAWZ-13. Trace element, Hf and O spot names and locations labeled


11.1
87 NAWZ13
85 NAWZ13
8.1
10.1
8.2
88 NAWZ13
86 NAWZ13

84 NAWZ13
8.1

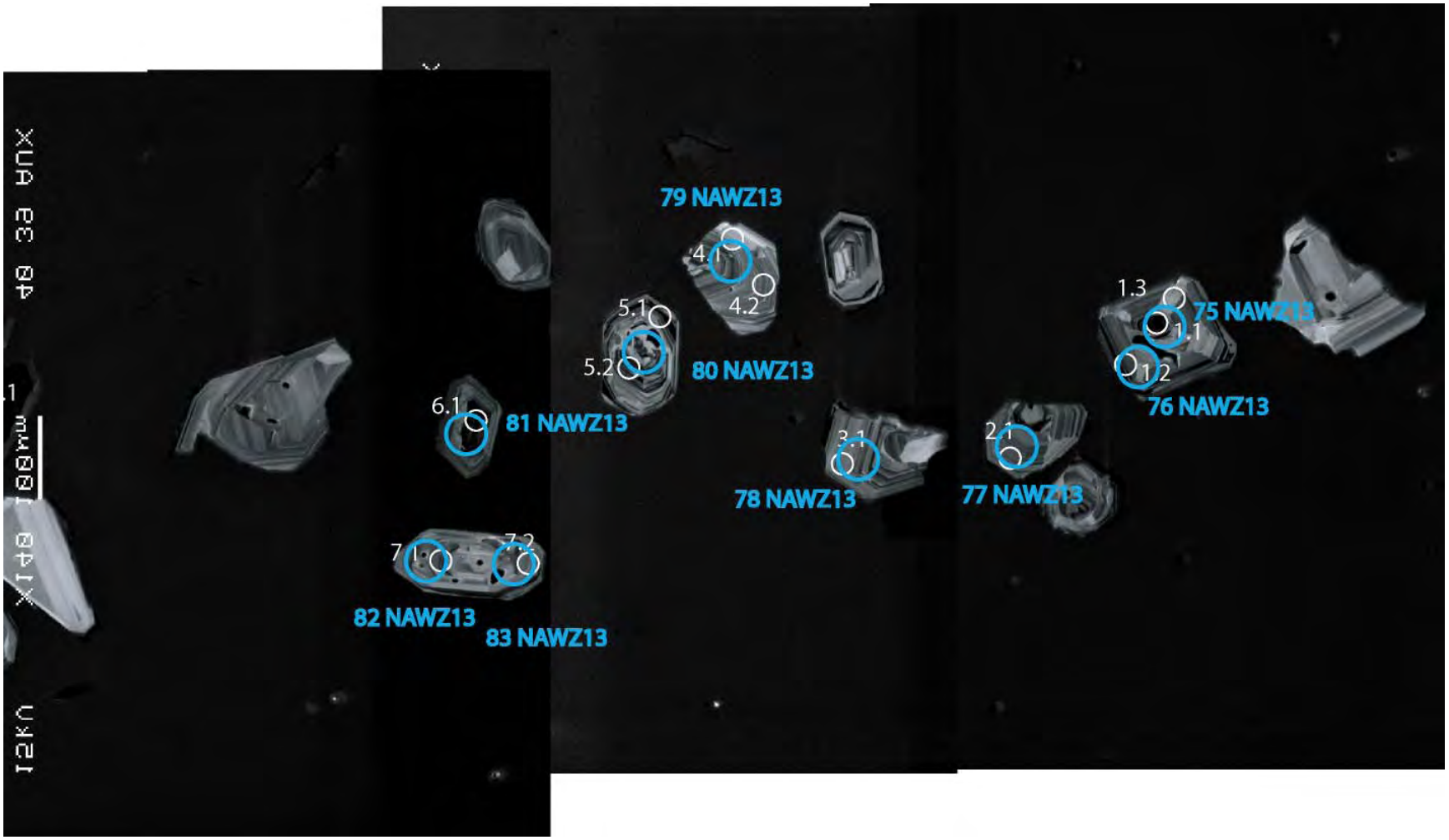
79 NAWZ13
4.1
4.2
5.1
5.2
80 NAWZ13
6.1
81 NAWZ13
7.1
7.2
82 NAWZ13
83 NAWZ13
3.1
78 NAWZ13
2.1
77 NAWZ13
1.3
75 NAWZ13
1.1
1.2
76 NAWZ13

Figure G2: Zircon images for sample NAWZ-16. Trace element, Hf and O spot names and locations labeled

12kV X180 100μm 30 30 44X
12kV X180 100μm 30 30 44X
12kV X180 100μm 30 30 44X

12kV X140 100μm 30 30 UNX
12kV X140 100μm 30 30 UNX

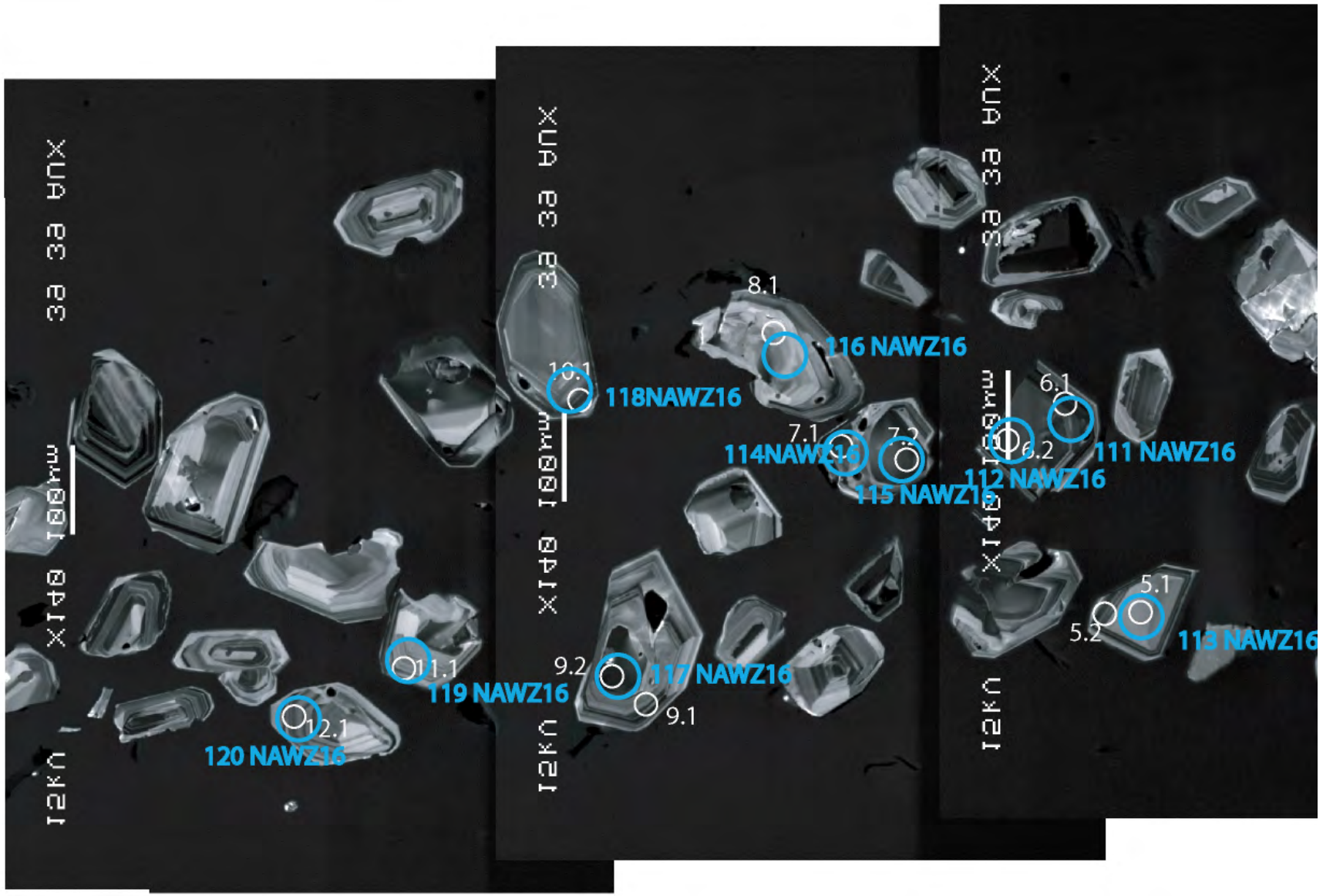
8.1
116 NAWZ16
10.1
118NAWZ16
7.1
7.2
114NAWZ16
115 NAWZ16
6.1
6.2
111 NAWZ16
112 NAWZ16
5.1
5.2
113 NAWZ16
11.1
119 NAWZ16
9.2
117 NAWZ16
9.1
12.1
120 NAWZ16

110 NAWZ16
109 NAWZ16
108 NAWZ1
107 NAW
4.1
4.2
1.1

Figure G3: Zircon images for sample NAWZ-26. Trace element, Hf and O spot names and locations labeled

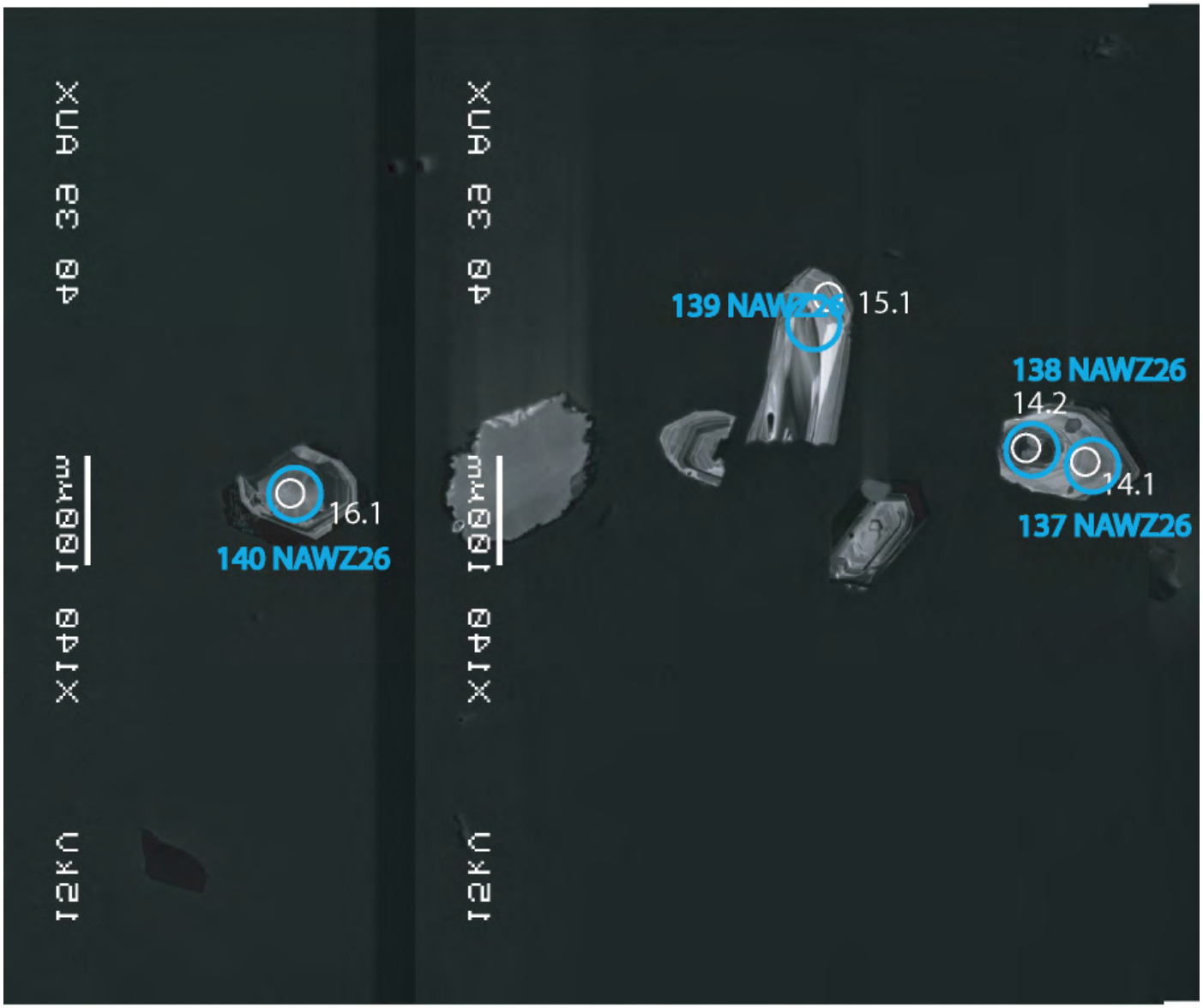
16.1
140 NAWZ26
15.1
139 NAWZ26
138 NAWZ26
14.2
14.1
137 NAWZ26


134 NAWZ26
13.1
12.1
10.1
136 NAWZ26
135 NAWZ26
133 NAWZ26

131 NAWZ26
9.1
133 NAWZ26
7.1
7.2
132 NAWZ26

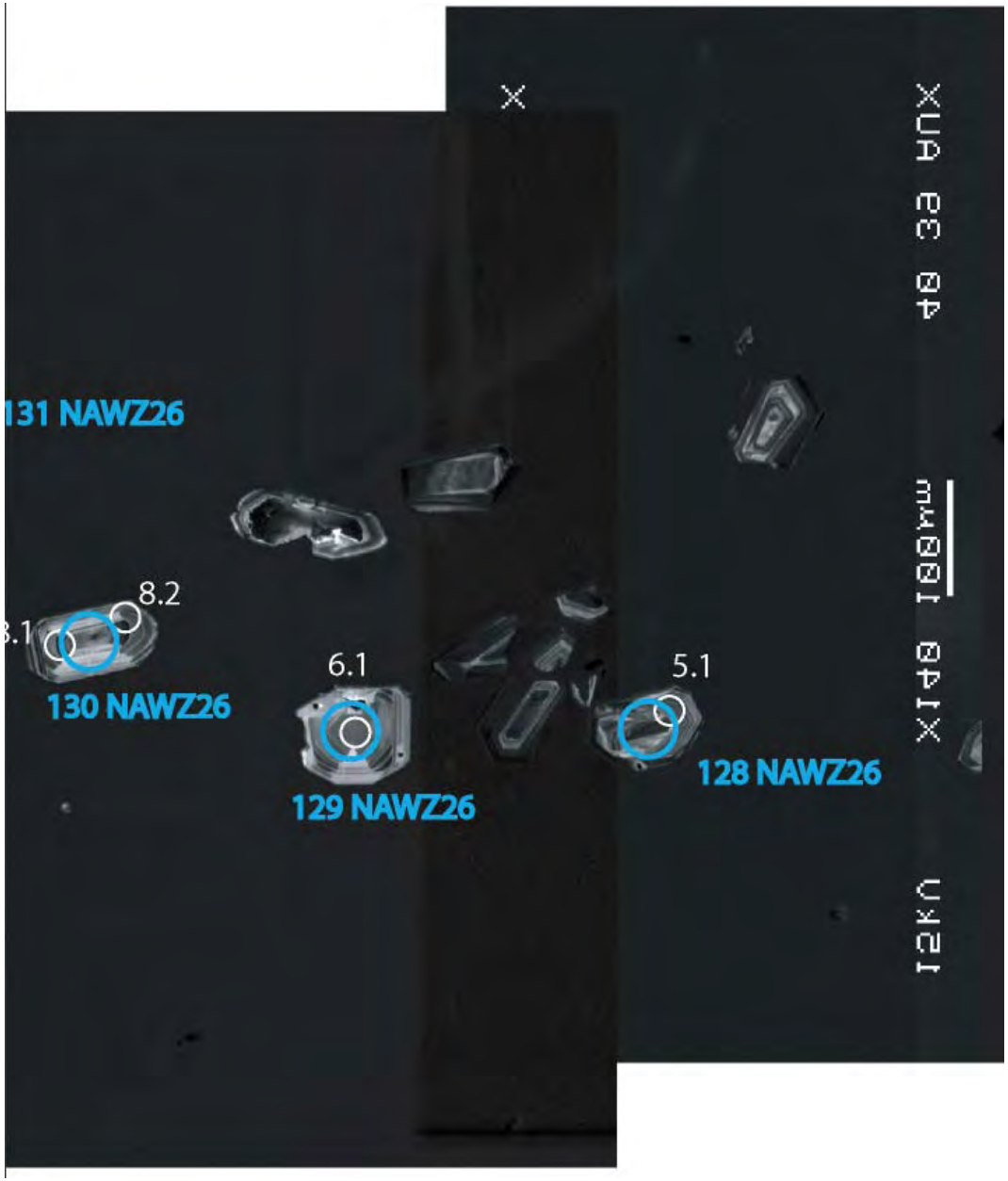
131 NAWZ26
8.2
130 NAWZ26
6.1
129 NAWZ26
5.1
128 NAWZ26

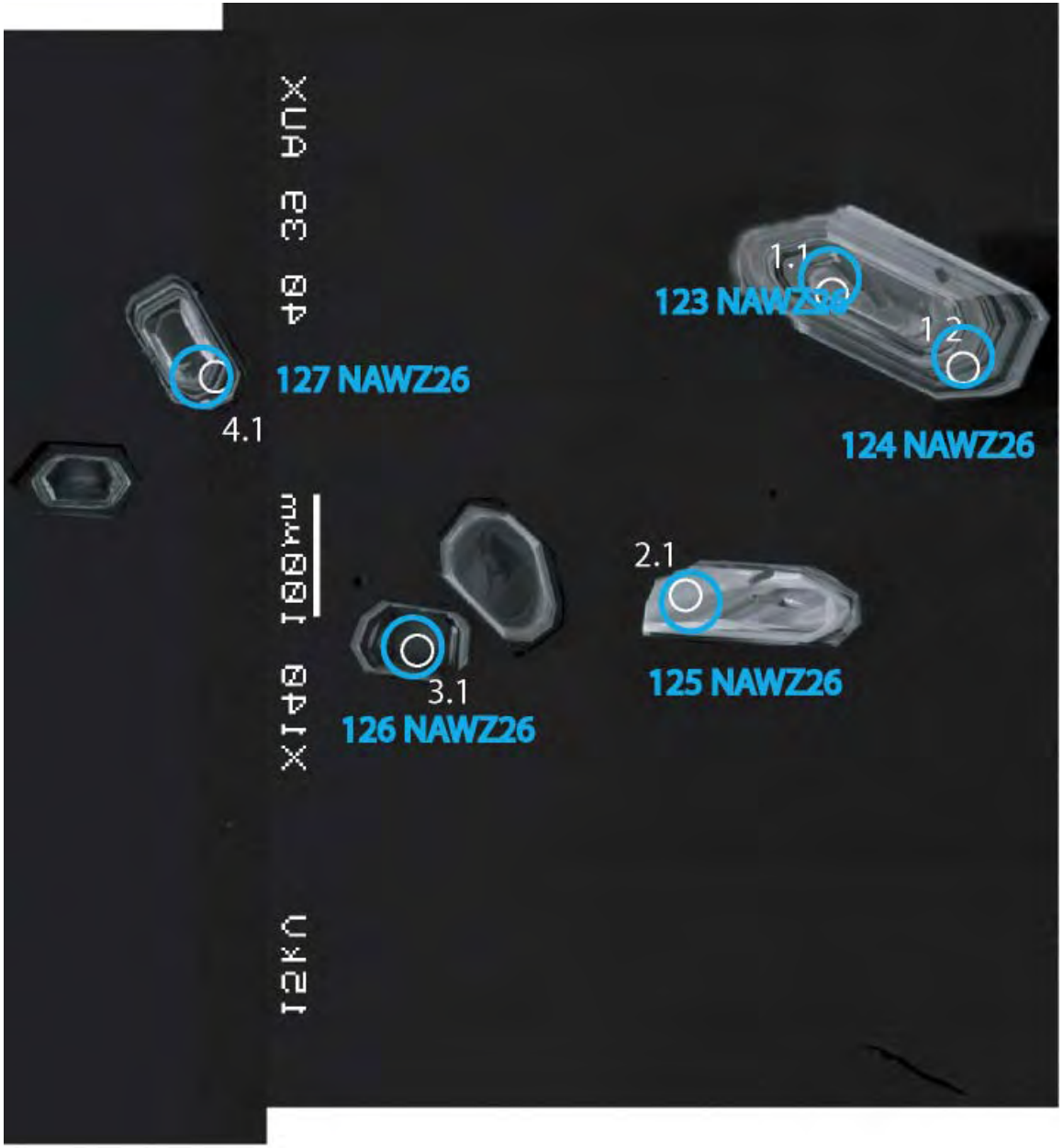
1.1
123 NAWZ26
1.2
124 NAWZ26
127 NAWZ26
4.1
2.1
125 NAWZ26
3.1
126 NAWZ26

Figure G4: Zircon images for sample NAWZ-50. Trace element, Hf and O spot names and locations labeled

1.1MGI
92 NAWZ50
1.2GZE
93 NAWZ50
9.2MGZE
9.1MGZI
94 NAWZ50

XUA 83 40
mm001 04IX 12kV
2.2MGZE
2.1DGC
95 NAWZ50
8.2MGZE
96 NAWZ50
10.2MGZE
10.1DGZC
97 NAWZ50

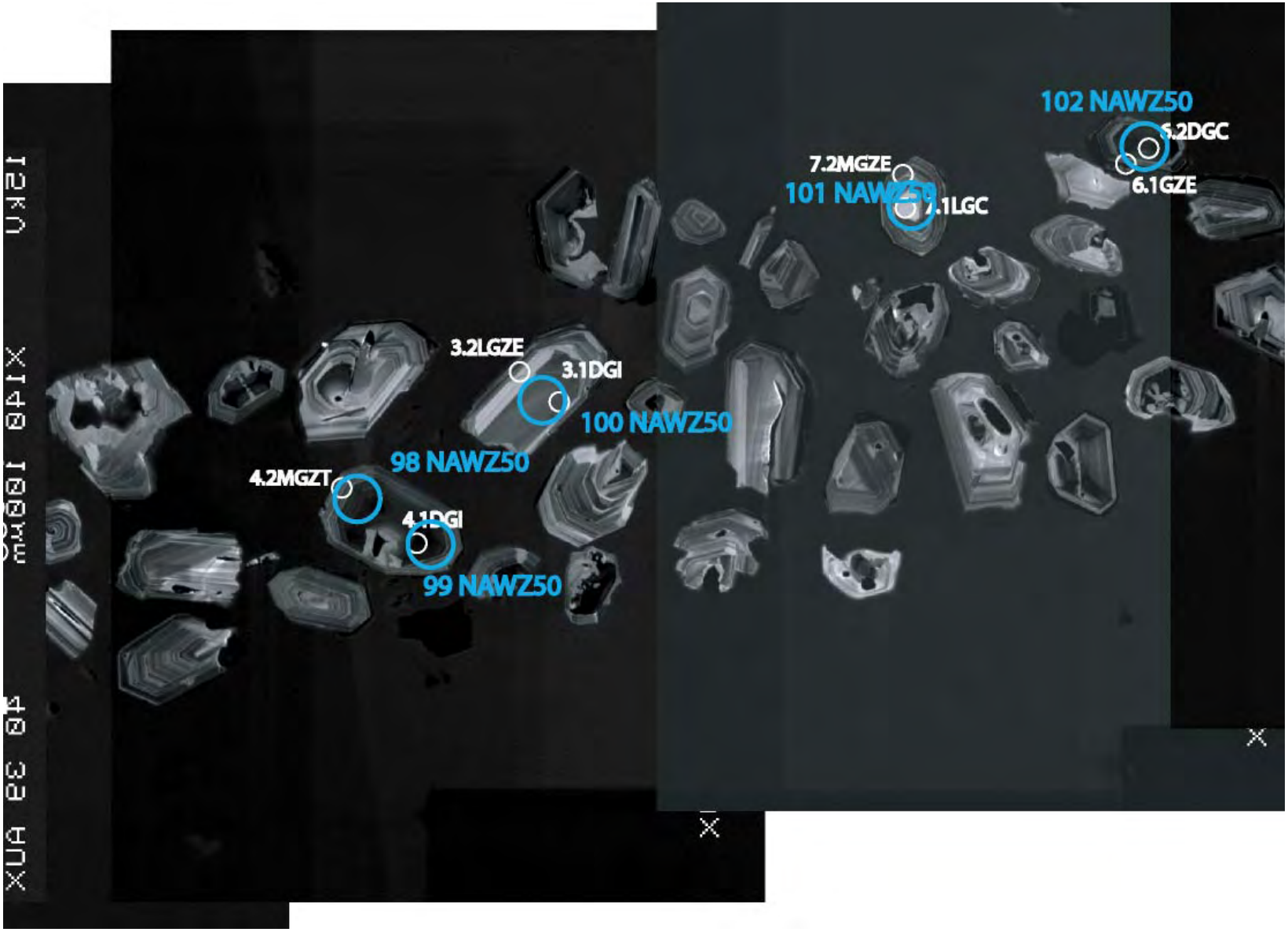
102 NAWZ50
6.2DGC
6.1GZE
7.2MGZE
101 NAWZ50
7.1LGC
3.2LGZE
3.1DGI
100 NAWZ50
98 NAWZ50
4.2MGZT
4.1DGI
99 NAWZ50


103 NAWZ50 5.2GZE
5.1MGC
12.1GZ4
12kV WD41.1mm X140 0.41µm

Figure G5: Zircon images for sample AWAG-1A. Trace element, Hf and O spot names and locations labeled

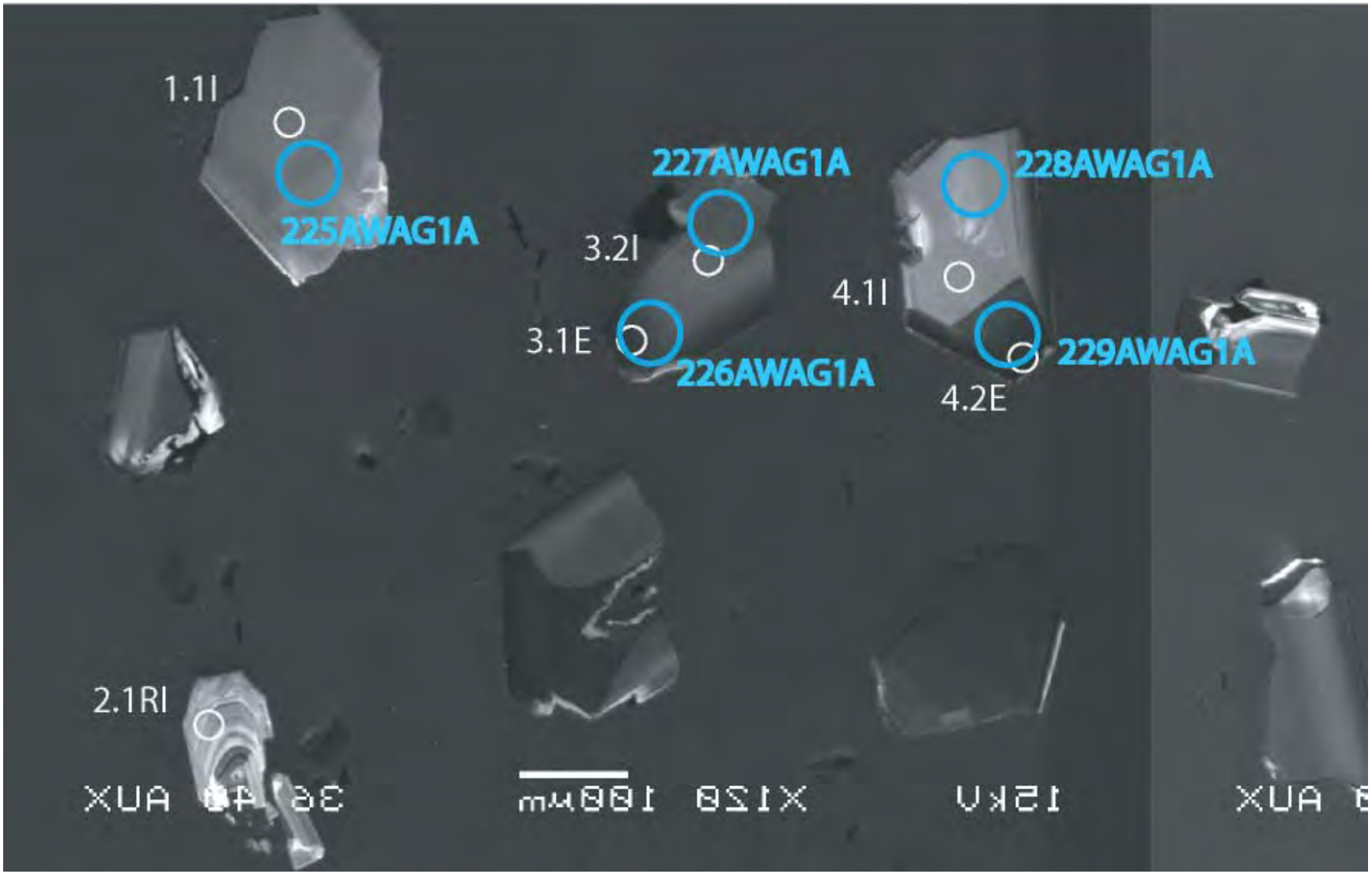
1.1I
225AWAG1A
227AWAG1A
228AWAG1A
3.2I
4.1I
3.1E
226AWAG1A
229AWAG1A
4.2E
2.1RI

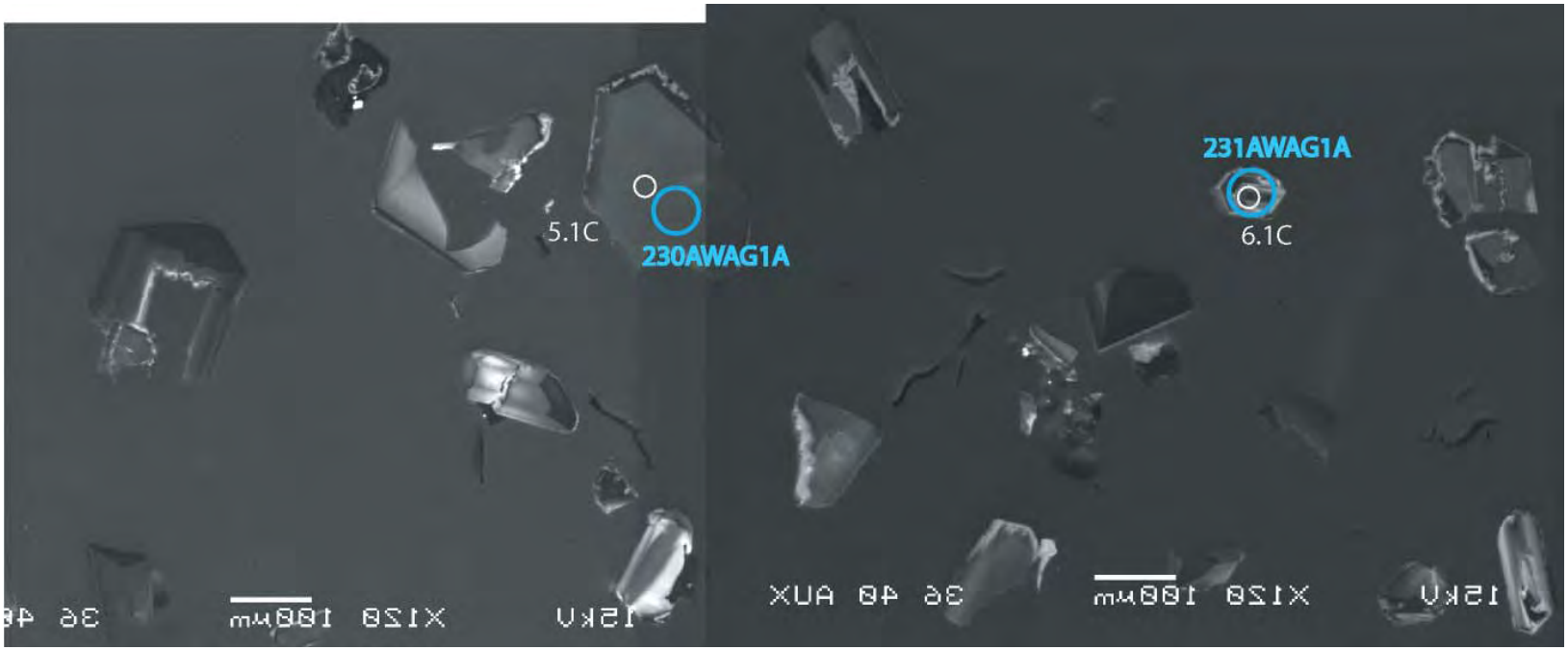
5.1C
230AWAG1A
231AWAG1A
6.1C

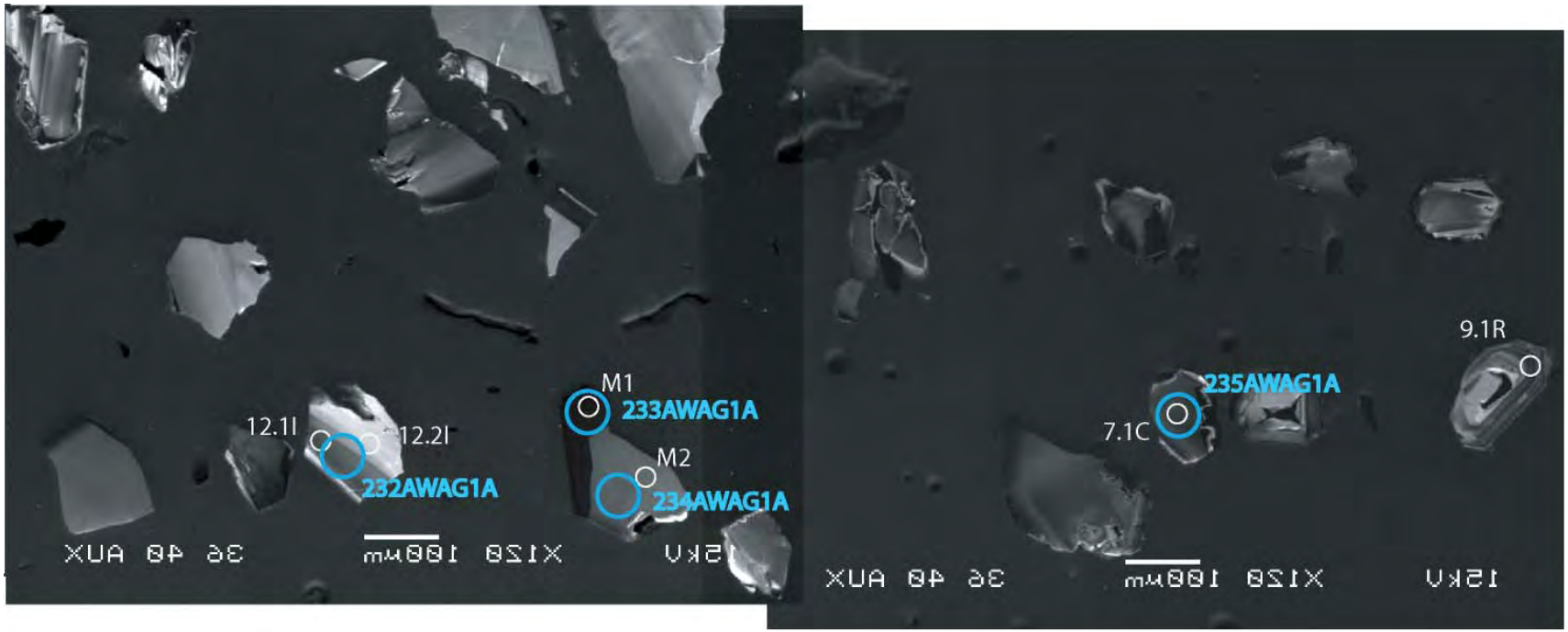
12.1I
12.2I
232AWAG1A
M1
233AWAG1A
M2
234AWAG1A
7.1C
235AWAG1A
9.1R


238AWAG1A
8.3C
237AWAG1A
8.2I
236AWAG1A
8.1R
10.1C
11.1C

Figure G6: Zircon images for sample AWAG-1B. Trace element, Hf and O spot names and locations labeled


1.4DGI2
1.2MGI
1.3DGI
268 AWAG1B
2.1EI
2.2C
269 AWAG1B
3.3MGIZ
3.2MGI
3.1E

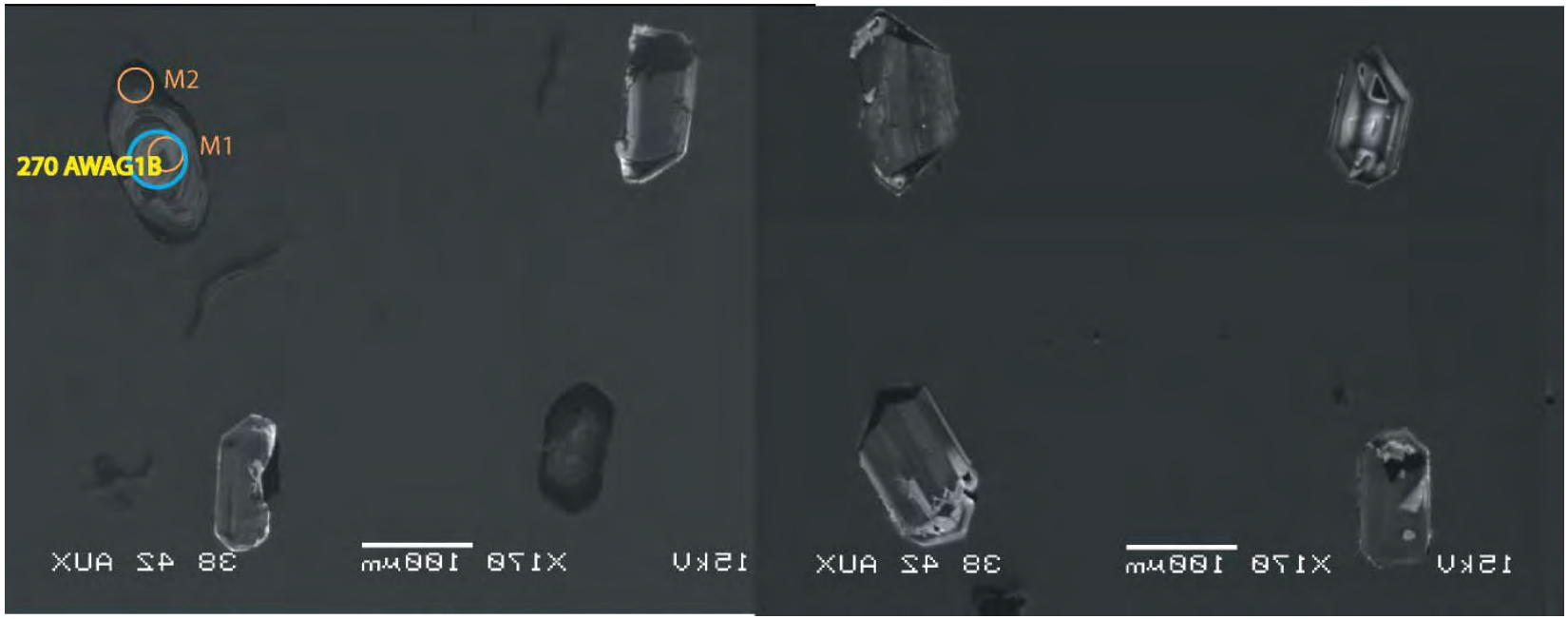
M2
M1
270 AWAG1B
15kV X170 100µm 38 42 AUX
15kV X170 100µm 38 42 AUX


M3
271 AWAG1B
5.2LGI
5.1DGIZ
6.1DGE
6.2LGI
7.1DGIZ


M4
273 AWAG1B
4.1MGIZ
4.1DGIZ
8.1DGIZ
272 AWAG1B
9.2LGI
8.1DGE

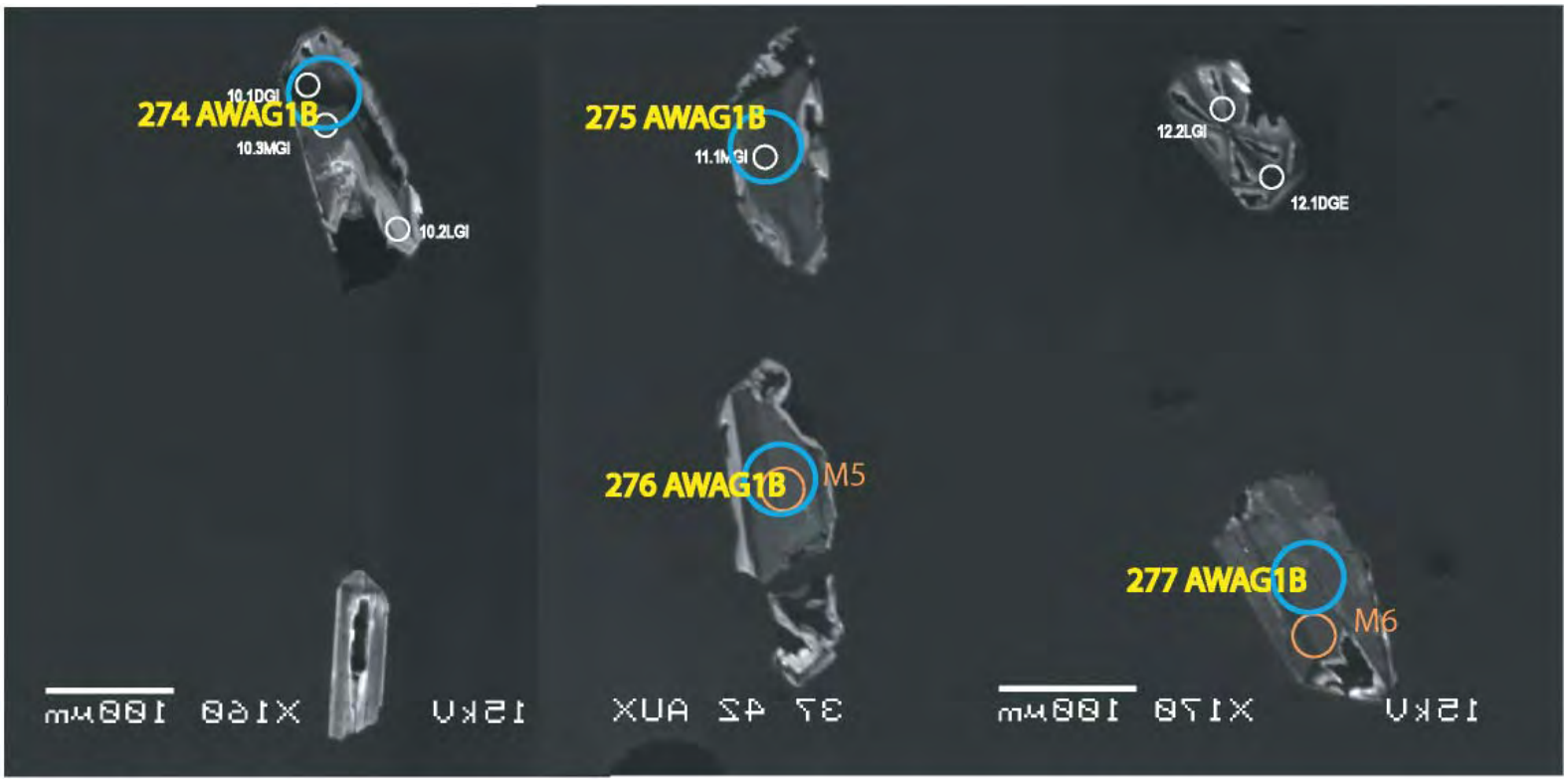
274 AWAG1B
10.1DGI
10.3MGI
10.2LGI
275 AWAG1B
11.1MGI
276 AWAG1B
M5
277 AWAG1B
M6
12.2LGI
12.1DGE

Figure G7: Zircon images for sample AWAG-1C. Trace element, Hf and O spot names and locations labeled


212AWAG1C
1.1 I
3.1 R
213AWAG1C
3.2 C
215AWAG1C
M1
2.1 E
214AWAG1C
5.1 I
4.1 R


M2
219AWAG1C
M3
220AWAG1C
221AWAG1C
217AWAG1C
216AWAG1C
218AWAG1C
222AWAG1C

Figure G8: Zircon images for sample AWAG-2. Trace element, Hf and O spot names and locations labeled

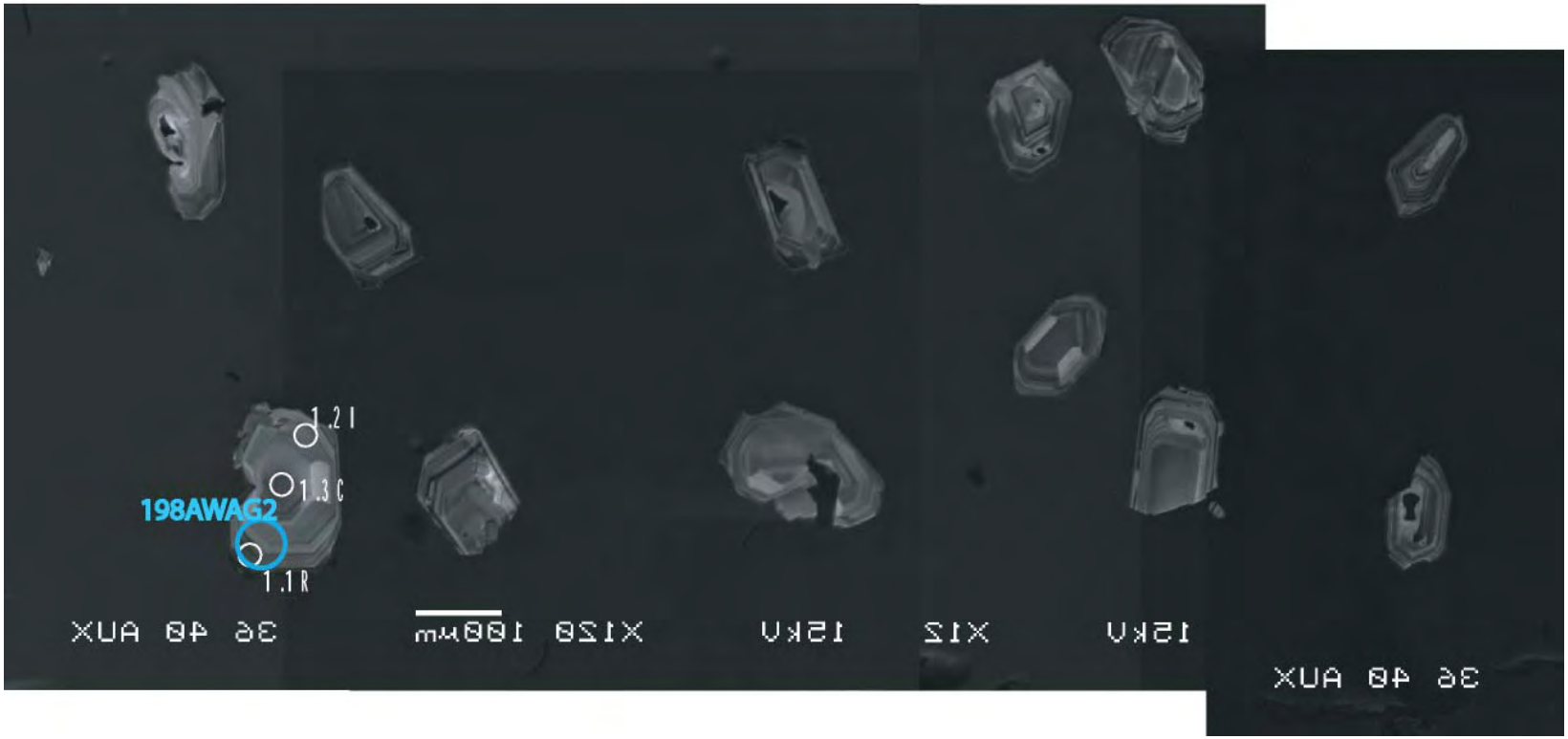
198AWAG2
1.2 I
1.3 C
1.1 R
15KV X12 15KV X120 100µm
36 40 AUX


M1
199AWAG2
15kU X120 100μm
15kU X120 100μm 36 40


202AWAG2
201AWAG2
200AWAG2
203AWAG2
204AWAG2


M3
209AWAG2
M2
208AWAG2
205AWAG2
206AWAG2
207AWAG2

Figure G9: Zircon images for sample AWAG-3. Trace element, Hf and O spot names and locations labeled


1.1C
183AWAG3
184AWAG3
1.2E1.


M1
185AWAG3
M2
2.3E
2.1C
186AWAG3
2.2I
3.2I
3.1C
187AWAG3
188AWAG3
4.1C
189AWAG3
4.2E
M4
M3
190AWAG3


5.3E
5.1C
5.2E

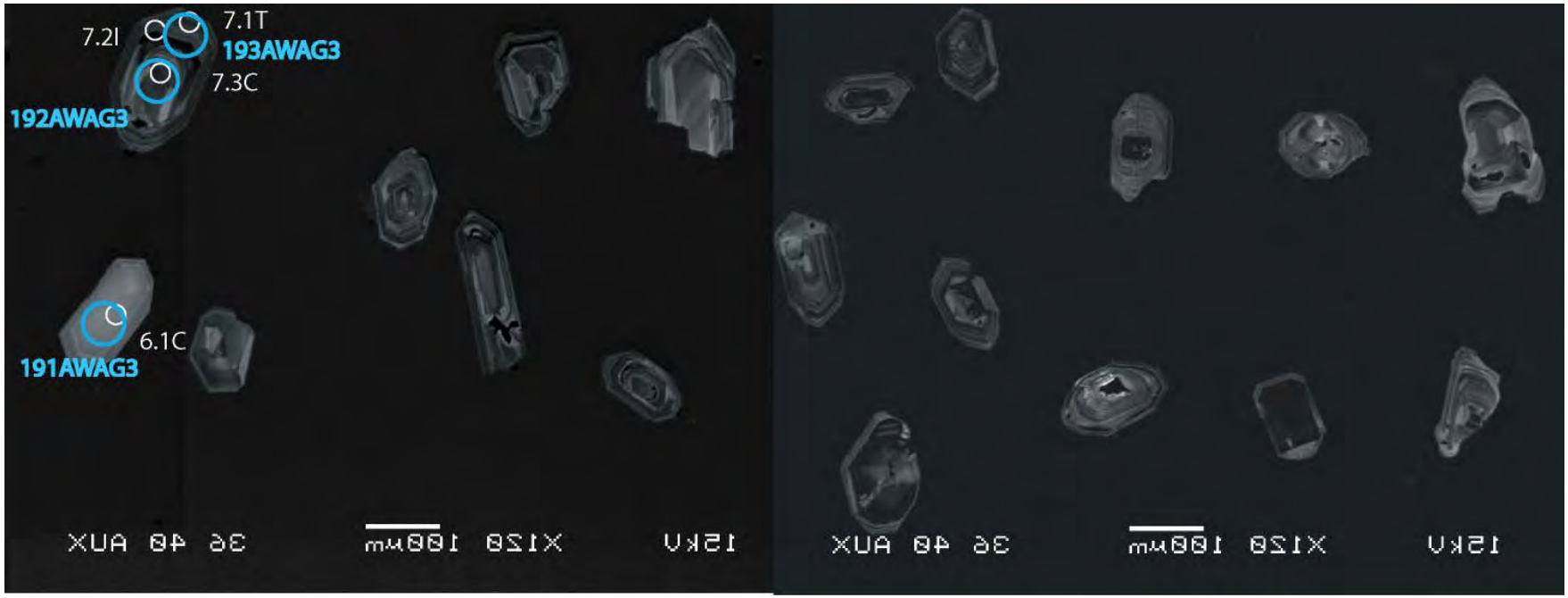
7.2I
7.1T
193AWAG3
7.3C
192AWAG3
6.1C
191AWAG3
15kV X120 100µm 36 40 AUX
15kV X120 100µm 36 40 AUX

Figure G10: Zircon images for sample AWAG-4. Trace element, Hf and O spot names and locations labeled


244 AWAG4
1.1MGI
1.2LGE
1.3DIE
2.1DGI
247 AWAG4
2.2LGIE
(labelled 3.1LGIE)
3.1LI
3.2MGI
3.3DGI
245 AWAG4
M1
246 AWAG4
M2

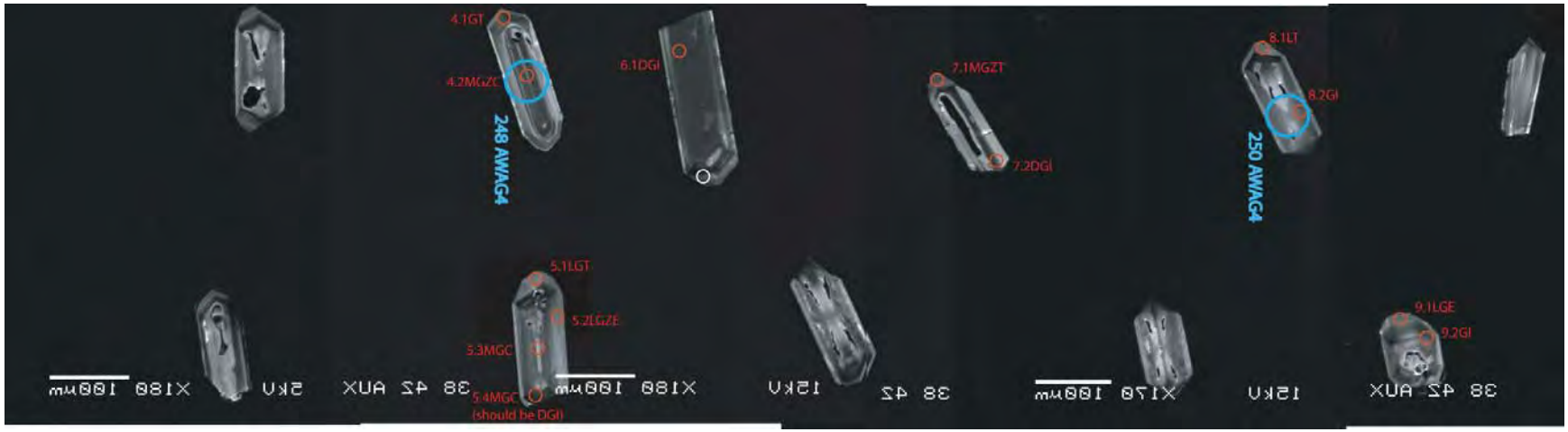
4.1GT
4.2MGZT
248 AWAG4
6.1DGI
5.1LGT
5.2LGZE
5.3MGC
5.4MGC
(should be DGI)
7.1MGZT
7.2DGI
8.1LT
8.2GI
250 AWAG4
9.1LGE
9.2GI


251 AWAG4
252 AWAG4
11.1LE
253 AWAG4
M3
254 AWAG4
M4
255 AWAG4
12.1GZI
15kV
X250 100nm
38 42 AUX

256 AWAG4
M5
257 AWAG4
M6
38 46 AUX
X130 100nm
15kU
38 46 AUX
X170 100nm
15kU

Figure G11: Zircon images for sample AWAG-5. Trace element, Hf and O spot names and locations labeled

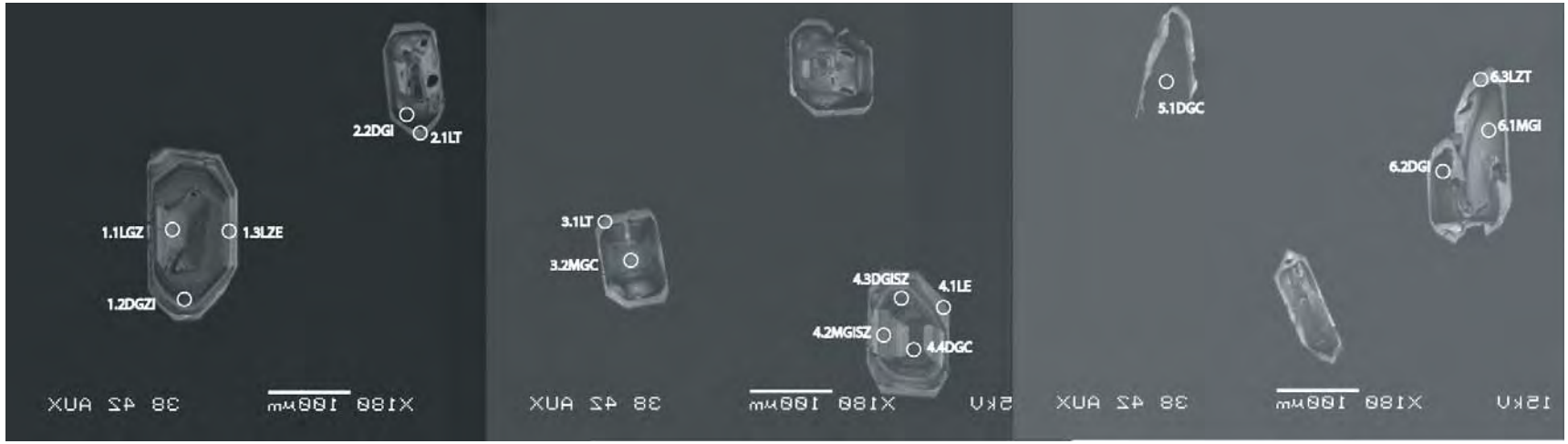
2.2DGI
2.1LT
1.1LGZ
1.3LZE
1.2DGZJ
3.1LT
3.2MGC
4.3DGISZ
4.1LE
4.2MGISZ
4.4DGC
5.1DGC
6.3LZT
6.1MGI
6.2DGI

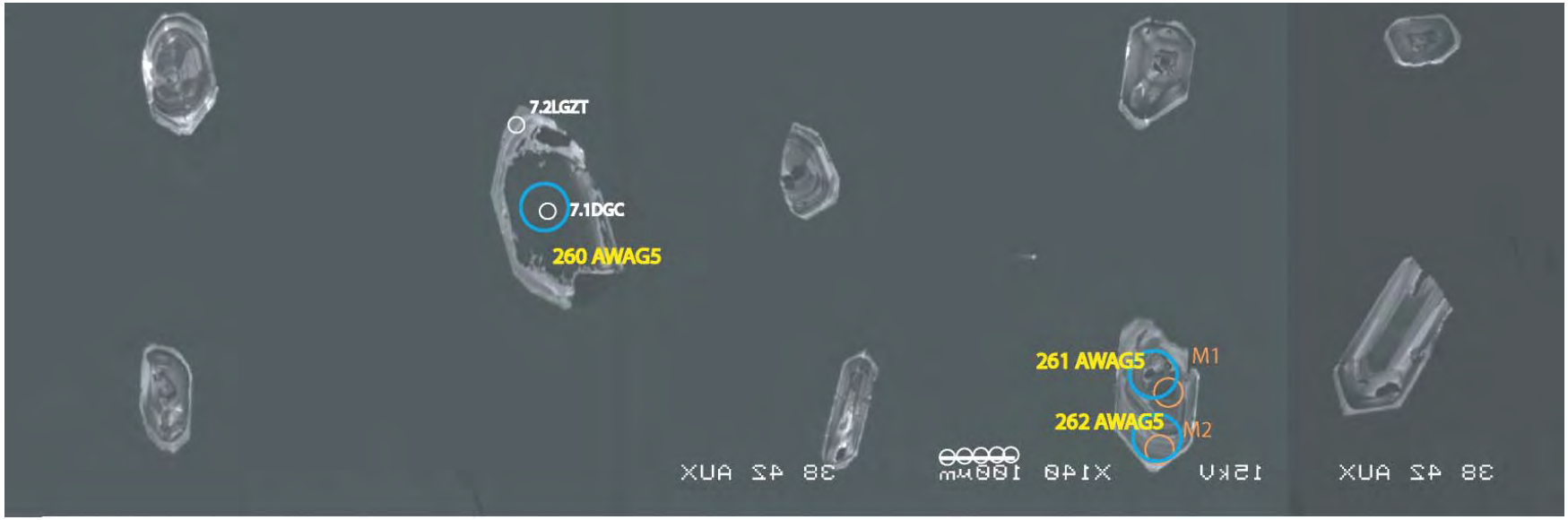
7.2LGZT
7.1DGC
260 AWAG5
261 AWAG5
M1
262 AWAG5
M2


M3
264 AWAG5
8.1LGI
8.2GI
263 AWAG5
10.2MGI
10.1LGT
9.1LE
9.2DGIZ
M4
M5
265 AWAG5
11.1LGE
11.2DGZI
12.1DGZC

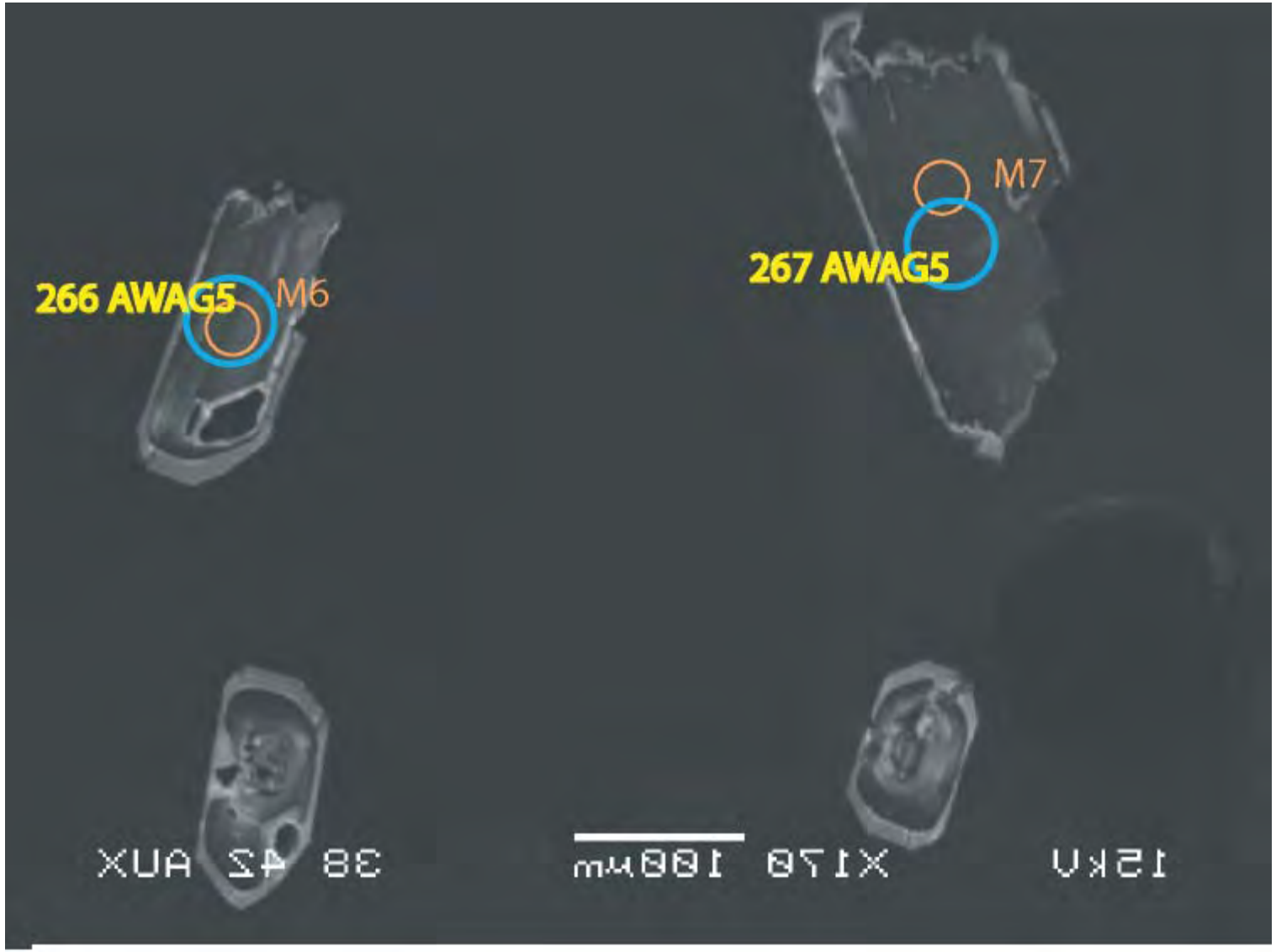
266 AWAG5
M6
267 AWAG5
M7
15kV X170 100µm 38 42 AUX

Figure G12: Zircon images for sample AWAG-6. Trace element, Hf and O spot names and locations labeled


M2
M1
166 AWAG6
M4
M3
167 AWAG6
1.1R
169 AWAG6
1.2C
2.1C
168 AWAG6

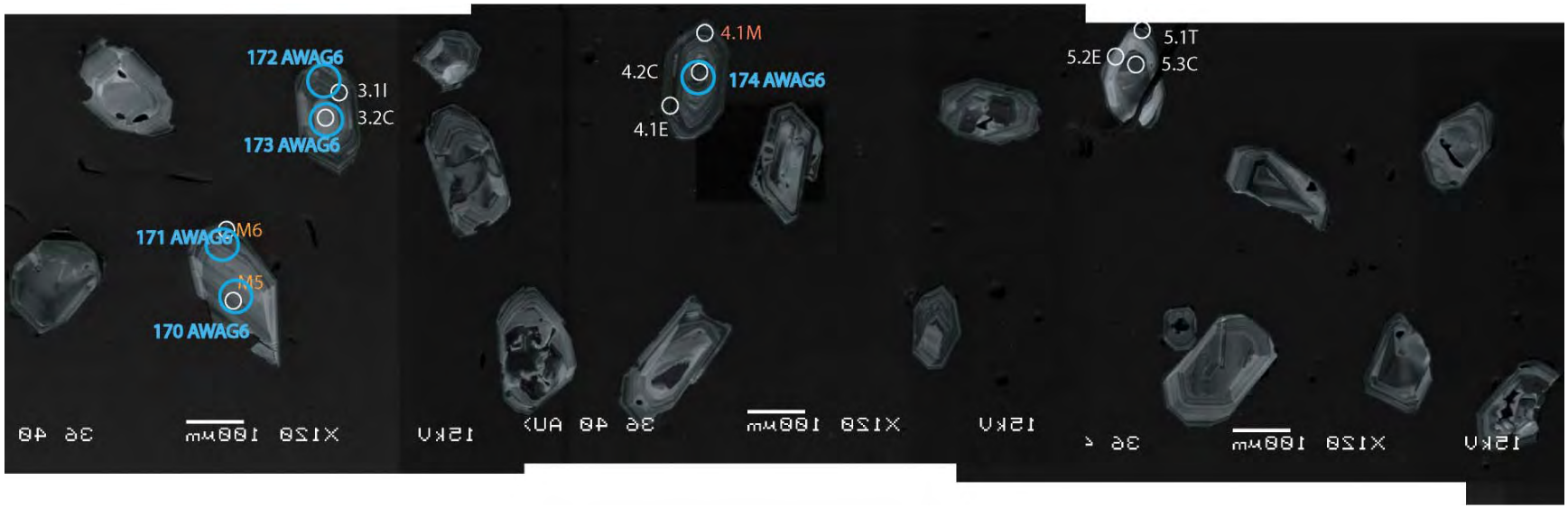
172 AWAG6
3.1I
3.2C
173 AWAG6
171 AWAG6
M6
M5
170 AWAG6
4.1M
4.2C
174 AWAG6
4.1E
5.1T
5.2E
5.3C

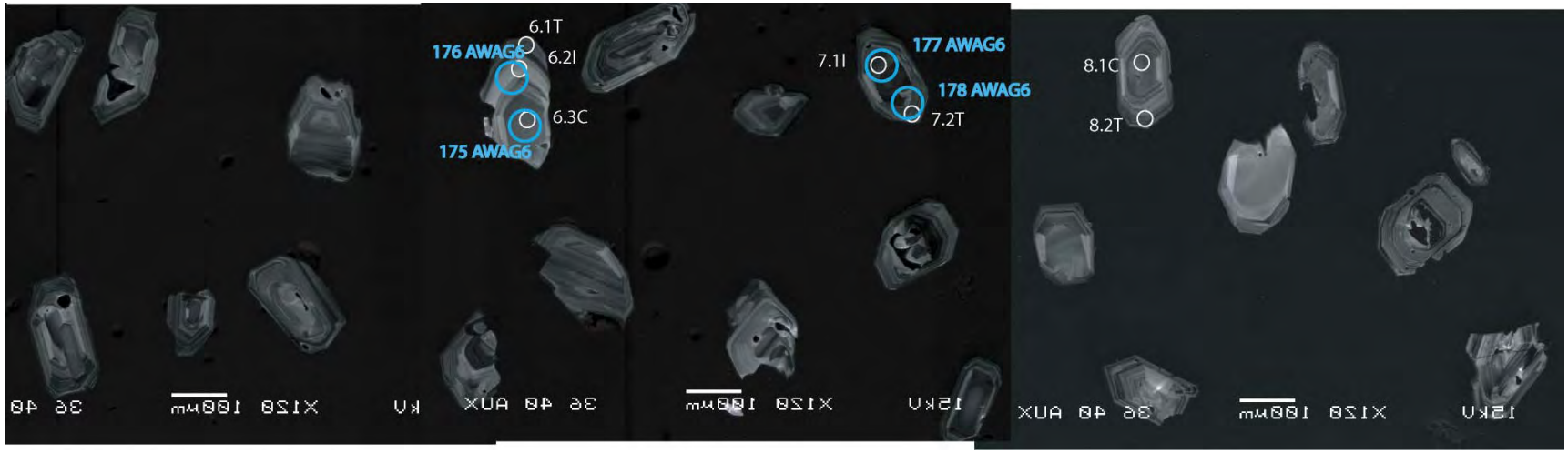
6.1T
176 AWAG6
6.2I
6.3C
175 AWAG6
7.1I
177 AWAG6
178 AWAG6
7.2T
8.1C
8.2T

Figure G13: Zircon images for sample AWAG-7. Trace element, Hf and O spot names and locations labeled

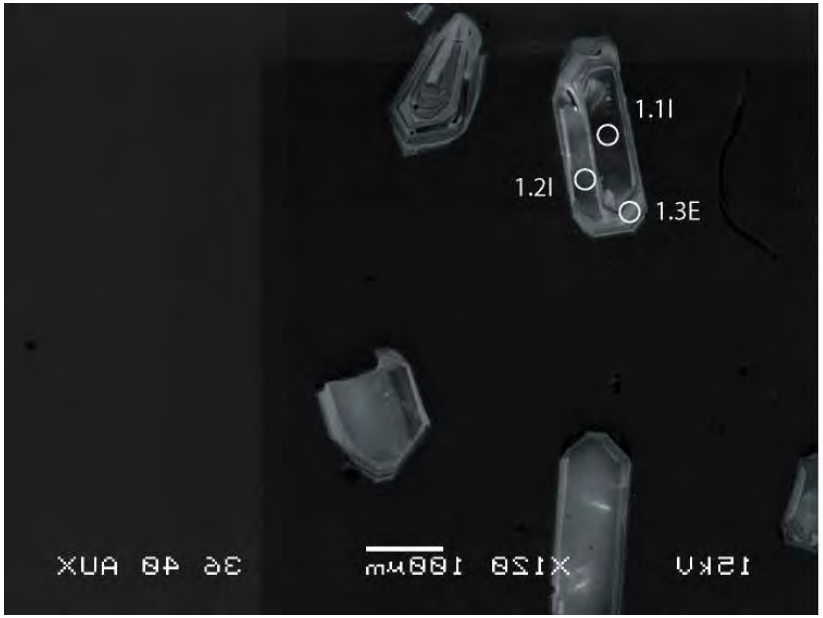
1.1I
1.2I
1.3E


150 AWAG7
2.3I
152 AWAG7
M2
149 AWAG7
2.2C
M1
2.1T
148 AWAG7
151 AWAG7

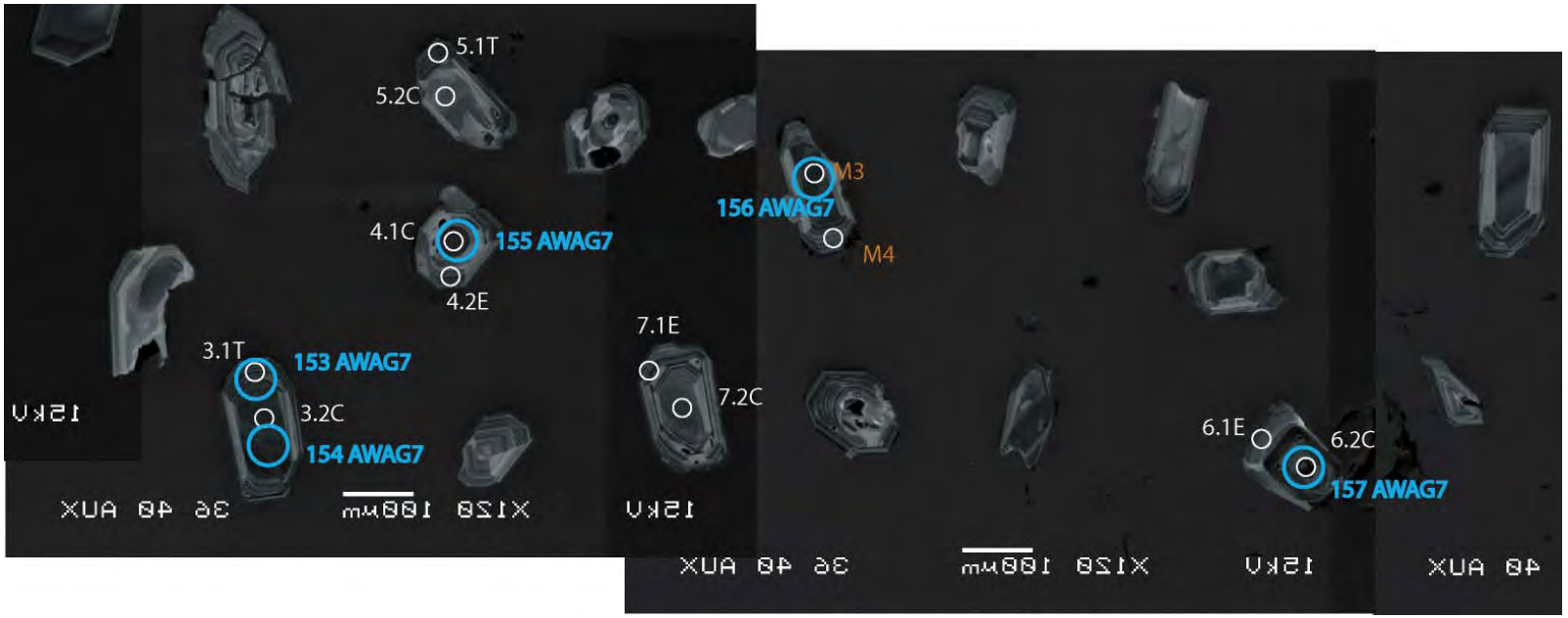
5.1T
5.2C
4.1C
155 AWAG7
4.2E
3.1T
153 AWAG7
3.2C
154 AWAG7
7.1E
7.2C
M3
156 AWAG7
M4
6.1E
6.2C
157 AWAG7

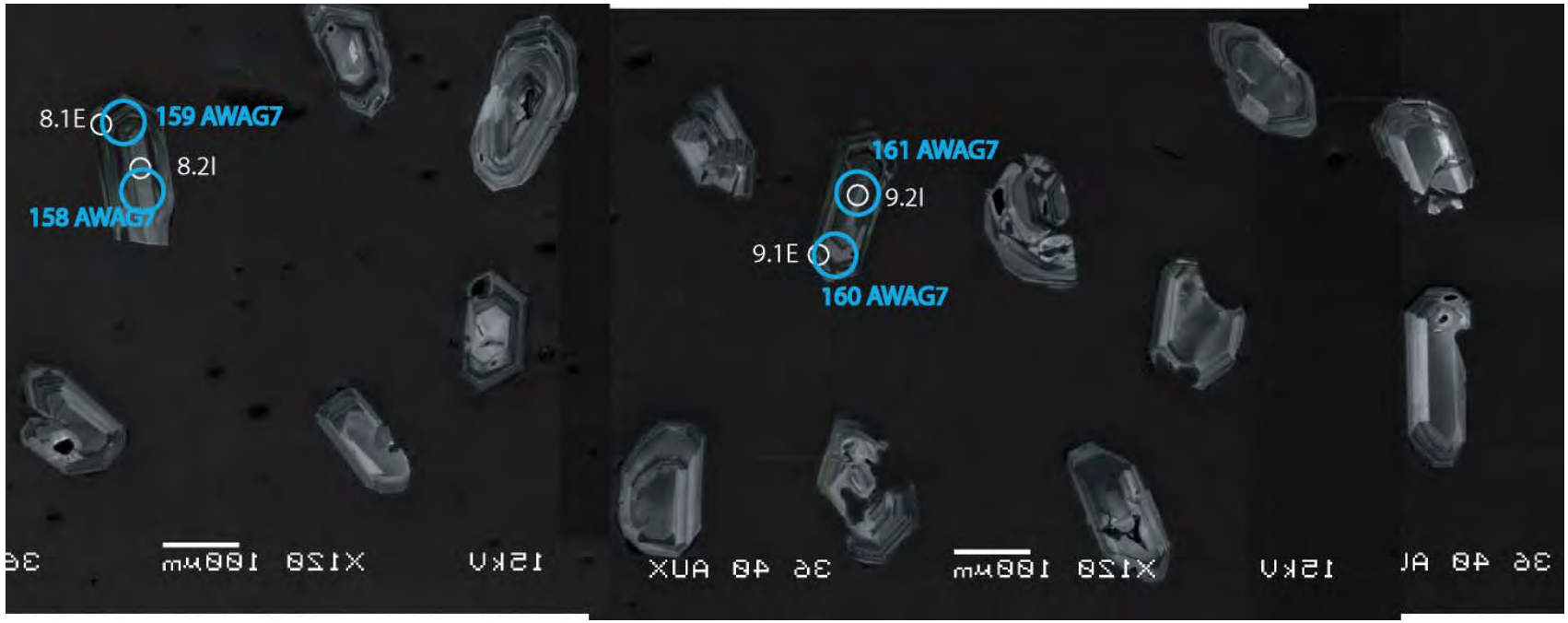
8.1E
159 AWAG7
8.2I
158 AWAG7
161 AWAG7
9.2I
9.1E
160 AWAG7

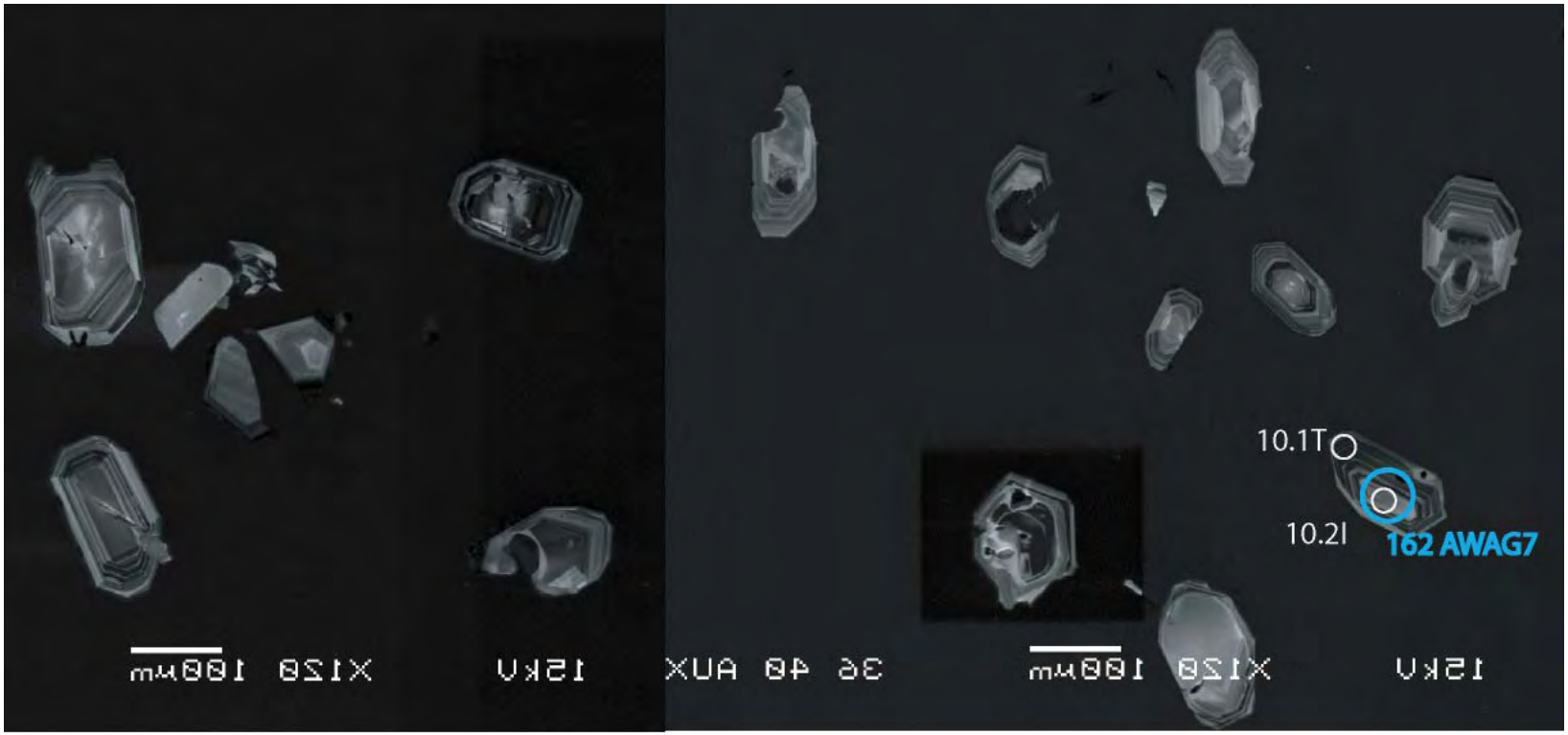
10.1T
10.2I
162 AWAG7

Figure G14: Zircon images for sample AWM-1. Trace element, age, Hf and O spot names and locations labeled

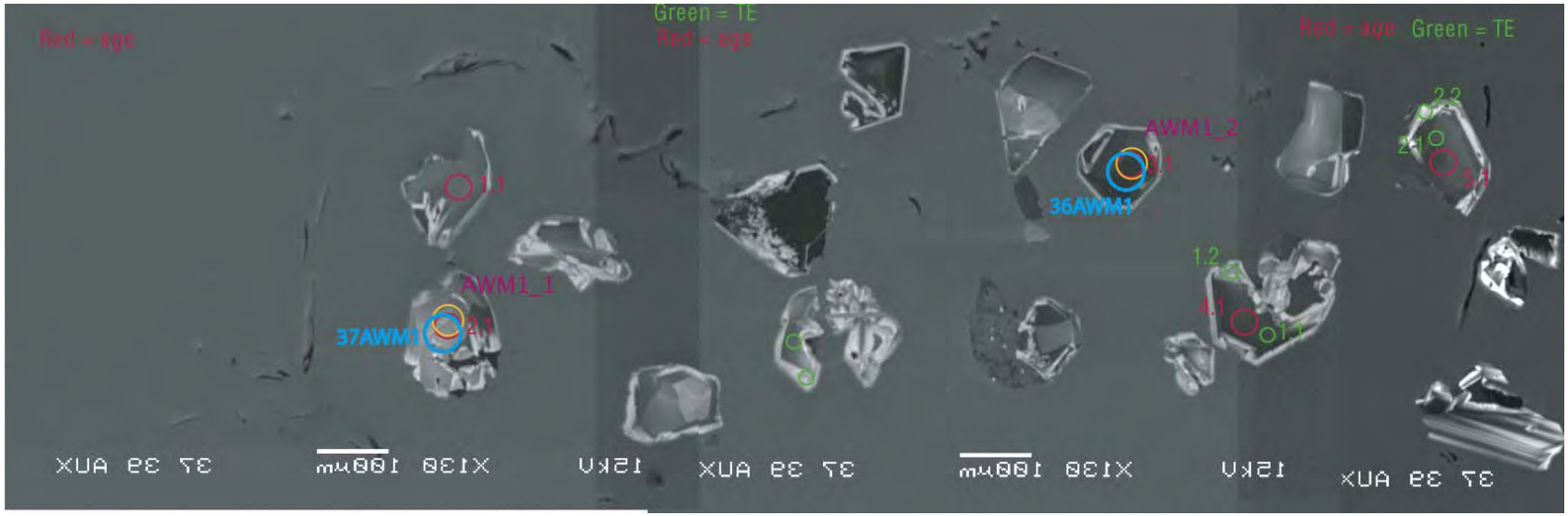
Red = age
1.1
AWM1_1
37AWM1
2.1
Green = TE
Red = age
AWM1_2
3.1
36AWM1
Red = age
Green = TE
2.2
2.1
5.1
1.2
4.1
1.1

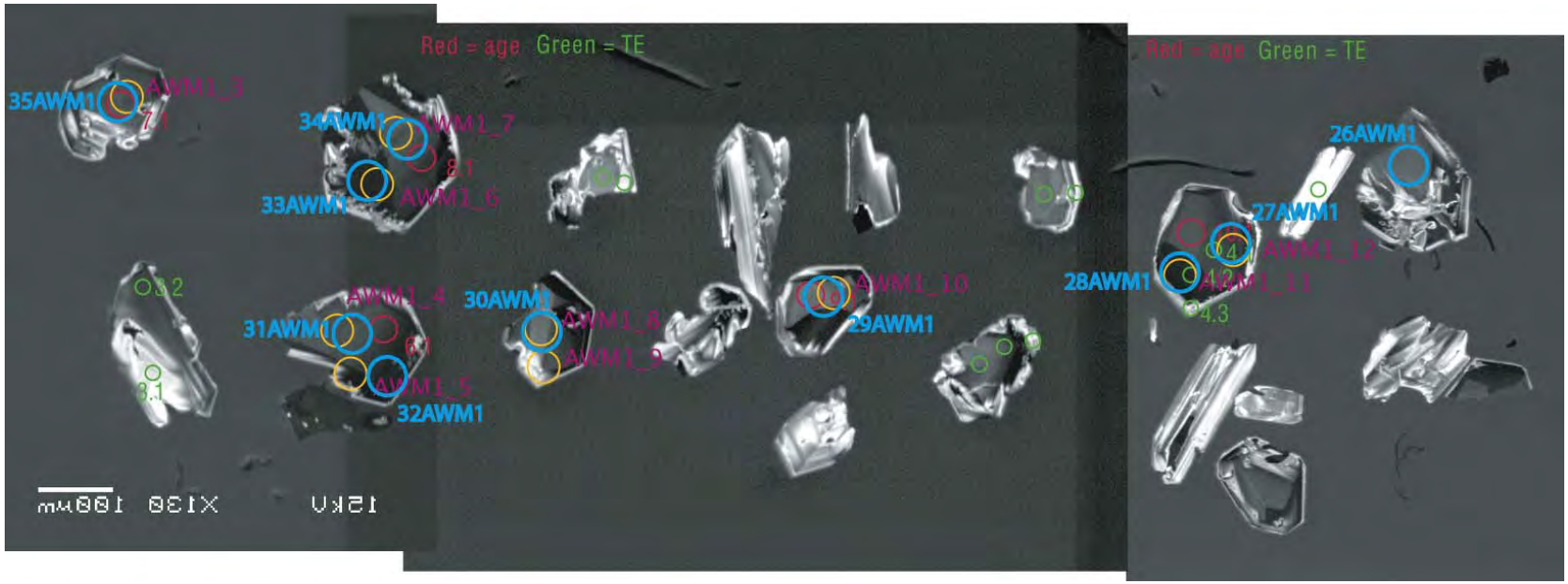
Red = age Green = TE
35AWM1
AWM1_3
7.1
34AWM1
AWM1_7
8.1
33AWM1
AWM1_6
3.2
31AWM1
AWM1_4
6.1
AWM1_5
32AWM1
3.1
30AWM1
AWM1_8
AWM1_9
AWM1_10
29AWM1
Red = age Green = TE
26AWM1
27AWM1
AWM1_12
28AWM1
AWM1_11
4.3

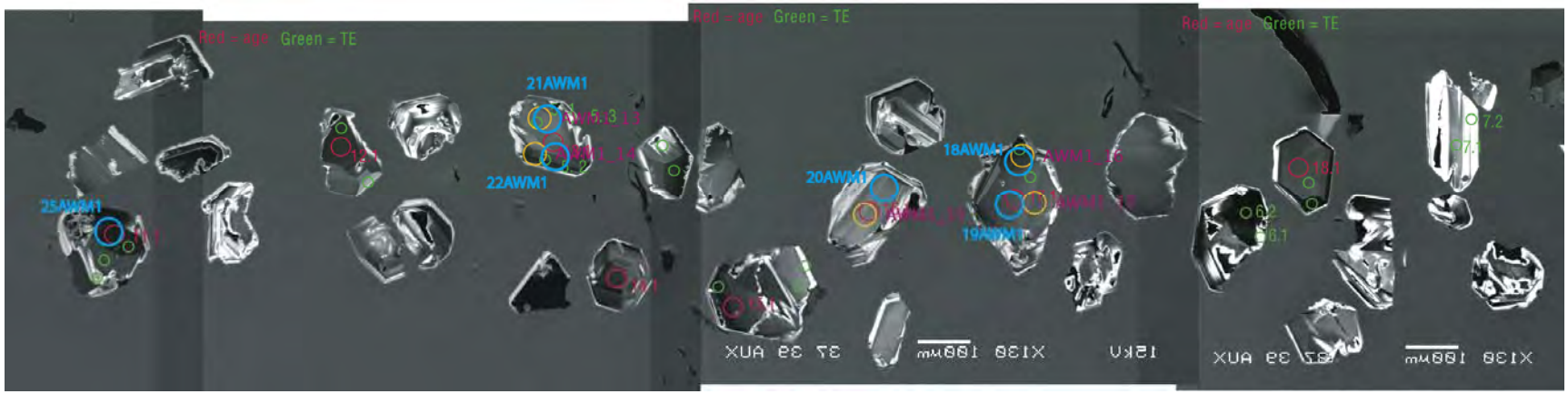
Red = age Green = TE
25AWM1
21AWM1
22AWM1
Red = age Green = TE
20AWM1
18AWM1
19AWM1
Red = age Green = TE
18.1
7.2
6.2
6.1


Red = age Green = TE
Green = TE
15AWM1
AWM1_19
16AWM1
AWM1_20
AWM1_18
14AWM1
17AWM1
13AWM1
9.2

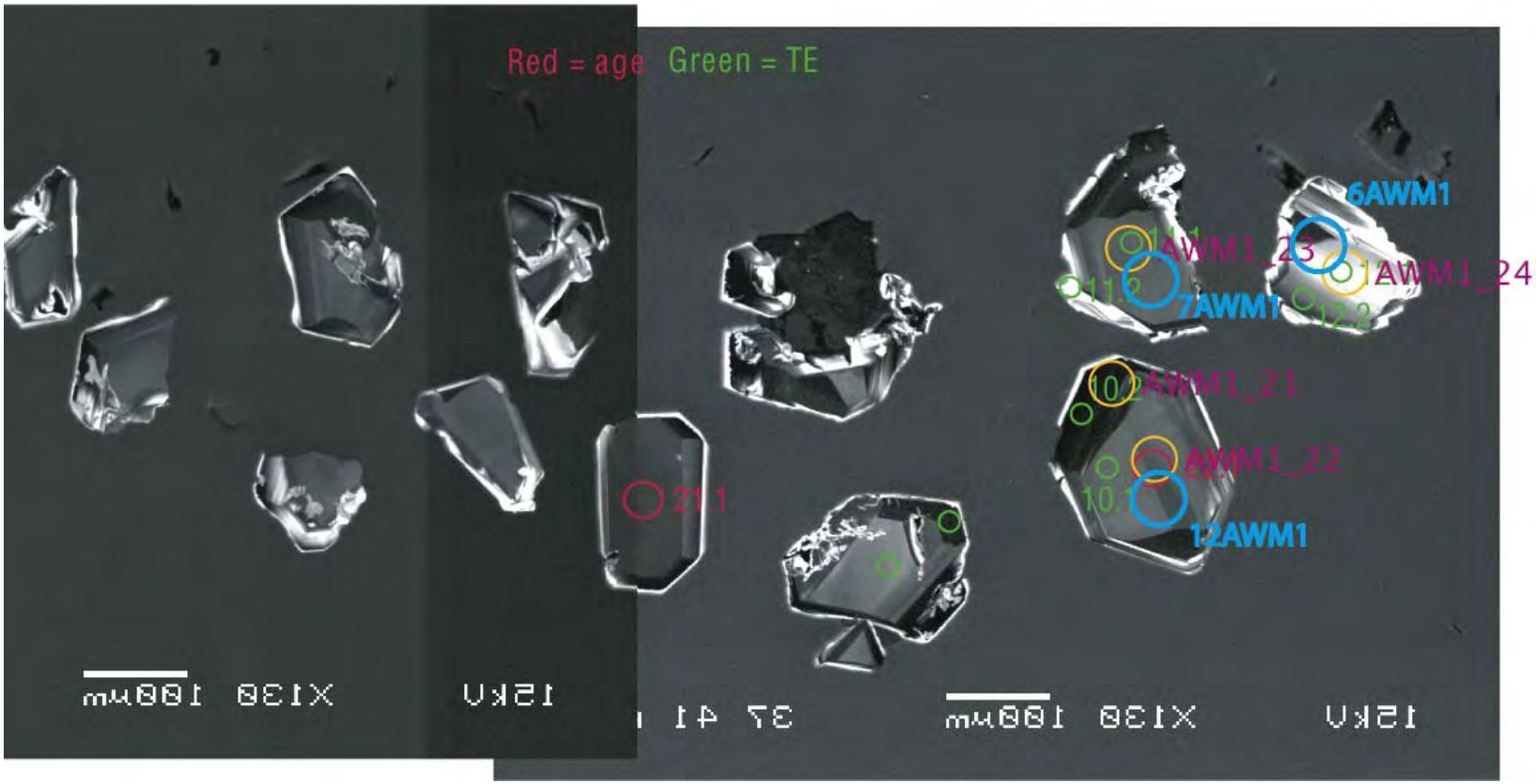
Red = age
Green = TE
6AWM1
7AWM1
12AWM1
211

Figure G14: Zircon images for sample AWM-2. Trace element, age, Hf and O spot names and locations labeled

SC045
SC046
SC047
SC048

SC003
SC001
SC002

SC013
SC014
SC012
SC011
SC043
SC010
SC044
SC009

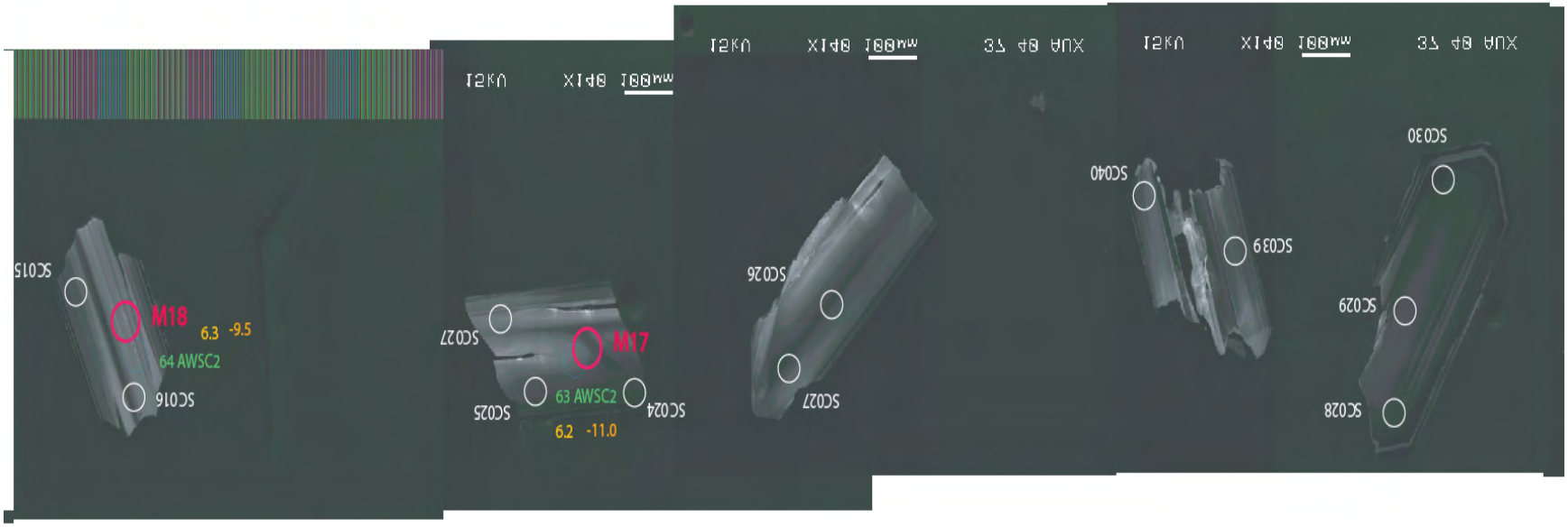
SC015
M18
6.3 -9.5
64 AWSC2
SC016
SC027
M17
SC025
63 AWSC2
6.2 -11.0
SC024
SC026
SC027
SC040
SC039
SC030
SC029
SC028

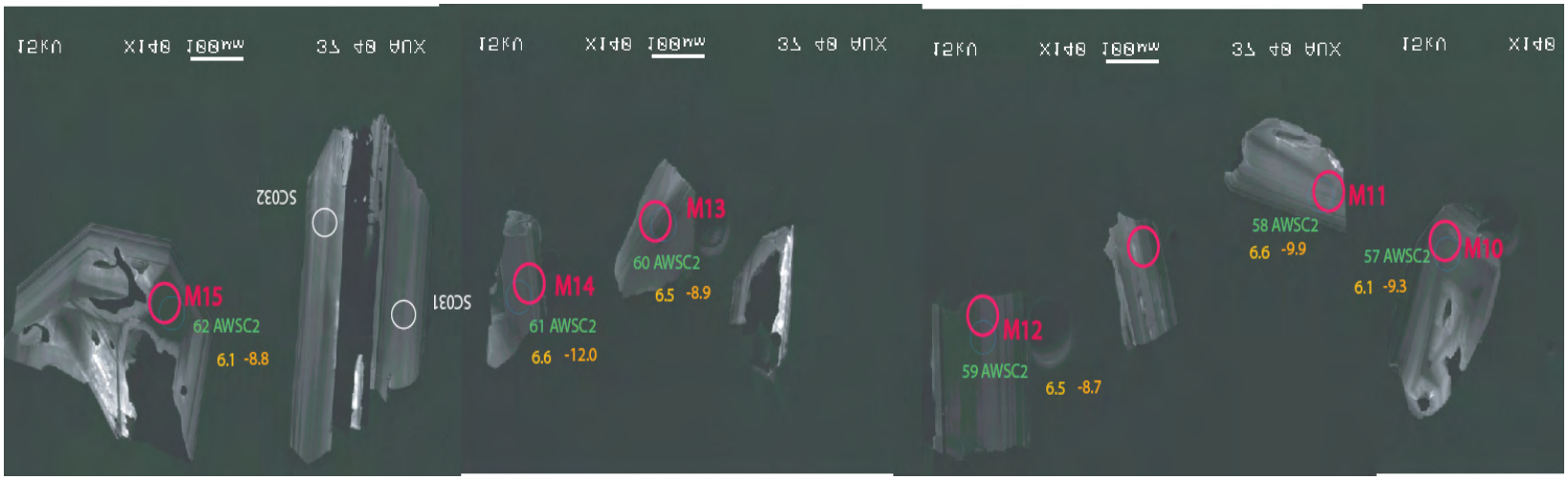
M15
62 AWSC2
6.1 -8.8
SC032
SC031
M14
61 AWSC2
6.6 -12.0
M13
60 AWSC2
6.5 -8.9
M12
59 AWSC2
6.5 -8.7
M11
58 AWSC2
6.6 -9.9
M10
57 AWSC2
6.1 -9.3

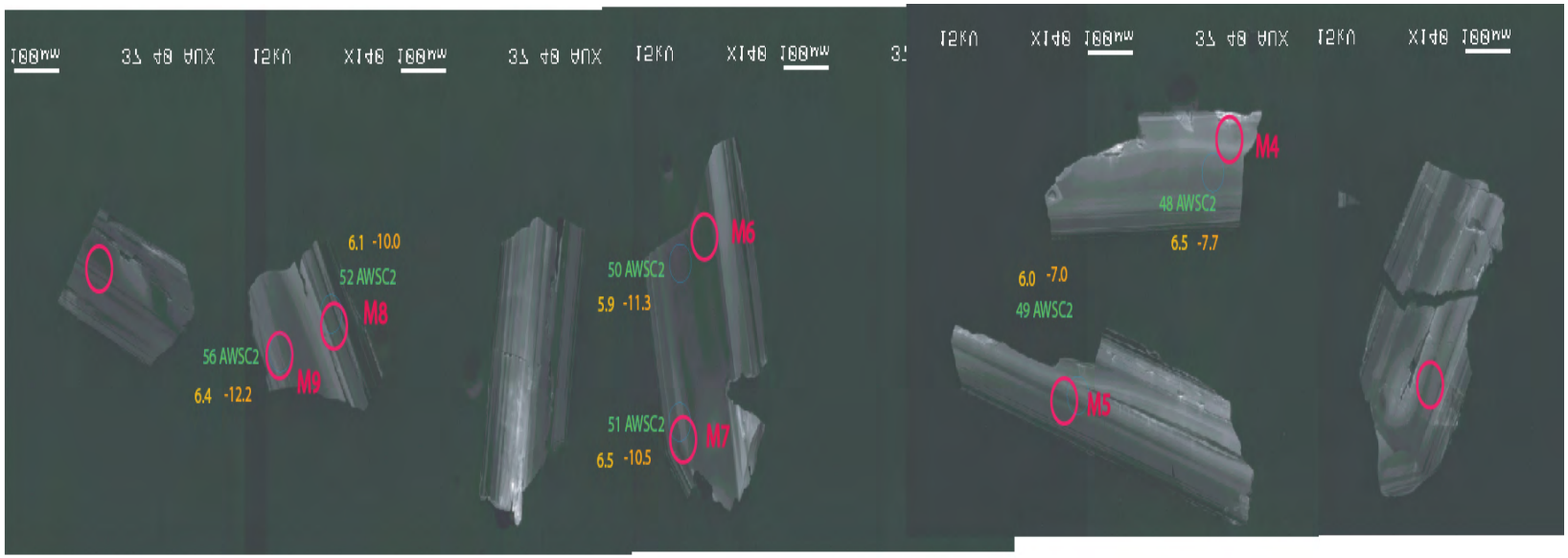
M4
48 AWSC2
6.5 -7.7
6.0 -7.0
49 AWSC2
M5
M6
50 AWSC2
5.9 -11.3
M7
51 AWSC2
6.5 -10.5
6.1 -10.0
52 AWSC2
M8
56 AWSC2
M9
6.4 -12.2


47 AWSC2
M3
46 AWSC2
6.2 -8.6
44 AWSC2
5.9 -9.4
M1
45 AWSC2
6.2
-10.0
M2

Appendix H

Back-scatter Electron Imaging of Sphene

Figure H1. Back-scatter Electron Imaging of AWAG-1A

Red spots and numbers indicate spot location and name
Yellow text indicates Zr-in-sphene thermometry temperatures (above) and Zr concentrations (lower)

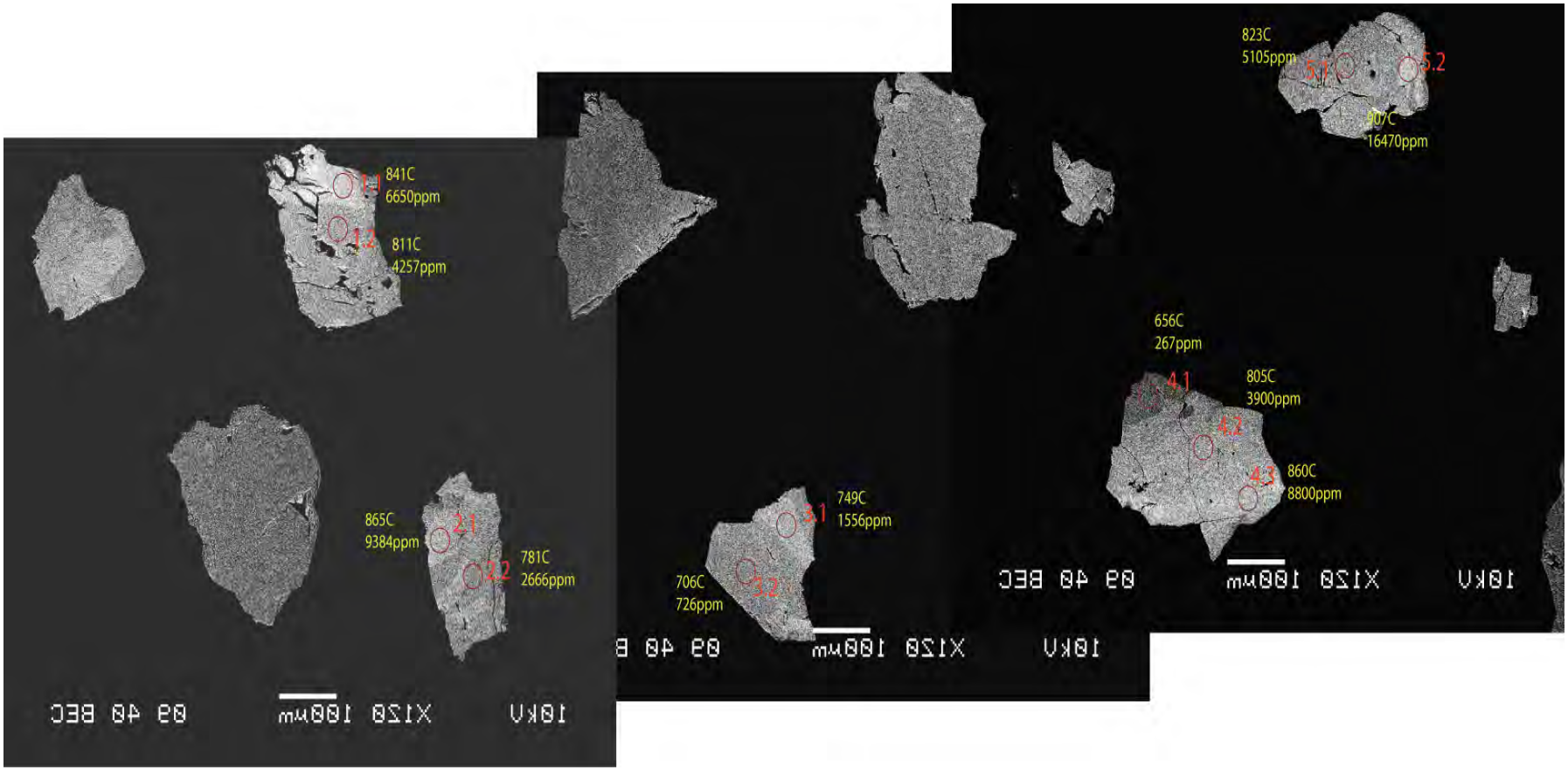
841C
6650ppm
1.1
1.2
811C
4257ppm
865C
9384ppm
2.1
2.2
781C
2666ppm
749C
1556ppm
3.1
706C
726ppm
3.2
656C
267ppm
4.1
805C
3900ppm
4.2
4.3
860C
8800ppm
823C
5105ppm
5.1
5.2
16470ppm
10kV X120 100µm 03 40 BEC

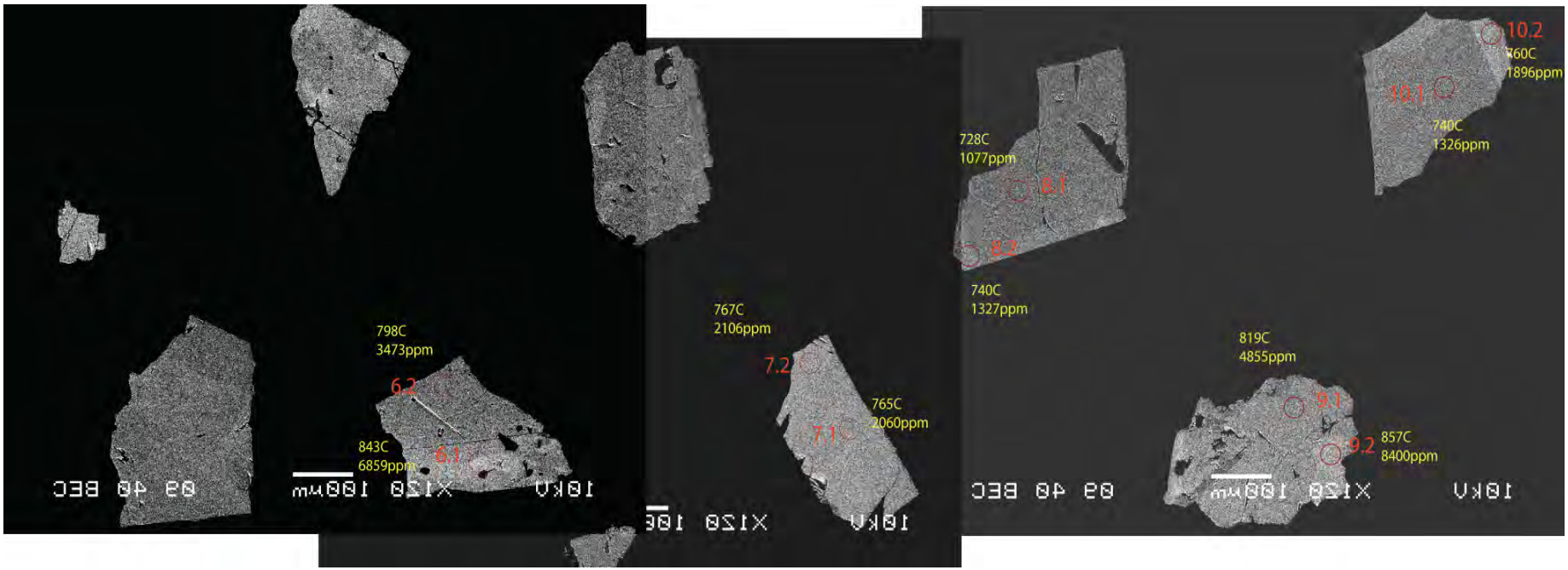
798C
3473ppm
6.2
843C
6859ppm
6.1
767C
2106ppm
7.2
765C
2060ppm
7.1
728C
1077ppm
8.1
8.2
740C
1327ppm
819C
4855ppm
9.1
9.2
857C
8400ppm
10.2
760C
1896ppm
10.1
740C
1326ppm

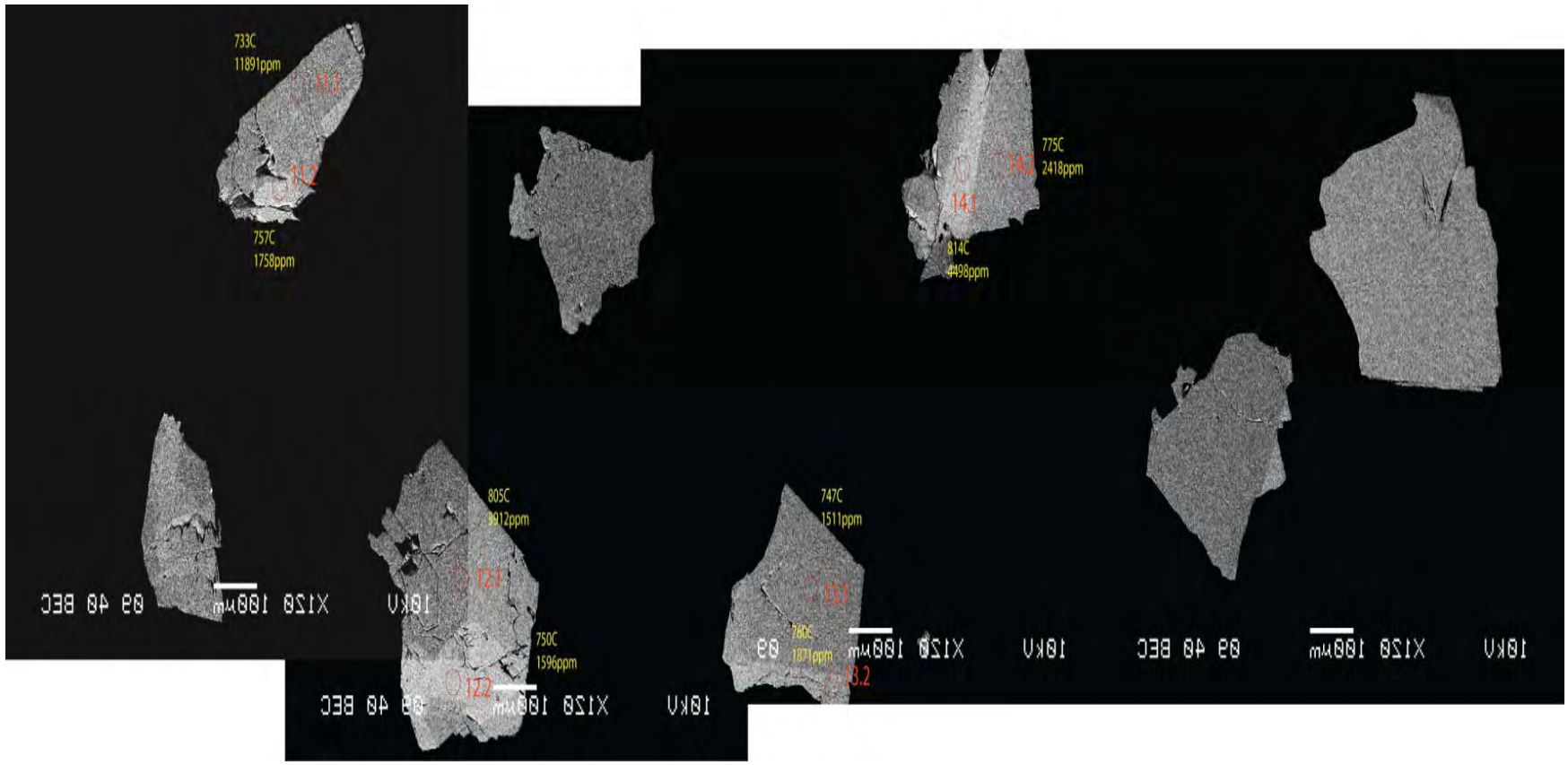
733C
11891ppm
11.1
11.2
757C
1758ppm
805C
9912ppm
12.1
12.2
750C
1596ppm
747C
1511ppm
13.1
13.2
775C
2418ppm
14.2
14.1
814C
4498ppm
10KV X120 100µm 09 40 BEC

Figure H2. Back-scatter Electron Imaging of AWAG-1B

Red spots and numbers indicate spot location and name
Yellow text indicates Zr-in-sphene thermometry temperatures (above) and Zr concentrations (lower)

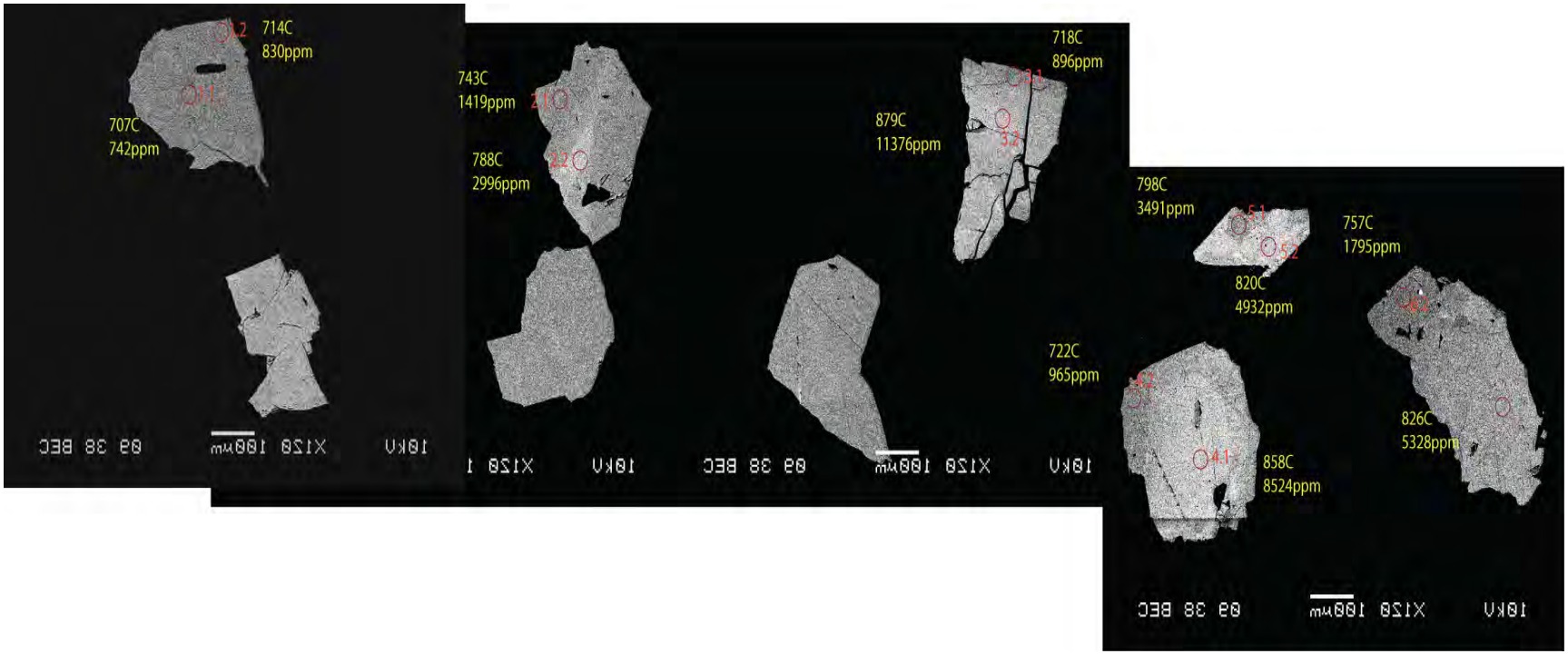
714C
830ppm
707C
742ppm
743C
1419ppm
788C
2996ppm
718C
896ppm
879C
11376ppm
798C
3491ppm
757C
1795ppm
820C
4932ppm
722C
965ppm
826C
5328ppm
858C
8524ppm

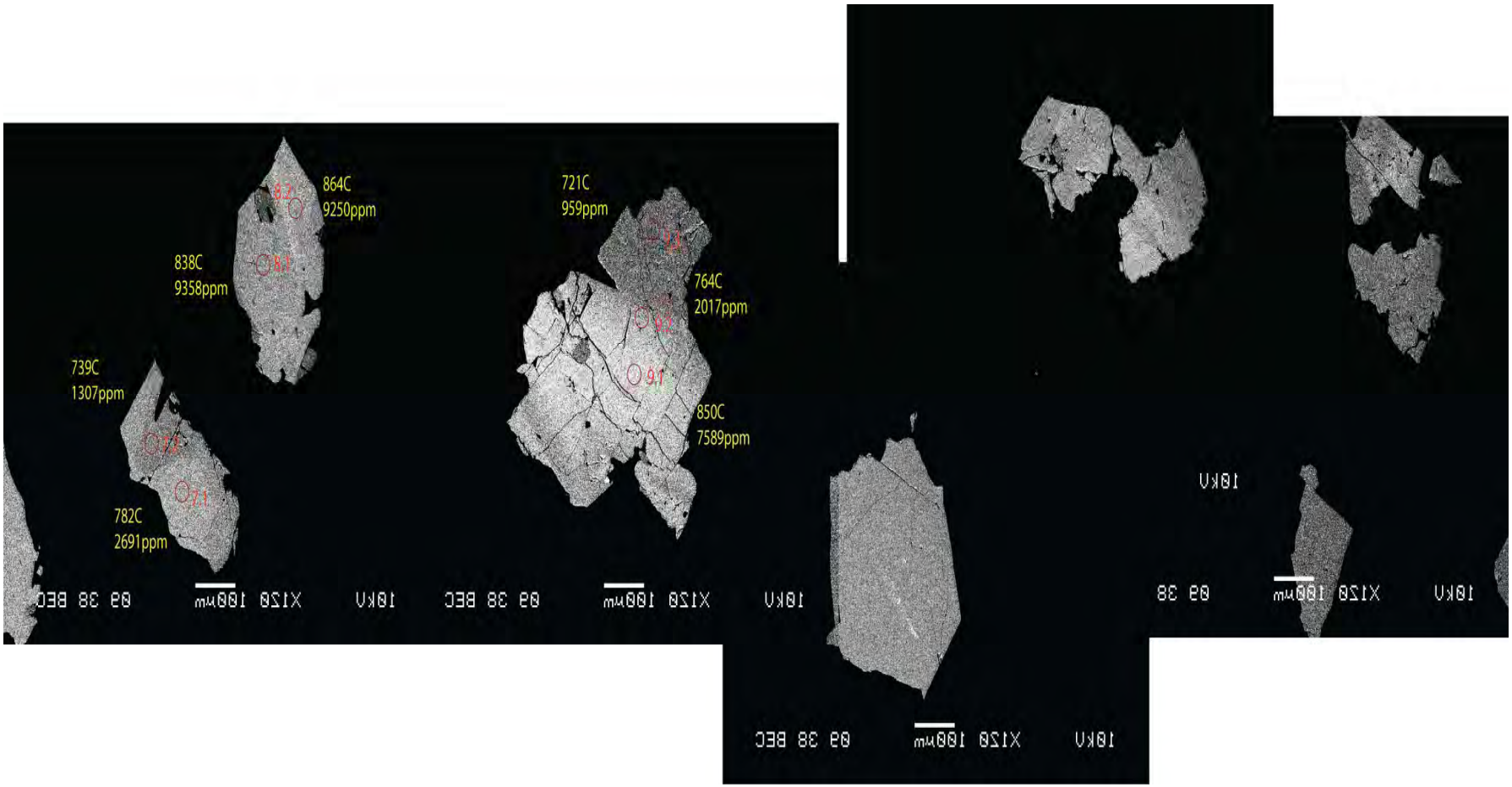
864C
9250ppm
838C
9358ppm
739C
1307ppm
782C
2691ppm
721C
959ppm
764C
2017ppm
850C
7589ppm
10kV X120 100µm 09 38 BEC

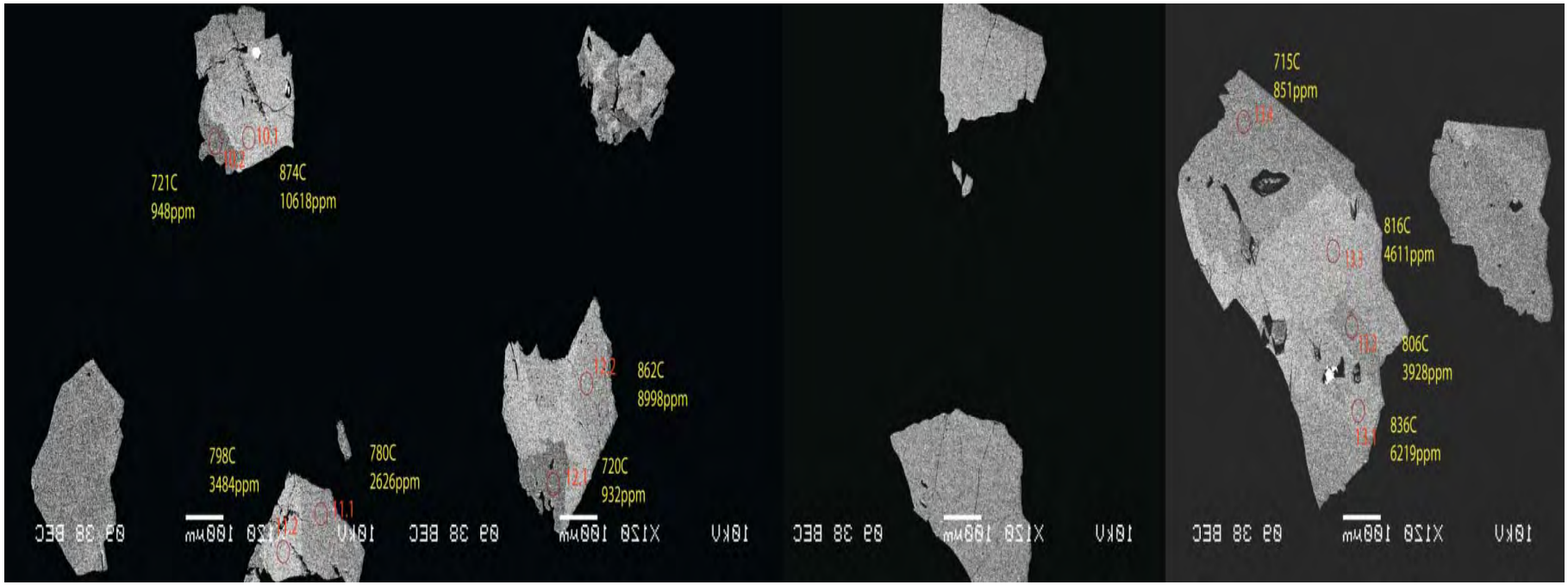
721C
948ppm
874C
10618ppm
862C
8998ppm
798C
3484ppm
780C
2626ppm
720C
932ppm
715C
851ppm
816C
4611ppm
806C
3928ppm
836C
6219ppm

Figure H3. Back-scatter Electron Imaging of AWAG-2

Red spots and numbers indicate spot location and name
Yellow text indicates Zr-in-sphene thermometry temperatures (above) and Zr concentrations (lower)

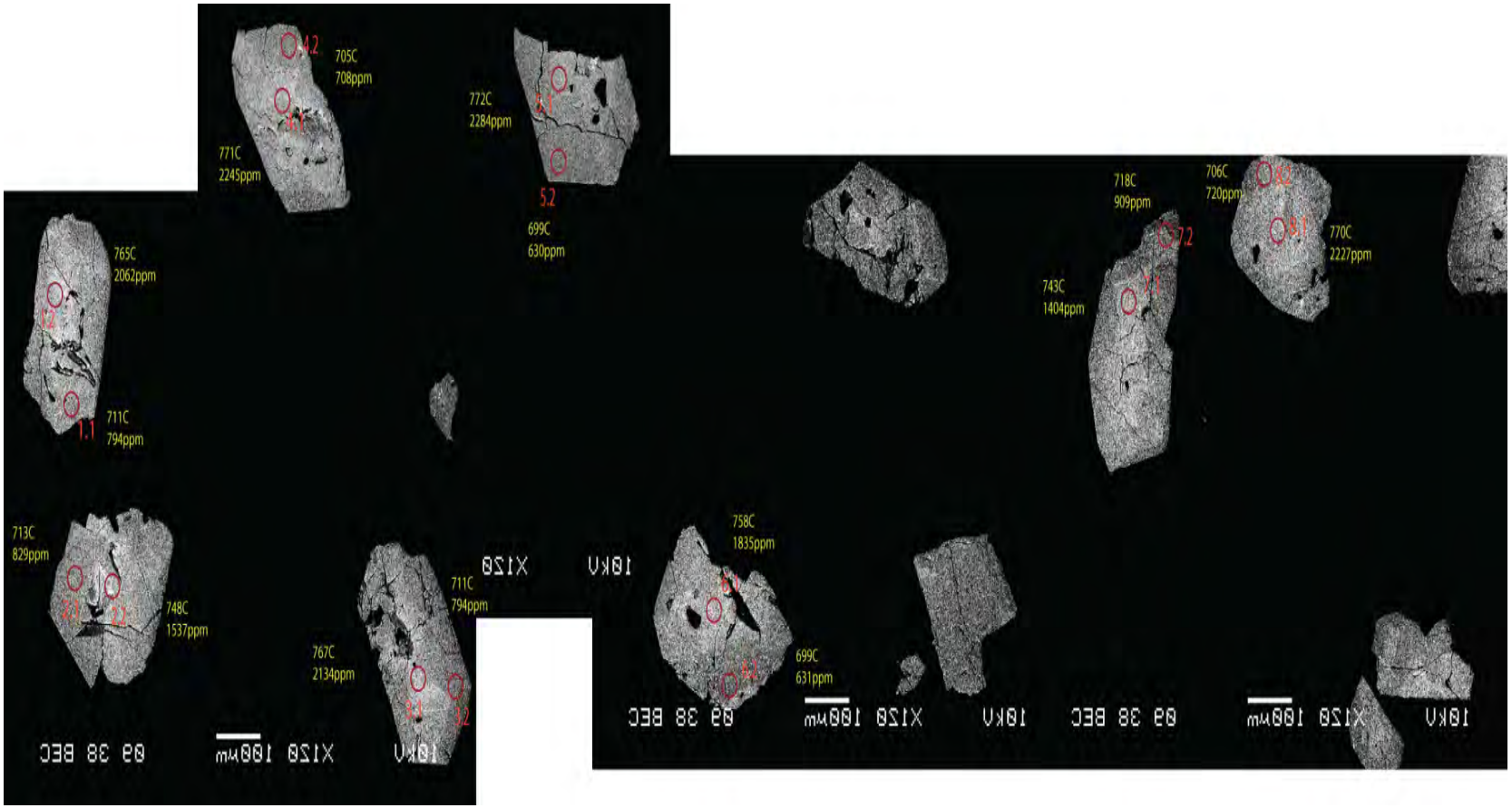
705C
708ppm
4.2
4.1
771C
2245ppm
772C
2284ppm
5.1
5.2
699C
630ppm
765C
2062ppm
1.2
1.1
711C
794ppm
713C
829ppm
2.1
2.2
748C
1537ppm
767C
2134ppm
3.1
3.2
711C
794ppm
X120
10kV
758C
1835ppm
6.1
6.2
699C
631ppm
718C
909ppm
7.2
7.1
743C
1404ppm
706C
720ppm
8.2
8.1
770C
2227ppm
09 38 BEC
X120 100µm
10kV

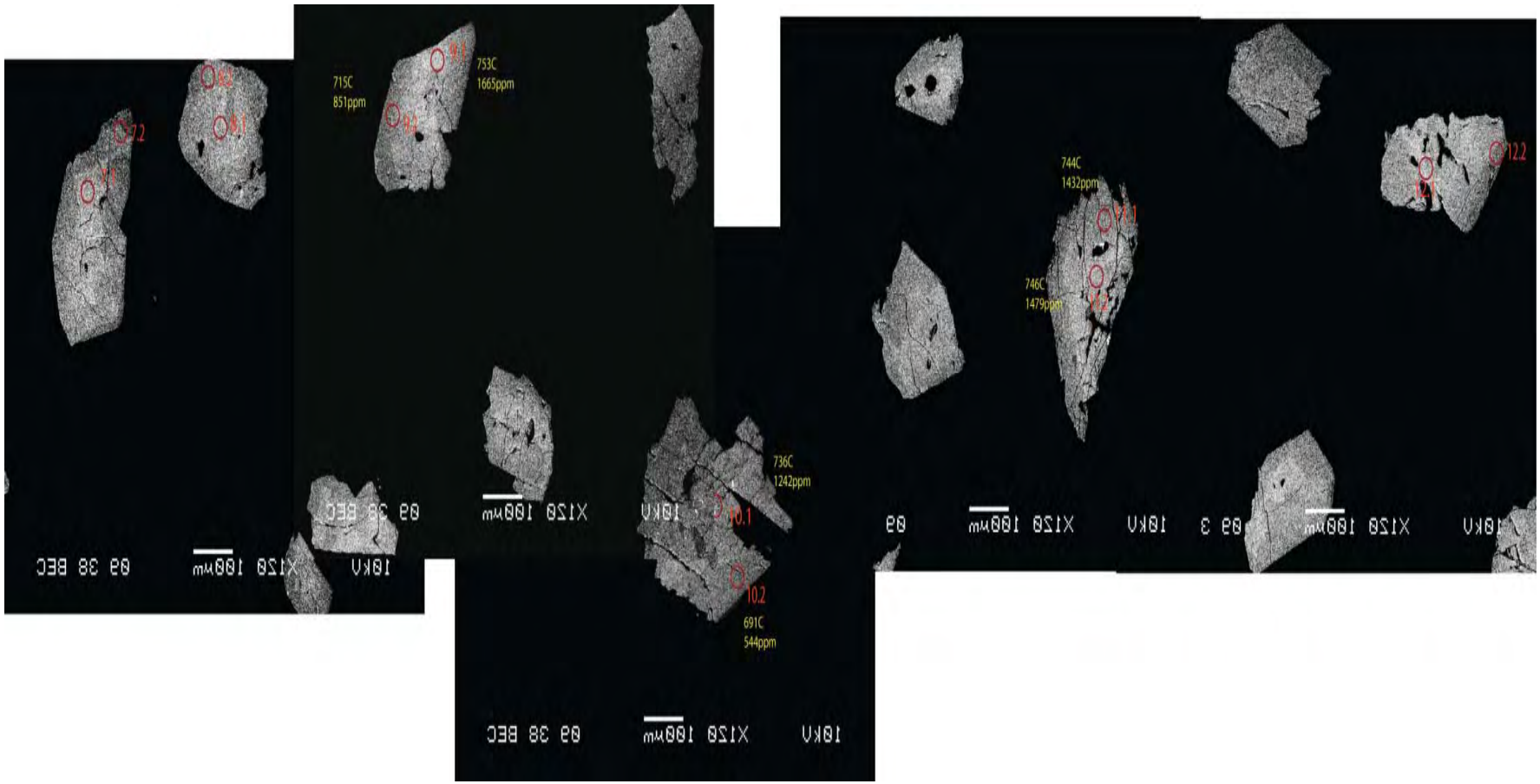
715C
851ppm
753C
1665ppm
744C
1432ppm
746C
1479ppm
736C
1242ppm
691C
544ppm

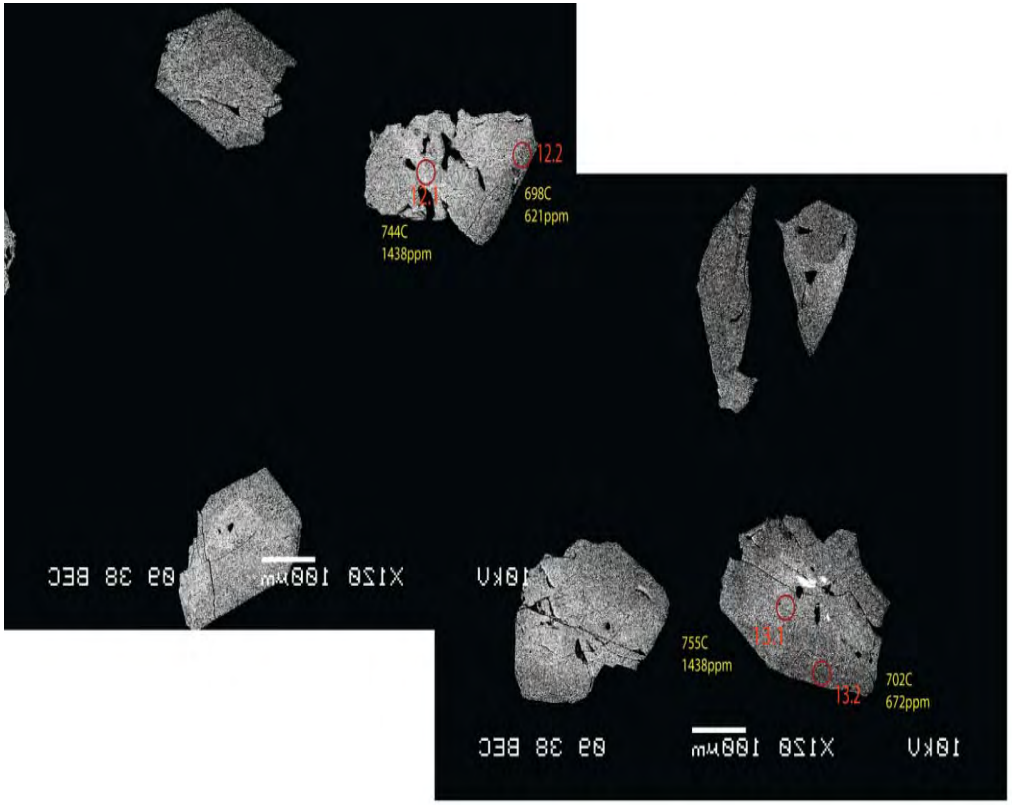
12.2
12.1
744C
1438ppm
698C
621ppm
13.1
13.2
755C
1438ppm
702C
672ppm

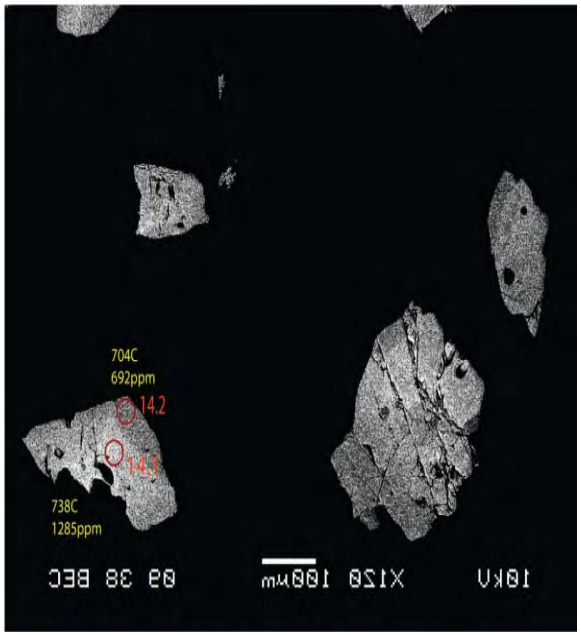
704C
692ppm
14.2
14.1
738C
1285ppm

Figure H4. Back-scatter Electron Imaging of AWAG-3

Red spots and numbers indicate spot location and name
Yellow text indicates Zr-in-sphene thermometry temperatures (above) and Zr concentrations (lower)

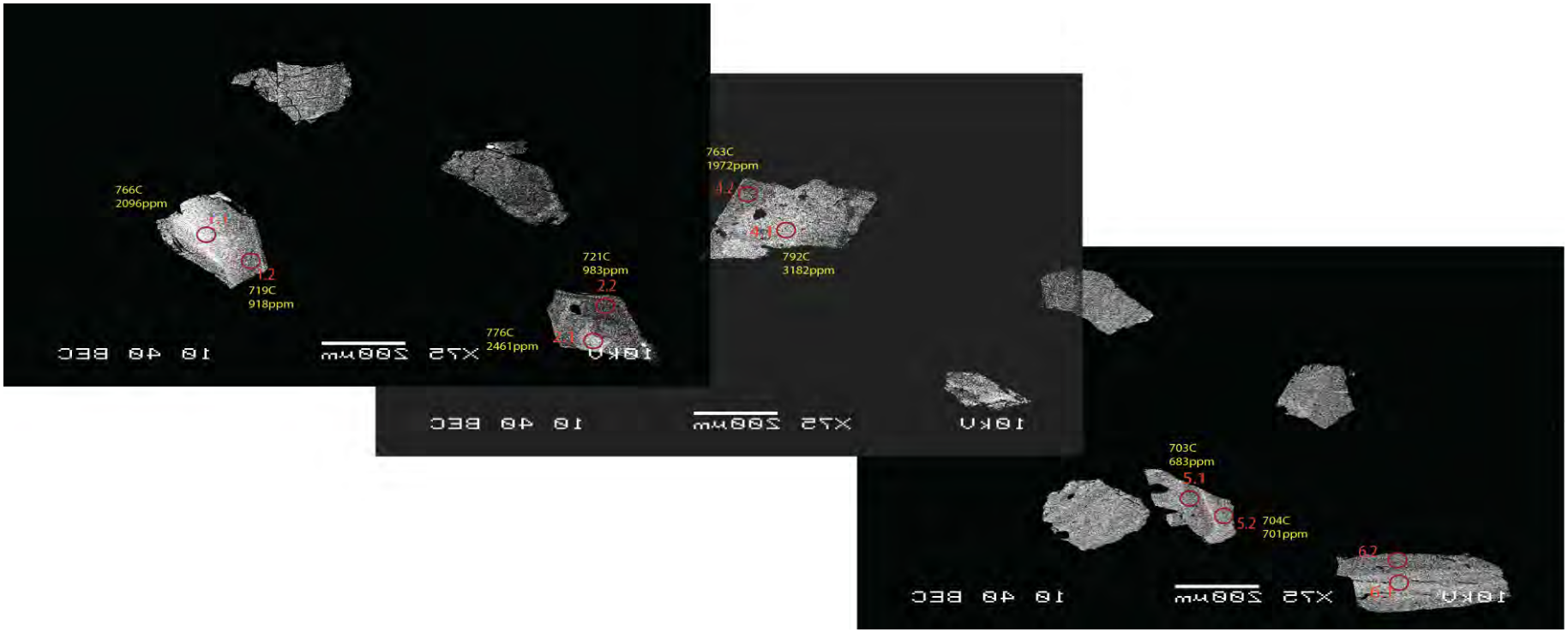
766C
2096ppm
1.1
1.2
719C
918ppm
721C
983ppm
2.2
776C
2461ppm
763C
1972ppm
4.2
4.1
792C
3182ppm
703C
683ppm
5.1
5.2
704C
701ppm
6.2
6.1

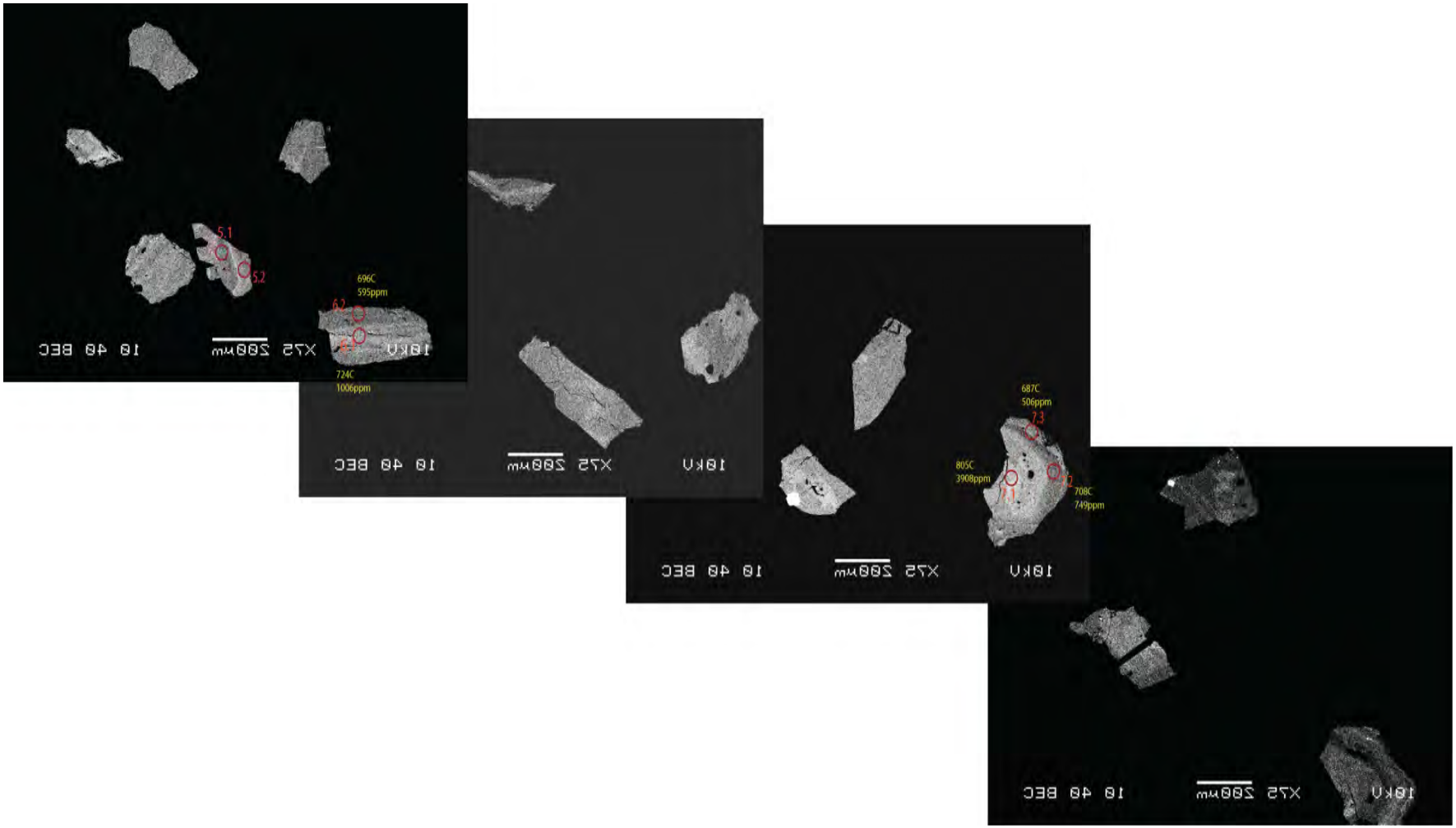
5.1
5.2
696C
595ppm
6.2
724C
1006ppm
687C
506ppm
7.3
805C
3908ppm
7.1
7.2
708C
749ppm
10 40 BEC
X25 200µm
10kV

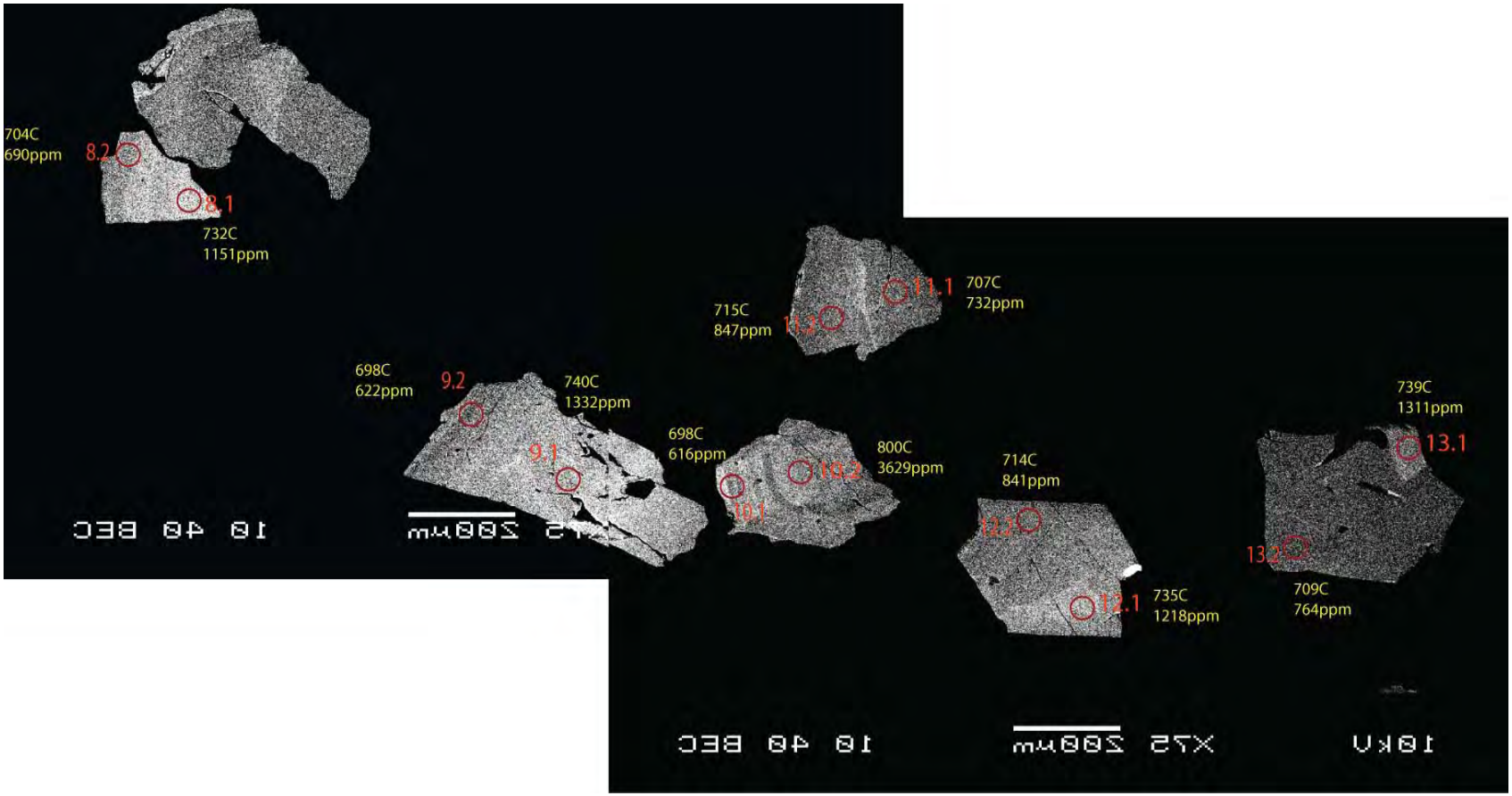
704C
690ppm
8.2
8.1
732C
1151ppm
715C
847ppm
11.3
11.1
707C
732ppm
698C
622ppm
9.2
740C
1332ppm
9.1
698C
616ppm
10.2
10.1
800C
3629ppm
714C
841ppm
12.2
12.1
735C
1218ppm
739C
1311ppm
13.1
13.2
709C
764ppm
200µm
10kV

Figure H5. Back-scatter Electron Imaging of AWAG-4

Red spots and numbers indicate spot location and name
Yellow text indicates Zr-in-sphene thermometry temperatures (above) and Zr concentrations (lower)

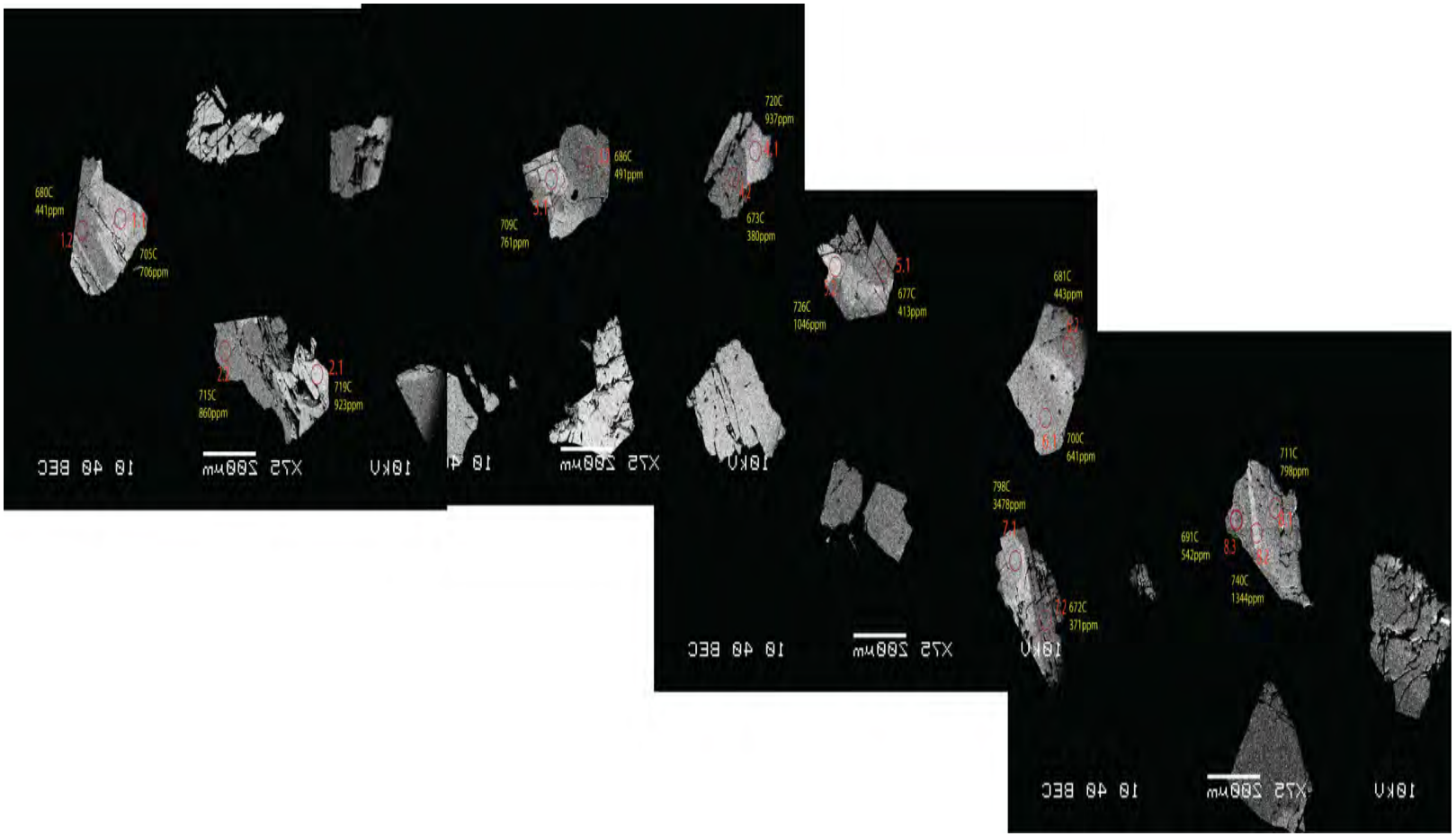
680C
441ppm
1.2
1.1
705C
706ppm
715C
860ppm
2.2
2.1
719C
923ppm
686C
491ppm
3.1
709C
761ppm
720C
937ppm
4.1
4.2
673C
380ppm
726C
1046ppm
5.2
5.1
677C
413ppm
681C
443ppm
6.2
6.1
700C
641ppm
798C
3478ppm
7.1
7.2
672C
371ppm
691C
542ppm
8.3
8.2
740C
1344ppm
711C
798ppm
8.1
10KV
X75 200µm
10 40 BEC

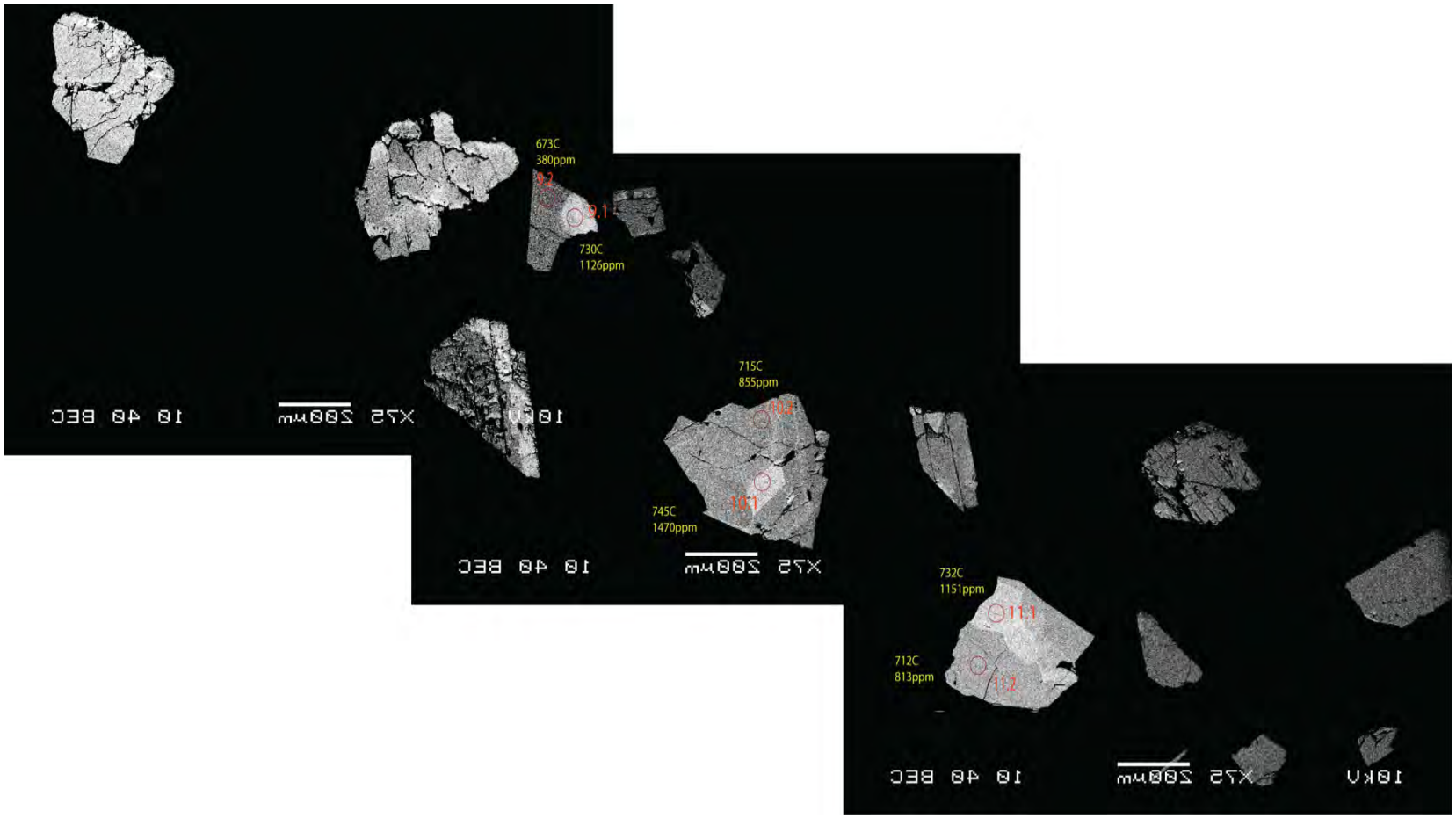
673C
380ppm
730C
1126ppm
715C
855ppm
745C
1470ppm
732C
1151ppm
712C
813ppm

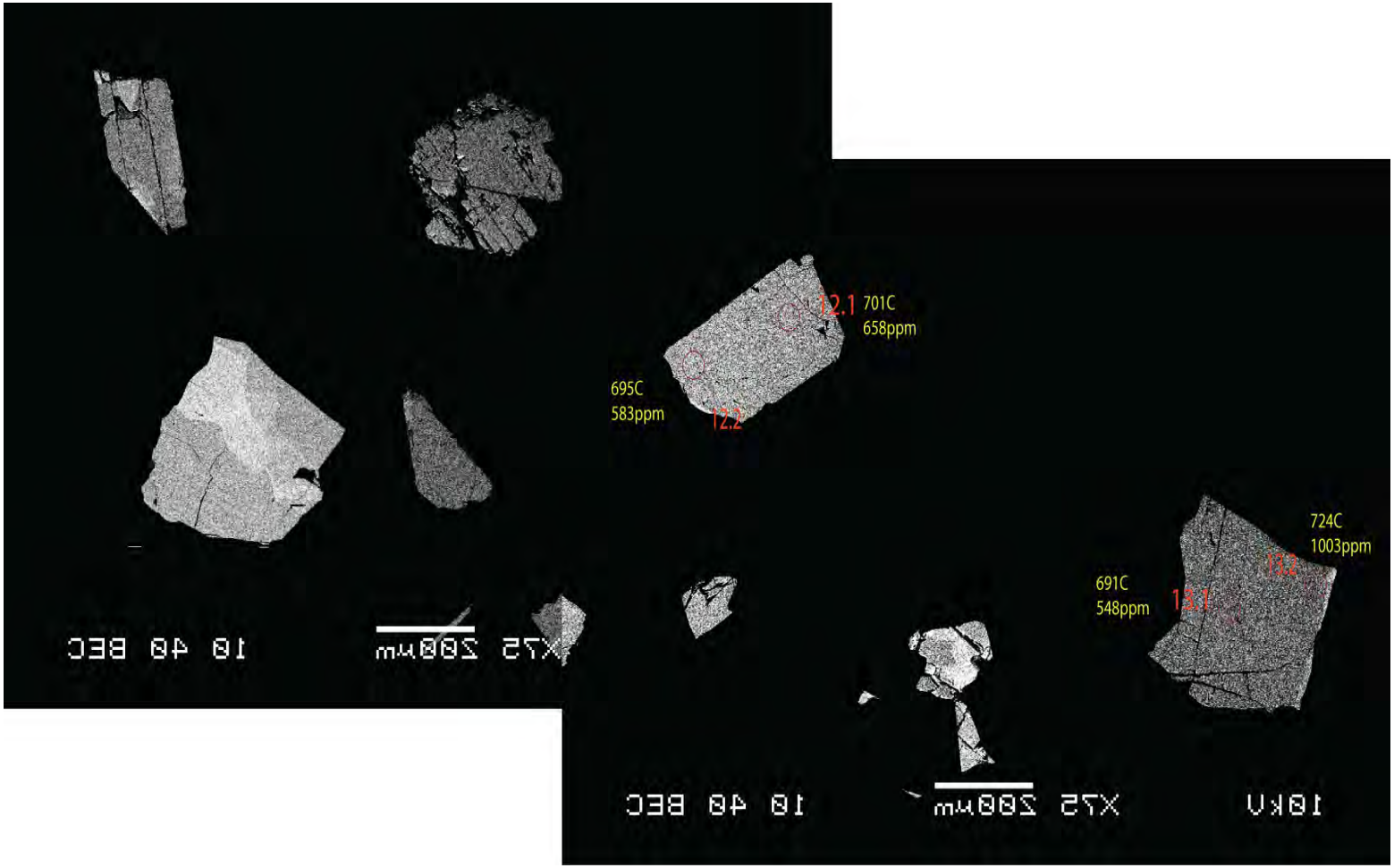
12.1
701C
658ppm
695C
583ppm
12.2
724C
1003ppm
13.2
691C
548ppm
13.1
10kV X75 200µm 10 40 BEC

Figure H6. Back-scatter Electron Imaging of AWAG-5

Red spots and numbers indicate spot location and name
Yellow text indicates Zr-in-sphene thermometry temperatures (above) and Zr concentrations (lower)

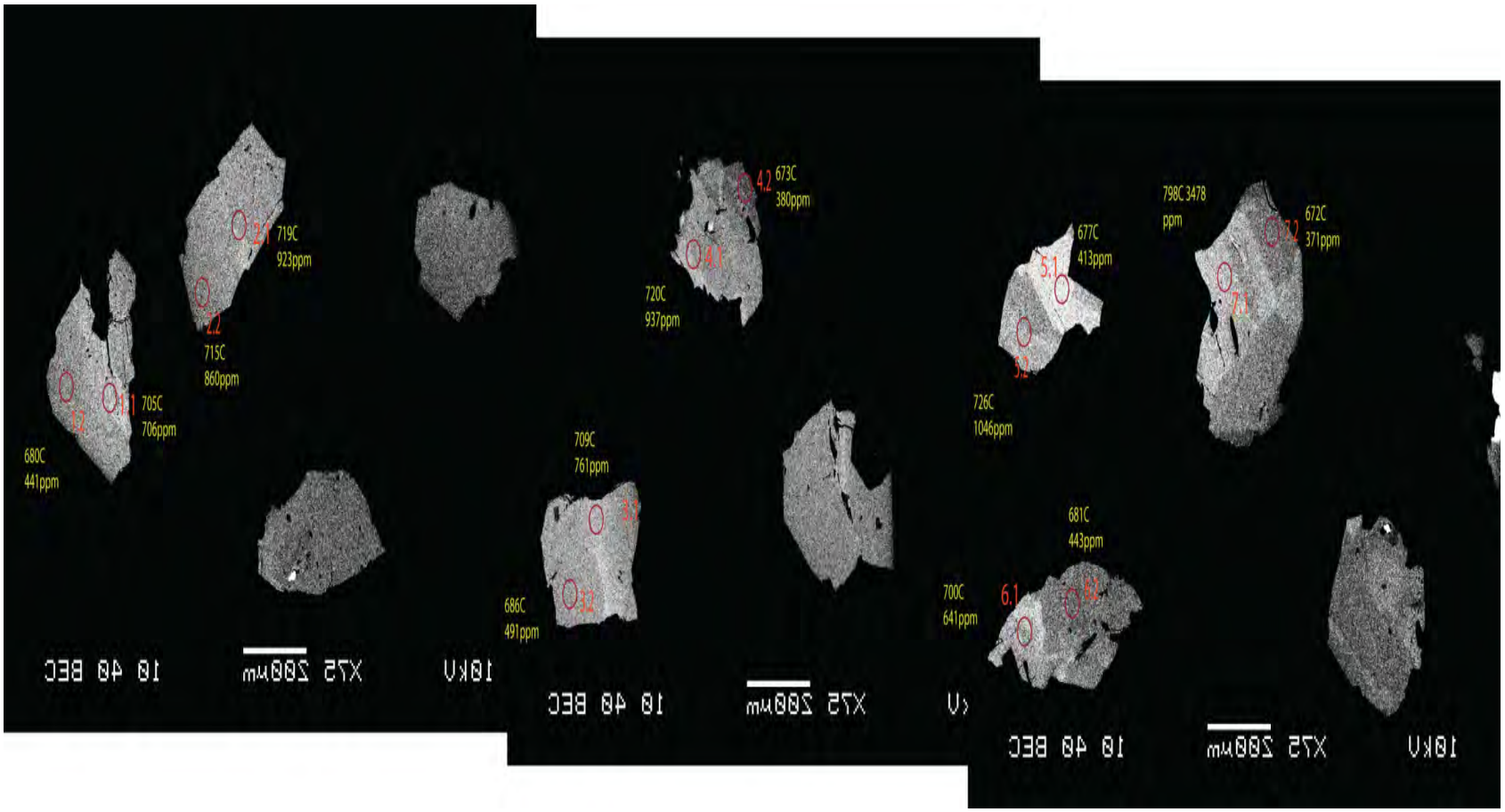
1.1
705C
706ppm
1.2
680C
441ppm
2.1
719C
923ppm
2.2
715C
860ppm
3.2
709C
761ppm
3.1
686C
491ppm
4.2
673C
380ppm
4.1
720C
937ppm
5.1
677C
413ppm
5.2
726C
1046ppm
7.2
672C
371ppm
7.1
798C 3478
ppm
6.2
681C
443ppm
6.1
700C
641ppm
10 40 BEC
X75 200µm
10kV

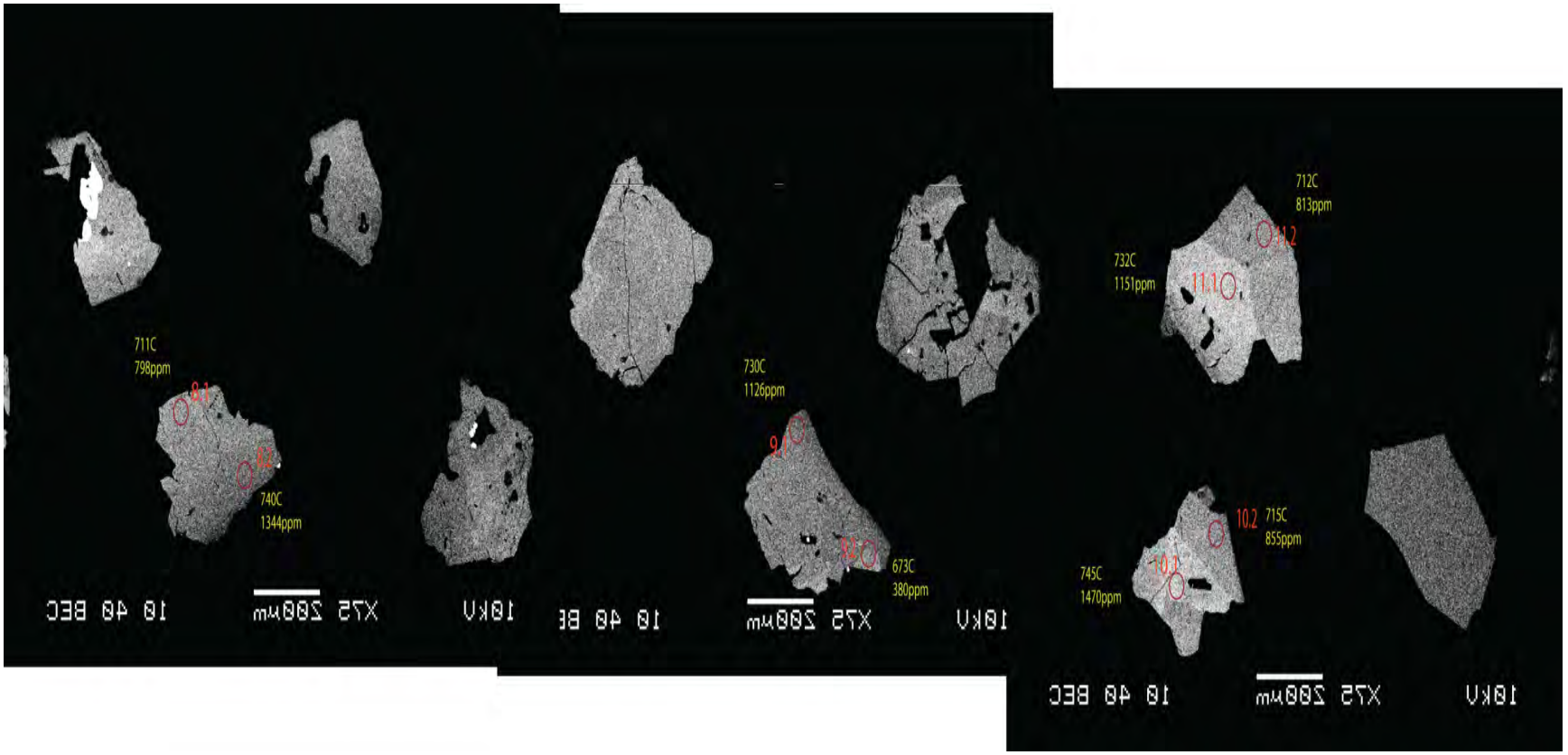
711C
798ppm
740C
1344ppm
730C
1126ppm
673C
380ppm
732C
1151ppm
712C
813ppm
715C
855ppm
745C
1470ppm
10KV
X75 200µm
10 40 BEC

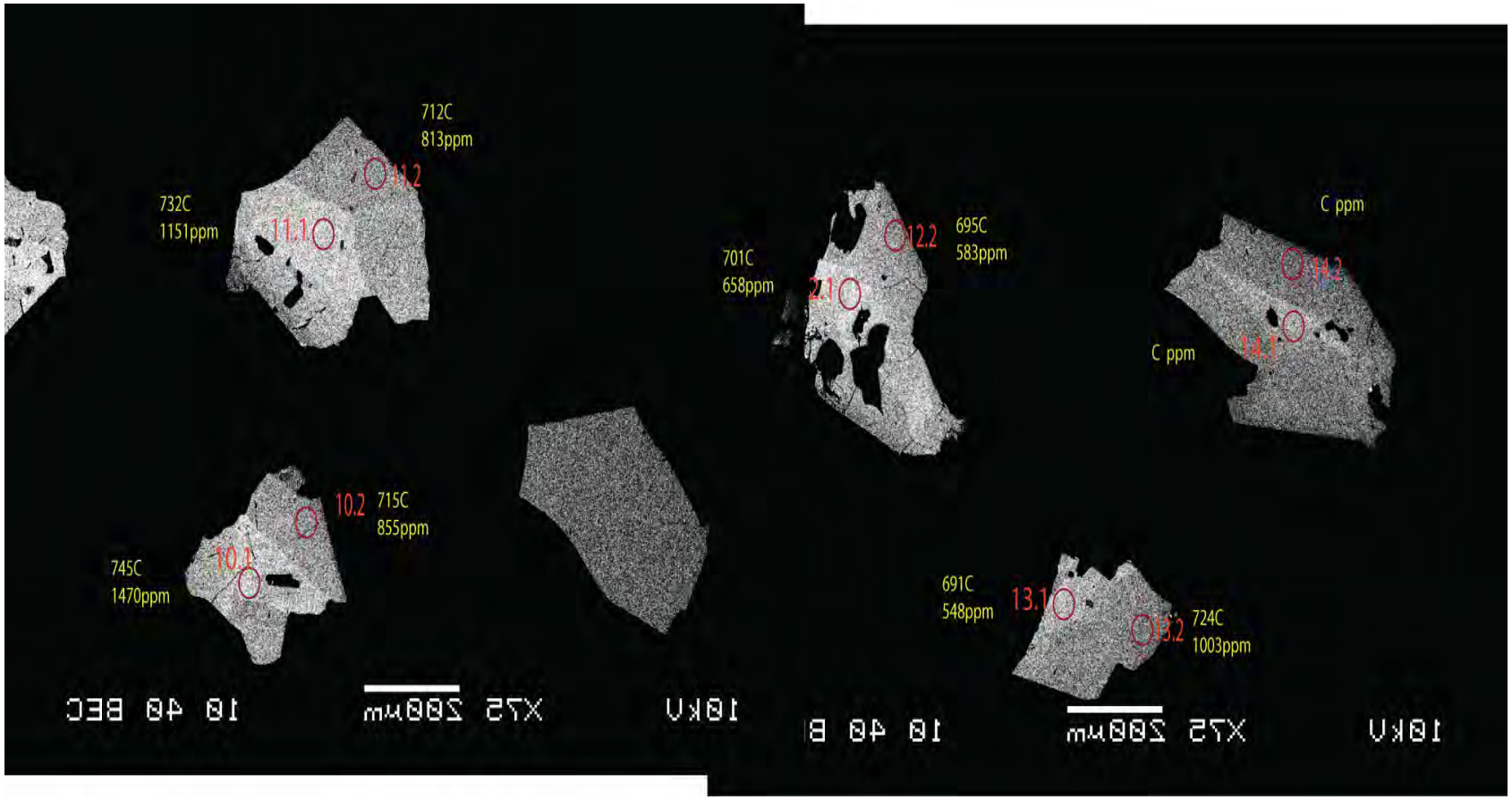
712C
813ppm
11.2
732C
1151ppm
11.1
701C
658ppm
12.2
695C
583ppm
2.1
C ppm
14.2
C ppm
14.1
10.2
715C
855ppm
745C
1470ppm
10.1
691C
548ppm
13.1
13.2
724C
1003ppm
10kV X75 200µm 10 40 BEC
10kV X75 200µm 10 40 B

Figure H7. Back-scatter Electron Imaging of AWAG-6

Red spots and numbers indicate spot location and name
Yellow text indicates Zr-in-sphene thermometry temperatures (above) and Zr concentrations (lower)

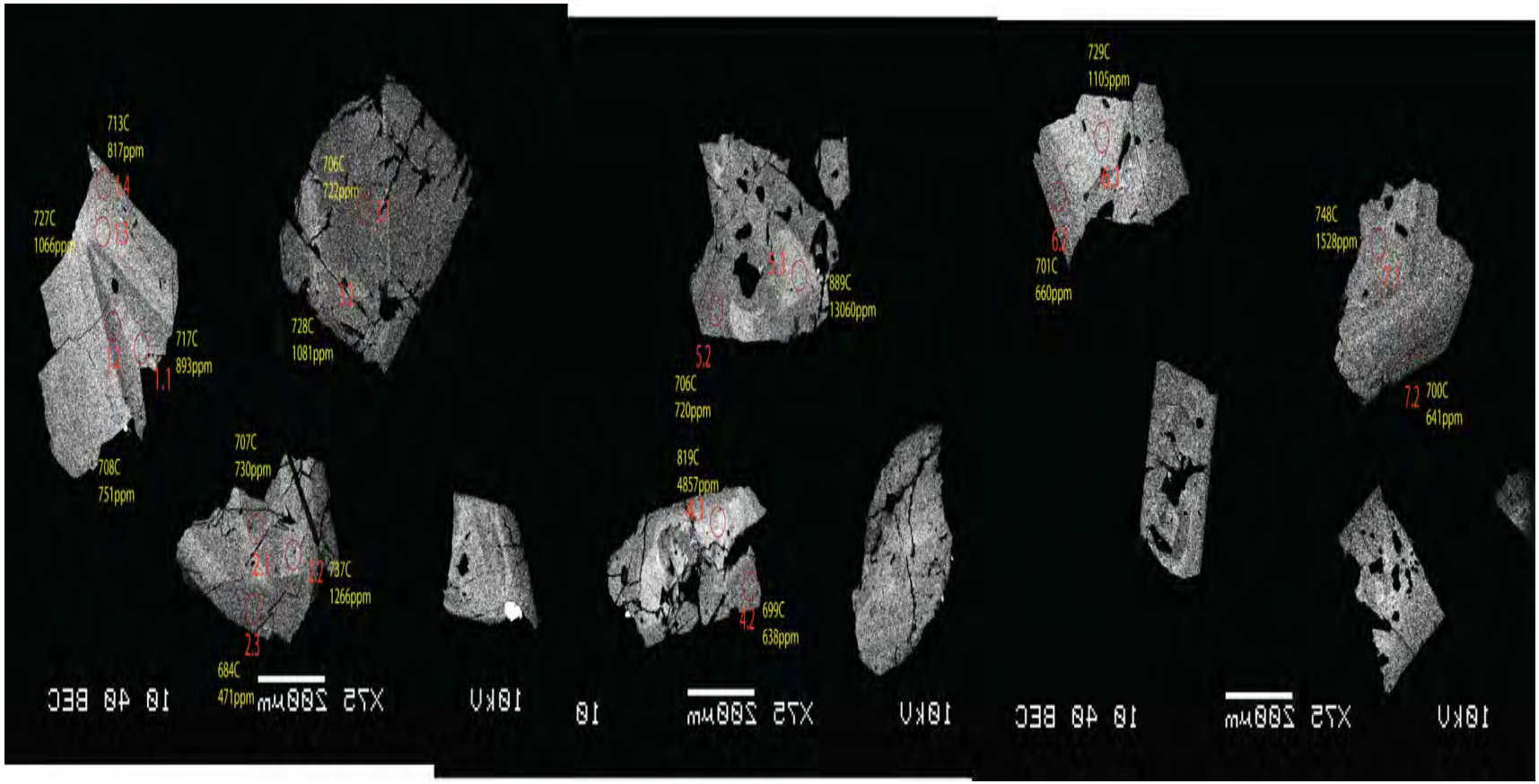
713C
817ppm
1.4
727C
1066ppm
1.3
717C
893ppm
1.2
1.1
708C
751ppm
706C
722ppm
3.1
3.2
728C
1081ppm
707C
730ppm
2.1
2.2
737C
1266ppm
2.3
684C
471ppm
10kV
X75 200µm
10 40 BEC
10
5.1
889C
13060ppm
5.2
706C
720ppm
819C
4857ppm
4.1
4.2
699C
638ppm
729C
1105ppm
6.1
6.2
701C
660ppm
748C
1528ppm
7.1
7.2
700C
641ppm

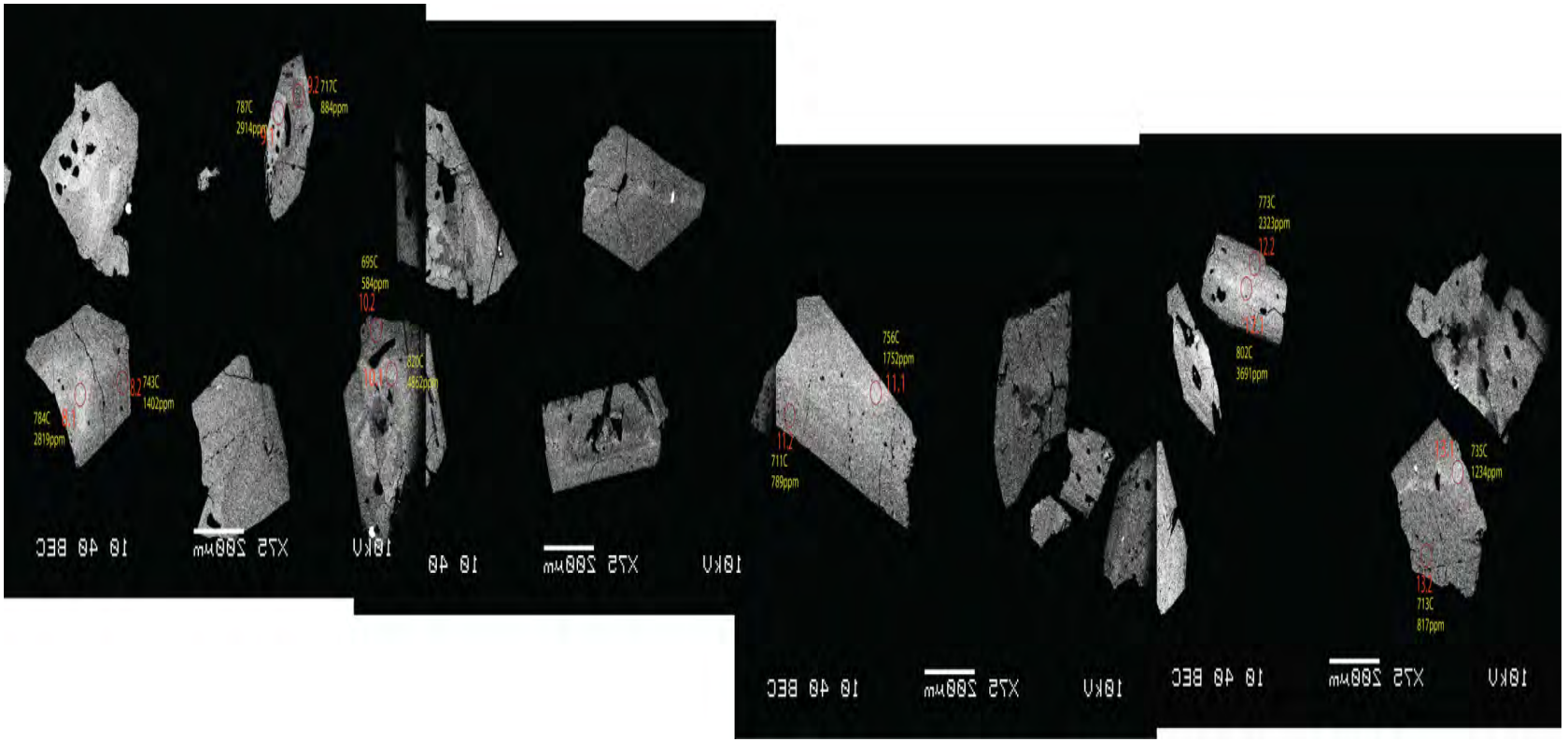
787C
2914ppm
9.2
717C
884ppm
695C
584ppm
10.2
784C
2819ppm
8.2
743C
1402ppm
10kV
X25 200µm
10 40 BEC
10kV
X25 200µm
10 40
711C
789ppm
11.2
756C
1752ppm
11.1
10kV
X25 200µm
10 40 BEC
773C
2323ppm
12.2
12.1
802C
3691ppm
13.1
739C
1234ppm
13.2
713C
817ppm
10kV
X25 200µm
10 40 BEC

Figure H8. Back-scatter Electron Imaging of AWAG-7

Red spots and numbers indicate spot location and name
Yellow text indicates Zr-in-sphene thermometry temperatures (above) and Zr concentrations (lower)

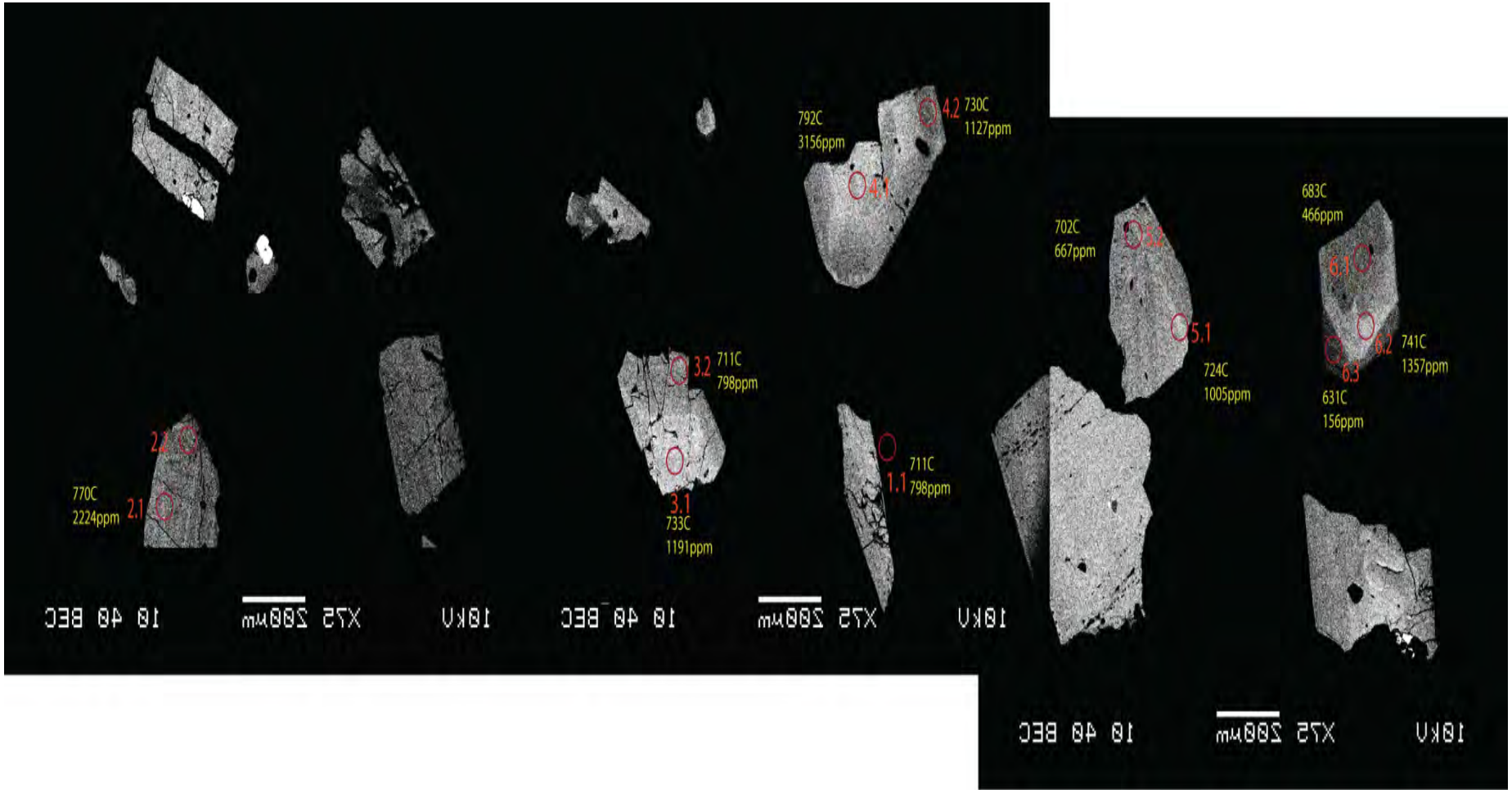
792C
3156ppm
4.2
730C
1127ppm
4.1
3.2
711C
798ppm
2.2
770C
2224ppm
2.1
3.1
733C
1191ppm
711C
1.1
798ppm
702C
667ppm
5.2
5.1
724C
1005ppm
683C
466ppm
6.1
6.2
741C
1357ppm
6.3
631C
156ppm
10 40 BEC
X75 200µm
10kV

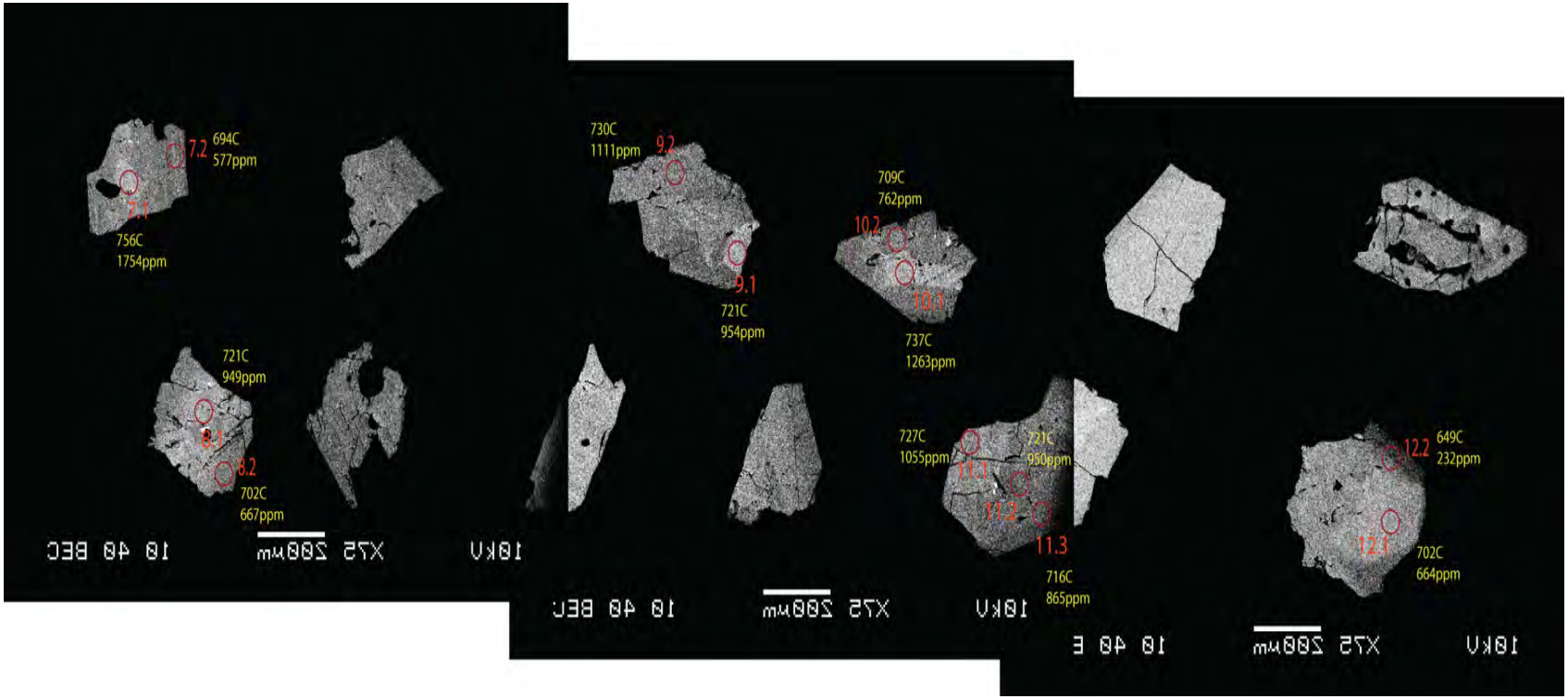
7.2
694C
577ppm
7.1
756C
1754ppm
721C
949ppm
8.1
8.2
702C
667ppm
10kV X75 200µm 10 40 BEC
730C
1111ppm
9.2
9.1
721C
954ppm
709C
762ppm
10.2
10.1
737C
1263ppm
10kV X75 200µm 10 40 BEC
727C
1055ppm
721C
950ppm
11.1
11.2
11.3
716C
865ppm
10kV X75 200µm 10 40 E
12.2
649C
232ppm
12.1
702C
664ppm

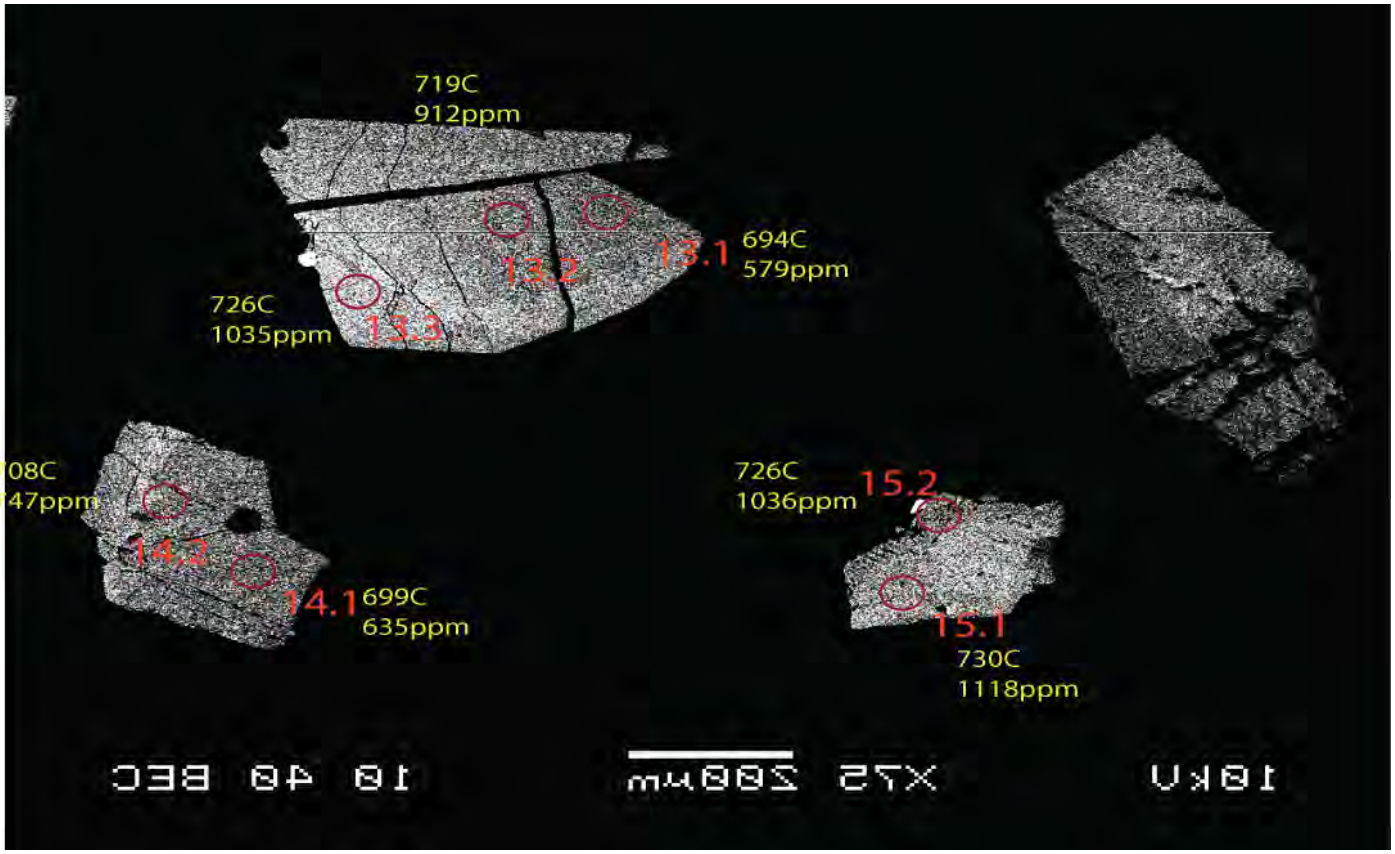
719C
912ppm
13.2
13.1
694C
579ppm
726C
1035ppm
13.3
708C
747ppm
14.2
14.1
699C
635ppm
726C
1036ppm
15.2
15.1
730C
1118ppm

Figure H9. Back-scatter Electron Imaging of AWM-1

Red spots and numbers indicate spot location and name
Yellow text indicates Zr-in-sphene thermometry temperatures (above) and Zr concentrations (lower)

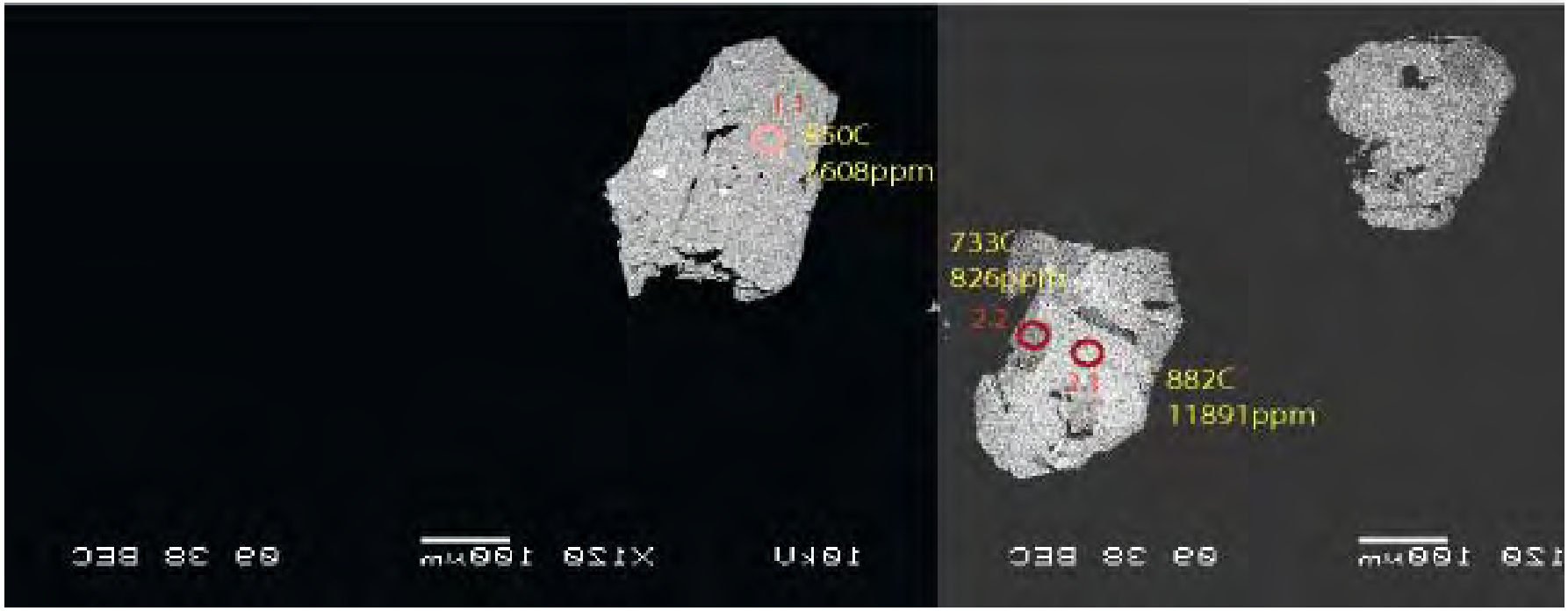
850C
7608ppm
733C
826ppm
882C
11891ppm

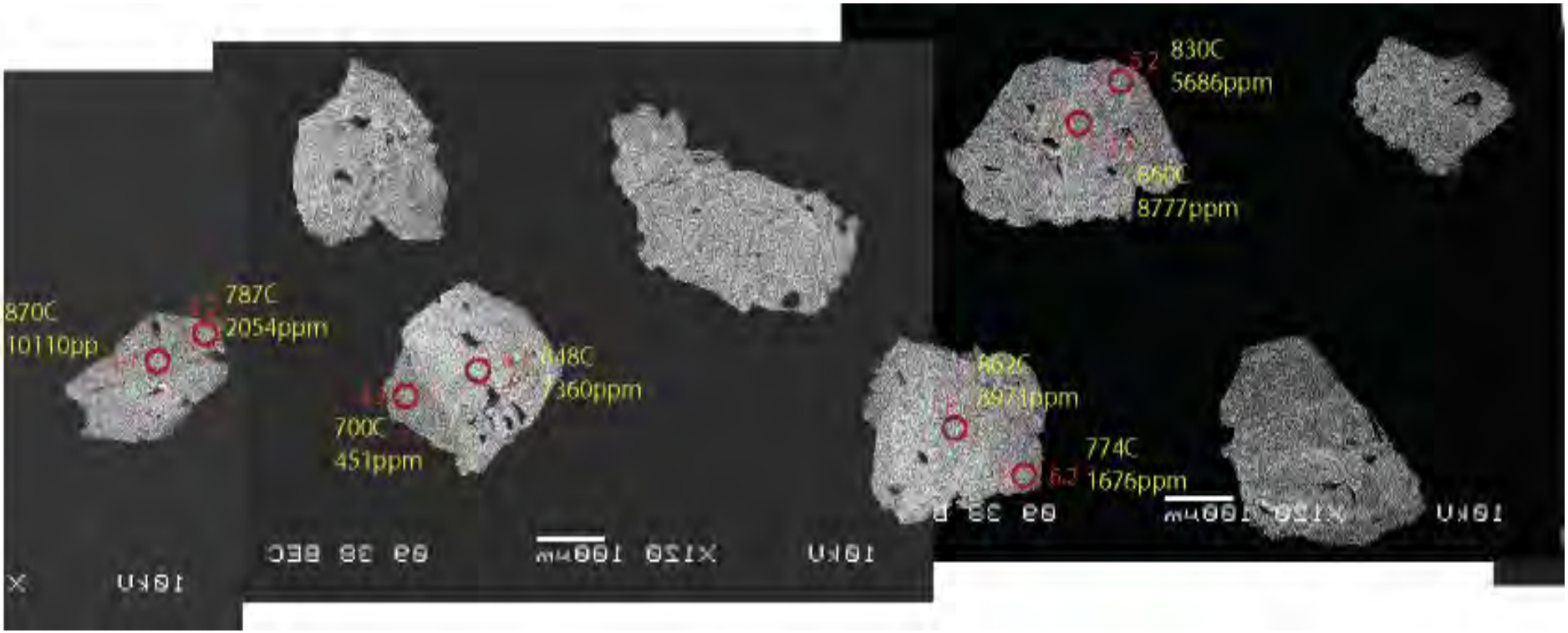
830C
5686ppm
8777ppm
787C
2054ppm
700C
451ppm
774C
1676ppm

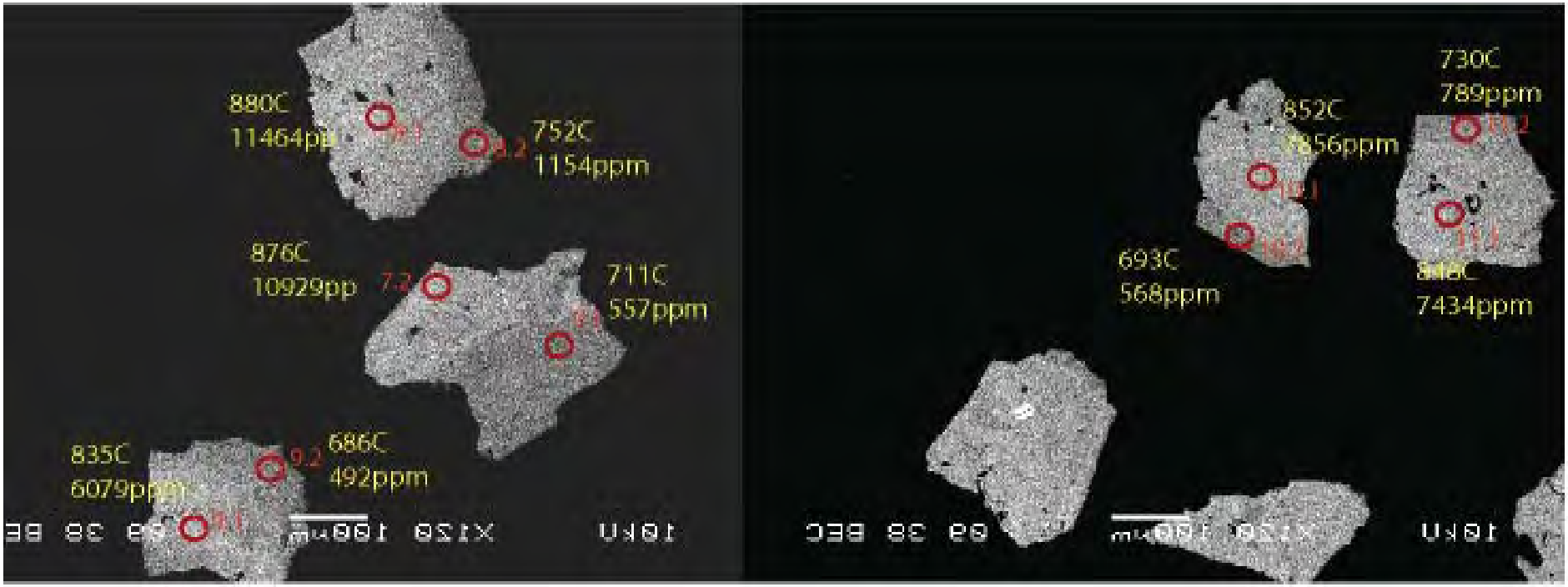
880C
11464pp
752C
1154ppm
876C
10929pp
711C
557ppm
835C
6079ppm
686C
492ppm
852C
730C
789ppm
693C
568ppm
7434ppm

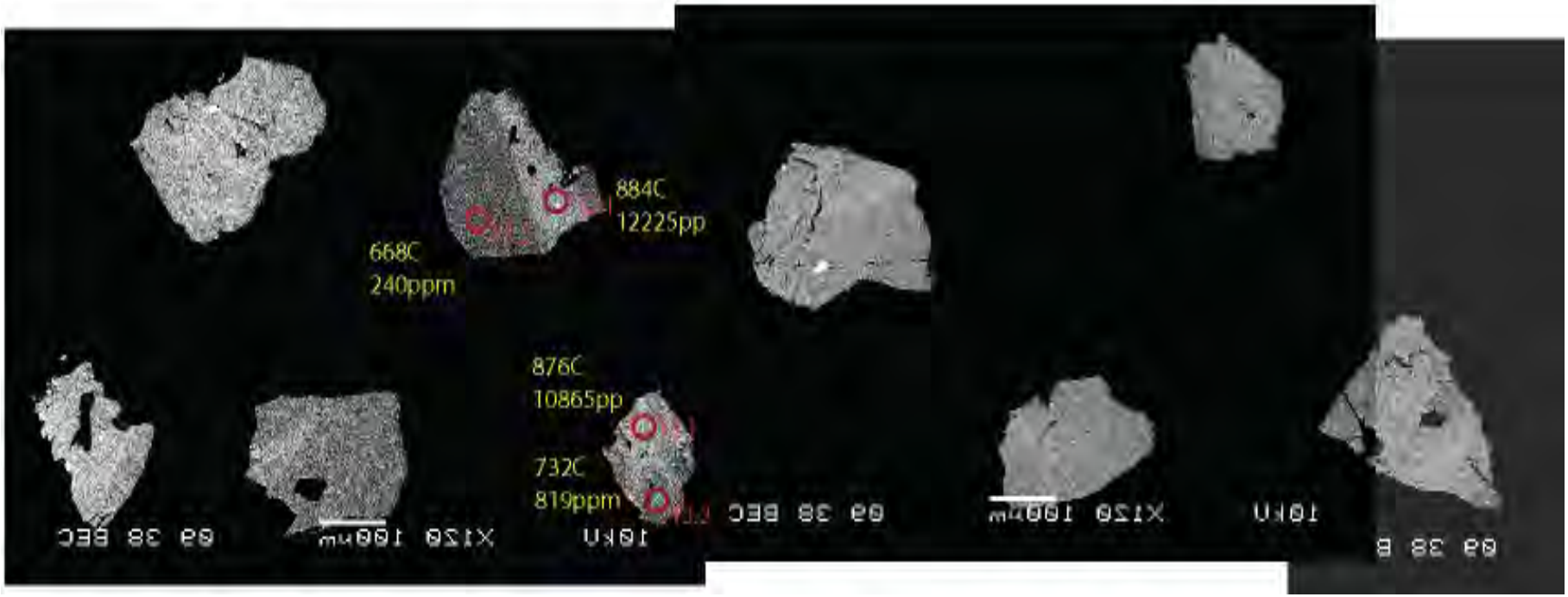
884C
12225pp
668C
240ppm
876C
10865pp
732C
819ppm

676C
406ppm
834C
6029ppm

Figure H10. Back-scatter Electron Imaging of AWM-2

Red spots and numbers indicate spot location and name
Yellow text indicates Zr-in-sphene thermometry temperatures (above) and Zr concentrations (lower)

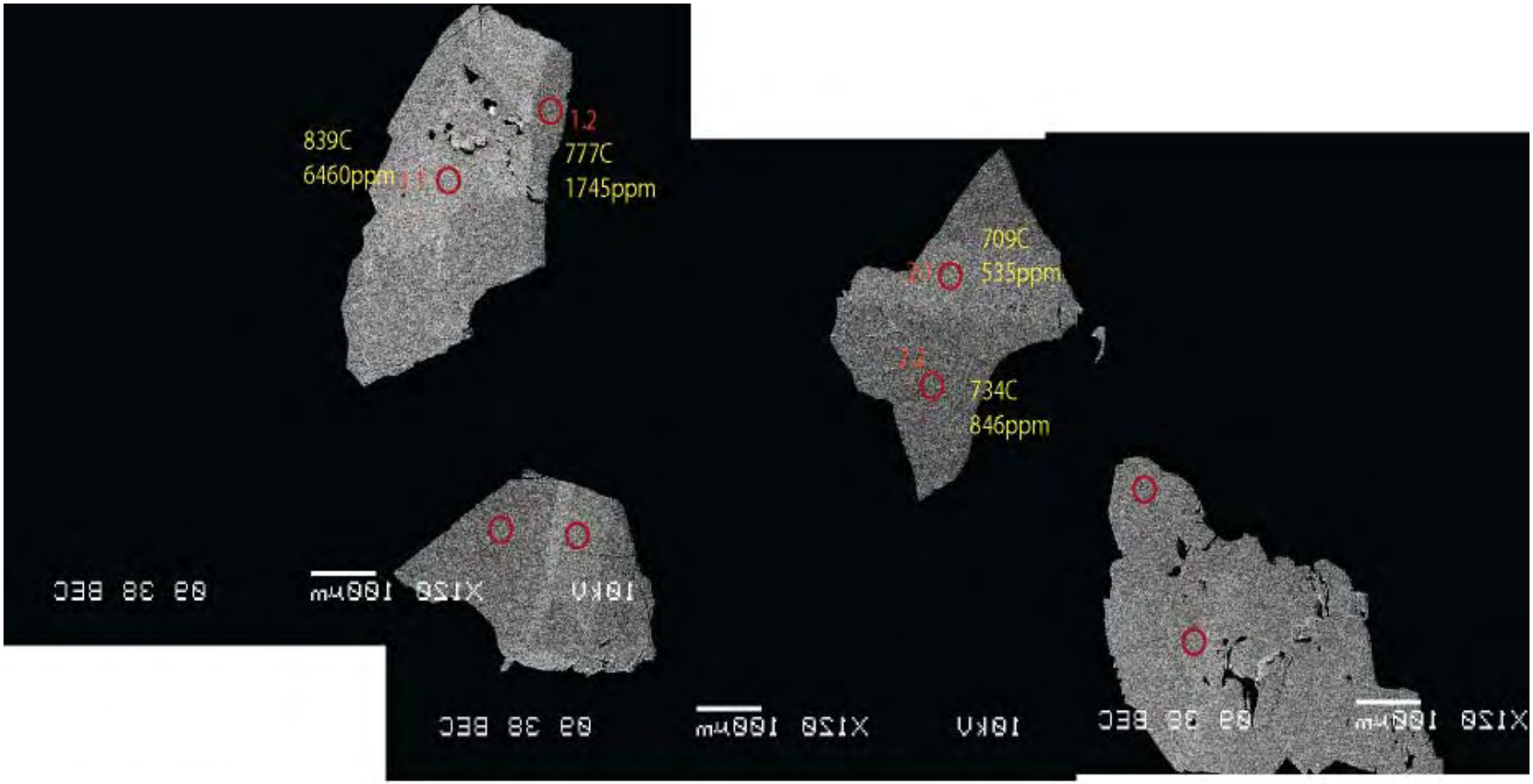
839C
6460ppm
1.2
777C
1745ppm
709C
535ppm
734C
846ppm

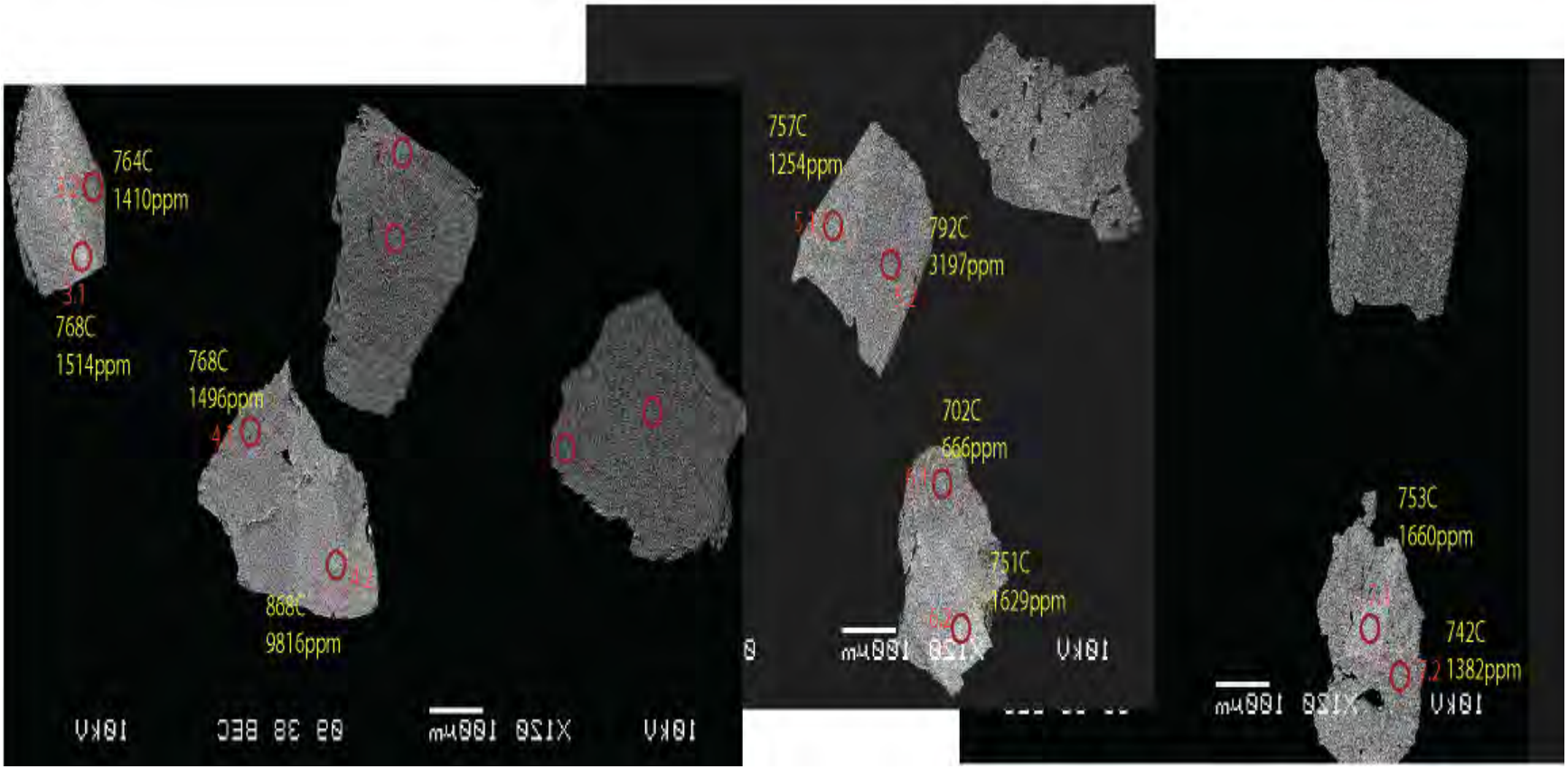
764C
1410ppm
768C
1514ppm
768C
1496ppm
868C
9816ppm
757C
1254ppm
792C
3197ppm
702C
666ppm
751C
1629ppm
753C
1660ppm
742C
1382ppm

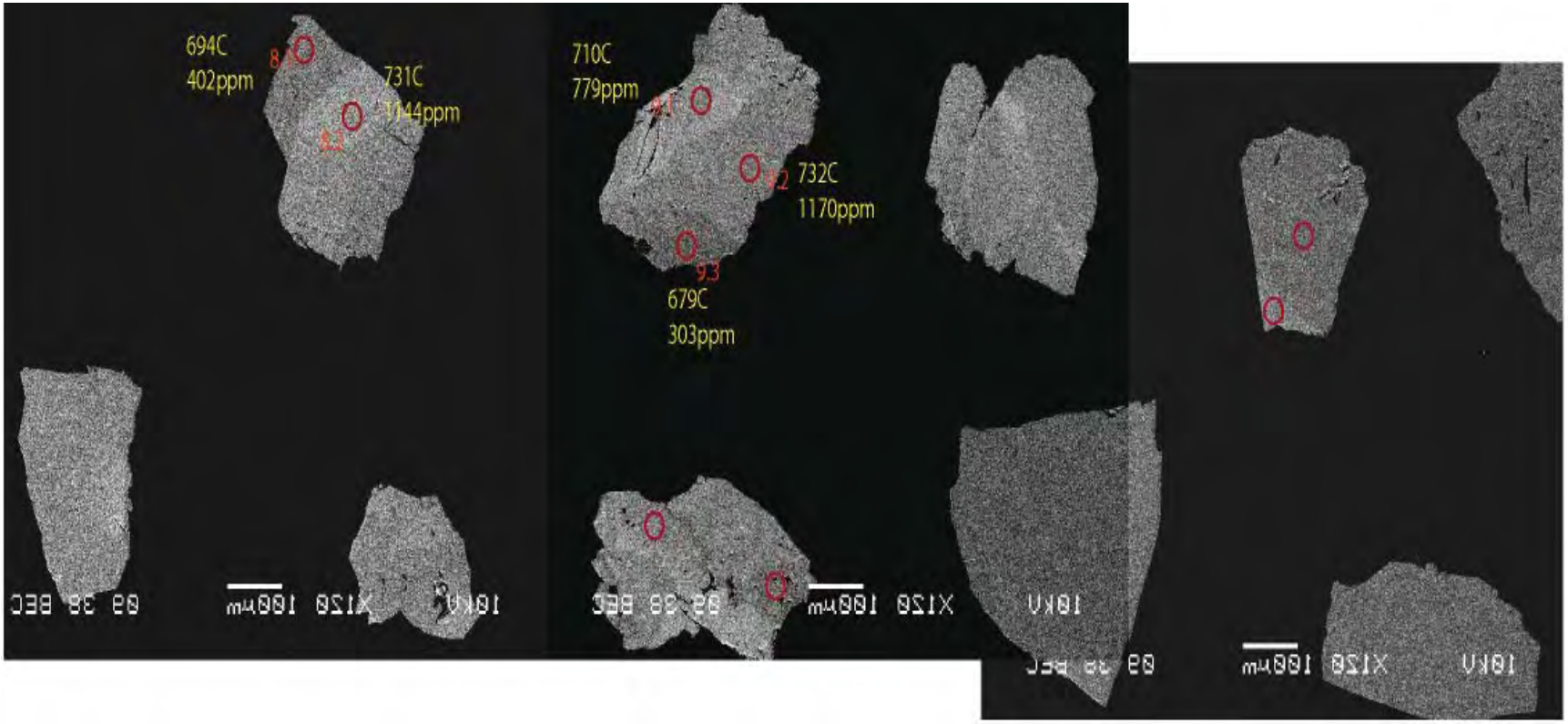
694C
402ppm
731C
1144ppm
710C
779ppm
732C
1170ppm
679C
303ppm

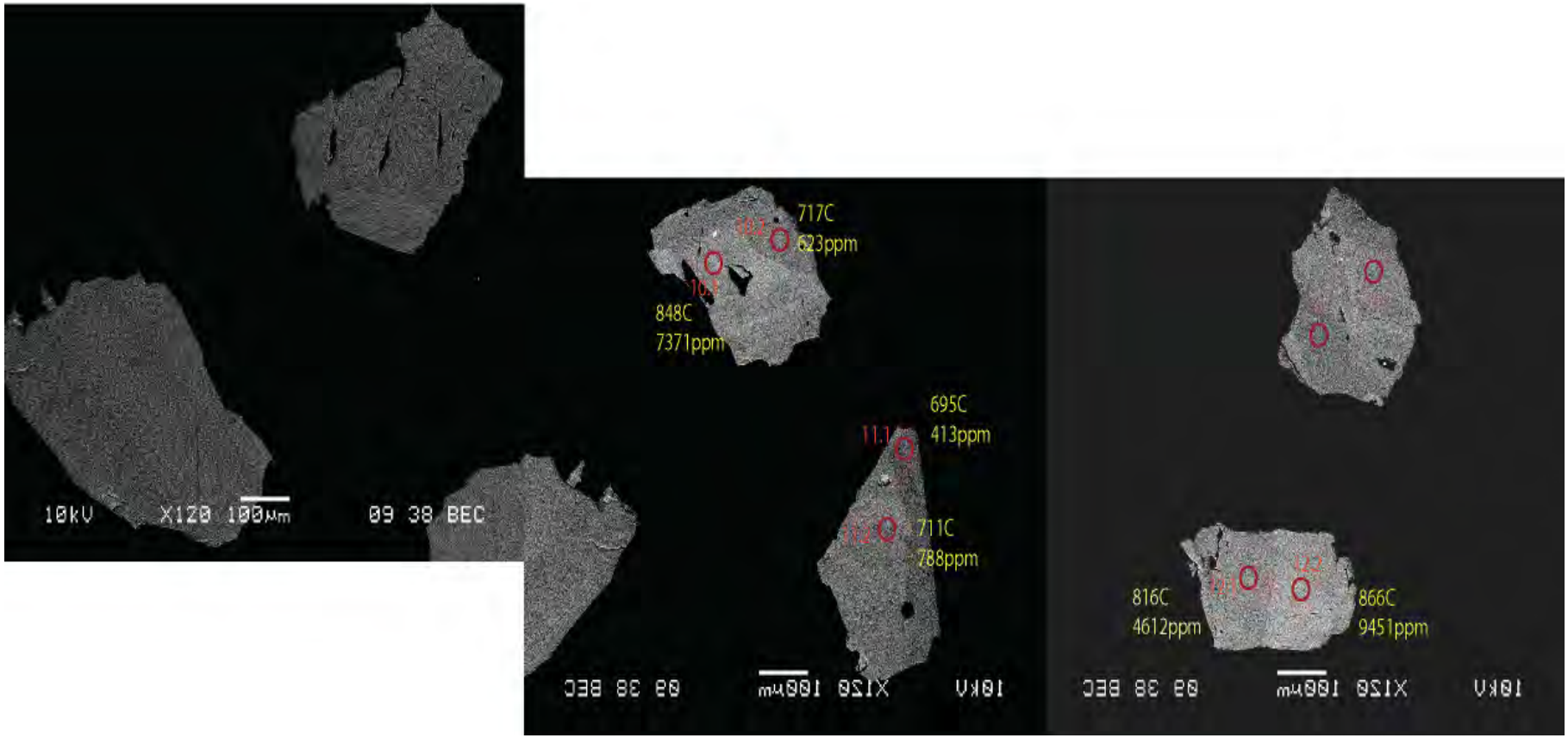
10kV X120 100µm 09 38 BEC
717C
623ppm
848C
7371ppm
695C
413ppm
711C
788ppm
816C
4612ppm
866C
9451ppm

Appendix I

Mixing curve data

Table I1 Calculated results for binary mixing of whole-rock Sr and Nd isotopic data

	Ireteba Granite[##]		Old Woman[†]		Crust Mean[‡]	
Fraction of EMB[#]	$^{87}Sr/^{86}Sr$	εNd	$^{87}Sr/^{86}Sr$	εNd	$^{87}Sr/^{86}Sr$	εNd
0	0.71500	-16.0	0.72000	-18.0	0.71900	-15.2
0.2	0.71303	-12.4	0.71431	-16.1	0.71534	-13.5
0.4	0.71139	-10.1	0.71146	-13.9	0.71269	-11.8
0.6	0.71001	-8.4	0.70975	-11.6	0.71067	-10.0
0.8	0.70883	-7.2	0.70861	-9.1	0.70908	-8.2

Enriched Mantle Basalt (EMB) figures taken from sample SAW17 (Ericksen, 2006).

Ireteba Granite data taken from Kapp et al., (2002).

† Old Woman Mountains data taken from Kapp et al., (2002).

‡ Mojave Crustal Mean data taken from Miller and Wooden (1994).

Table I2 Calculated results for binary mixing of in-situ zircon Hf and O isotopic data

	EnrichedMantle-Precambrian I†		Enriched Mantle-Precambrian II‡		Depleted Mantle##-Precambrian II	
Melt fraction of mantle end-member	εHf	$\delta^{18}O^{\#}$	εHf	$\delta^{18}O^{\#}$	εHf	$\delta^{18}O^{\#}$
0.0	-28.0	8.5	-28.0	12	-28.0	12
0.2	-25.1	7.86	-21.4	10.66	-19.9	10.66
0.4	-21.8	7.22	-16.1	9.32	-12.3	9.32
0.6	-18.0	6.58	-11.8	7.98	-5.1	7.98
0.8	-13.5	5.94	-8.1	6.64	1.6	6.64
1.0	-8.0	5.3	-5.0	5.3	8.0	5.3

$\delta^{18}O$ values calculated without O concentrations due to large abundance likely present in all samples.

Calculation of Depleted Mantle using the following data: Hf = 7ppm, εHf = +8 (Beard and Johnson, 1997), $\delta^{18}O$ = 5.3 (Vallet et al., 2003).

† Calculation of Precambrian I using following data: Hf = 6ppm (Taylor and McLennan, 1995), εHf = -28, $\delta^{18}O$ = 8.5 (Kapp et al., 2002).

‡ Calculation of Precambrian II using following data: Hf = 6ppm (Taylor and McLennan, 1995), εHf = -28 (Kapp et al., 2002), $\delta^{18}O$ = 12 (Bender et al., 1993).